K.D. Sen *Editor*

Electronic Structure of Quantum Confined Atoms and Molecules

Springer

Electronic Structure of Quantum Confined Atoms and Molecules

K.D. Sen
Editor

Electronic Structure of Quantum Confined Atoms and Molecules

Springer

Editor
K.D. Sen
School of Chemistry
University of Hyderabad
Hyderabad, Telangana
India

ISBN 978-3-319-09981-1 ISBN 978-3-319-09982-8 (eBook)
DOI 10.1007/978-3-319-09982-8

Library of Congress Control Number: 2014950050

Springer Cham Heidelberg New York Dordrecht London

Printed on acid-free paper

Springer is part of Springer Science+Business Media (www.springer.com)

Dedicated to my teacher
Professor P.T. Narasimhan (1928–2013)

Preface

Due largely to their relevance in the design and synthesis of new materials and futuristic devices, quantum confined model systems incorporating the repulsive as well as attractive confining potentials have become a subject of growing research interest. A diverse set of experiments involving, e.g. atoms and molecules under pressure, quantum dots and atoms in metallofullerenes are analysed using such models which are essentially defined by the given shape and strength of confinining potential. Comprising a set of nine contributed chapters, dealing with the simplest among the quantum confined model systems, this monograph records the significant developments in the field subsequent to the two published volumes of Advances in Quantum Chemistry (Academic Press, New York, 2009), Vol. 57–58. In Chap. 1, Eugenio Ley-Koo and Guo-Hua Sun present their work on surface effects in light atoms confined by dihedral angles in spherical, parabolic and prolate spheroidal coordinates. In Chap. 2, Vladimir Pupyshev and Andrey Scherbinin discuss the effect of symmetry lowering of the confining impenetrable cavity, including the deformation of large cavity on the eigen-spectrum of hydrogen atom. In Chap. 3, Norberto Aquino and A. Flores-Riveros discuss their work covering the effect of soft spherical confinement on the popular information theoretical measures due to Shannon and Fisher for the hydrogen atom in the position and momentum space. In Chap. 4, H.E. Montgomery Jr. and K.D. Sen present the accurate total energy calulations on the two electron isoelectronic systems in excited electronic states within the impenetrable spherical boundary wall using variational perturbation method. The following Chap. 5 contributed by Frederico Prudente and Marcilio Guimarães describes the finite element and discrete variable representation under the variational ansatz for the treatment of the few electrons under the spherical, endohedral and plasmatical confinement conditions. Chapter 6, by L.G. Jiao and Y.K. Ho, presents a set of highly accurate calculations on the bound and resonant states in confined quantum dots. In the contribution under Chap. 7, S.A. Ndengué and O. Motapon use the Galerkin variational method with the wave functions obtained as expansions on B-splines basis sets in spherical, cylindrical or prolate spheroidal coordinates. The authors describe how the electronic energy levels of hydrogen atom, its wave functions and static and dynamic electric dipole

polarizabilities are significantly changed under the spherical, cylindrical or prolate spheroidal, endohedral or shell confinement conditions. The latter model potential is frequently used to model the confinenment effects arising from a single and multi-wall fullerene cage. The study is extended to the investigation of the H_2^+ molecular ion and its isotopologues. In Chap. 8, J. Garza and R. Vargas formulate the scheme of carrying out the Thomas-Fermi, modified Thomas-Fermi and the density functional theory (DFT) calculations within the Kohn-Sham model for the spherically confined many electron atoms. The influence of confinement on the correlation energy has been studied within the DFT. Finally, in Chap. 9, A. Sarsa and C. Le Sech study the effect of quantum confinement on the H_2^+ molecular ion and H_2 molecule. For these molecules confined by impenetrable surfaces the trial wave functions are computed using the variational and diffusional Monte Carlo approaches. The study is carried out beyond the Born-Oppenheimer approximation so that the motion of the nuclei is included in the trial wave function. It is hoped that the theoretical formulations, algorithms and their applications contained in this monograph will serve as a ready reference material to the interdiscipliniary research community interested in studying confined quantum electronic systems.

Hyderabad, June 2014

K.D. Sen
J.C. Bose National Fellow

Contents

Contributors

N. Aquino Departamento de Física, Universidad Autónoma Metropolitana-Iztapalapa, México, D.F., Mexico

A. Flores-Riveros Instituto de Física, Benemérita Universidad Autónoma de Puebla, Puebla, PUE, Mexico

Jorge Garza Departamento de Química, Universidad Autónoma Metropolitana-Iztapalapa, México, D.F., México

Marcilio N. Guimarães Centro de Formação de Professores, Universidade Federal Do Recôncavo Da Bahia, Amargosa, BA, Brazil

Y.K. Ho Institute of Atomic and Molecular Sciences, Academia Sinica, Taipei, Taiwan

L.G. Jiao Institute of Atomic and Molecular Sciences, Academia Sinica, Taipei, Taiwan

Eugenio Ley-Koo Instituto de Física, Universidad Nacional Autónoma de México, México, D.F., Mexico; Centro Universitario Valle de Chalco Universidad Autónoma del Estado de México Chalco, México, D.F., Estado de México, Mexico

H.E. Montgomery Jr. Chemistry Program, Centre College, Danville, USA

O. Motapon Laboratoire de Physique Fondamentale, UFD Mathématiques, Informatique Appliquée et Physique Fondamentale, University of Douala, Douala, Cameroon

S.A. Ndengué Laboratoire de Physique Fondamentale, UFD Mathématiques, Informatique Appliquée et Physique Fondamentale, University of Douala, Douala, Cameroon

Frederico V. Prudente Instituto de Física, Universidade Federal Da Bahia, Salvador, BA, Brazil

Vladimir I. Pupyshev Laboratory of Molecular Structure and Quantum Mechanics, Department of Chemistry, M.V. Lomonosov Moscow State University, Moscow, Russia

Antonio Sarsa Departmento de Física, Campus de Rabanales Edif. C2, Universidad de Córdoba, Córdoba, Spain

Andrey V. Scherbinin Laboratory of Molecular Structure and Quantum Mechanics, Department of Chemistry, M.V. Lomonosov Moscow State University, Moscow, Russia

Claude Le Sech CNRS, Institut des Sciences Moleculaires d'Orsay-ISMO (UMR 8214), Université Paris Sud 11, Orsay Cedex, France

K.D. Sen School of Chemistry, University of Hyderabad, Hyderabad, Telangana State, India

Guo-Hua Sun Instituto de Física, Universidad Nacional Autónoma de México, México, D.F., Mexico

Rubicelia Vargas Departamento de Química, Universidad Autónoma Metropolitana-Iztapalapa, México, D.F., México

Chapter 1
Surface Effects in the Hydrogen Atom Confined by Dihedral Angles

Eugenio Ley-Koo and Guo-Hua Sun

1.1 Introduction

The contributions contained in the present Monograph on "Quantum Confined Electronic Structure of Atoms and Molecules" constitute a representative sample of the most recent developments in this field. They are intended to serve as guides, on some specific recent and current problems, for the colleagues with theoretical and experimental interests in the area. The updating has been implemented by taking the chapters of volumes 57 [1–9] and 58 [10–15] of Advances in Quantum Chemistry on "Theory of Confined Quantum Systems" Parts I and II, as the background in contents and in time. The readers, according to their interests, may identify in some of these chapters the variety of confined systems and confining environments, their respective modelings, the changes of their physical properties in comparison with those of the free systems, the diversity of effects and processes allowing the measurement of those properties, etc.

The present contribution has its roots and trunk in Ref. [3], involving confinement in semi-infinite spaces limited by conoidal boundaries. It can be remarked that [8] is the only other chapter dealing explicitly with this type of confinement, while [9] treats confined systems as open systems, and most of the other chapters involve confinements inside spheres or spheroids. Reference [3] is also restricted to the hydrogen atom, taking into consideration the separability of its Schrödinger

E. Ley-Koo (✉) · G.-H. Sun
Instituto de Física, Universidad Nacional Autónoma de México,
Apartado Postal 20-364 Mexico, D.F., Mexico
e-mail: eleykoo@fisica.unam.mx

G.-H. Sun
Centro Universitario Valle de Chalco Universidad Autónoma del Estado de México Chalco,
México, D.F., Estado de México, Mexico
e-mail: sunghdb@yahoo.com

K.D. Sen (ed.), *Electronic Structure of Quantum Confined Atoms and Molecules*,
DOI 10.1007/978-3-319-09982-8_1

equations in spherical, spheroconal, parabolic and prolate spheroidal coordinates, as well as their exact solvability for the free system and also for confinement by the natural boundaries defined by the successive coordinates, as reviewed and overviewed in its Sects. 1.3 and 1.4, respectively. The reference contains also Sect. 1.2 "Sample of Comments on Articles about Confined Atoms and Molecules", and Sect. 1.5 "Preview of Problems on Confined Atoms and Molecules of Current and Future Investigations"; Sect. 2.4 and the sections 5.1–5.4 can be identified as the off-shoots for the branches in the updating of Sect. 1.2 and the main body of Sect. 1.3 in the Contents of this contribution.

In fact, the articles in [16, 17] gave the title of Section 2.4 in [3], and also formed the basis of the Comment in [18]. Afterwards, the Letter in [19] motivated the writing of the Comment in [20]. Both sets dealing with the binding of an electron by a polar molecule, in confined and free configurations, respectively, justify the title of the present Sect. 1.2.1, where the reasons for the Comments are illustrated. On the other hand, our articles [21] briefly reviewed in Sect. 1.2.2, [22–25] in Sect. 1.2.3, [26] in Sect. 1.2.4, and [27, 28] in Sect. 1.2.5, are in direct correspondence with the Preview sections in [3]: 5.3, 5.1, 5.2 and 5.4, as a comparison of their titles show. In this way, Sect. 1.2 illustrates the updating of problems formulated 5 years earlier, and some of their extensions already developed within that period. Specifically, the confinement of the hydrogen atom by elliptical cones [22] was shown to be also applicable to any central potential [23], and to the rotations of asymmetric molecules [24]; furthermore the theory of angular momentum in the bases of spheroconal harmonics is now on a par with the familiar one in the basis of spherical harmonics [25]. On the other hand, Ref. [26] established the superintegrability of the harmonic oscillator and the hydrogen atom under dihedral angle confinement, by identifying complete sets of ladder operators for their eigenstates in the respective sets of separating coordinates. Finally, the complete electric dipole fields and their sources inside, outside and on spheres and spheroids, respectively [27], are alternatives for the analysis of the binding of an electron by a polar molecule. In addition, the corresponding quadrupole magnetic fields [28] are alternatives of interest in nuclear magnetic resonance and neutral atom traps.

Section 1.3 is the main body of this contribution. Its immediate antecedent is Ref. [26], establishing the superintegrability and exact solvability of the Schrödinger equation for the hydrogen atom confined by dihedral angles in spherical, parabolic and prolate spheroidal coordinates. In Sect. 1.3.1 their respective eigenfunctions, eigenenergies and degeneracies are identified. Original results on the surface effects in the hydrogen atom and the confining meridian half planes defining the dihedral angle are evaluated and reported for the first time: Sect. 1.3.2 Electric dipole moments for ground and excited states, in the different coordinates and as functions of the confining angles, and the relationships among them, Sect. 1.3.3 Pressure distributions on the boundary meridian half-planes, Sect. 1.3.4 Hyperfine structure for the ground state with the suppression of the Fermi contact contribution and enhancement of the anisotropic contribution, and Sect. 1.3.5 Zeeman effect with the suppression of the first order perturbation theory contribution, and of the degenerate perturbation theory contributions for confining angles $2\pi/(2N+1)$, and

identification of nonuniform splitting patterns for other confining angles. The remaining two sections include Sect. 1.3.6 a comparison with the confinements in spheres and circular cones, as well as the description and an analysis of Sect. 1.3.7 single-electron quantum dots confined by dihedral angles.

Section 1.4 contains our perspective on future work on multielectron systems confined by dihedral angles. The only available points of comparison involve central confinement in spheres or spheroids, which give us a chance to emphasize the qualitative differences between both types of confinement for Sect. 1.4.1 two-electron atoms and quantum dots, Sect. 1.4.2 the filling of shells for the successive elements and Sect. 1.4.3 the hydrogen molecular ion and neutral molecule. The discussion in Sect. 1.5 summarizes the main results in the successive sections, the relationships among them, and most important the anticipation of future theoretical and experimental developments.

1.2 Updating and Extensions of Comment and Preview in "The Hydrogen Atom Confined in Semi-infinite Spaces Limited by Conoidal Boundaries"

This section takes the Comment 2.4 and the Preview Section 5 in [3] as the points of reference to guide the readers to some of our published investigations in the last 5 years since the writing of that chapter.

1.2.1 On the Binding of an Electron by a Polar Molecule

Comment 2.4 in [3] was limited to point out conceptual inconsistencies in Refs. [16, 17] in their analysis of the binding of an electron by a polar molecule confined inside spherical boxes and spheroidal boxes, respectively. At that moment we had just written and submitted a Comment on both works, mentioning it in Sect. 1.2.4 and inviting to read [16, 17]. Our own Comment [18] was published in the Fall of 2008 and was included as Ref. [11] in [3]. Now, the interested readers are invited to read [16, 17, 18] together and appreciate the difference in the binding energies of free systems and of confined systems, which is the key point of interest in Sect. 1.2.4 and other sections in [3].

One year later, we learned about the Letter [19] proposing new sets of angular and radial eigenfunctions for the same problem in the free configuration. Our familiarity with the solutions in the existing literature led us to try to understand the new elements in [19], and in the process we decided to write our Comment [20]. Indeed, the Schrödinger equation with the potential energy of a negative electron and a point electric dipole $\vec{p}$, $U(\vec{r}) = ep\cos\theta/r^2$, is known to be separable in spherical coordinates. The polar angle part corresponds to the eigenvalue equation of the operator $\hat{\ell}^2 + 2mep\cos\theta$ with eigenvalue $\hbar^2 E_\theta$, where $\hat{\ell}^2$ is the square of the

angular momentum and E_θ is dimensionless. The radial part is simply the radial Schrödinger equation with an effective potential $\hbar^2 E_\theta / 2mr^2$, inversely proportional to the square of the radial coordinate. The Letter in [19] proposed angular eigenfunctions as expansions of Jacobi polynomials, with coefficients satisfying three-term recurrence relations, and radial eigenfunctions as expansions of Laguerre polynomials, also with coefficients satisfying three-term recurrence relations, for the bound states which have $E_\theta < 0$ and energy $E < 0$. In the Comment [20] it was pointed out that while for the angular eigenfunction the three-term recurrence relations are determined by the selection rules $\ell' = \ell$ for $\hat{\ell}^2$ and $\ell' = \ell \pm 1$ for $\cos\theta$, reflected by the tridiagonal character of the matrix representation of their combined operators, for the radial equation the corresponding representation does not hold. Consequently, the radial functions in [19] are not bonafide solutions of the problem.

1.2.2 Ground State Energy Shift of the Helium Atom Close to a Plane Surface

The title for this section is the first part of the title of Ref. [21]; the other parts of the title "relation with the scattering potential" and "A confinement model" describe the physical problem of interest and part of its modeling, respectively. In fact, the problem belongs to the area of low-energy ion scattering by surfaces as a tool to investigate the surface structure and topology as well as the dynamical changes in the projectiles. One of the recent practical implementations involves grazing-scattering experiments of low-energy ion beams impinging on insulator and metal surfaces. Specifically in Refs. [3, 4] of [21], Wetherkam and Winter obtained evidence on the ground state evolution of the helium atom near an Al(111) surface from the He^+ grazing-scattering experiments after Auger neutralization, motivating the investigation in [21]. The confinement model for both He and He^+ is the one for atoms in semi-infinite spaces limited by a plane boundary in prolate spheroidal coordinates [3, 8]. Figure 1.1 in [21] illustrates (A) the energies of the ground states of the atom and the ion as functions of their distances to the plane surface, while Fig. 1.2 shows the changes in the electron probability distribution for the atom as it approaches the surface, and Table 1.1 contains the electric dipole moments acquired by the atom and the ion due to the confinement, from variational calculations performed within the Born-Oppenheimer approximation. The interested readers may follow in [21]: (B) The identification of the atom-surface interaction energy in general, and specifically in this model; the comparison with its counterparts for He interacting with a graphitic plane and with Aluminum (111), (110) and (100) surfaces, from the continuum average over the surface of the He–C and He–Al interactions, (C) The dynamic response of a perfectly conducting surface to the presence of an atom or ion possessing a net electric charge and an electric dipole moment, is modeled by including the image potential arising from those sources, Eq. (1.21), with the results of Fig. 1.9 [21]. The summary and conclusions are presented in Sect. 1.4.

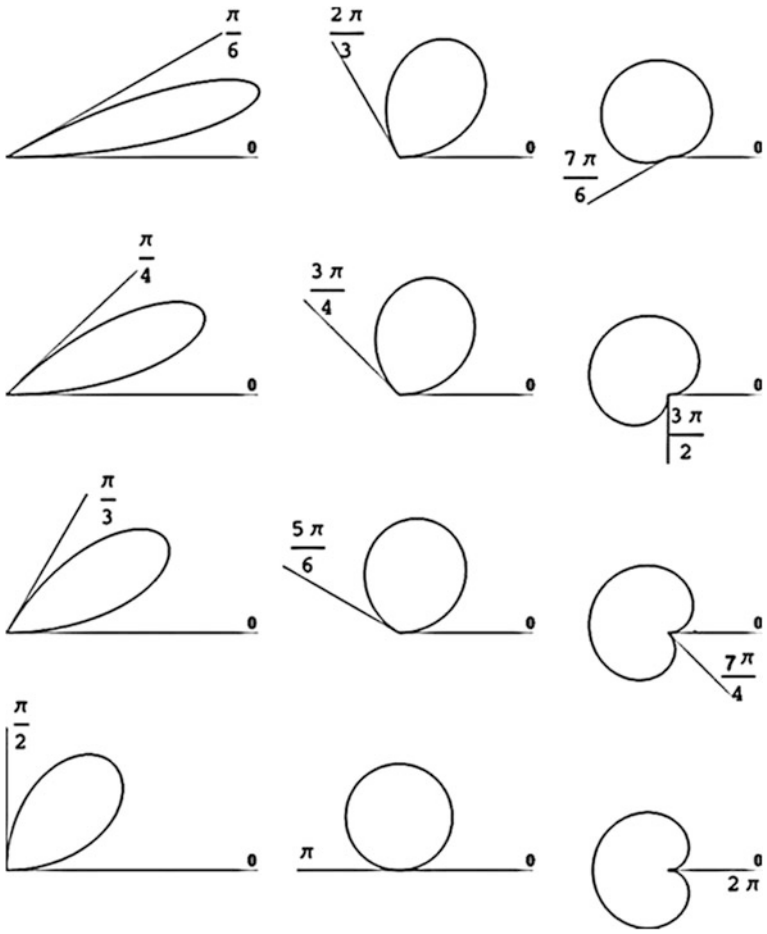

Fig. 1.1 Circular polar graphs of the eigenfunctions of Eq. (1.4) for the states with $n_\varphi = 1$, exhibiting their variations with the value of the confining angle $\varphi_0 = \pi/6, \pi/4, \ldots, \pi, 7\pi/4$ and 2π

1.2.3 Hydrogen Atom and Asymmetric Molecules Confined by Elliptical Cones

Section 5.1 in [3] shared the same title as the present one excluding "and asymmetric molecules". In fact, the investigation for the future previewed in that section was implemented and published as Ref. [22]. The key difference between the evaluation of the free spheroconal harmonics and the confined in an elliptical cone spheroconal harmonics consists in the following: while the former involves polynomial solutions with coefficients satisfying three-term recurrence relations, the latter are infinite series with coefficients satisfying four-term recurrence relations.

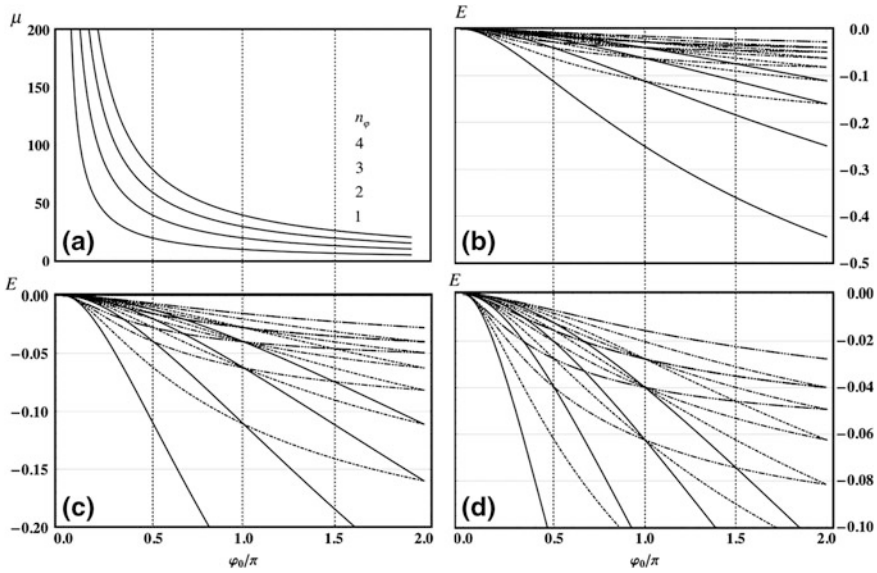

Fig. 1.2 (**a**) Angular momentum z-component eigenvalueμ, (**b**) Energy spectra$E_{n_1 n_2 n_\varphi}[e^2/2a_0]$ and amplifications for (**c**) $-0.2 < E_v < 0$ and (**d**) $-0.1 < E_v < 0$ for $n_1 + n_2 = 0$ (——)$n_1 + n_2 = 1$ (–·–), $n_1 + n_2 = 2$ (–··–), $n_1 + n_2 = 3$ (–···–), as functions of $0 < \varphi_0/\pi < 2$

In both cases the separation constants and the expansion coefficients are evaluated via matrix diagonalizations of finite and infinite sizes, respectively. The latter are approximated with finite but large enough sizes guaranteeing convergence and precision. In Ref. [22], we identified for the first time that the pressure distribution on the walls of the confining cone include positive and negative values corresponding to coexisting regions of high pressure and low tension.

While completing the above work we realized that we could also analyze the rotations of asymmetric molecules, and also any central potential system, in the same situation of confinement in elliptical cones. Preliminary results were presented at the 50th Sanibel Symposium and published in its Proceedings [23]. Shortly after the acceptance of the latter, we received the invitation to write a chapter reviewing our recent works for a volume in Advances in Quantum Chemistry, on some of the topics discussed at the Symposium [24], in which we included original results for the rotations of the confined asymmetric molecules, and also started the identification of spheroconal tools to construct a theory of angular momentum based on spheroconal harmonics.

In February 2012, we participated in the International Symposium on "Superintegrability, Exact Solvability and Special Functions". The contribution by Ricardo Méndez Fragoso was on "The Symmetries of Asymmetric Molecules". The invitation to write original contributions on the topics of the Symposium for a special volume of SIGMA was the motivation to identify and construct the raising and lowering operators connecting the different kinds and species of spheroconal

Table 1.1 Order of energy levels $E_{n_1 n_2 n_\varphi}(\varphi_0)$ and their degeneracies D for different openings of the confining dihedral angle

φ_0/π 1/3			1/2			2/3			1			3/2			2		
n_1+n_2	n_φ	D	n_1+n_2	n_φ	D		n_1+n_2		n_φ	D		n_1+n_2	n_φ	D	n_1+n_2	n_φ	D
n_1+n_2	n_φ	D															
0	1	1	0	1	1	0	1	1	0	1	1	0	1	1	0	1	1
1	1	2	1	1	2	0	2	1	1	1	3	0	2	1	0	2	1
2	1	3	2	1	4	1	1	2	0	2		1	1	2	1	1	3
3	1	5	0	2		1	2	2	2	1	6	0	3	1	0	3	
0	2		3	1	6	2	1	3	1	2		1	2	2	1	2	3
4	1	7	1	2		3	1	5	0	3		2	1	4	0	4	
1	2		4	1	9	0	3		3	1	10	0	4		2	1	6
5	1	9	2	2		2	2	3	2	2		1	3	2	1	3	
2	2		0	3		4	1	7	1	3		2	2	4	0	5	
6	1	12	5	1	12	1	3		0	4		0	5		2	2	6
3	2		3	2		3	2	5	4	1	15	3	1	6	1	4	
0	3		1	3		0	4		3	2		1	4		0	6	
7	1	15	6	1	16	5	1	9	2	3		2	3	4	3	1	10
4	2		4	2		2	3		1	4		0	6		2	3	
1	3		2	3		4	2	7	0	5		3	2	6	1	5	
			0	4		1	4		5	1	21	1	5		0	7	
			7	1	20	6	1	12	4	2		4	1	9	3	2	10
			5	2		3	3		3	3		2	4		2	4	
			3	3		0	5		2	4		0	7		1	6	
			1	4					1	5		3	3	6	0	8	
									0	6		1	6		4	1	15
												4	2	9	3	3	
												2	5		2	5	
												0	8		1	7	

harmonics, common eigenfunctions of the square of the angular momentum and the asymmetry distribution Hamiltonian, bringing the theory of angular momentum based in spheroconal harmonics on a par with the familiar one based in spherical harmonics [25].

1.2.4 Harmonic Oscillators and Hydrogen Atom Confined by Dihedral Angles

Our other contribution to the Symposium mentioned in the last paragraph of the previous section was "Superintegrability in the Confined Hydrogen Atom". For our written contribution to the volume in SIGMA [26], we constructed sets of ladder operators connecting the eigenstates of the harmonic oscillators confined by dihedral angles in circular cylindrical and spherical coordinates, and for the hydrogen atom in the same situation of confinement in spherical, parabolic and prolate spheroidal coordinates. The dihedral angle coordinate is common to all of them, and the same happens with the canonically conjugate momentum, and its square. Consequently, the different systems also share the same raising and lowering operators for the common eigenstates of the square of the z-component of the angular momentum, with non-integer eigenvalues μ. The constants of motion associated with the other coordinates, for the respective physical systems, keep their polynomial eigenfunctions and integer eigenvalues, with the non-integer index of associativity μ. The corresponding ladder operators are modified accordingly, from their free system forms.

1.2.5 Electric Dipole and Magnetic Quadrupole Fields and Sources in Spheres and Spheroids

The writing of [27] was anticipated in Preview 5.4 of [3], recognizing the need of a complete description of the electric dipole field, not only outside but also inside a polar molecule, in order to analyze more realistically its binding of an electron without the falling to the center of the point dipole, which is a mathematical and not a physical effect. The corresponding electrostatic fields and their sources on the surfaces of spheres and both prolate and oblate spheroids were explicitly identified.

As an extension of the same idea, and motivated for the needs in Nuclear Magnetic Resonance imaging as well as in neutral atom traps, the magnetic quadrupole fields and sources were constructed in the same geometries Ref. [28].

1.3 Surface Effects in the Hydrogen Atom Confined by Dihedral Angles in Spherical, Parabolic and Prolate Spheroidal Coordinates

As anticipated in the Introduction, this section deals with the hydrogen atom confined by dihedral angles and its properties in three different coordinates systems, in Sects. 1.3.1–1.3.5. The last Sect. 1.3.6 and 1.3.7 establish the comparison with the same system in spherical and circular cone confinements, and with quantum dots confined by dihedral angles, respectively.

The Schrödinger equation for the motion of the electron relative to the nucleus is considered in spherical (r, θ, φ), parabolic (ξ, η, φ), and prolate spheroidal coordinates (u, v, φ), which are connected by their transformation equations to cartesian coordinates [29]:

$$\begin{aligned} x &= r\sin\theta\cos\varphi = \xi\eta\cos\varphi = f\sqrt{(u^2-1)(1-\mathrm{v}^2)}\cos\varphi, \\ y &= r\sin\theta\sin\varphi = \xi\eta\sin\varphi = f\sqrt{(u^2-1)(1-\mathrm{v}^2)}\sin\varphi, \\ z &= r\cos\theta = \frac{\xi^2-\eta^2}{2} = fu\mathrm{v}, \end{aligned} \tag{1.1}$$

The Schrödinger equation is separable in the three coordinate systems when the nucleus occupies the center, the focus and one of the focii, respectively, with factorizable solutions of the common form:

$$\begin{aligned} \psi(r,\theta,\varphi) = R(r)\Theta(\theta)\Phi(\varphi), \quad \psi(\xi,\eta,\varphi) = \Xi(\xi)H(\eta)\Phi(\varphi), \\ \psi(u,\mathrm{v},\varphi) = U(u)V(\mathrm{v})\Phi(\varphi). \end{aligned} \tag{1.2}$$

The confining angle is defined by the positions of its meridian half-planes $\varphi_1 = 0$ and $\varphi_2 = \varphi_0$. The confinement of the hydrogen atom by the dihedral angle imposes the boundary conditions that its eigenfunctions vanish at the positions of those meridian half-planes, which involve only the common third factor in Eq. (1.2):

$$-\frac{d^2\Phi(\varphi)}{d\varphi^2} = \mu^2\Phi(\varphi); \quad \Phi(\varphi=0) = 0, \quad \Phi(\varphi=\varphi_0) = 0. \tag{1.3}$$

Since the z component of the angular momentum is canonically conjugate to the angle φ, and it appears quadratically in the Schrödinger equation, the corresponding eigenfunctions satisfying the boundary conditions of Eq. (1.3) and their eigenvalues are

$$\Phi_\mu(\varphi) = \sqrt{\frac{2}{\varphi_0}}\sin(\mu\varphi), \quad \mu = \frac{n_\varphi\pi}{\varphi_0}, \quad n_\varphi = 1,2,3,\ldots \tag{1.4}$$

1.3.1 Eigenfunctions, Eigenenergies and Degeneracies

The readers are referred to [26] for the details on the construction of the eigenfunctions and eigenvalues in the successive coordinates, which are written in their general forms, commented and illustrated next. Farther on, their degeneracies are also counted and illustrated as functions of the confining angle. The eigenfunctions in the respective coordinates have basically the same structure as in the free atom [3], replacing the integer quantum magnetic number m with the label μ in Eq. (1.4):

$$\psi^{s} = N_{n_r n_\theta \mu}\, e^{-\frac{r}{a_0 v}} (r\sin\theta)^{\mu}\, \sin(\mu\varphi)\, r^{n_\theta}\, {}_1F_1\left(-n_r; 2n_\theta + 2\mu + 2; \frac{2r}{a_0 v}\right)$$
$$\left[{}_2F_1\left(-n_\theta, n_\theta + 2\mu + 1; \mu + 1; \frac{1-\cos\theta}{2}\right) + (-1)^{n_\theta}\, {}_2F_1\left(-n_\theta, n_\theta + 2\mu + 1; \mu + 1; \frac{1+\cos\theta}{2}\right)\right], \tag{1.5}$$

$$\psi^{P} = N_{n_\xi n_\eta \mu}\, e^{-\frac{\xi^2+\eta^2}{2a_0 v}} (\xi\eta)^{\mu} \sin(\mu\varphi)\, {}_1F_1\left(-n_\xi; \mu + 1; \frac{\xi^2}{a_0 v}\right) {}_1F_1\left(-n_\eta; \mu + 1; \frac{\eta^2}{a_0 v}\right), \tag{1.6}$$

$$\psi^{PS} = N_{n_u n v \mu}\, e^{-\frac{f(u+\mathrm{v})}{a_0 v}} \left[f\sqrt{(u^2-1)(1-\mathrm{v}^2)}\right]^{\mu} \sin(\mu\varphi) S^{\mu}_{n_u}(u) S^{\mu}_{n v}(\mathrm{v}). \tag{1.7}$$

Notice their common singularity removing factors: μ powers of $r\sin\theta, \xi\eta$ and $\sqrt{(u^2-1)(1-\mathrm{v}^2)}$ close to the z-axis, Eqs. (1.1); and decreasing exponentials of the proton-electron radial separation at infinity. The other factors are polynomials of degrees $n_r, n_\theta, n_\xi, n_\eta, n_u$ and n_v in the first two independent variables of the respective coordinates. Additionally, notice in spherical coordinates: the extra n_θ power factor of r needed to remove the singularity at the origin, recognizing that $n_\theta + \mu = \lambda$ is the quantum label for the magnitude of the orbital angular momentum; the same label is explicitly identified in the second entries of the hypergeometric functions inside the brackets; if μ were an integer, either function would be a polynomial of even or odd powers of $\cos\theta$ and parity defined by their degree n_θ; when μ is non integer as in Eq. (1.4), both functions contain even and odd powers of $\cos\theta$, implying that the breaking of the rotation symmetry around the z-axis also breaks the $z \to -z$ parity symmetry; the combination of both functions in Eq. (1.5) is needed to restore their z parity. The eigenfunctions in parabolic coordinates have the formal structure of a two-dimensional harmonic oscillator in circular coordinates [3, 26]. The S functions in prolate spheroidal coordinates are polynomials in powers of $u-1$ and $\mathrm{v}-1$, solutions of the same differential equation in the domains of the respective spheroidal and hyperboloidal variables $[1,\infty]$ and $[-1,1]$; the coefficients in their expansions satisfy three-term recurrence relations [3, 26, 30]. The eigenenergies are given by the familiar parametrization:

$$E_v = -\frac{e^2}{2a_0 v^2} \tag{1.8}$$

involving the principal quantum label in the respective coordinates:

$$v = n_r + n_\theta + \mu + 1 = n_\xi + n_\eta + \mu + 1 = n_u + n_\mathrm{v} + \mu + 1 \tag{1.9}$$

Figure 1.1 illustrates the circular polar graphs of the eigenfunctions of Eq. (1.4) for the states with $n_\varphi = 1$ exhibiting their variations with the value of the confining angle $\varphi_0 = \pi/6, \pi/4, \ldots, \pi, \ldots, 7\pi/4$ and 2π. The value of π corresponds to confinement by a plane [31] where the graph is a circle tangent to the plane at the position of the nucleus. For the other angles the lobes are also tangent to the planes defining the confining angle, getting more elongated as the latter becomes smaller, and becoming heart-shaped as the angle increases up to 2π. Notice that the bisecting angle exhibits also the reflection symmetry of the respective graphs. The generalization for the excited states with $n_\varphi = 2, 3, 4, \ldots$ having $1, 2, 3, \ldots$ equally spaced azimuthal meridian nodes, and exhibiting alternatively antisymmetry and symmetry under reflection in the bisecting meridian plane, follows from Eq. (1.4).

Figure 1.1 illustrates the variations of the label μ of Eq. (1.4) and the eigenenergies of Eqs. (1.8, 1.9) as functions of the confining angle. The variations of μ are inversely proportional to the angle, and they can be followed for $n_\varphi = 1, 2, 3, 4, \ldots$ in Fig. 1.2a. Starting from Levine's plane with $\varphi_0 = \pi$ and $\mu = m$ integer, the reader may follow the increasing values to the left and the decreasing values to the right up to half integer numbers for $\varphi_0 = 2\pi$. The variations of the eigenergies are exhibited in Fig. 1.2b, c, and d for the ground and increasingly excited states, in successively amplified energy intervals. Notice that each level increases the value of its eigenenergy as the confinement of the atom increases when going from right to left in each graph, which is correlated with the corresponding increases in μ already recognized in Fig. 1.2a. This is trivial for the ground state, shared by the three coordinate systems with $n_1 = n_2 = 0$. It is also true for the degenerate excited states with $n_1 + n_2$ and any value of μ, which are $n_1 + n_2 + 1$ in number. Consequently, the reader's attention is also called to follow the removal of degeneracies, signaled by the separation of energy levels; and also to identify new degeneracies, signaled by new crossing of levels and associated with combinations in Eq. (1.9) such that $n_1 + n_2 + \mu = n_1' + n_2' + \mu'$. Both types of signals can be recognized in Fig. 1.2b and increasingly in Fig. 1.2c and d. For very small angles of confinement on the left of each figure, μ increases towards infinity and the eigenenergies tend to zero, becoming infinitely degenerate at the ionization limit. This situation is also shared by the hydrogen atom confined in semi-infinite spaces with other boundaries [22, 24, 32, 33]. It is also important to understand that for $\varphi_0 = 2\pi$, the eigenfunctions and eigenenergies are different from those of the free atom due to the boundary conditions of Eq. (1.3).

Table 1.1 illustrates the degeneracies of the energy levels of the hydrogen atom for a sample of confining dihedral angles. The basic degeneracy is of order

$D_{(n_1+n_2)} = n_1 + n_2 + 1$, determined by the sum of the number of nodes in the other two degrees of freedom, reminiscent of the degeneracy of the two-dimensional harmonic oscillator [26]. Additional degeneracies may occur for coinciding values of $n_1 + n_2 + \mu$ in Eq. (1.9); and the sum of the basic degeneracies of the respective combinations

$$D = \sum_{n_1+n_2} D_{(n_1+n_2)}$$

gives the accumulated degeneracy of the energy levels crossing at the specific angle. Both types of degeneracies are counted for the successive combinations of the quantum numbers $n_1 + n_2$ and n_φ compatible with Eqs. (1.4) and (1.9) for each confining angle. The counting extends to about sixty orbital states so that when the electron spin degree of freedom is considered all the known chemical elements are covered. Not surprisingly, these degeneracies differ from the n^2 familiar counterpart of the free atom.

1.3.2 Electric Dipole Moment

The electric dipole moment is defined by the charge of the electron times the expectation value of the relative position vector of the electron from the proton:

$$\langle \psi_{n_1 n_2 \mu} \Big| \overrightarrow{d} \, | \psi_{n_1 n_2 \mu} \rangle = -e \langle \psi_{n_1 n_2 \mu} \big| \left(\hat{i}\, x + \hat{j}\, y + \hat{k}\, z \right) | \psi_{n_1 n_2 \mu} \rangle \tag{1.10}$$

Here we report the results for the common ground state $(n_1 = 0,\ n_2 = 0,\ n_\varphi = 1)$, and the pairs of eigenstates with lowest excitation $\left(n_1 + n_2 = 1,\ n_\varphi = 1\right)$, in the three coordinate systems. The integration over φ is common for all of them and the expressions for the dipole moment also have the common structure:

$$\left\langle \overrightarrow{d} \right\rangle = -e \left\{ \frac{2}{\varphi_0} \frac{4\mu^2 \sin\left(\frac{\varphi_0}{2}\right)}{4\mu^2 - 1} \left[\hat{i} \cos\left(\frac{\varphi_0}{2}\right) + \hat{j} \sin\left(\frac{\varphi_0}{2}\right) \right] I_\perp(n_1 n_2) + \hat{k} I_z(n_1 n_2) \right\} \tag{1.11}$$

Notice the distinction between the axial and transverse components. In fact, the φ integration for the axial component is simply the normalization constant, while for the transverse component coincides with the expression for the electric dipole moment of the hydrogen atom in two dimensions confined by the same angle [34], in the direction of the bisecting angle. $I_z(n_1 n_2)$ and $I_\perp(n_1 n_2)$ are the integrals over the two other degrees of freedom for the respective cartesian components in the successive coordinates. In spherical coordinates, the eigenfunctions have a well-defined z parity and the corresponding component of the dipole moment vanishes. In parabolic coordinates, the 01μ and 10μ states have the same transverse

components, while their axial components share the same magnitude with opposite directions, upward and downward, respectively. In prolate spheroidal coordinates, the respective dipole moments interpolate between their counterparts in spherical and parabolic coordinates in the limits of very small and very large focal distances.

Table 1.2 and Fig. 1.3 illustrate the numerical values of the magnitudes of the transverse and axial components of the electric dipole moment of the hydrogen atom as functions of the confining dihedral angle. The data for the ground state 001 are common for the three coordinate systems. For the excited states 011 and 101: in S, the axial components vanish and only the transverse components are reported with different numerical values; in P, both states share the same magnitudes for both components, the transverse with the same direction and the axial in opposite directions; in PS, three entries for small, intermediate and large focal distances are included, with different values for the transverse components, and equal magnitudes and opposite directions for the axial components. The transverse components increase monotonically as the confining angle is reduced; notice the ground state value of $3.75ea_0$ for Levine's plane as the familiar reference; going from the ground to the excited states, the magnitudes of the dipole moments change, but not too much. The following relationships among their values in the different degenerate excited states and coordinates can be recognized for the transverse components:

$$\begin{aligned} d_{\perp}^{S}(011) \leq d_{\perp}^{PS}(011, f = 0.1) < d_{\perp}^{PS}(011, f = 5) \\ < d_{\perp}^{PS}(011, f = 100) \approx d_{\perp}^{P}(011) = d_{\perp}^{P}(101) \\ = \frac{1}{2}\left[d_{\perp}^{S}(011) + d_{\perp}^{S}(101)\right] \approx d_{\perp}^{PS}(101, f = 100) \\ < d_{\perp}^{PS}(101, f = 5) < d_{\perp}^{PS}(101, f = 0.1) \leq d_{\perp}^{S}(101). \end{aligned} \tag{1.12}$$

The equalities at the middle follow from the equivalence of the parabolic coordinates ξ and η, and from the fact that the P and S $n_1 + n_2 = 1$ degenerate states are connected by the sum or difference of the other two, as illustrated in Sect. 7 of [26]. The interpolation by the PS states between the S and P states is explicitly exhibited. On the other hand, the axial components have small magnitudes, increasing monotonically with the confining angle.

1.3.3 Pressure Distributions

The average pressure of a quantum system confined in a finite volume is identified with the rate of change of its energy with respect to the change in the confining volume. This concept when applied to the hydrogen atom confined in a semi-infinite space leads to a vanishing average pressure because the change of energy is finite when the boundary is changed while the change in volume is infinite. Here, we adopt the concept of pressure distribution on the confining boundary, assuming that the latter is divided into elements of area $h_1 \Delta q_1 h_2 \Delta q_2$ associated with cylinders

Table 1.2 Magnitude of electric dipole moment transverse $d_\perp(\varphi_0)$ and axial $d_z(\varphi_0)$ components in unit [ea_0] for 001, 011 and 101 states in the three coordinate systems as functions of φ_0/π

$\frac{\varphi_0}{\pi}$	001	*S* 011	*S* 101	*P* 011 and *P* 101		*PS* 011 and *PS* 101($f = 0.1a_0$)			*PS* 011 and *PS* 101($f = 5a_0$)			*PS* 011 and *PS* 101($f = 100a_0$)		
	$d_\perp$	$d_\perp$	$d_\perp$	$d_\perp$	d_z	$d_\perp$	d_z	$d_\perp$	$d_\perp$	d_z	$d_\perp$	$d_\perp$	d_z	$d_\perp$
0.1	123.459	140.294	157.130	148.712	1.8	140.295	0.00428	157.13	140.319	0.21359	157.106	144.075	2.3598	153.349
0.2	37. 169	46.4619	55.7543	51.2081	2.1	46.4632	0.01571	55.753	46.5883	0.76404	55.6279	50.1532	3.22826	52.063
0.3	32.9736	26.2332	32.9789	29.6061	2.4	26.2364	0.03262	32.9758	26.5106	1.49708	32.7016	29.2189	3.74499	29.9932
0.4	12.7051	18.1501	23.5952	20.8726	2.7	18.1556	0.05385	23.5897	18.5743	2.27329	23.171	20.6589	4.22806	21.0864
0.5	9. 2807	13.9212	18.5616	16.2414	3.0	13.9292	0.07853	18.5535	14.4589	3.0168	18.0238	16.1024	4.70393	16.3863
0.6	7. 2565	11.3384	15.4202	13.3793	3.3	11.349	0.10601	15.4096	11.9524	3.70633	14.8061	13.2796	5.17744	13.4789
0.7	5.92949	9.59182	13.2542	11.4230	3.6	9.60488	0.13579	13.2411	10.2513	4.34564	12.5947	11.3468	5.64997	11.4992
0.8	4.99291	8.32152	11.6501	9.98582	3.9	8.33687	0.16749	11.6348	9.00344	4.94503	10.9682	9.92501	6.12202	10.0466
0.9	4.29424	7.34541	10.3966	8.87100	4.2	7.3628	0.20080	10.3792	8.03349	5.51433	9.7085	8.82093	6.59379	8.92107
1.0	3.75000	6.56250	9.37500	7.96875	4.5	6.5816	0.23548	9.35587	7.24524	6.06126	8.69226	7.92658	7.0654	8.01092
1.1	3.31113	5.91273	8.51433	7.21353	4.8	5.9333	0.27135	8.49374	6.58196	6.5915	7.84509	7.17742	7.53692	7.24964
1.2	2.94714	5.35844	7.76974	6.56409	5.1	5.3801	0.30822	7.74800	6.00833	7.10916	7.11985	6.53278	8.00836	6.59539
1.3	2.63823	4.87500	7.11176	5.99338	5.4	4.8976	0.34579	7.08917	5.50132	7.6172	6.48544	5.96599	8.47976	6.02077
1.4	2.37107	4.44576	6.52045	5.48311	5.7	4.4689	0.38449	6.49729	5.04548	8.11777	5.92073	5.45898	8.95112	5.50723
1.5	2.13641	4.05918	5.98194	5.02056	6.0	4.0826	0.42369	5.95849	4.6301	8.61247	5.41101	4.9992	9.42245	5.04192
1.6	1.92767	3.70705	5.48644	4.59675	6.3	3.7305	0.46348	5.46296	4.24767	9.10248	4.94582	4.57778	9.89377	4.61572
1.7	1.74008	3.38350	5.02691	4.20521	6.6	3.4068	0.50380	5.00363	3.89279	9.58871	4.51762	4.18832	10.3651	4.22209
1.8	1.57014	3.08420	4.59826	3.84123	6.9	3.1071	0.54460	4.57539	3.56158	10.0178	4.12089	3.82619	10.8364	3.85628
1.9	1.41519	2.80598	4.19678	3.50138	7.2	2.8283	0.585824	4.17451	3.25119	10.5504	3.75157	3.48797	11.3076	3.51478
2.0	1.27307	2.54648	3.81972	3.18310	7.5	2.57049	0.62743	3.80187	2.95957	11.0309	3.40663	3.17147	11.7789	3.19813

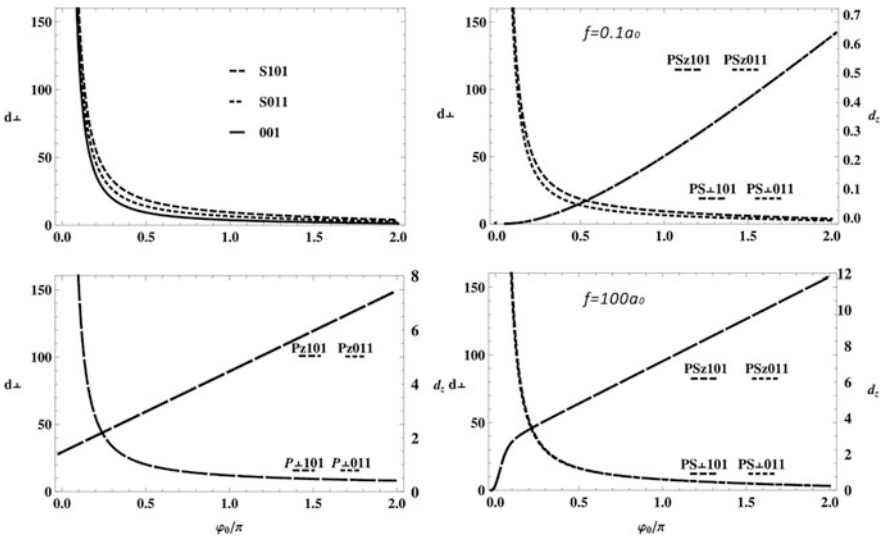

Fig. 1.3 Magnitude of electric dipole moment transverse $d_{\perp}(\varphi_0)$ and axial $d_z(\varphi_0)$ components in unit [ea_0] with the *left* and *right* side scales, respectively, in the successive coordinates, as functions of φ_0/π

of infinitesimal height $h_3\Delta q_3$. For such cylinders with infinitesimal volumes the corresponding pressure is expressed as [35, 36],

$$P(q_1,q_2,q_3) = -\frac{1}{h_1h_2\Delta q_1\Delta q_2}\frac{1}{h_3}\frac{\partial}{\partial q_3}\left[\varepsilon(q_1,q_2,q_3)\Delta q_1\Delta q_2\right]\Big|_{q_3=q_{30}} \tag{1.13}$$

where $\varepsilon(q_1,q_2,q_3)$ is the associated energy, such that

$$\varepsilon(q_1,q_2,q_3)\Delta q_1\Delta q_2 = \int_{q_3}^{q_3+\Delta q_3} h_1h_2h_3dq_3\psi^*\hat{H}\psi\Delta q_1\Delta q_2. \tag{1.14}$$

In the specific case of confinement in the dihedral angles with $q_{30} = \varphi_0$, the scale factors$h_r = 1, \quad h_\theta = r, h_\varphi = r\sin\theta = \xi\eta = f\sqrt{(u^2-1)(1-\mathrm{v}^2)}, h_\xi = h_\eta = \sqrt{\xi^2+\eta^2}$and $h_u = f\sqrt{(u^2-\mathrm{v}^2)/(u^2-1)}, \quad h_\mathrm{v} = f\sqrt{(u^2-\mathrm{v}^2)/(1-\mathrm{v}^2)}$ do not depend on the variable φ; consequently their presence in Eq. (1.13) when Eq. (1.14) is substituted, gives a quotient of one. Furthermore, the Hamiltonian $\hat{H}$ operating on its eigenfunctions $\psi_{n_1n_2\mu}$ gives the same eigenfunctions multiplied by the eigenvalue of the energy $E_v(\varphi_0)$ as a function of the opening of the dihedral angle. Thus the

evaluation of the pressure in Eq. (1.13) is reduced to the numerical evaluation of the derivative

$$P(q_1, q_2, \varphi_0) = -\frac{\partial}{\partial \varphi_0}\left[E_v(\varphi_0)\psi^*_{n_1 n_2 \mu}(q_1, q_2, \varphi_0)\psi_{n_1 n_2 \mu}(q_1, q_2, \varphi_0)\right]. \qquad (1.15)$$

Table 1.3 and Fig. 1.4 illustrate the numerical values of the pressure distributions for the $00\mu, 01\mu, 10\mu$ states in the successive coordinates for confining angles φ_0/π. The entries in the Table cover the maximum pressure, the corresponding position $q_1$max, and the position where the pressure vanishes q_{10}, at fixed positions in q_2. Figure 1.4 provides more details for the pressure as functions of q_1, for the chosen values of q_2 and φ_0/π. Specifically, the entries in the first two rows and the first two columns in the figure, correspond to the ground state S001 at the polar angle position $\theta = \pi/6$, with diminishing azimuthal angles of confinement $\varphi_0/\pi = n/6$ for $n = 12, \ldots, 1$ as functions of the radial coordinate. The entries in the first two rows and third column illustrate the corresponding information for the S011 and S101 excited states and a more restricted set of confining angles. The entries in the third row and first two columns are samples for the PS011 and PS101 excited states at the hyperboloidal v = 0.5 position, as functions of the spheroidal coordinate and

Table 1.3 Pressure distribution for the lower states in the three coordinates

The lower states	φ_0/π	1/2	1	3/2	2
$S:001$ $\theta = \pi/6$	P_{max} [10^{13} Pa]	0.097935	2.87159	9.57853	17.6420
	r_{max} [$2r/a_0$]	4.958000	1.53800	0.81000	0.51390
	R_0 [$2r/a_0$]	15.03650	7.29019	5.31829	4.44664
$S:011$ $\theta = \pi/6$	P_{max} [10^9 Pa]	0.409302	2.61103	3.92984	4.21405
	r_{max} [$2r/a_0$]	10.10600	4.85300	3.51800	2.92800
	R_0 [$2r/a_0$]	23.91210	13.6544	10.8319	9.53006
$S:101$ $\theta = \pi/6$	P_{max} [10^9 Pa]	0.223558	3.31064	7.97022	11.7285
	r_{max} [$2r/a_0$]	4.188000	1.32560	0.69800	0.44690
	R_0 [$2r/a_0$]	8.496770	3.87037	2.72494	2.22524
$P:011$ $\eta/\sqrt{a_0} = 1.2$	P_{max} [10^8 Pa]	4.361670	53.8539	84.3179	90.2903
	$\xi_{max}[\xi/\sqrt{a_0}]$	1.821000	0.93800	0.65780	0.49860
	$\xi_0[\xi/\sqrt{a_0}]$	3.006700	1.95444	1.59566	1.41341
$PS:011$ $v = 0.5$ $f/a_0 = 1.2$	P_{max} [10^{11} Pa]	9.332620	27.4735	35.8610	36.6268
	$u$max	8.017000	3.87900	2.78900	2.28300
	u_0	16.15730	9.59709	7.77068	6.90960
$PS:011$ $v = 0.5$ $f/a_0 = 0.6$	P_{max} [10^{12} Pa]	1.159450	4.87012	25.4137	6.74402
	$u$max	6.700000	2.38900	1.21900	1.58960
	u_0	12.69170	5.74147	4.04930	3.32243

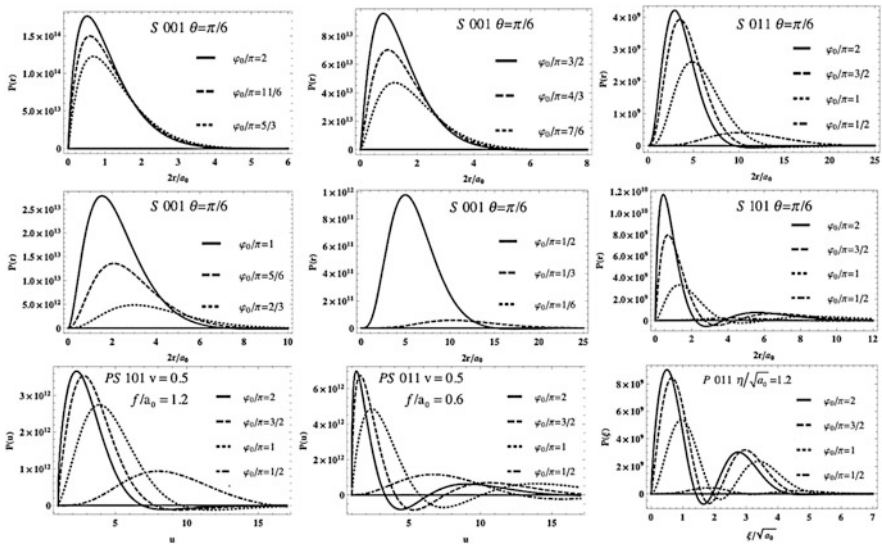

Fig. 1.4 Pressure as function of q_1 for the chosen values of q_2 and φ_0/π for the lower states 001, 011 and 101 in three coordinate systems

the indicated values of the focal distance. The third row and third column corresponds to the P011 state for the same set of confining angles at the chosen $\eta/\sqrt{a_0}$ position as functions of the $\xi/\sqrt{a_0}$ coordinate. The same information is also valid for the P101 state, with the exchange of the roles of the η and ξ coordinates. All the curves have the same shape starting from the origin displaying a fast increase up to a maximum, then a slower decrease, vanishing and taking negative values and tending to zero asymptotically after a finite number of oscillations; the latter part shows the coexistence of high pressure and low tension regions in the confining planes. In this work, we evaluated the pressure for excited states in order to establish that the alternation of its values and signs is a common happening, which had not been noticed before our investigation of the ground states of the hydrogen atom confined by elliptical cones [22].

1.3.4 Hyperfine Structure

The proton and electron spin-spin magnetic dipole interaction Hamiltonian, leading to the hyperfine structure of the hydrogen atom, has the form [37]:

$$\hat{H}_{\vec{\mu}_s^p,\vec{\mu}_s^e} = -\frac{3\left(\vec{\mu}_s^p\cdot\hat{r}\right)\left(\vec{\mu}_s^e\cdot\hat{r}\right)-\vec{\mu}_s^p\cdot\vec{\mu}_s^e}{r^3}+\frac{8\pi}{3}\vec{\mu}_s^p\cdot\vec{\mu}_s^e\delta\left(\vec{r}_e-\vec{r}_p\right), \tag{1.16}$$

where the last term corresponds to the Fermi contact interaction. In the case of the free hydrogen atom in its ground state with zero orbital angular momentum, the contribution of the first term vanishes; and the second term depending on the probability density of finding the electron at the position of the nucleus, $\left|\psi_{00\mu}(\vec{r}=0)\right|^2$, which is the expectation value of the Dirac delta function, determines the well-known hyperfine splitting of its eigenstates with total atomic angular momentum $F=1$ and $F=0$ arising from the coupling of the proton and electron one-half spins. In contrast, the hydrogen atom confined by dihedral angles exhibits the suppression of the Fermi contact contribution, and the appearance of anisotropic contributions from the first term in Eq. (1.16). In fact, $\psi_{00\mu}(\vec{r}=0)$ from Eq. (1.5) contains the radial singularity removing factor r^μ, which reduces the probability of finding the electron at the position of the proton to zero, thereby suppressing completely the Fermi contact contribution to the hyperfine splitting in the confined atom. On the other hand, concerning the first term in Eq. (1.16), the space dependence of its different terms correspond to the harmonic quadrupole tensor with five independent components: $xy/r^5, xz/r^5, yz/r^5, (x^2-y^2)/r^5$ and $(3z^2-r^2)/r^5$, which give a measure of the departure of the electron distribution from a spherical one. It follows that for the hydrogen atom confined in the dihedral angle, the first, fourth and fifth components provide finite contributions, while those from the second and third terms vanish due to their negative z-parity; if we took an x' axis along the bisecting angle $\varphi_0/2$, then the contribution of the first component $\langle x'y'/r^5\rangle$, would vanish due to its odd y' reflection parity, while its companion $\langle (x'^2-y'^2)/r^5\rangle$ does not vanish. The reader need not worry about the presence of the singular $1/r^3$ factor in the respective components; it is compensated by the presence of the factors $r^{(2+2\mu)}$ from the volume element and the square of the wave function, which becomes r^3 for the smallest value of $\mu=1/2$ for $\varphi_0=2\pi$. The hydrogen atom confined by dihedral angles acquires a quadupole moment responsible for its anisotropic contribution to the hyperfine splitting.

Next, we concentrate on the evaluation of the expectation values of the operators $(3\cos^2\theta-1)/r^3$ and $\sin^2\theta\,\left(\cos^2\varphi'-\sin^2\varphi'\right)/r^3$ for the ground state,

$$\psi_{00\mu}(r,\theta,\varphi)=N_{00\mu}r^\mu\,e^{-r/(\mu+1)a_0}\sin^\mu\theta\cos\mu\varphi',$$

from Eq. (1.5) with the change in coordinate $\varphi'=\varphi-\frac{\varphi_0}{2}$, in the interval $-\varphi_0/2<\varphi<\varphi_0/2$:

$$A_{33}=\langle\psi_{00\mu}|\frac{2-3\sin^2\theta}{r^3}|\psi_{00\mu}\rangle,$$

$$A_{x'^2-y'^2}=\langle\psi_{00\mu}|\frac{\sin^2\theta\cos 2\varphi'}{r^3}|\psi_{00\mu}\rangle.$$

The integrals over $r^2 dr \sin\theta d\varphi'$ share the common radial integrals with the integrands $r^{2\mu+3} e^{-2r/(\mu+1)a_0}$ and $r^{2\mu} e^{-2r/(\mu+1)a_0}$ for the normalization constant and the operator, leading to the net factor:

$$I^{radial} = \left[\frac{2}{(\mu+1)a_0}\right]^3 \frac{\Gamma(2\mu)}{\Gamma(2\mu+3)},$$

in terms of the respective gamma functions. The integrals over the polar angles can be rewritten in terms of the respective integrands $\sin^{2\mu+1}\theta$ and $\sin^{2\mu+3}\theta$, and can be expressed in terms of beta functions with the results:

$$I_{33}^{polar} = 2 - 3\frac{B(\mu+2,1/2)}{B(\mu+1,1/2)} = -\frac{2\mu}{2\mu+3}$$

$$I_{x'^2-y'^2}^{polar} = \frac{B(\mu+2,1/2)}{B(\mu+1,1/2)} = \frac{2(\mu+1)}{2\mu+3}.$$

The integrations over φ' for the normalization and the operator of A_{33} give a net factor of one. The corresponding factor for the other operator is

$$I_{x'^2-y'^2}^{\varphi'} = \frac{2}{\varphi_0} \int_{-\phi_0/2}^{\phi_0/2} d\varphi' \cos 2\varphi' \frac{1}{2}(1+\cos 2\mu\phi') = \frac{\mu^2 \sin\varphi_0}{(\mu^2-1)\,\varphi_0}.$$

Correspondingly, the products of the respective factors give the final forms:

$$A_{33} = -\left(\frac{1}{a_0^3}\right)\frac{4}{(\mu+1)^4(2\mu+1)(2\mu+3)}$$

$$A_{x'^2-y'^2} = \left(\frac{1}{a_0^3}\right)\frac{4\mu}{(\mu+1)^4(\mu-1)(2\mu+1)(2\mu+3)}\frac{\sin\varphi_0}{\varphi_0}$$

Table 1.4 contains the numerical values of these anisotropic components of the hyperfine structure for the hydrogen atom confined by dihedral angles in units of $1/a_0^3$, for the interval $[0, 2\pi]$ of φ_0. Figures 1.5a, b contain the respective plots illustrating the monotonic increase in the magnitude of A_{33}, and the increasing and decreasing values of $A_{x'^2-y'^2}$ as the confining angle changes from zero to 2π. Notice the vanishing of both components for $\varphi_0 = 0$, the vanishing of the transverse component for $\varphi_0 = 2\pi$, and the equal values of 1/60 of both components for Levine's plane with $\varphi_0 = \pi$. It is also pertinent to recall that the corresponding magnitude of the Fermi contact isotropic hyperfine contribution for the free hydrogen atom is $8/3a_0^3$.

Table 1.4 Numerical values of longitudinal and transverse components of the anisotropic hyperfine structure contributions in units $\left[1/a_0^3\right]$ for the successive values of the confining angle

φ_0/π	A_{33}	$A_{x'^2-y'^3}$
0	0	0
0.1	-5.65643×10^{-7}	6.18204×10^{-7}
0.2	-2.15834×10^{-5}	2.52387×10^{-5}
0.3	-1.53069×10^{-4}	1.87705×10^{-4}
0.4	-5.55324×10^{-4}	7.00474×10^{-4}
0.5	-1.41093×10^{-3}	1.79646×10^{-3}
0.6	-2.88224×10^{-3}	3.63560×10^{-3}
0.7	-5.08985×10^{-3}	6.24156×10^{-3}
0.8	-8.10773×10^{-3}	9.48087×10^{-3}
0.9	-1.19675×10^{-2}	1.30796×10^{-2}
1.0	-1.66667×10^{-2}	1.66667×10^{-2}
1.1	-2.21769×10^{-2}	1.98308×10^{-2}
1.2	-2.84524×10^{-2}	2.21808×10^{-2}
1.3	-3.54358×10^{-2}	2.33984×10^{-2}
1.4	-4.30638×10^{-2}	2.32799×10^{-2}
1.5	-5.12703×10^{-2}	2.17598×10^{-2}
1.6	-5.99895×10^{-2}	1.89174×10^{-2}
1.7	-6.91574×10^{-2}	1.49658×10^{-2}
1.8	-7.87132×10^{-2}	1.02271×10^{-2}
1.9	-8.86001×10^{-2}	5.09648×10^{-3}
2.0	-9.87654×10^{-2}	0

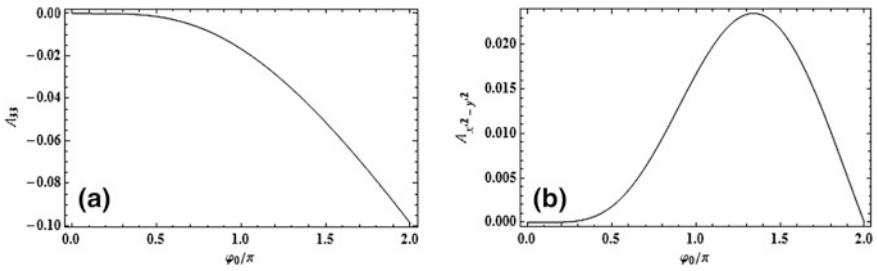

Fig. 1.5 Longitudinal (**a**) and transverse (**b**) components of the anisotropic hyperfine structure contributions in units $\left[1/a_0^3\right]$, as functions of the confining angle ϕ_0

1.3.5 Zeeman Effect

The Hamiltonian for the interaction of the hydrogen atom with an external axial uniform magnetic induction field, $\vec{B} = \hat{k}B$, including the orbital and spin contributions of its electron magnetic moment, is

$$\hat{H}_{\vec{\mu}^e,\vec{B}} = -\vec{\mu}^e \cdot \vec{B} = \frac{eB}{2m_e c}\left[l_z + g_s^e s_z\right]. \tag{1.17}$$

Here we concentrate on the orbital contribution, for the cases of the hydrogen atom in its free and confined by dihedral angle configurations, successively. In the familiar situation of the free atom, its wave functions are eigenfunctions of the z-component of the angular momentum with integer m eigenvalues, leading to the $2l+1$ uniformly split Zeeman pattern. The situation is radically changed for the hydrogen atom confined by dihedral angles because its wave functions are eigenfunctions of the square of the z-component of the angular momentum, Eqs. (1.3, 1.4). The changes can be analyzed and identified by constructing the matrix of the operator l_z in the basis of eigenfunctions of Eqs. (1.5)–(1.7). Indeed, the typical form of any matrix element:

$$\left\langle \psi_{n_1' n_2' n_\varphi'} | l_z | \psi_{n_1 n_2 n_3} \right\rangle = k\left(n_1' n_2' n_\varphi'; n_1 n_2 n_\varphi\right) \left\langle n_\varphi' | l_z | n_\varphi \right\rangle, \tag{1.18}$$

$$\begin{aligned} \left\langle n_\varphi' | l_z | n_\varphi \right\rangle &= \frac{2(-ih)}{\varphi_0} \int_0^{\varphi_0} d\varphi \sin\frac{n_\varphi' \pi\varphi}{\varphi_0} \frac{d}{d\varphi} \sin\frac{n_\varphi \pi\varphi}{\varphi_0} \\ &= \begin{cases} 0 & \text{for } n_\varphi' \pm n_\varphi \text{ even} \\ \frac{-i\hbar}{\varphi_0}\left[\frac{4n_\varphi n_\varphi'}{n_\varphi'^2 - n_\varphi^2}\right] & \text{for } n_\varphi' \pm n_\varphi \text{ odd} \end{cases} \end{aligned} \tag{1.19}$$

includes the selection rule that the matrix elements with $n_\varphi' \pm n_\varphi$ even vanish, and only the matrix elements with odd sums contribute; the constants $k\left(n_1' n_2' n_\varphi'; n_1 n_2 n_\varphi\right)$ represent the integrals over the other two degrees of freedom.

We proceed now to enumerate the consequences of such selection rules on the contributions to the Zeeman effect: (1) The first order perturbation theory contribution is suppressed, because it involves the expectation value with $n_\varphi' = n_\varphi$. Examples: All the entries of states with D = 1 for the different confining angles in Table 1.2. (2) There are also suppressed contributions for all the degenerate states associated with the confining angles of 2π and $2\pi/3$, because their n_φ values differ in even numbers as illustrated in the same Table; the situation is the same for all angles $2\pi/(2n+1)$. (3) The D by D square matrix representations of l_z in the bases of degenerate states for the other confinement angles in the Table have diagonal blocks with zero entries of the successive $D_{n_1+n_2}$ times $D_{n_1+n_2}$ dimensions, alternating with neighboring rectangular blocks with non-zero entries of dimensions

$D_{n'_1+n'_2}$ times $D_{n_1+n_2}$ and vice versa; the alternation of blocks with zero entries and non-zero entries with diminishing dimensions continues until the entire matrix is completed. The diagonalization of these hermitian matrices provides the Zeeman effect non-uniform orbital energy shifts and eigenfunctions. It is also feasible to include the spin contributions in the Hamiltonian of Eq. (1.16), as well as the spin up and spin down spinors in the basis functions for a complete treatment of the Zeeman effect in the confined hydrogen atom. Here, we restrict ourselves only to emphasize the differences with the free hydrogen atom; the corresponding results will be reported in the future.

1.3.6 Comparison with Other Confinements

In this section we revisit the hydrogen atom confined in spheres [38] and circular cones [33] under the light of confinement in dihedral angles. The exercise turns out to be instructive on more than one account, illustrating the differences between confinements in finite volumes versus in semi-infinite spaces.

We start out from the free hydrogen atom and its chain of $0(4) \supset 0(3) \supset 0(2)$ group symmetries, in spherical coordinates. Then we recognize that the successive confinements correspond to the breaking of the $0(4)$ symmetry in the spherical case with eigenstates $|v_r \ell m>$ maintaining the $0(3) \supset 0(2)$ symmetries; of the $0(3)$ symmetry in the case of the circular cone with eigenstates $|n_r, v_\theta, m>$ keeping the other symmetries; and of the $0(2)$ symmetry for the dihedral angles with eigenstates $|n_r, n_\theta, \mu>$.

The basic degeneracies are respectively $D_\ell = 2\ell + 1$ typical of a central potential for the spherical case, $D_{n_r+|m|} = n_r + |m| + 1$ for the circular cone, and $D_{n_r+n_\theta} = n_r + n_\theta + 1$ for the dihedral angle. Additional degeneracies may appear for specific values of the radius of the confining sphere when v_r becomes an integer; likewise for specific values of the polar angle defining the aperture of the confining cone when v_θ becomes an integer; Table 1.1 illustrates the systematics for dihedral angles in which μ becomes also an integer. The differences can be traced to the regular spacings of the zeros of the sine functions, versus the spacings of the corresponding zeros of the Laguerre and Legendre polynomials.

Speaking about the physical effects on the properties of the hydrogen atom under confinement, we can contrast the differences among the successive geometries. In fact, for the sphere: the spherical harmonics survive the confinement, and consequently, the pressure is uniform, the changes in the polarizability and the Fermi contact contribution to the hyperfine structure are due to the changes in the radial function. In the cases of confinement in semi-infinite spaces with a plane boundary and its natural extensions of circular cones and dihedral angles: the free spherical harmonics are replaced by their confined versions, already illustrated in Fig. 1.1 for the dihedral angles, and also now for the circular cone in Fig. 1.6. Correspondingly, the respective $0(3)$ and $0(2)$ symmetry breakings lead to non uniform pressures on

the confining boundaries, electric dipole moments instead of polarizabilities, the suppression of the Fermi contact contribution to the hyperfine structure with the concomitant enhancement of the anisotropic contribution associated with the acquired quadrupole moment. The survival of the $0(2)$ symmetry in the spherical and circular cone confinements guarantees uniform orbital Zeeman splittings, in contrast with the situation of Sect 1.3.5.

1.3.7 Single-Electron Quantum Dots Confined by Dihedral Angles

The discussion in this section has been focused so far on the hydrogen atom. In this final section we go back to [26], in which both the harmonic oscillator and the hydrogen atom were investigated together, in order to recognize that the results for the first system are immediately applicable in the description of single-electron quantum dots confined by dihedral angles.

Indeed, Ref. [14] describes the modeling of quantum dots in sphere and spheroids using isotropic harmonic oscillators, and anisotropic oscillators with frequencies $\omega_x = \omega_y = \omega_z$ and $\omega_x = \omega_y \neq \omega_z$, respectively. The spheroids may be prolate if $\omega_z < \omega_x$,or oblate if $\omega_z > \omega_x$.

Here we limit ourselves to point out that [26] contains the eigenfunctions and eigenergies for the oscillators confined by dihedral angles in spherical coordinates and circular cylindrical coordinates. The analysis of the surface effects for the single-electron quantum dot confined by dihedral angles can be readily implemented.

1.4 Outlook for Multielectron Atoms and Molecules Confined by Dihedral Angles

In the following discussion, the references [2, 4, 7, 39–44], dealing with confinement in spherical volumes, serve as points of comparison for their counterparts in confinement by dihedral angles. Concerning the hydrogen atom, Ref. [2] recognized that its orbitals for confinement in spherical boxes interpolate between those of the free atom for very large boxes, and the free-electron orbitals in a box for very small boxes. On the other hand, the confinement of the hydrogen atom centered in a fullerene cage was modeled by superposing a spherical attractive shell to the nucleus-electron Coulomb potential, recognizing the changes in the orders of the $4s$-$3d$ and $5s$-$4d$ orbitals including their dissolution [40]. In contrast, for confinement by dihedral angles, the hydrogen orbitals and their degeneracies behave systematically as functions of the confining angle φ_0 in its domain $[0, 2\pi]$, as illustrated in Table 1.1. These differences are expected to play an important role for the multielectron systems.

1.4.1 Two Electron Systems: *He*-Like Atoms and Quantum Dots

References [4, 7] reviewed the confinement of the helium atom at the center of a rigid spherical box, while [39] characterized the spectroscopic changes of two-electron systems: atoms and quantum dots in spheres and spheroids, using harmonic oscillator confinement.

Now, we propose the study of the same systems for the alternative confinement by dihedral angles. The hydrogenic orbitals in Sect. 1.3.1 or their harmonic oscillator orbitals in Sect. 1.3.7 are the natural basis for variational calculations. More noticeable changes are anticipated for confinement by dihedral angles versus in spheres, relative to the free system.

1.4.2 The Filling of Shells in Multielectron Systems

The effect of isotropic compression of multielectron atoms was investigated in [41] via Hartree-Fock averaged calculations for atoms with nuclear charge Z and Z electrons, and their atomic ions with $(Z-1)$ electrons, using the simple familiar model of central confinement inside a sphere of decreasing radius. The results of such calculations in the *3d* and *4d* periods of the transition metals showed that "In general, the periodic table for confined (compressed) atoms can differ from that for free atoms". More specifically, while the filling of the shells follows the order of increasing values of $n+l$ for free atoms according to the aufbau principle [42, 43], the compression favors the filling of the hydrogenic orbitals with increasing values of n.

The entries in our Table 1.1 on the degeneracies of the hydrogen atom confined by dihedral angles suggest that the changes of the filling of shells for multielectron atoms in the same situations of confinement will be even more noticeable compared to the free atoms, for any angle of confinement. The corresponding multielectron atomic calculations will have to be implemented in order to establish the specific changes and their consequent surface effects. The work in [8] involving both closed and open boundaries is a good point of reference.

1.4.3 The Hydrogen Molecular Ion and Molecule

The hydrogen molecular ion and the neutral hydrogen molecule have been investigated under confinement by prolate spheroidal boxes [44].

We are also considering the alternative confinement by dihedral angles of some molecular systems. The starting point is the molecular ion in its simplest configuration, which in prolate spheroidal coordinates implies that the nuclei positions are the foci. According with the results the step to the neutral molecule will be taken at the appropriate moment.

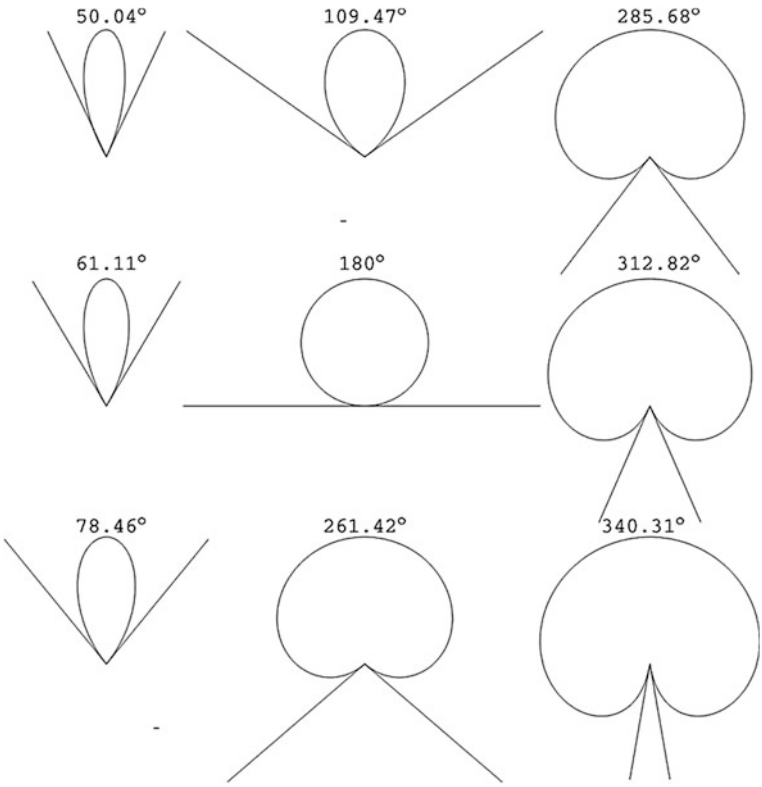

Fig. 1.6 Polar angle graphs of Legendre function orbitals $P_\lambda(\cos\theta)$ confined in *circular cones* for increasing values of $2\theta_0$

1.5 Discussion

The topics in the Contents and some of their relationships, as described in the Introduction, have been presented, successively and with varying details, in Sect. 1.2 as a brief review of some of our recent works; in Sect. 1.3 on our current work about the surface effects in the hydrogen atom confined by dihedral angles, including a comparison with its confinement in spherical boxes and circular cones, and an extension for single-electron quantum dots; and in Sect. 1.4 our perspective on some multielectron atoms and molecules confined by dihedral angles, which are interesting and we have started to analyze.

The updating on the binding of an electron by a polar molecule includes Comment [18] on [16, 17], in which the binding energy of the electron to form the anion in situations of confinement used the energy $E = 0$, without any physical basis; and Comment [20] on [19], identifying the invalidity of the proposal for new

exact radial eigenfunctions for the bound states of an electron in a point electric dipole molecule.

The work in [21] was contemporary to the writing of [3], belonging to the latter's Preview 5.3; however the time frame did not allow for including it there. Section 1.2.2 in this chapter can be read as an updating or as an extension. The remaining contributions [22–25] on free and confined-by-elliptical-cone atoms and molecules, [26] on the harmonic oscillator and hydrogen atom confined by dihedral angles, as well as [27, 28] on the complete electric dipole and magnetic quadrupole fields and sources had been previewed in 5.1, 5.2 and 5.4 of [3], respectively.

Concerning the main section of this chapter, its natural connection with Ref. [26] has already been mentioned. While the superintegrability of the free hydrogen atom is familiar, its occurrence in the hydrogen atom confined by dihedral angles is unique compared with the confinements in the other natural boundaries. The relationships between the degenerate eigenstates in the spherical, parabolic and prolate spheroidal coordinates were explicitly established in [26], for any confining angle. The main consequences are reflected in the common validity of the orbitals of Eq. (1.4), illustrated in Fig. 1.1, and of the degeneracies illustrated in Table 1.1 for the eigenstates in the different coordinates; and also in the relationships among the electric dipole moments in the different excited states in the different coordinates, Table 1.2 and Fig. 1.3. The alternation of regions of high pressure and low tension, identified for the first time in the ground state of the hydrogen atom confined by elliptical cones [22], is also exhibited by the ground and excited states in Table 1.3 and Fig. 1.4. The suppression and enhancement of the hyperfine structure and Zeeman effects due to the confinement by dihedral angles should be easily detectable experimentally. We hope this will encourage the practical implementation of such a confinement in the proper environments.

The comparison of the successive confinements in Sect. 1.3.6 allows to appreciate their different effects. Specifically, the confinement in the circular cone shares the suppression and enhancement effects of the hyperfine structure contributions, to be expected from the comparison of the orbitals in Figs. 1.1 and 1.6. For confinement in spheres and spheroids, we suggest evaluating and measuring pressure distributions instead of average pressures: for off-center confinement in spheres, and for atoms with the nucleus at one focus of spheroids, the distributions are expected to be non uniform and may allow the identification of weak spots in the confining environment. It can also be mentioned that the spheroconal elliptical coordinates interpolate between the polar angle and dihedral coordinates, justifying a careful comparison of existing and additional results from [22, 33] and this chapter.

Section 1.4 contains some problems for atoms and molecules confined by dihedral angles, that we think can be solved with the orbitals of Eqs. (1.4)–(1.7), or their variants. We hope other members of the community will elaborate their own lists.

Acknowledgments The authors warmly thank Professor Kalidas Sen for his initiative to edit this Monograph, and for inviting us to write this Chapter. They also wish to dedicate this work to Professor Salvador Cruz, Universidad Autónoma Metropolitana-Iztapalapa, and to Professor

Jocele Allegra Wild Wolf, formerly at UAM-I and China University of Science and Technology, for their respective, scientific and linguistic, expert collaborations through decades, and most specially for their friendship and love. The professional typing of the manuscript and continuous help of Ms. Lizette Ramírez are also gratefully acknowledged. This research has been supported by Consejo Nacional de Ciencia y Tecnología (ELK, SNI-1796).

References

1. Patil SH, Varshni P (2009) Properties of Confined Hydrogen and Helium Atoms. In: Sabin JR, Brändas E. Cruz SA (eds) Advances quantum chemistry: theory of confined quantum systems part I, vol 57. Academic Press, New York, Chap. 1, pp 1
2. Sen KD, IPupyshev V, Montgomery HE (2009) Exact relations for confined one-electron systems. In: Sabin JR, Brändas E. Cruz SA (eds) Advances quantum chemistry: theory of confined quantum systems part I, vol 57. Academic Press, New York, Chap. 2, p 25
3. Ley-Koo E (2009) The hydrogen atom confined in semi-infinite spaces limited by conoidal boundaries. In: Sabin JR, Brändas E. Cruz SA (eds) Advances quantum chemistry: theory of confined quantum systems part I, vol 57. Academic Press, New York, Chap. 3, p 79
4. Aquino N (2009) The hydrogen and helium atoms confined in spherical boxes. In: Sabin JR, Brändas E. Cruz SA (eds) Advances quantum chemistry: theory of confined quantum systems part I, vol 57. Academic Press, New York, Chap. 4, p 123
5. Burrows BL, Cohen M (2009) Exact solutions for confined model systems using Kummer functions. In: Sabin JR, Brändas E. Cruz SA (eds) Advances quantum chemistry: theory of confined quantum systems part I, vol 57. Academic Press, New York, Chap. 5, p 173
6. Laughlin C (2009) Perturbation theory for a hydrogen-like atom confined within an impenetrable spherical cavity. In: Sabin JR, Brändas E. Cruz SA (eds) Advances quantum chemistry: theory of confined quantum systems part I, vol 57. Academic Press, New York, Chap. 6, p 203
7. Garza J, Vargas R (2009) Comparative study between the Hartree-Fock and Kohn-Sham models for the lowest singlet and triplet states of the confined helium atom. In: Sabin JR, Brändas E. Cruz SA (eds) Advances quantum chemistry: theory of confined quantum systems part I, vol 57. Academic Press, New York, Chap. 7, p 241
8. Cruz SA (2009) Thomas-Fermi-Dirac-Weizsäcker density functional formalism applied to the study of many-electron atom confinement by open and closed boundaries. In: Sabin JR, Brändas E. Cruz SA (eds) Advances quantum chemistry: theory of confined quantum systems part I, vol 57. Academic Press, New York, Chap. 8, p 255
9. Bader RFW (2009) Confined atoms treated as open quantum systems. In: Sabin JR, Brändas E. Cruz SA (eds) Advances quantum chemistry: theory of confined quantum systems part I, vol 57. Academic Press, New York, Chap. 9, p 285
10. Guerra D, Vargas R, Fuentealba P and Garza J (2009) Modeling pressure effects on the electronic properties of Ca, Sr, and Ba by the confined atoms model. In: Sabin JR, Brändas E. Cruz SA (eds) Advances quantum chemistry: theory of confined quantum systems part II, vol 58. Academic Press, New York, Chap. 1, p 1
11. Dolmatov VK (2009) Photoionization of atoms encaged in spherical fullerenes. In: Sabin JR, Brändas E. Cruz SA (eds) Advances quantum chemistry: theory of confined quantum systems part II, vol 58. Academic Press, New York, Chap. 2, p 13
12. Charkin OP, Klimenko NM and Charkin DO (2009) DFT study of molecules confined inside fullerene and fullerene-like cages. In: Sabin JR, Brändas E. Cruz SA (eds) Advances quantum chemistry: theory of confined quantum systems part II, vol 58. Academic Press, New York, Chap. 3, p 69

13. Sil AN, Canuto S, Mukherjee PK (2009) Spectroscopy of confined atomic systems: effect of plasma. In: Sabin JR, Brändas E. Cruz SA (eds) Advances quantum chemistry: theory of confined quantum systems part II, vol 58. Academic Press, New York, Chap. 4, p 115
14. Sako T, Paldus J, Diercksen GHF (2009) The energy level structure of low-dimensional multi-electron quantum dots. In: Sabin JR, Brändas E. Cruz SA (eds) Advances quantum chemistry: theory of confined quantum systems part II, vol 58. Academic Press, New York, Chap. 5, p 177
15. Degoli E, Ossicini S (2009) Engineering quantum confined silicon nanostructures: Ab initio study of the structural, electronic and optical properties. In: Sabin JR, Brändas E. Cruz SA (eds) Advances quantum chemistry: theory of confined quantum systems part II, vol 58. Academic Press, New York, Chap. 6, p 203
16. Ronen S (2003) Electron structure of a dipole-bound anion confined in a spherical box. Phys Rev A 68:012106
17. Ronen S (2003) Addendum to electron structure of a dipole-bound anion confined in a spherical box: the case of a finite dipole. Phys Rev A 68:064101
18. Ley-Koo E (2008) Comment on electron structure of a dipole-bound anion confined in a spherical box and addendum to electron structure of a dipole-bound anion confined in a spherical box: the case of a finite dipole. Phys Rev A 78:036102
19. Alhaidari AD, Bahlouli H (2008) Electron in the field of a molecule with an electric dipole moment. Phys Rev Lett 100:110401
20. Sun GH, Ley-Koo E (2010) Comment on electron in the field of a molecule with an electric dipole moment. Phys Rev Lett 104:118901
21. Cruz SA, Ley-Koo E, Cabrera-Trujillo R (2008) Ground-state energy shift of He close to a surface and its relation with the scattering potential: a confinement model. Phys Rev A 78:032905
22. Méndez-Fragoso R, Ley-Koo E (2010) The hydrogen atom in a semi-infinite space with an elliptical cone boundary. Int J Quant Chem 111:2882–2897
23. Méndez-Fragoso R, Ley-Koo E (2010) Lamé spheroconal harmonics in atoms and molecules. Int J Quant Chem 110:2765–2780
24. Méndez Fragoso R, Ley-Koo E (2011) Rotations of asymmetric molecules and the hydrogen atom in free and confined configurations. In: Advances quantum chemistry, vol 62. Chap. 4, p 137–213
25. Méndez-Fragoso R, and Ley-Koo E (2012) Ladder operators for lamé spheroconal harmonic polynomials. SIGMA 8:074
26. Ley Koo E, Sun GH (2012) Ladder operators for quantum systems confined by dihedral angles. SIGMA 8:060
27. Ley-Koo E (2009) Complete pure dipole spheroidal electrostatic fields and sources. Rev Mex Fis E55(1):1–7
28. Medina L, Ley-Koo E (2012) Surface current distributions on spheres and spheroids as sources of pure quadrupole magnetic fields. Revista Mexicana de Física E57:87–95
29. Morse PM, Feshbach H (1953) Methods of theoretical physics part II. Mc Graw-Hill), New York
30. Coulson CA, Robinson PD (1958) Wave functions for the hydrogen atom in spheroidal coordinates I: the derivation and properties of the functions. Proc Phys Soc 71:815
31. Levine JD (1965) Nodal hydrogenic wave functions of donors on semiconductor surfaces. Phys Rev 140:A586
32. Ley-Koo E, Mateos-Cortés S (1993) The hydrogen atom in a semi-infinite space limited by a hyperboloidal boundary. Int J Quantum Chem 46:609
33. Ley-Koo E, Mateos-Cortés S (1993) The hydrogen atom in a semi-infinite space limited by a conical boundary. Am J Phys 61:246
34. Chaos-Cador L, Ley-Koo E (2005) Two-dimensional hydrogen atom confined in circles, angles, and circular sectors. Int J Quantum Chem 103:369
35. Ley-Koo E, Garcia-Castelán RMG (1991) The hydrogen atom in a semi-infinite space limited by a paraboloidal boundary. J Phys A Math Gen 24:1481
36. Hirschfelder JO (1978) Quantum mechanical equations of change. I. J Chem Phys 68:5151

37. Fermi E (1930) Über die magnetischen Momente der Atomkerne. Zeitschrift für Physik 60 (5–6):320
38. Ley-Koo E, Rubinstein S (1979) The hydrogen atom within spherical boxes with penetrable walls. J Chem Phys 71:351
39. Sako T, Diercksen GHF (2003) Confined quantum systems: a comparison of the spectral properties of the two-electron quantum dot, the negative hydrogen ion and the helium atom. J Phy B: At Mol Opt Phys 36:1681
40. Connerade JP, Dolmatov VK, Manson ST (1999) Electron structure of endohedrally confined atoms: atomic hydrogen in an attractive shell. J Phys B: At Mol Opt Phys 32:L239
41. Connerade JP, Dolmatov VK, Manson ST (2000) The filling of shells in compressed atoms. J Phys B: At Mol Opt Phys 33:251
42. Bohr N (1922) The theory of spectra and atomic constitution. Cambridge University Press), Cambridge
43. Stoner EC (1924) The distribution of electrons among atomic levels. Philos Mag Ser 6 48 (286):719
44. Colin-Rodriguez R, Diaz Garcia C, Cruz SA (2011) The hydrogen molecule and the H2+ molecular ion inside padded prolate spheroidal cavities with arbitrary nuclear positions. J Phys B: At Mol Opt Phys 44:241001

Chapter 2
Symmetry Reduction and Energy Levels Splitting of the One-Electron Atom in an Impenetrable Cavity

Vladimir I. Pupyshev and Andrey V. Scherbinin

2.1 Introduction

The splitting of a degenerate energy level is one of the oldest quantum-chemical problems. Here we consider this problem for some simple one-electron systems placed in an impenetrable cavity. The Hamiltonian of the model systems considered here has the form

$$\mathrm{H} = -\frac{1}{2}\Delta + \mathrm{V}(|\mathbf{r}|) \tag{2.1}$$

where **r** is electron radius-vector and V is the spherically symmetric potential; here and later we use only atomic units. Problems of this type appeared first in the Solid State Theory, where one of the first models was closely connected with the solution of the one-electron Schrödinger equation in a bounded region Ω with Neumann boundary conditions on the wavefunctions φ(**r**) [1, 2]: the derivative along the external normal **n** to the boundary ∂Ω of the region vanishes. That is,

$$\partial_n \varphi(\mathbf{r})|_{\mathbf{r}\in\partial\Omega} = 0 \tag{2.2}$$

Here the normal derivative is denoted as $\partial_n = (\mathbf{n},\nabla_{\mathbf{r}})$; $\nabla_{\mathbf{r}}$ is the gradient symbol with respect to the particle coordinates.

It is natural, that one of the first problems studied was the problem of the particle in a spherical cavity and corresponding energy changes under the sphere extension [3–5]. For this problem some other types of the boundary conditions also were studied; for example, the Dirichlet conditions that define the impenetrable cavity

V.I. Pupyshev (✉) · A.V. Scherbinin
Laboratory of Molecular Structure and Quantum Mechanics, Department of Chemistry, M.V. Lomonosov Moscow State University, Moscow 119991, Russia
e-mail: vip@classic.chem.msu.su

K.D. Sen (ed.), *Electronic Structure of Quantum Confined Atoms and Molecules*,
DOI 10.1007/978-3-319-09982-8_2

$$\varphi(\mathbf{r})|_{\mathbf{r}\in\partial\Omega} = 0 \tag{2.3}$$

The general self-adjoint boundary conditions were also studied in [6] for some parameter κ:

$$\partial_n\varphi(\mathbf{r}) - \kappa\varphi(\mathbf{r})|_{\mathbf{r}\in\partial\Omega} = 0 \tag{2.4}$$

For a review of mathematical problems for boundary conditions (2.1–2.4), in particular for the case when κ depends on some parameters, see in [7, 8]. We restrict this study to Dirichlet boundary conditions (2.3).

The work of Michels et al. [9] is often regarded as a first example of how the Dirichlet boundary conditions can be applied to study real physical problems. In this work, the hydrogen atom under high pressure was studied. Note that the approach is still in use, especially in astrophysics [10]. Another domain of applicability is connected with modeling of defects in solids, superlattice structures, quantum dots and quantum wires.

For example, excitons in semiconductors may be described as an electron-hole pair. The differences with the hydrogen-like systems are here mainly in the effective masses of particles and the polarization of the medium around the cavity. A large number of examples and applications for the model of the atom embedded in a cavity may be found in [11–13]. In [14] the interaction of embedded particles with the cavity walls is considered. See also the other papers from the issue cited.

The problem of a spherically symmetric system placed at the centre of impenetrable spherical cavity allows for reduction to independent 1D problems; see e.g. [15, 16]. The hydrogen atom problem in impenetrable spherical cavity is described in details in [17]. The works [7, 16, 18, 19] summarize the energy spectrum description for boundary conditions of general type (2.4). The 2D and 3D harmonic oscillator in a spherical cavity problem is described in details in [20, 21].

The model of an atom in a cavity is often used to simulate the states of atoms embedded in fullerenes or carbon nanotubes [22]. Note that the question of how free is the atom or the molecule inside the cavity of a nanotube or a fullerene is raised from time to time [23–26].

Closely related to the confined atom problems are the problems of the Crystal Field theory and this is well known (see e.g. [27–31]). Effect of restrictions of the region of free movement of electrons on the matrix elements of the perturbation operator associated with the system of point charges was discussed, for example, in the context of the crystal field theory in [31, 32].

The most common effect of symmetry reduction of the spherically symmetric system under the influence of applied external field consists of splitting of degenerate energy levels. In this paper, we consider similar effects for one-electron systems in a cavity when Dirichlet boundary conditions are imposed. Such problems require the study of cavities of more general form than purely spherical ones.

Below we use the symbols $\varphi_j(\mathbf{r}, \Omega)$, $E_j(\Omega)$ (or φ_j when the region is fixed and clear) for eigenfunctions of the Hamiltonian (2.1) under the Dirichlet boundary

conditions (2.3). For the free atom problem (i.e. for $\Omega = R^3$ and the condition that the wavefunctions are square-integrable) the eigenfunctions of H and corresponding energies of the discrete spectrum are denoted as ψ_j, E_j. The energy levels are enumerated in increasing order. All the functions used here are real-valued.

2.2 Effects of Symmetry Lowering for Cavities of Different Type

2.2.1 Spherical Cavity

The symmetry reduction in passing from the free system to the system in a cavity is a well-known phenomenon. For example, the particle moving in the pure Coulomb field possesses a higher dynamic symmetry than a general spherical one. This is the reason for the high degeneracy of the energy levels. The energy is the same for the states (n, ℓ) with the same principal quantum number n and different angular momentum values [33]. However, for the hydrogen atom with the nucleus placed in the center of impenetrable spherical cavity of finite radius R, the degeneracy mentioned disappears. See the analysis of the energy levels for this problem in [17].

There exist a number of explanations for this phenomenon, but here we mention only one of them. The extra degeneracy of the free hydrogen atom energy levels is the result of the so called Lenz vector conservation [33] being a specific integral of the motion for the Kepler problem in classical mechanics; this conservation law implies constant orientation and shape of the elliptical orbit. When the atom is placed in a spherical cavity, then the classical electron moves along the elliptical orbit, but is then reflected from the spherical surface. The orbit is formed by the system of elliptical fragments and the Lenz vector does not conserve. (The quantum mechanical description of the problem in terms of Dirichlet boundary conditions violations may be found in [34]). Nevertheless one may find that when the cavity radius R equals the square of the angular momentum for any energy value, all the orbits are closed and consist of exactly two elliptical fragments. This is the case when the system "remembers" the additional conservation law [35] of its free state. This is followed by a surprising degeneracy of quantum states (n, $\ell + 2$) and ($n - 1$, ℓ), being simultaneous for any $n > \ell + 2$ when $R = (\ell + 1)(\ell + 2)$ [17, 34]. For example, for R = 2 au one may find relations $E_{2s}(R) = E_{3d}(R)$, $E_{3s}(R) = E_{4d}(R)$, …. For the specific R noted the lowest energy of the state with momentum ℓ of the hydrogen atom equals exactly to the energy of the free atom in the state ($\ell + 2$, ℓ).

These regularities are closely connected with the properties of confluent hypergeometric function that defines the radial wavefunctions of hydrogen-like atom [17]. It is not strange that simultaneous degeneracy can be found in some other problems, for example, for the confined isotropic harmonic oscillator in an impenetrable spherical cavity [36]. For the description of the details in similar situations, see also [20, 21, 37].

In a more general case of the spherically symmetric potential one may find only the usual $2\ell + 1$-fold degeneracy of the states with different angular momentum projections, that is, due to the conventional spherical symmetry of the problem. One may note only, that the energy of the state (n, ℓ) increases both with n and ℓ. Extension of any cavity is accomplished with monotonic decreasing of each of the energy levels (see [38], Sect. XIII.15, or [39]) that converge to the corresponding $E_{n\ell}$ levels of the free system. A general statement also holds for convergence of stationary state wavefunctions and their gradients [39, 40]. In particular, for the 3D hydrogen-like atom in a sphere with large radius R, the lowest energy values are ordered in energy as follows:

$$1s, \{2p, 2s\}, \{3d, 3p, 3s\} \ldots \tag{2.5}$$

Here we use brackets to denote the groups of levels with the same limits as $R \rightarrow \infty$ [15, 17, 41]. For the spherically confined 3D isotropic harmonic oscillator, for large R values, the order of the states differs from (2.5) [21]:

$$1s,\ 1p,\ \{1d,\ 2s\},\ \{1f, 2p\},\ \{1g,\ 2d,\ 3s\}, \ldots \tag{2.6}$$

It is difficult to find general statements on the energy spectrum for arbitrary potential. However it may be demonstrated for a wide class of potentials, including the Coulomb one, that for small enough cavity size the potential does not influence the state's ordering and in case of the Dirichlet problem the levels are in the same order as of the free particle in the same box. For the spherical cavity, the following order can be found [33]:

$$1s, 2p, 3d, 2s, 4f, 3p, 5g, 4d, 6h, 3s \ldots \tag{2.7}$$

(the hydrogen-like notations are used here, that is, $n \geq \ell + 1$, in contrast with Eq. 2.6).

2.2.2 The Cavity of the More Complex Form

For the system in a non-spherical cavity, one may expect the additional splitting of the energy levels that were degenerate for the free system. Application of perturbation theory methods would seem natural, but a caution should be addressed here. Let us consider the simplest case of a non-degenerate level, as the generalization to the case of degenerate level is rather obvious. When the effect of the finite potential walls of the height U_0 around the cavity Ω is described, one may introduce the perturbation of the form $U_0\chi^c_\Omega(\mathbf{r})$, where χ^c_Ω is the characteristic function of the complement Ω^c of the region Ω in R^3. In the first order of the perturbation theory, one may write

$$E_j(\Omega, U_0) \approx E_j + U_0 \int\limits_{\Omega^c(R)} |\psi_j(\mathbf{r})|^2 d\mathbf{r} \tag{2.8}$$

The exact energy levels $E_j(\Omega, U_0)$ are lower than the Dirichlet energies $E_j(\Omega)$ and converge to $E_j(\Omega)$ in the limit $U_0 \to \infty$ monotonically [40]. Unfortunately, relation (2.8) itself cannot describe this limit correctly, as the right hand side obviously diverges (recall that the ψ_j and E_j notations correspond to the free system, i.e. they are independent of U_0). Note that it was demonstrated in the classic work by Wigner [42] that perturbation theory requires carefulness when applied to the "box" problems. However, the use of such a perturbation for large R values seems be useful at least for qualitative discussions. One may hope, that at least the state ordering may be estimated correctly for some finite U_0 value when Ω is large enough and the wavefunctions of the free system decrease exponentially. Note that it is a common situation that the radial functions of quantum mechanical problems may be asymptotically described as $Br^n\exp(-\alpha r^\beta)$ for some positive constants. All the calculations below will be performed within this supposition.

Let R be the distance from the potential center O to the boundary $\partial\Omega$, that is R is equal to the radius of the sphere with the center O inscribed in the cavity Ω. The sphere mentioned touches the boundary $\partial\Omega$ at points $\{\mathbf{r}_k\}$ ($|r_k| = R$). Let us suppose, that any ray starting from the potential center crosses the boundary $\partial\Omega$ in exactly one point (for example, this is true for any convex region Ω). Then one may estimate the integral in Eq. (2.8) by the Laplace method (see Sect. 4.1–4.3 of [43]) for the radial variable. The resulting surface integral also may be evaluated by the Laplace method. A simple idea, but a very cumbersome calculation shows that the integral is reduced to the sum of the wavefunction values at the points $\{\mathbf{r}_k\}$. Hence for large enough R one may write

$$E_j(\Omega(R)) \approx E_j + \frac{\pi U_0}{2(\alpha\beta)^2} R^{3-2\beta} \sum_k \left|\psi_j(\mathbf{r}_k)\right|^2 \tag{2.9}$$

where α, β are the parameters of the above mentioned asymptotical form of the wavefunction ψ_j. The modification of these relations to the case of the degenerate level is now trivial. Nevertheless one may use Eq. (2.9) for the degenerate states when one component of a certain symmetry type is considered.

For us, these formulas are not interesting in themselves, but only as qualitative results that show that the values of the free problem wave functions at the points $r_k(R)$ of $\partial\Omega$ determine the asymptotic behavior of the energy shifts.

2.2.3 Polyhedral Cavity

In the case of highly symmetrical cavities and the location of the potential origin at the center of symmetry, one may apply the standard group-theoretical methods

primarily developed in the framework of the Crystal Field Theory for the analysis of reduction of the rotational group of R^3 on a given subgroup (in this case—the symmetry point group of the cavity). For example, the splitting laws of states with the lowest values of the angular momentum are well known [27–29]. Thus one may note for the cubic or octahedral cavities (the symmetry group O_h) the following reduction laws

$$s \to a_{1g}, p \to f_{1u}, d \to e_g + f_{2g}, \ldots \tag{2.10}$$

According to the conventional symmetry notations, the *a*-states are non-degenerate, while *e*- and *f*-states are doubly and triply degenerated, respectively. Note that sometimes O_h states of the *f*-type are denoted in literature as *t*.

Among the symmetry operations there is no inversion for the tetrahedral cavity (T_d). This is followed by more complex form of reduction. The symmetry type f_2 appears both for p and d-levels:

$$s \to a_1, p \to f_2, d \to e_g + f_2, \ldots \tag{2.11}$$

Relations like (2.9) for energy shifts and levels splitting allow us to expect that the symmetry of the cavity Ω may be enough to determine the order of the splitted states. Unfortunately, this is not the case.

Let us consider some numerically calculated data for the hydrogen atom at the center of the impenetrable cubic cavity. Here we will not describe energy changes under the displacements of the nucleus away from the center (see the analysis in [44]). For the present calculations, we have used the method presented in [45] (see Sect. 2.3.3).

Let the vertices of the cube be truncated with conservation of the O_h symmetry of the cavity. This truncation may be described by the dimensionless parameter X that defines the proportion of the truncated edge from the side of each of vertices. The value X = 0 corresponds to the regular cube, while at X = 0.5 the cube edges disappear, and the truncated cube is the cuboctahedron. The same polyhedron is the result of truncation of the octahedron of the appropriate size. The results of truncation of the cube and the tetrahedron are jointly represented in Fig. 2.1. for the initial cube edge length of 4 au. As an abscissa, the variable t is used that defines the cube truncation when $t < 0.5$ by the relation $t = X$; for $t > 0.5$ we use the definition $t = 1 - X$, where X defines the octahedron truncation. The point t = 1 corresponds to the regular octahedron.

Note that for any truncated cube with $X \le 0.5$, the inscribed sphere radius is the same and, based on relation (2.9), one could expect the conservation of the state ordering. The Fig. 2.1 shows that this is indeed the case. For the hydrogen atom in the spherical cavity with $R \approx 2$ au, the levels are ordered as 1s, 2p, 2s, 3d,… and the levels 2s and 3d are degenerated for R = 2. As it was explained, the compression that accomplishes the truncation of both cube and octahedron is followed by energy increase [38]. These details are well represented in Fig. 2.1.

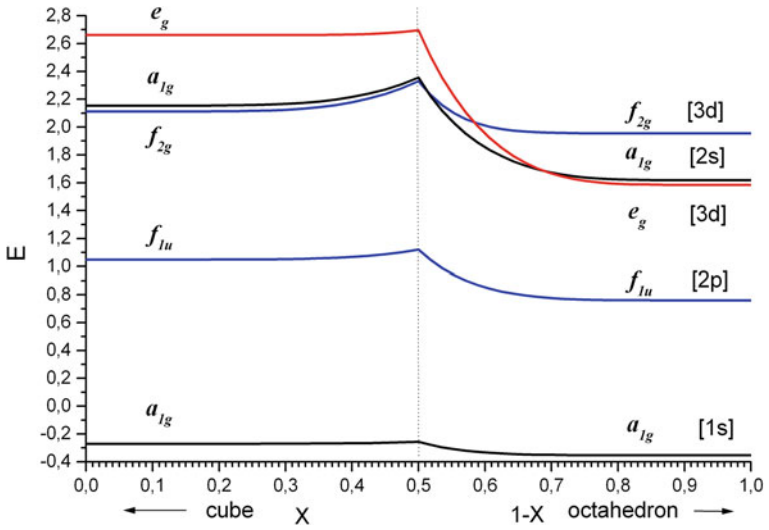

Fig. 2.1 Energy levels (au) for hydrogen atom placed at the centre of the cavity formed by joint symmetrical truncation of both the cube with the edge 4 au and the octahedron. For an explanation of the choice of dimensionless abscissa axis, see the text. In *brackets*, the corresponding states of the free atom are supplied

It is interesting that the most essential changes in the state ordering occur near the point $t \approx 0.58$ where the points of the cavity boundary closest to the center of the truncated octahedron replace that ones for the truncated cube. The relative position of the state a_{1g} [2s] changes near this point. When the size of the initial cube increases, the energies of the states decrease and the corresponding curve for the state $2a_{1g}$ is much closer to the state $1f_{1u}$ in accordance with the scheme (2.5). The intersection point for the states e_g and f_{2g} remains practically unchanged with the cavity size increase, and one may expect relations like (2.9) to be useful for similar considerations, though the positive U_0 value is undefined and the cavity size is small.

In a similar way change the energy values in other confined systems. For example, Fig. 2.2 demonstrates energies of an isotropic harmonic oscillator in a tetrahedral cavity truncated in a symmetric way into an octahedron. It is interesting that the qualitative behavior of the states for the harmonic oscillator is close to that of a hydrogen atom (one may compare Fig. 2.2 with the Fig. 6 of the work [45]). The position of the degeneracy point for the states e and f_2 varies essentially with the size of the tetrahedron and one can not use any simple geometrical arguments here.

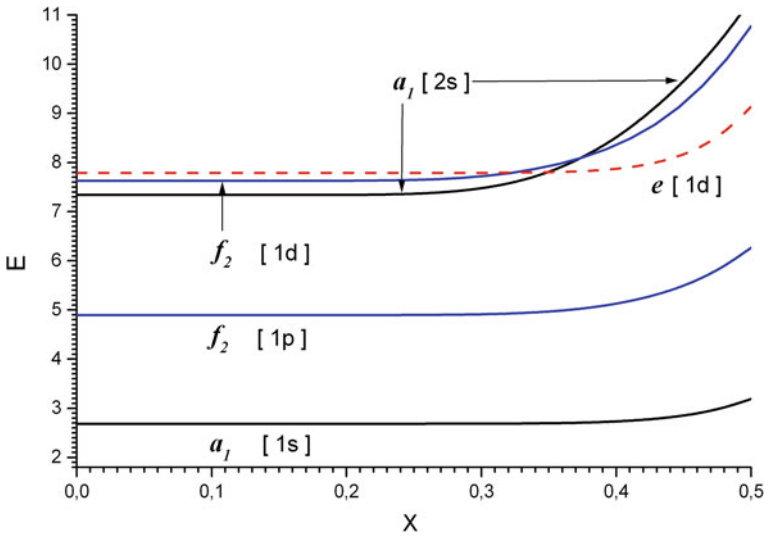

Fig. 2.2 The energies of the isotropic harmonic oscillator with the force constant K = 1 au placed at the center of the tetrahedral cavity with the edge 5.65 au (X = 0) truncated to octahedron (X = 0.5)

2.2.4 Note on the State Ordering

In certain cases, at least some of details of the state ordering can be explored by means of simple qualitative arguments. Let us consider the 3D isotropic harmonic oscillator with a variable force constant K in some fixed polyhedral cavity. When K is large enough, one may consider the system as being practically free (indeed, the wave functions of the lowest states are localized near the origin and the effect of the boundaries can be shown to be negligible [39]). In this limiting case, the states are ordered according to Eqs. (2.6), (2.10). When the force constant is negative-valued, there are no discrete spectrum states in the free system, but for the same system in an impenetrable cavity, only a discrete spectrum exists. It is quite clear that, in the latter case, the wave functions of the low lying states are localized near the vertexes of the polyhedral cavity. One may further consider conventional correlation diagrams to establish the state ordering in between the two limiting cases, $K \to -\infty$ and $K \to +\infty$.

For example, for a cubic cavity, it is quite evident that when $K < 0$ and $|K|$ is large enough, at least 8 lowest states may be adequately represented as proper linear combinations of 8 symmetry-equivalent basis functions, each being localized near one of the vertexes. The corresponding 8-fold representation of the point group O_h is easily decomposed into the following irreducible components: a_{1g}, a_{2u}, f_{1u} and f_{2g}. The fact that e_g-states are absent in this list implies that such states are situated much higher in energy. Therefore, in the study of the d-state splitting of the harmonic oscillator in a cubic cavity, in accordance with the symmetry reduction law

(2.10), it is natural to expect that the e_g-state is higher in energy than f_{2g}-state, at least for the 1d-level. For octahedral cavity, one may apply the same method to find that six localized states define the lowest states of the types a_{1g}, f_{1u} and e_g.

Note that one may use similar arguments for the Coulomb potential case. In this case one should use negative nuclear charges to construct the correlation diagram instead of negative K values for the case of harmonic oscillator. This difference is unessential for the method presented. In particular, this makes it clear the $e_g - f_{2g}$ state inversion when the cube is transformed into the octahedron (see e.g. Fig. 2.1). This is well known in the Crystal Field theory, though the state ordering on Fig. 2.1 differs from the usual one for the atomic states when the one-electron atom is surrounded by negatively charged ligands.

For the tetrahedral cavity, the constructions described above are practically useless, as for the tetrahedron the four lowest states are of the types a_1 and f_2 correlated with the free atomic states 1s and 2p. For example, one may find for the harmonic oscillator in a tetrahedral cavity with the edge 6.53 au, that the splitting of the harmonic oscillator 1d-state state into $2f_2$ and e is inverted near the force constant value of K ≈ 1.5 au. This example demonstrates that the real level splitting results from the interplay of numerous factors that require special attention and care.

2.3 Some Methods for Systems in Bounded Cavities

Practically each of the works on confined systems uses some original numerical method for the real states analysis. Here we describe only some of them, mainly important for qualitative description of the state order.

2.3.1 On the Numerical Methods for the Problems in the Sphere

The simplest way for solution of the confined system problem with the full spherical symmetry is the analysis of the radial wave functions R_ℓ(r, E) for a given angular momentum and arbitrary energy value E. For quantum-chemical problems, any acceptable solution should be bounded at the origin and therefore behaves like r^ℓ. The energy values of the stationary states with a given ℓ value for the Dirichlet problem within an impenetrable spherical cavity of radius R are defined by solutions of the following equation

$$R_\ell(\mathrm{R}, \mathrm{E}) = 0 \tag{2.12}$$

Radial functions and solutions of Eq. (2.12) may be determined analytically or numerically for any E values. Similar methods are used to study the systems in cavities like combinations of some spheres [46]. On the numerical methods for the

problem with fixed nucleus see [47]. For the use of the perturbation theory and other constructions see [41, 48, 49].

Of course, the finite difference calculations and combined methods are also used in practice. For example, a combination of numerical methods was implemented to describe both electronic and nuclear motion in the adiabatic approximation and to estimate the rovibronic energy levels and transition probabilities for the fully-dimensional problem of hydrogen atom in a spherical cavity [50]. Similar constructions were used for modeling of vibrational and rotational energy levels of diatomic molecules in an impenetrable sphere and to analyze the isotopic substitution effects in molecular spectra [51, 52]. Note also an interesting study of diatomics in cavity in [53, 54]. The methods for nuclear motion [55, 56] are closely related with methods for two-electron systems [57, 58].

The effective potentials for the cavity simulation also may be used. This makes it possible to use more traditional methods of quantum chemistry and molecular modeling, but this line is far from the subject of this text, though the techniques mentioned are developing rapidly in recent years.

2.3.2 The Method of Cutting Functions

It was suggested in [6] to consider the wave functions of the system in a cavity in the form $f(\mathbf{r})\psi(\mathbf{r})$, where ψ is some square-integrable solution of the Schrödinger equation for the problem in the whole space, and $f(\mathbf{r})$ is a "cutting factor", which ensures fulfillment of the desired boundary conditions. For example, for the Dirichlet problem one may use functions with special property $f|_{\partial\Omega} = 0$ (it is supposed here that for $\mathbf{r} \notin \Omega$ one puts $f(\mathbf{r}) = 0$). At one time this idea was popular and often used for numerical estimates [59], for example, in the perturbation theory. For the history of the method and its applications see also [40, 60]. For the application of this technique to the confined system problems see [60–66].

Within the linear variational method, the use of cutting functions is particularly efficient. For example, when the boundary is not too curvy, one may calculate the matrix of the Hamiltonian in the basis of functions like $\{f\psi_j\}$ by using the sesquilinear form

$$\varepsilon(u, v) = \frac{1}{2}\langle \nabla u | \nabla v \rangle_\Omega + \langle u | V | v \rangle_\Omega \tag{2.13}$$

where the index Ω indicates the integration over the region only. Continuation of all the functions out of Ω by zero value allows omitting this index.

Note that when the function v is in the domain of definition of the Hamiltonian operator, then one may use the Green's relation to find

$$\varepsilon(u,v)=\frac{1}{2}\int\limits_{\partial\Omega} u\partial_n v d\sigma+\langle u|Hv\rangle_\Omega \tag{2.14}$$

Here, u may be any piecewise smooth function and this property extends the possible class of cutting functions. For example, let f be the piecewise smooth function with properties $|f|\le 1$ and $f=0$ in Ω^c; in particular, $f|_{\partial\Omega}=0$. Let us use the wavefunctions ψ_m and φ_k for the free and the Dirichlet problems, correspondingly, to calculate the values $\varepsilon(f\psi_m, \varphi_k)$ and $\varepsilon(\psi_m, f\varphi_k)$ with the help of relation (2.14). One may find that

$$(E_k(R)-E_m)\langle f\psi_m|\varphi_k\rangle=\frac{1}{2}\int\limits_{\Omega}(\nabla f,\psi_m\nabla\varphi_k-\varphi_k\nabla\psi_m)dr \tag{2.15}$$

where (,) means the inner product of 3D-vectors. The surface integrals are absent in this relation due to boundary properties of functions f and φ_k. One may note that the integrand in the right hand side of (2.15) is non-zero only in the region where the cutting function f differs from 1. Usually this region is some neighborhood of the boundary $\partial\Omega$. Sometimes one may suppose that in this neighborhood the functions φ_m and ψ_m are proportional and one may find the function $f=f_0$ such that for all the points where $\nabla f_0(\mathbf{r})\neq 0$, one may write $\varphi_m(\mathbf{r})=f_0(\mathbf{r})\psi_m(\mathbf{r})$ (in other points of Ω, where $f_0=1$, this relation may fail). For the function f_0 one may write (2.15) in the form

$$(E_m(R)-E_m)\langle f_0\psi_m|\varphi_m\rangle=\frac{1}{2}\langle\psi_m(\nabla f_0,\nabla f_0)\psi_m\rangle \tag{2.16}$$

The other important relation of this type is the Kirkwood-Buckingham relation [40] that may be written for any function $f(\mathbf{r})$ as

$$\begin{aligned}H_{mn}&=\varepsilon(f\psi_m,f\psi_n)\\&=\frac{1}{2}(E_m+E_n)\langle\psi_m|f^2|\psi_n\rangle+\frac{1}{2}\langle\psi_m|(\nabla f,\nabla f)|\psi_n\rangle\end{aligned} \tag{2.17}$$

In particular, for the finite set of N basis functions $f\psi_1$, $f\psi_2$, … $f\psi_N$ one may compose the $N\times N$ Hamiltonian matrix $\mathbf{H}$ with the elements H_{mn} and calculate the variational energy estimates for the Dirichlet problem in the region Ω. In recent years similar variational methods in the basis of cutting functions were often applied to many-electron systems; see, for example, [58]. The overlap matrix $\mathbf{W}$ for the set $\{f\psi_j\}$ has the form $\mathbf{W}=\mathbf{1}-\mathbf{Q}$ where $\mathbf{Q}$ is the matrix with elements $Q_{ij}=\langle\psi_i|1-f^2|\psi_j\rangle$. It is important here that the matrix $\mathbf{Q}$ is nonnegatively defined when $|f|\le 1$. In particular, its largest eigenvalue does not exceed the trace of $\mathbf{Q}$.

The generalized eigenvalue problem with the Hamiltonian matrix $\mathbf{H}$ and the overlap matrix $\mathbf{W}$ gives upper bounds E_j^* for the exact energies $E_j(\Omega)$ ("the Hylleraas-Undheim-MacDonald theorem" [67]). Hence the sum of N lowest

energies $E_j(\Omega)$ is estimated by the sum of N numbers E_j^*. The standard method allows to estimate the sum:

$$\sum_{j=1}^{N} E_j(\Omega) \le \sum_{j=1}^{N} E_j^* = \mathrm{tr}\mathbf{H}\mathbf{W}^{-1} \tag{2.18}$$

Due to relations (2.17) for the matrix elements, it is easy to rewrite this inequality in the form

$$\sum_{j=1}^{N} (E_j(\Omega) - E_j) \le \frac{1}{2}\left(\sum_{j=1}^{N} \left\langle \psi_j \middle| |\nabla f|^2 \middle| \psi_j \right\rangle\right) / (1 - \mathrm{tr}\mathbf{Q}) \tag{2.19}$$

where $1 - \mathrm{tr}\mathbf{Q}$ gives the lower bound for the lowest eigenvalue of the overlap matrix **W**. Of course, it is supposed in inequality (2.19) that the tr**Q** is small enough.

All the terms in the sum in the left hand side of Eq. (2.19) are positive numbers only and one may estimate each of the energy differences by the right hand side of this relation. We will use Eq. (2.19) below. An alternative way to derive Eq. (2.19) is presented in [39].

2.3.3 The Cavity of the More Complex Form

The main problem with cavities of a complex form is the compact description of the cavity boundary surface. When the surface $\partial\Omega$ is not too complex one may use the method described in [45], similar to the Shooting Method for 1D problems: for one-electron problems one may define the energy values by imposing the boundary conditions on the trial function $\varphi(\mathbf{r}, E)$. Here $\varphi(\mathbf{r}, E)$ is a solution of the differential Schrödinger equation for some trial energy value E. For example, for the spherically symmetric potential, the radial functions $R_\ell(r, E)$ are known analytically or numerically. For low symmetry cavities, one may construct the functions of a definite symmetry type Γ as linear combinations $Y_\ell^{(\Gamma)}(\theta, \varphi)$ of spherical harmonics with some appropriate ℓ values. Thus the functions $u_\ell(\mathbf{r}, E)$ of the form $R_\ell(r, E)Y_\ell^{(\Gamma)}(\theta, \varphi)$ may be considered as a basis set for determination of a trial function of the form

$$\varphi^{(L)}(\mathbf{r}, E, \mathbf{c}) = \sum_{\ell=0}^{L} c_\ell u_\ell(\mathbf{r}, E) \tag{2.20}$$

Later on we use the **c** symbol for the vector with coefficients $\{c_\ell\}$. The (2.20) define some solution of the Schrödinger equation for each energy E and vector **c** for a given symmetry species. For normalized functions $\varphi(\mathbf{r}, E, \mathbf{c})$ the Dirichlet boundary condition (2.3) can be replaced with the relation $D(\varphi, E, \mathbf{c}) = 0$, where the functional D is defined as

$$D(\varphi, \mathrm{E}, \mathbf{c}) = \int\limits_{\partial\Omega} |\varphi(\mathbf{r}, \mathrm{E}, \mathbf{c})|^2 \mathrm{d}\sigma \tag{2.21}$$

This is the qualitative idea of the method described. It is based on the statement, that when for some functions $\varphi^{(\mathrm{L})}(\mathbf{r}, \mathrm{E}^{(\mathrm{L})}, \mathbf{c}^{(\mathrm{L})})$, being solutions of the differential Schrödinger equation, for $\mathrm{L} \to \infty$ one may state that $\{D(\varphi^{(\mathrm{L})}, \mathrm{E}^{(\mathrm{L})}, \mathbf{c}^{(\mathrm{L})})\} \to 0$ and $\mathrm{E}^{(\mathrm{L})} \to \mathrm{E}_*$, then the limiting value E_* defines the point of the discrete spectrum of the Hamiltonian (2.1) with the Dirichlet boundaries. This is not a trivial statement but restrictions on the functions $\{\varphi^{(\mathrm{L})}\}$ are not too strong; see [45].

When one tries to minimize the functional D (2.21) with trial functions of the form (2.20) with respect to the vector **c,** it is clear that the quadratic form optimization results in a generalized eigenvalue problem

$$\mathbf{\Sigma c} = \delta^{(\mathrm{L})}(\mathrm{E})\mathbf{Sc} \tag{2.22}$$

where **S** is the usual $\mathrm{L} \times \mathrm{L}$ overlap matrix for the basis functions $\{\mathrm{u}_\ell\}$, calculated by integration over the region Ω, while $\mathbf{\Sigma}$ is a similar overlap matrix, but for the restrictions of the functions $\{\mathrm{u}_\ell\}$ only to the surface $\partial\Omega$. The vector **c** defines optimal approximation for $\varphi^{(\mathrm{L})}$, while the lowest eigenvalue $\delta^{(\mathrm{L})}(\mathrm{E})$ gives the optimal value of the functional for a given energy value E.

When the function $\delta^{(\mathrm{L})}(\mathrm{E})$ is known, one may find the set of its local minima $\mathrm{E}_1^{(\mathrm{L})}$, $\mathrm{E}_2^{(\mathrm{L})}$,… with respect to E. These local minima define, with increasing L, the estimates for the energy levels $\mathrm{E}_1(\Omega)$, $\mathrm{E}_2(\Omega)$, … for the Dirichlet problem. The L values required for calculations of low lying states are usually not too large.

There exist a variety of realizations of the idea described. One may note that when there exists a zero eigenvalue of the matrix $\mathbf{\Sigma}$, then it is the solution of Eq. (2.22) for any form of the matrix **S**. In particular, in order to optimize the calculation time, one may use approximate forms of the matrix **S**; this is equivalent to the use of some weights for calculation of the functional D. For example, one may use the diagonal part of **S** only, or **S** = 1. Of course, the results are stable to such modifications only when the optimal values of $\delta^{(\mathrm{L})}(\mathrm{E})$ are small enough. For example, in [45] we used the exact **S** matrix, while in [44, 68] simpler forms of overlap matrices were also tested. Note that the complete form of the method gives the most stable computational results. The numerical data used for Figs. 2.1 and 2.2 were prepared by this method.

Note that for the spherical cavity Ω, the described method is simplified and reduces to the usual solution of Eq. (2.12), and one may consider the construction described as “the Shooting Method”. One may use both analytical and numerical estimates for radial functions. One may consider the integral D minimization as looking for approximate solution of the problem $\varphi^{(\mathrm{L})}|_{\partial\Omega} = 0$ at some grid points. So one may consider the method as a variety of the Least Squares Method with weights or as the collocation method.

For the excited states, the stability of the method decreases and it is sensitive to the choice of the grid points used for calculations. The search of local minima for

$\delta^{(L)}(E)$ function becomes a very difficult problem as the minima are too sharp for large L values. Nevertheless, when compared with other numerical tools such as finite difference, perturbational or variational approaches [48, 49], the present methods are quite reliable. In particular, they may be used for other types of boundary value problems like Eq. (2.4).

2.4 Cavities of the Large Size

2.4.1 Evaluation of the Energy Shift

Let us evaluate the energy shift for a system in an impenetrable cavity with respect to the free system. There exist a number of ways to do it. In any case, we consider a parametric family of cavities expanding with the parameter growth. As a parameter mentioned, the radius R of an inscribed sphere with the centre at the origin of the potential is convenient. It is possible to prove L_2 convergence of the wavefunctions $\varphi_j(\mathbf{r}, \Omega(R))$, continued as identically zero-valued outside $\Omega(R)$, to the solutions $\psi_j(\mathbf{r})$ of the free problem. For 1D or equivalent problems it was first demonstrated in [69] with Ω being a sphere. A similar in spirit but different in realization approach developed in [70, 71] allows to asymptotically estimate the energies, wave functions, oscillator strengths and polarizabilities for the confined hydrogen atom in selected states. Some analytical approaches were also developed in [72–76]. (However, the detailed theoretical description of the R-dependence for oscillator strength of the hydrogen atom, estimated in the wide range of the spherical cavity radii in [77], does not exist up to now.)

The convergence of the energy levels $E_j(R)$ to E_j is almost evident. For example, one may use the cutting function f that differs from 1 in a neighborhood of $\partial\Omega$ for points $|\mathbf{r}| > \gamma R$ where $\gamma < 1$ is fixed. The function f decreases to zero value at $\partial\Omega$. As it was already mentioned, we use the asymptotic form $Br^{\eta}\exp(-\alpha r^{\beta})$ for the radial parts of the free problem wavefunctions (this idea was proposed in [69]). It is obvious in this case, that the $\langle\psi_k|(1-f^2)|\psi_k\rangle$ integrals converge to zero exponentially. Hence one may use inequality (2.19) in the form

$$\sum_{j=1}^{N}\left[E_j(R) - E_j\right] \le \frac{1}{2}\sum_{j=1}^{N}\left\langle\psi_j\left||\nabla f|^2\right|\psi_j\right\rangle(1 + o(R)) \tag{2.23}$$

with some positive function o(R) that vanishes exponentially. As the integrals in this relation are calculated for the region $|\mathbf{r}| > \gamma R$, the right hand side of Eq. (2.23) also converges to zero when $|\nabla f|$ is bounded.

One may rewrite (2.23) in a simpler form. It is a usual situation that the rate of decay of discrete energy spectrum wave functions at infinity decreases with the excitation level. Hence, for a non-degenerate energy level, one may write the following asymptotic relation for large enough R values and $|\mathbf{r}| > \gamma R$:

$$\sum_{j=1}^{N} |\psi_j|^2 \cong |\psi_N|^2 \tag{2.24}$$

and one may rewrite (2.23) in a much weaker form

$$E_N(R) - E_N \leq \frac{1}{2}\left\langle \psi_N || \nabla f|^2 | \psi_N \right\rangle (1 + o(R)) \tag{2.25}$$

Relations of this kind may be used to prove convergence of wavefunctions and their gradients [39] by means of a combination of the Eckart relations [78] and the Katriel trick [79]. Alternatively, this can be established by virtue of the Löwdin's results (see (3.41) in [80]).

More refined approval can be obtained if one uses (2.16) with some appropriate function f_0. This is true, for example, in one-dimensional problems or for the radial equation, when for a sufficiently large distance from the centre, the potential values are higher than the energy studied. It follows from the bilateral estimate $0 \leq f_0 \leq 1$ and the convergence of $f_0\psi_m$ to φ_m with increasing R, that the integrals $\langle f_0\psi_m|\varphi_m\rangle$ converge to 1, not exceeding 1. Hence one may estimate the energy shift from below, as follows:

$$E_m(R) - E_m \geq \frac{1}{2}\left\langle \psi_m || \nabla f_0|^2 | \psi_m \right\rangle \tag{2.26}$$

Relations (2.25) and (2.26) are similar, but obviously not equivalent. However, in the problems that may be reduced to one-dimensional ones, one may look for the optimal form of the function f from the minimization of the integral in the right hand side of (2.25) (see e.g. Sect. 4.4 in [16]). As simple estimates show, with optimal choice of $f = f_{opt}$, the leading asymptotic term essentially depends on the behavior of the wave functions at the boundary only, and this circumstance allows us to combine estimates (2.25) and (2.26) in the case of spherical regions. The energy shift is evaluated asymptotically through the radial part of the wave function of the corresponding state of the free problem (here and later we use the radial functions that are normalized with the weight factor r^2):

$$\begin{aligned} E_m(R) - E_m &\cong \frac{1}{2}\left\langle \psi_m || \nabla f_{opt}|^2 | \psi_m \right\rangle \\ &\cong -rR_m(r)\partial_r[rR_m(r)]|_{r=R} \cong -R^2 R_m(R)\partial_r R_m(R) \end{aligned} \tag{2.27}$$

Here, the symbol ∂_ξ is used for the derivative with respect to the variable ξ. The same estimate was described in [69]. For the next asymptotic terms of the energy shift, see [70, 71, 81].

2.4.2 The Large Polyhedral Cavity

For regions of general type we cannot guarantee the relations like (2.26) to be true, but one may suppose the estimates of the form (2.25) to be not too poor. The optimal form of the cutting function in Eq. (2.25) for convex polyhedral cavities (or cavities described in Sect. 2.2.2) may be estimated by a solution of a pair of one-dimensional problems. We will not give here fairly cumbersome intermediate stages of asymptotic calculations, leading to qualitatively clear relations.

The upper bound for the optimal integral $\langle\psi_m||\nabla f^*|^2|\psi_m\rangle$ value can be found if one uses the functions $f(\mathbf{x})$ specified only by the distance from the point $\mathbf{x}$ to the nearest plain face of the polyhedron. This is the case when one may reduce the three-dimensional integrals to one-dimensional ones using the density of the state averaged over the planes parallel to the polyhedron faces. All the calculations may be performed on the basis of the method of Laplace (see Sects. 4.1–4.3 of [43]) for the wave functions ψ_m of the above mentioned form.

For the polyhedron, the lower bound for the optimal integral value can be also found when optimizing the cutting function along the radial direction from the center to the boundary and omitting all the angular contributions in $|\nabla f|^2$. The remaining integral over the angular variables is calculated again using the method of Laplace.

It is interesting that the leading terms of asymptotic expansions for the integral under consideration are the same for both the upper and lower bounds, and the resulting asymptotical value of the integral is expressed through the points $\{\mathbf{r}_k\}$ where the inscribed sphere touches the faces of the polyhedron (see also Sect. 2.2.2). Thus one may write for $R \to \infty$

$$\frac{1}{2}\left\langle\psi_m||\nabla f_{opt}|^2|\psi_m\right\rangle \cong 2\pi R\sum_k |\psi_m(\mathbf{r}_k)|^2 \tag{2.28}$$

This estimate differs from the perturbation theory result (2.9) by a radial factor only, but the factor does not change the state ordering, according to Eqs. (2.9) or (2.28). So the role of the points $\{\mathbf{r}_k\}$ in evaluating the energy shifts is confirmed in an independent way.

The modification of Eq. (2.28) for the degenerate case is almost trivial. For example, let us consider the splitting of the degenerated energy level of hydrogen atom with the given principal quantum number n. The free atom radial wave functions have the form $r^{n-1}e^{-r/n}$ at large distances from the nucleus, and they differ in the numerical factors $B_{n\ell}$ only [33]:

$$B_{n\ell} = \frac{2^n}{n^{n+1}\sqrt{(n+\ell)!((n-\ell-1))!}} \tag{2.29}$$

If one is interested in the state ordering, the radial contributions may be omitted and the splitting of the states with respect to the exact free atom value $E_n = -1/2n^2$

Table 2.1 The energy splitting (t_k in relative units) of the hydrogen atom states with n = 3 in some large polyhedral cavities

Polyhedron	Assignment and t_k			
$\boldsymbol{O_h}$	$\boldsymbol{1f_{2g}}$	$\boldsymbol{1e_g}$	$\boldsymbol{2f_{1u}}$	$\boldsymbol{3a_{1g}}$
Cube	0	0.97	1.94	3.88
Octahedron	0.86	0	2.59	5.17
$\boldsymbol{T_d}$	$\boldsymbol{2f_2}$	$\boldsymbol{1e}$	$\boldsymbol{3f_2}$	$\boldsymbol{3a_1}$
Tetrahedron (3s, 3p, 3d)	0	0	1.72	2.59
Tetrahedron (3d)	0.43	0	–	–

is defined by eigenvalues $\{t_j\}$ of the matrix $\mathbf{T}$ defined as follows. The matrix elements of $\mathbf{T}$ are expressed through the B-factors (2.29) and the values of the spherical harmonics at the respective points $\{\omega_k = \mathbf{r}_k/R\}$ on a unit sphere:

$$T_{i,j} = B_{n\ell_i} B_{n\ell_j} \sum_k Y_i(\omega_k) Y_j(\omega_k) \tag{2.30}$$

For some classical polyhedra, the calculated energy splittings for n = 3 are collected in Table 2.1.

Recall that for the hydrogen-like atom in a large spherical cavity the levels with the principal quantum number n = 3 are ordered as 3d, 3p, 3s. This is consistent with the data from Table 2.1, where the 3p and 3s levels are referred to as ($2f_{1u}$, $3a_{1g}$) and ($3f_2$, $3a_1$) for cubic and tetrahedral systems, respectively. For the case of the tetrahedron, the reduction laws (2.11) make it possible to consider also the splitting of 3d states, also presented in Table 2.1.

Note, however, that for the tetrahedron in the case n = 3, the 5-fold degeneracy conserves within the leading asymptotic order. The rank of the matrix $\mathbf{T}$ is small (it equals 4) and the splitting of the 3d levels has to be studied in the next orders of the asymptotic expansion. In [45] we mention too small energy gap between $1e$ and $2f_2$ states originated from the 3d atomic levels in tetrahedral cavities even of relatively small sizes. For our discussion it is sufficient to notice that the small splitting of these levels makes them very sensitive to a variety of other factors that can be seen from discussion at the end of Sect. 2.2.4.

It is also worth noting that (2.28) and (2.9) look naturally in the context of the method presented in Sect. 2.3.3 (see Eq. 2.21). There exists an intrinsic relation between the energy shifts or splittings and the behavior of the free system wave functions at the boundary.

2.4.3 Wave Functions Near the Boundary

One may find a large number of different relations for the energy shifts. For example, one may estimate the value $\varepsilon(\psi_j, \varphi_j)$ as it was described in Sect. 2.3.2. The resulting relation was known to Fröhlich [6] and later it was re-derived many times:

$$(E_j(\Omega) - E_j)\langle\psi_j|\varphi_j\rangle_\Omega = -\frac{1}{2}\int\limits_{\partial\Omega} \psi_j \partial_n \varphi_j d\sigma \tag{2.31}$$

In particular, one may note that for spherical cavities Ω the size increase is accomplished by convergence of $\langle\psi_j|\varphi_j\rangle_{\Omega(R)}$ to 1. Let us denote as $R_j(r|R)$ the radial parts of eigenfunctions of the Dirichlet problem normalized over the sphere with the weight factor r^2. Then (2.31) is immediately followed by the asymptotic relation

$$E_j(R) - E_j \cong -\frac{1}{2}r^2 R_j(r)\partial_r R_j(r|R)|_{r=R} \tag{2.32}$$

This equation is close to (2.27) where only free problem functions $R_j(r)$ are used. The detailed comparison of (2.27) and (2.33) clearly demonstrates an interesting relation, that was found in [73] on the basis of analysis of explicit asymptotic relations for radial functions. For the Dirichlet problem, one may write that the following asymptotic relation holds in the $R \to \infty$ limit:

$$\partial_r R_j(r|R)|_{r=R} \cong 2\partial_r R_j(r)|_{r=R} \; (R \to \infty) \tag{2.33}$$

It interesting that, for numerical estimates, Fröhlich used in [6] (see p. 946 near Eq. 6) the natural analog of this relation without the factor 2. The nature of this multiplier is clear from the simplified model that illustrates the discussion of [73]. Suppose that the Schrödinger equation has two solutions, one of which $R(r)$ decreases exponentially, while the other one grows exponentially. For large R values, one may write the solution of the Dirichlet problem in the form

$$R(r|R) \approx C[\exp(-\alpha r) - \exp(-2\alpha R)\exp(+\alpha r)] \tag{2.34}$$

The coefficient C is defined by normalization condition and may be thought to be a constant. The coefficient at the growing exponent is defined by the Dirichlet condition at the point R. It is evident that relation (2.33) holds indeed, as:

$$\partial_r R(r|R)|_{r=R} \approx 2C[-\alpha\exp(-\alpha R)] \approx 2\partial_r R(r)|_{r=R} \tag{2.35}$$

Surprisingly, although the convergence of the sequence of energies and the norm-convergence of functions is insufficient to ensure the pointwise convergence for the functions or their derivatives, and such groundless conclusions are dangerous (see, e.g. (2.33) as an example, or [82, 83]), relation (2.33) may be obtained by using the optimal cutting function (see the text before Eq. 2.27).

For the hydrogen atom in a spherical cavity, asymptotics of wave functions are known. The use of estimates for the radial functions from [41, 71] immediately gives the following asymptotic relations

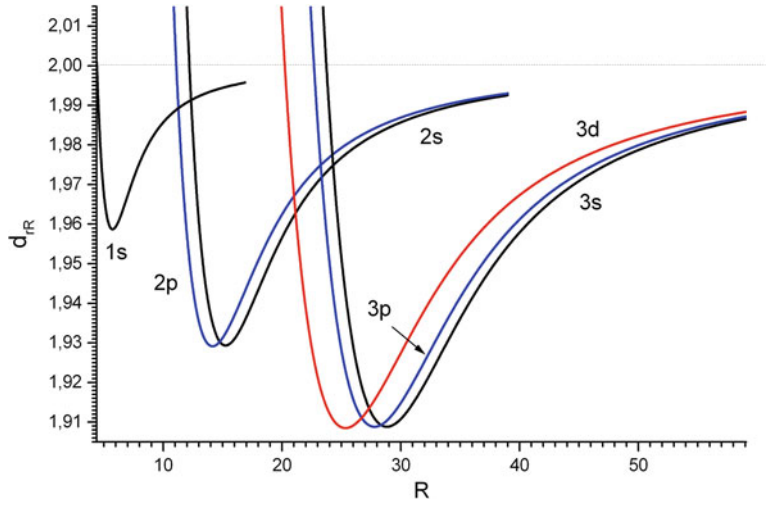

Fig. 2.3 The ratio of derivatives $d_{rR}(R)$ for radial wave functions of the hydrogen atom in the spherical cavity at the point r = R (au)

$$d_R(R) = \left.\frac{\partial_r R_{1s}(r|R)}{\partial_r R_{1s}(r)}\right|_{r=R} \cong 2 - \frac{2}{R} + \cdots \tag{2.36}$$

$$d_{rR}(R) = \left.\frac{\partial_r [rR_{1s}(r|R)]}{\partial_r [rR_{1s}(r)]}\right|_{r=R} \cong 2 - \left(\frac{1}{R^2} + \frac{5}{R^3} + \cdots\right) \tag{2.37}$$

Clearly, ratio (2.37) for the functions normalized with a unit weight seems to be more accurate for relatively small values of R. But even for the region R ~ 10 au, where the 1s-state wave function practically vanishes, both d_R and d_{rR} values are markedly different from 2. This is evident from the numerical representation of these ratios, presented in Fig. 2.3. Interestingly, the results of numerical estimations of the derivatives at the boundary are close to the relations presented for R > 7 au. Note that, in accordance with the energy ordering, among a group of states with the same principal quantum number value, the higher the angular momentum, the faster the limiting value 2 is approached.

For the case of general boundary conditions one may repeat all the calculations on the basis of energy estimates from [16]. For example, for the Neumann conditions (2.2) for R → ∞ one may state that $R_j(r|R)|_{r=R} \cong 2R_j(r)|_{r=R}$ [73].

2.5 Deformation of the Cavity of Large Size

2.5.1 The Basic Relations

Some almost obvious conclusions on the relative position of the energy levels of simple systems can be derived using the results for the spherical cavity. Let us consider the Dirichlet problem for cavities $\Omega(\lambda)$ that deform with the parameter λ changes. Let the point $\lambda = 0$ correspond to $\Omega(0) = \Omega$. The orthonormalized wavefunctions for the region $\Omega(\lambda)$ are denoted as $\varphi_k(\lambda)$; for $\lambda = 0$ we use the standard notations $\Omega(0) = \Omega$ and φ_k.

Differentiation of the identity

$$\varepsilon(\varphi_j, \varphi_k(\lambda)) - E_k(\Omega(\lambda))\langle\varphi_j|\varphi_k(\lambda)\rangle = 0 \tag{2.38}$$

with respect to the parameter λ gives immediately (by using the Green's formula) a simple relation that may be written for $\lambda = 0$ as follows:

$$\begin{aligned}\partial_\lambda E_k(\Omega)\langle\varphi_j|\varphi_k\rangle = \\ = \frac{1}{2}\int\limits_{\partial\Omega} \partial_n\varphi_j\partial_\lambda\varphi_k d\sigma + [E_j(\Omega) - E_k(\Omega)]\langle\varphi_j|\partial_\lambda\varphi_k\rangle\end{aligned} \tag{2.39}$$

where the symbols $\partial_\lambda\varphi_k$ and $\partial_\lambda E_k(\Omega)$ denote the derivatives $\partial_\lambda\varphi_k(\lambda)$ and $\partial_\lambda E_k(\Omega(\lambda))$ at the point $\lambda = 0$. One may suppose that, under small deformation of the cavity, the point $\mathbf{z} \in \partial\Omega$ moves in the direction of the outer normal $\mathbf{n}$ to $\partial\Omega$ at the point $\mathbf{z}$ and transforms to the point $\mathbf{z} + \rho(\mathbf{z})\mathbf{n}d\lambda$. Then differentiation of the Dirichlet condition $\varphi_k(\mathbf{z}(\lambda), \lambda) = 0$ at the point $\lambda = 0$ allows one to estimate

$$\partial_\lambda\varphi_k = -\rho\partial_n\varphi_k \quad \text{for} \quad \mathbf{z} \in \partial\Omega \tag{2.40}$$

(see the details, e.g. in [72] or [16]). Hence the orthogonality of the functions φ_k implies the simple relation

$$\partial_\lambda E_k\delta_{jk} = -\frac{1}{2}\int\limits_{\partial\Omega} \rho\partial_n\varphi_j\partial_n\varphi_k d\sigma + [E_j(\Omega) - E_k(\Omega)]\langle\varphi_j|\partial_\lambda\varphi_k\rangle \tag{2.41}$$

Note that the functions $\{\varphi_k\}$ in (2.41) are *the limits* of the functions $\{\varphi_k(\lambda)\}$ when $\lambda \to 0$. It means, for example, that for an *arbitrary* set of M degenerated functions with the same energy one has to calculate the $M \times M$ matrix $\mathbf{G}$ with the elements

$$G_{jk} = -\frac{1}{2}\int\limits_{\partial\Omega} \rho\partial_n\varphi_j\partial_n\varphi_k d\sigma \tag{2.42}$$

and diagonalize it to find the derivatives $\partial_\lambda E_k$ as eigenvalues of the matrix $\mathbf{G}$; the corresponding eigenvectors define linear combinations for which Eq. (2.41) holds. (Similar constructions are usual for perturbation theory for degenerate energy levels. Here is one of variants of such constructions).

Relation (2.41) in a slightly modified form is described in a large number of works, for example, [6, 84]. Note that for degenerate states, the second term in Eq. (2.41) vanishes.

2.5.2 Example: Expansion of a Spherical Cavity

For a large enough spherical cavity, one may use relations of Sect. 2.5.1 in combination with the asymptotical relations (2.33). For example, one may consider the expansion of the spherical cavity using R as the parameter. It is clear that the normal derivative to a sphere is the derivative with respect to the radial variable. Orthogonality of the spherical harmonics means that for a degenerate set of states with a given angular momentum one may write (see the text near Eq. 2.29)

$$\partial_R E_{n\ell} \cong G_{n\ell,n\ell} \cong -\frac{2}{n^2} B_{n\ell}^2 R^{2n} e^{-2R/n} \tag{2.43}$$

In agreement with Eq. (2.27), this relation is followed by

$$E_{n\ell}(R) = E_{n\ell}(\infty) - \int_R^\infty \partial_r E_{n\ell}(r)dr \cong E_{n\ell} + \frac{B_{n\ell}^2}{n} R^{2n} e^{-2R/n} \tag{2.44}$$

In particular, it is clear that the $B_{n\ell}$'s (2.29) define the state ordering in large cavities. The higher the ℓ, the smaller is $B_{n\ell}$. That is, the atomic states are ordered according to the decrease of the angular momentum (see Eq. 2.5). This statement is popular in the literature and may be explained by a variety of arguments [17, 41, 81]. It is presented here to explain the main ideas of the next subsections.

2.5.3 Asymptotically Degenerate States

When one considers the deformation of a very large cavity, relation (2.41) deserves more careful treatment. For example, for the hydrogen atom one has to consider the whole group of the asymptotically degenerate states with the same principal quantum number. Only for the case considered in Sect. 2.5.2 may one analyze states with different angular moments in the independent way due to the spherical symmetry of the problem.

When Ω is a sphere (or a slightly deformed sphere) of large radius R, one may use relations (2.33) to see that the contribution of the matrix **G** in the right hand side of Eq. (2.41) is of the same order as the energy shifts or their derivatives. But there exists one more term in the right hand side of this equation. The energy difference $E_j(\Omega) - E_k(\Omega)$ vanishes for the states corresponding to the strictly degenerate energy level, but for a large enough region Ω this difference has the same order as the energy shifts and one may suppose it to be of approximately the same order as the energy shifts under consideration. This means that in the general case, one has to consider all the terms in Eq. (2.41).

In general, it is difficult to describe all the features of the wave function changes under deformations of the cavity. But it is possible when the states studied are localized mainly near the potential center, while the main changes in the densities are localized near the boundary. The examples of optimal cutting functions for similar problems [16, 39] confirm this statement. One may suppose the essential changes in $\partial_\lambda \varphi_k$ mainly in the region $|r| > \gamma R$, for some linear size R of the cavity. It means that one may suppose that for large enough cavity size, the matrix elements $\langle \varphi_j | \partial_\lambda \varphi_k \rangle$ are small and decrease to zero with the cavity extension. But this is the case when the last term in the right hand side of Eq. (2.41) vanishes asymptotically in comparison with the first term.

For the situation considered one may reduce the derivative calculations to evaluation of the **G** matrix for *all* asymptotically degenerate states. For example, for the one-electron atom, one should calculate the matrix **G** in the basis of the states ns, np, nd, … simultaneously. Nevertheless, it is difficult to exclude situations when the splitting of the states with different angular momenta is essential and it is desirable to consider also the splitting of the states with a given angular momentum separately.

2.5.4 The Polyhedral Deformation of the Sphere

Now we are ready to study the state ordering for the polyhedral deformations of the large spherical cavity Ω of radius R. We consider the set of similar polyhedrons P (x) with the same center and parallel faces. The dimensionless parameter x describes extension of polyhedrons from inscribed in the sphere (for x = 0) to circumscribed around the sphere Ω (for x = 1). One may define the set of regions $\Omega^*(x) = \Omega \cap P(x)$ that may be considered as polyhedrons with vertices smoothed by the sphere or as a result of the "polyhedral" truncation of the sphere.

It would be interesting to analyze the changes in the hydrogen atom spectrum for the nucleus placed in the centre of an impenetrable cavity $\Omega^*(x)$. But we cannot use explicit relations for wavefunction derivatives on $\partial\Omega^*(x)$ and solve here another problem that may be considered as the sphere deformation "in the direction of the region $\Omega^*(x)$".

For a pair of points $\mathbf{z} = R\mathbf{m}$ on ∂Ω and $\mathbf{z}^* = Rq(\mathbf{m}, x)\mathbf{m}$ on $\partial\Omega^*(x)$ we consider the deformation family Ω(λ, x) by the relation $\mathbf{z}(\lambda) = (1 - \lambda)\mathbf{z} + \lambda\mathbf{z}^*$ for the boundary ∂Ω(λ, x). It means that, in relations (2.40)–(2.42), one may use the function

$$\rho(\mathbf{z}) = R(\mathrm{q}(\mathbf{m}, \mathrm{x}) - 1) = R\rho_0(\mathbf{m}, \mathrm{x}) \tag{2.45}$$

In order to calculate the matrix elements of $\mathbf{G}$ (see Eq. 2.42) for the hydrogen atom, it is sufficient to use ρ_0 and spherical harmonics $\mathrm{Y_k}$ only. The radial functions are the same and may be omitted to analyze the energy level splitting (it may be considered as the use of a specific scale). That is, for each x we calculate the matrix $\mathbf{\Lambda}$ with elements defined as

$$\Lambda_{\mathrm{kj}} = -\mathrm{B}_{\mathrm{n}\ell_\mathrm{k}}\mathrm{B}_{\mathrm{n}\ell_\mathrm{j}} \int \mathrm{Y}_\mathrm{k}^* \mathrm{Y}_\mathrm{j}\, \rho_0(\mathbf{m}, \mathrm{x})\mathrm{d}\omega \tag{2.46}$$

The energy derivatives (2.41) are proportional to the eigenvalues Λ_j of this matrix.

It is clear that, due to relation $\Omega^*(\mathrm{x}) \subseteq \Omega$, the energy derivatives with respect to λ are nonnegative. When the energy levels for large enough region Ω are considered as degenerate or almost degenerate, it is clear that the bigger the derivative Λ_j, the higher is the energy of the corresponding atomic state.

The results of the $e - f_2$ splitting in derivatives that may be attributed to the components of the 3d-state are presented for the hydrogen atom in Fig. 2.4 for different cavities $\Omega^*(\mathrm{x})$. We consider the families of the cavities defined by classical polyhedrons: cube, octahedron and tetrahedron.

Recall that, in the case of the cavities of the symmetry type O_h [cube, octahedron and associated families $\Omega^*(\mathrm{x})$], there exists parity that distinguishes the 3d and 3p

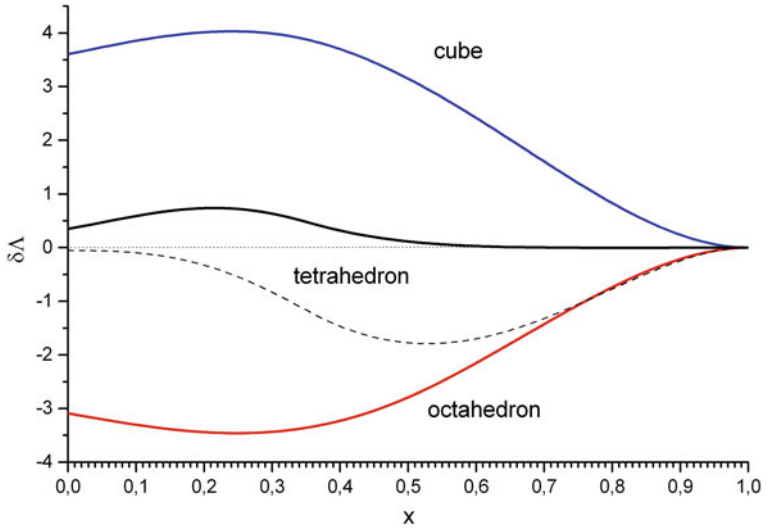

Fig. 2.4 The differences $\delta\Lambda = \Lambda(e) - \Lambda(f_2)$ for the sphere deformations "in the direction $\Omega^*(\mathrm{x})$" in relative units. The *solid lines* describe the difference for the system of states {3s, 3p, 3d}; the *dashed line* corresponds to the pure 3d-state in the tetrahedral family of cavities

states. But for tetrahedral systems, there is an essential difference between the splitting in the case of almost-degenerate 3s, 3p, 3d states and selected 3d states. As is clear from the Fig. 2.4 the interaction with 3p states drastically changes the splitting of the atomic 3d state and sometimes it is negligible. This observation can also be tied with the conclusions made on the basis of asymptotic estimates in Sect. 2.3 (see also Table 2.1 and the end of Sect. 2.1). Crudely speaking, for the 3d state, the levels are ordered in tetrahedral case so that the e level is below the f_2 one, but the 3p state of the same type f_2 shifts the lowest f_2 state below the e level.

One should stress the similarity of Eqs. (2.30) and (2.46), especially for the region $x \approx 1$.

2.6 Further Insights

Discussion of the problems of the relative positions of the energy levels of atomic and molecular systems in cavities of different types stimulates a lot of further insights of interaction between the system and the environment. The most serious problems here are those concerning the structured nature of the surrounding medium. This area is developing nowadays especially rapidly. In this regard, more sophisticated models were formulated, based on the use of systems of point charges or distributed multipoles, also taking into account the effects of polarization and short-range interactions [85]. One could also mention different embedded cluster and periodic models for a localized inhomogenity in an extended medium which are increasingly used in practice, especially within the Density Functional Theory (DFT) framework. See, e.g. the comprehensive reviews [86, 87] and references therein for further details.

However, even in the simplest one-electron models new effects arise, e.g. when considering a potential model with finite height walls. For example, in the case of the hydrogen-like system in a cylindrical cavity, there were cases when the wave functions were pushed out of the too-small potential well [88]. It is interesting to note that similar effects occur in many-electron atoms [89] because the behavior of the wave functions inside and outside of the potential well in the field of the other electrons is considerably different [90].

Another kind of serious problems is associated with displacement of the atomic nucleus or other force center away from the highly-symmetric position in the cavity. Qualitative methods for this sort of problems were described, in particular, for cavities of small size, for spherical cavities [48], for cylindrical cavities [68, 91], for cubic [44], tetrahedral and similar cavities [45]. On the methods useful for icosahedral systems, see [92].

Many years ago [93–95] the energy changes were estimated for the hydrogen nucleus shifted from the center to the points of the cavity boundary for the quantum wire of square section. In this case, the results are almost evident when one uses the simple model [96], initially proposed to describe the atomic states on the surface.

For example, it is evident that when the nucleus is placed on the impenetrable plane, the 2p-orbital oriented in the direction of its normal defines the ground state. Indeed, this function is the solution of the Schrödinger equation that satisfies the Dirichlet boundary conditions in the half-space and has no nodal surfaces (except for the Dirichlet boundary). Similar considerations are very useful for the purpose of qualitative analysis. One may consider approaches of this sort as a clever development of ideas of classical works [97, 98] in which the energy of systems with spatial restrictions was assessed using the known energy values of the states of a free system, the wave functions of which have nodes in the right places. For more complex situations, but for the ground state only, one may use the simple geometric method proposed in [99] on the basis of some of comparison theorems [100].

In principle, for the study of the nuclear shift effects in degenerated states of atomic systems in a cavity, it would be natural to use the Jahn-Teller theorem (on its proof and some connected problems see also [101, 102]). Obviously, for the atomic system in the cavity of a fixed form, there are not more than three nuclear displacements that could be Jahn-Teller active in a conventional sense, while there exist a lot of asymmetrical cavity deformations that would play a similar role here.

2.7 Conclusion

In the present work, we have considered the simplest effect of symmetry reduction, namely, the splitting of degenerate energy levels of some model systems like the hydrogen atom or the isotropic harmonic oscillator under transition from a free system to a system in the cavity. Special attention was paid to the cavities of a large size. In some cases, the asymptotic analysis of the splitting was proposed. It was demonstrated that the observed energy level ordering in cavities results from interplay of numerous factors and the relative positions of the energy levels could change significantly with variations of the cavity shape within the fixed point symmetry group.

The problems discussed here are closely related to those often encountered within the Crystal Field Theory. However, the laws of the energy levels splitting are determined by similar but slightly different relations. For example, relations like Eq. (2.9) or (2.28) for cavities of a large size are reminiscent of the formulas of the Crystal Field Theory. But to study the splitting of levels of an atom in a polyhedral cavity, one should consider not the positions of the polyhedron vertices, but the positions of the touch points for the faces and the inscribed sphere. For regular polyhedra, these points specify the location of the vertices *of the dual polyhedron*. This circumstance itself leads to some peculiarities of the problem when one tries to compare the state ordering for atoms in polyhedral cavities and for the same atoms surrounded by systems of point charges.

Another important detail is a need for analysis of a number of sets of degenerate states with a given angular momentum in some cases and quasi-degenerated groups of states. In the case of cubic or octahedral systems, it has no essential influence on

the structure of the energy levels. For tetrahedral cavities, on the contrary, this is an additional complication, leading to inversion of the state ordering in some cases.

Obviously, a more consistent consideration of the effects of spatial restrictions on the motion of particles, taking into account all degrees of the freedom of the system and estimating, e.g. the transition probabilities, is desirable. As an example, the fully-dimensional quantum-mechanical problem of a hydrogen atom in a spherical cavity, studied numerically in [50], has been already mentioned. Implementation of the same ideas for more complicated cavities (and, perhaps, for more realistic models for the environment) requires, even in one-electron case, further development of more powerful and efficient tools for the analysis of the boundary value problems for the molecular Schrödinger equation.

Acknowledgments The authors are grateful to Prof. H.E. Montgomery for valuable discussions and comments on the text. The work was financially supported by the Russian Foundation for Basic Research (projects 10-03-00665-a and 13-03-00640-a)

References

1. Wigner E, Seitz F (1933) Phys Rev 43(10):804–810
2. Wigner E, Seitz F (1934) Phys Rev 46(6):509–524
3. Brillouin L (1937) Compt Rend 204:1863–1865
4. Frohlich H (1937) Proc Roy Soc (London) Ser A, Math Phys Sci 158(893):97–110
5. Bardeen J (1938) J Chem Phys 6(7):372–378
6. Froehlich H (1938) Phys Rev 54(11):945–947
7. Al-Hashimi MH, Wiese U-J (2012) Ann Phys 327(11):2742–2759
8. Al-Hashimi MH, Wiese U-J (2012) Ann Phys 327(1):1–28
9. Michels A, de Boer J, Bijl A (1937) Physica 4(10):981–994
10. Pang H, Dai W-S, Xie MJ (2011) Phys A: Math Theor 44(36):365001 (19 pp)
11. Jaskólski W (1996) Phys Rep 271(1):1–66
12. Ley-Koo E (2009) Theory of confined quantum systems: part one. In: Sabin JR, Brändas E, Cruz SA (eds), Special edition. Academic Press, USA, (Adv Quant Chem 57), pp 79–122
13. Sveshnikov K, Roenko A (2013) Physica B 427:118–125
14. Cruz SA (2009) Theory of confined quantum systems: part one. In: Sabin JR, Brändas E, Cruz SA (eds), Special Edition. Academic Press, USA (Adv Quant Chem 57), pp 255–283
15. Fowler PW (1984) Mol Phys 53(4):865–889
16. Sen KD, Pupyshev VI, Montgomery HE (2009) Theory of confined quantum systems: part one. In: Sabin JR, Brändas E, Cruz SA (eds), Special edition. Academic Press, USA, (Adv Quant Chem 57), pp 25–77
17. Scherbinin AV, Pupyshev VI, Ermilov AY (1998) Physics of clusters. In: Lakhno VD, Chuev GN (eds), World scientific, Singapore. pp 273–292
18. Pupyshev VI (2000) Rus J Phys Chem 74(1):50–54 (Engl transl)
19. Shcherbinin AV, Pupyshev VI (2000) Rus J Phys Chem 74(2):292–295 (Engl transl)
20. Stevanović L, Sen KD (2008) J Phys A: Math Theor 41(26):265203(14 pp)
21. Stevanović L, Sen KD (2008) J Phys B: At Mol Opt Phys 41(22):225002 (6 pp)
22. Dolmatov VK (2009) Theory of confined quantum systems: part one. In: Sabin JR, Brändas E, Cruz SA (eds), Special edition. Academic Press, USA, (Adv Quant Chem 57). pp 13–68
23. Movilla JL, Planelles J (2005) Comp Phys Commun 170(2):144–152

24. Baltenkov AS, Becker U, Manson ST, Msezane AZ (2010) J Phys B: At Mol Opt Phys 43 (11):115102 (9 pp)
25. Cross RJ (2008) J Phys Chem A 112(31):7152–7156
26. Korol AV, Solov'yov AV (2010) J Phys B: At Mol Opt Phys 43(20):201004
27. Bersuker I (2010) Electronic structure and properties of transition metal compounds: introduction to theory. Wiley, New York
28. Flurry RL (1980) Symmetry groups. Theory and chemical applications. Prentice-Hall, Englewood Cliffs
29. Ballhausen CJ (1962) Introduction to ligand field theory. McGraw-Hill, New York
30. Van Vleck JH (1939) J Chem Phys 7(7):72–84
31. Kleiner WH (1952) J Chem Phys 20(11):1784–1791
32. Julg A, Julg O (1985) Canad J Chem 63(7):1955–1959
33. Landau LD, Lifshitz EM (1977) Quantum mechanics: non-relativistic theory, vol 3. Pergamon Press, Oxford
34. Pupyshev VI, Scherbinin AV (1998) Chem Phys Lett 295:217–222
35. Pupyshev VI, Scherbinin AV (2002) Phys Lett A 299(4):371–376
36. Montgomery HE, Aquino NA, Sen KD (2007) Int J Quant Chem 107(4):798–806
37. Stevanović L, Sen KD (2008) J Phys B: At Mol Opt Phys 41(20):205002 (9 pp)
38. Reed M, Simon B (1978) Methods of modern mathematical physics, vol 4: analysis of operators. Academic Press, New York
39. Pupyshev VI, Scherbinin AV (1999) J Phys B: At Mol Opt Phys 32(19):4627–4634
40. Pupyshev VI, Scherbinin AV, Stepanov NF (1997) J Math Phys 38(11):5626–5633
41. Laughlin C (2009) Theory of confined quantum systems: part one. In: Sabin JR, Brändas E, Cruz SA (eds), Special edition. Academic Press, USA, (Adv Quant Chem 57). pp 203–239
42. Wigner EP (1954) Phys Rew 94(1):77–78
43. de Bruijn NG (1958) Asymptotic methods in analysis. North-Holland Pub Co, Amsterdam)
44. Kretov MK, Scherbinin AV, Pupyshev VI (2009) Phys Scripta 80(4):048125 (4 pp)
45. Pupyshev VI (2011) Int J Quant Chem 111(11):2510–2518
46. Motapon O, Ndengue SA, Sen KD (2011) Int J Quant Chem 111(15):4425–4432
47. Aquino N (2009) Theory of confined quantum systems: part one. In: Sabin JR, Brändas E, Cruz SA (eds), Special edition. Academic Press, USA, (Adv Quant Chem 57). pp 123–171
48. Changa ME, Scherbinin AV, Pupyshev VI (2000) J Phys B: At Mol Opt Phys 33(3):421–432
49. Ciftci H, Hall RL, Saad N (2009) Int J Quant Chem 109(5):931–937
50. Changa ME, Scherbinin AV, Pupyshev VI (2004) Int J Quant Chem 96(2):167–174
51. Pupyshev VI, Bobrikov VV (2004) Int J Quant Chem 100(4):528–538
52. Bobrikov VV, Pupyshev VI (2005) Rus Chem Bull 54(1):55–61 (Engl transl)
53. Colín-Rodríguez R, Cruz SA (2010) J Phys B: At Mol Opt Phys 43(23):235102 (10 pp)
54. Sarsa A, Le Sech C (2012) J Phys B: At Mol Opt Phys 45(20):205101 (7 pp)
55. Korol AV, Solov'yov AV (2011) J Phys B: At Mol Opt Phys 44(8):085001 (17 pp)
56. Fernández FM, Aquino N, Flores-Riveros A (2012) Int J Quant Chem 112(3):823–828
57. Wilson CL, Montgomery HE, Sen KD, Thompson DC (2010) Phys Lett A 374 (43):4415–4419
58. Le Sech C, Banerjee A (2011) J Phys B: At Mol Opt Phys 44(10):105003 (9 pp)
59. Kirkwood JG (1932) Phys Z 33(2):57–60
60. Montgomery HE, Pupyshev VI (2013) Eur Phys J H 38(4):519–534
61. Gorecki J, Byers-Brown W (1987) J Phys B: At Mol Opt Phys 20(22):5953–5957
62. Gorecki J, Byers-Brown W (1989) J Phys B: At Mol Opt Phys 22(17):2659–2668
63. Gallardo J, Mattis D (1979) Phys Stat Sol (b) 93(1):229–235
64. Liu Z, Lin DL (1983) Phys Rew B 28(8):4413–4418
65. Singh KK (1964) Physica 30(1):211–222
66. Barton G, Bray AJ, McKane AJ (1990) Am J Phys 58(8):751–755
67. Epstein ST (1974) The variational method in quantum chemistry. Academic Press, New York
68. Yurenev PV, Scherbinin AV, Pupyshev VI (2008) Int J Quant Chem 108(14):2666–2677
69. Hull TE, Julius RS (1956) Can J Phys 34(9):914–919

70. Laughlin C, Burrows BL, Cohen M (2002) J Phys B: At Mol Opt Phys 35(3):701–715
71. Laughlin C (2004) J Phys B: At Mol Opt Phys 37(20):4085–4099
72. Berman DH (1991) Am J Phys 59(10):937–941
73. Wilcox W (2000) Ann Phys 279:65–80
74. Núñez MA (1995) Int J Quant Chem 53(1):15–25
75. Núñez MA (1994) Int J Quant Chem 50(2):113–134
76. Núñez MA (1997) Int J Quant Chem 62(5):449–460
77. Stevanović L (2010) J Phys B: At Mol Opt Phys 43(16):165002 (11 pp)
78. Eckart C (1930) Phys Rev 36(5):878–892
79. Katriel J (1983) Int J Quant Chem 23(5):1767–1780
80. Löwdin P-O (1959) Adv Chem Phys 2:207–322
81. Wilcox W (1989) Am J Phys 57(6):526–528
82. Klahn B, Bingel WA (1977) Theor Chim Acta 44:9–26
83. Núñez MA, Piña E (1998) Phys Rev A 57(2):806–814
84. Gonda I, Gray BF (1975) J Chem Soc, Faraday Trans Ser 2: Molec Chem Phys 71:2016–2024
85. Gordon MS, Freitag MA, Bandyopadhyay P, Jensen JH, Kairys V, Stevens WJ (2001) J Phys Chem A 105(2):293–307
86. Jug K, Bredow T (2004) J Comput Chem 25(13):1551–1567
87. Huang P, Carter EA (2008) Annu Rev Phys Chem 59:261–290
88. Bryant GW (1984) Phys Rev B 29(12):6632–6639
89. Connerade JP, Dolmatov VK (1998) J Phys B: At Mol Opt Phys 31(16):3557–3564
90. Dolmatov VK, King JL (2012) J Phys B: At Mol Opt Phys 45(22):225003 (5 pp)
91. Yurenev PV, Scherbinin AV, Pupyshev VI (2006) Int J Quant Chem 106(10):2201–2207
92. Nikolaev AV, Plakhutin BN (2010) Russ Chem Rev 79(9):729–755
93. Bryant GW (1985) Phys Rev B 31(12):7812–7818
94. Bastard G (1981) Phys Rev B 24(8):4714–4722
95. Brum JA (1985) Solid State Commun 54(2):179–181
96. Levine JD (1965) Phys Rev 140(2A):A586–A589
97. Sommerfeld A, Welker H (1938) Ann Phys 32(F 5):56–65
98. Sommerfeld A, Hartmann H (1940) Ann Phys 37(F 5):333–343
99. Pupyshev VI (2000) J Phys B.: At Mol Opt Phys 33(5):961–970
100. Hoffmann-Ostenhof T (1980) J Phys A: Math Gen 13(2):417–424
101. Pupyshev VI (2005) Int J Quant Chem 104(2):157–166
102. Pupyshev VI (2007) Int J Quant Chem 107(6):1446–1453

Chapter 3
The Confined Hydrogen Atom Revisited

N. Aquino and A. Flores-Riveros

3.1 Introduction

The present work is intended to be a continuation of the chapter "The hydrogen and helium atoms confined in spherical boxes", published in *Advances in Quantum Chemistry* (AQC), Vol. 57 (2009). Although many of the methods used in the confined hydrogen atom studies were reviewed in that chapter, we here describe some of the contributions that were not included in that review. It should be noted that volumes 57 and 58 of the AQC were dedicated to the study and applications of a variety of quantum confined systems.

The present work is based on two recently published articles: In the first, we consider a hydrogen atom confined in spherical impenetrable boxes of various dimensions, taking into account the nuclear motion, where the Hamiltonian contains the kinetic energy corresponding to two charged particles of different masses. In the second, we have computed the Shannon and Fisher entropies for the ground state of a hydrogen atom confined in soft spherical boxes of varying radius. In previous works, these entropies have been shown to be associated with some interesting physical properties.

The organization of this chapter is as follows: In Sect. 3.2, a brief description is given of the various model potentials used to confine the hydrogen atom in a spherical box. In Sect. 3.3, we discuss the confined hydrogen atom where the nucleus is allowed to move inside a spherical box of hard walls by using the variational method. Section 3.4 is devoted to the analysis of Shannon and Fisher

N. Aquino (✉)
Departamento de Física, Universidad Autónoma Metropolitana-Iztapalapa, Apartado Postal 55-534, 09340 México, D.F., Mexico
e-mail: naa@xanum.uam.mx

A. Flores-Riveros
Instituto de Física, Benemérita Universidad Autónoma de Puebla, Apartado Postal J-48, 72570 Puebla, PUE, Mexico

K.D. Sen (ed.), *Electronic Structure of Quantum Confined Atoms and Molecules*,
DOI 10.1007/978-3-319-09982-8_3

entropies as obtained for the ground state of an H atom spherically confined in penetrable boxes of varying size and strength. Finally, in Sect. 3.5 we give our conclusions.

3.2 An Overview

Because of a wide variety of applications in physics and chemistry, there has been a growing interest in the study of quantum confined systems [1–13]. Atoms and molecules confined by cavities of different geometrical forms and dimensions [14–17] have been used to study the electronic structure, chemical reactivity and ionization potentials of those systems under very high pressures [1–20] or, for example, when embedded into fullerenes, and also to model zeolite molecular sieves [21]. The confined harmonic oscillator has been used to model electrons in a quantum dot [22, 23], quantum wells and quantum wires, where electric and magnetic properties as well as the specific heat of metals can be analyzed [24].

Hydrogen atom represents the simplest and most frequently analyzed atomic system under confinement. It has been studied when inside a spherical box of penetrable or impenetrable walls [1–13] and in hard boxes of different geometrical forms and varying size. The hydrogen atom confined in a spherical box and the free hydrogen atom, have both exact solutions [2]. Many efforts have been devoted to finding approximate analytical and numerical solutions and comparing their accuracy to the exact solution. The helium atom spherically confined by hard walls is the simplest system where the role played by electron correlation can be systematically studied. However, all studies of the confined helium atom have been restricted to the ground and a few excited states. On the other hand, the analysis of many electron atoms has been carried out by using a variety of approximate methods [9] such as pseudopotential method, Hartree-Fock, CI, Fermi statistical method, DFT, and recently, the variational and diffusive quantum Monte Carlo methods [12].

In the late 70s, Ley-Koo and Rubinstein proposed a model in which the hydrogen atom is confined in a soft spherical box of radius r_c. They aimed at explaining the ionization of a hydrogen atom trapped in the α quartz as experimentally observed [25].

The Hamiltonian of the system is given by

$$H = -\frac{1}{2}\nabla^2 + V_c,$$

where the potential is defined as

$$V_c = \begin{cases} -1/r; & 0 \le r \le r_c \\ V_0; & r_c < r\infty \end{cases}.,$$

in which V_0 is a barrier with a constant height value. When $V_0 \to \infty$ the barrier becomes impenetrable and the particle cannot escape from it. Being V_c a central potential, the problem has a well defined angular momentum where the solution to the time independent Schrödinger equation $H\psi = E\psi$ can be written as

$$\psi_{Elm}(r, \theta, \phi) = R_{El}(r) Y_{l,m}(\theta, \phi)$$

By Substituting this solution in the above Schrödinger equation, one is led to the radial Schrödinger equation

$$-\frac{1}{2}\frac{1}{r^2}\frac{d}{dr}\left(r^2 \frac{dR_{El}}{dr}\right) + \frac{l(l+1)R_{El}}{2r^2} + V_c R_{El} = E R_{El}$$

Ley-Koo and Rubinstein separated the problem in an *interior region* (*i*), $0 \leq r \leq r_c$, and an *exterior region* (*e*), $r_c < r < \infty$, and found the solution of the radial Schrödinger equation in each.

For the interior region they expand the solution as a power series

$$R_{El}^{(i)}(x) = A_l \, x^l \sum_{s=0}^{\infty} c_s^{(l)} x^s,$$

where A_l is a normalization constant and

$$x = \frac{r}{\kappa}, \quad \kappa = \pm\frac{1}{2E},$$

whereas for the exterior region they found

$$R_{El}^{(e)} = B_l \, y^{-(l+1)} e^{-y} \, {}_1F_1(-l; -2l; 2y),$$

in which B_l is a normalization constant, ${}_1F_1$ is the confluent hypergeometric function, $y = kr$ and $k^2 = 2(V_0 - E)$.

Ley-Koo and Rubinstein computed the energy for a few of the lowest states as a function of r_c and the barrier height V_0. They also calculated the polarizability, the Fermi contact term, the screening constant and pressure as a function of r_c and V_0.

Montgomery and Sen, following the work of Ley-Koo and Rubinstein, improved the accuracy attained by these authors in their calculations, where the energies are determined by imposing continuity of the wave function and its derivative at $r = r_c$. Montgomery and Sen noted that the continuity condition at $r = r_c$ is more easily accomplished by matching the logarithmic derivatives at $r = r_c$. By taking the difference between the logarithmic derivatives of $R_{El}^{(i)}(r)$ and $R_{El}^{(e)}(r)$ at $r = r_c$, the problem of finding the energy eigenvalues is replaced by the search of roots—which are precisely the energy eigenvalues—of a transcendental function. They used the Maple program to perform the numerical computation of the energy eigenvalues

and reported their results with a 15-digit accuracy, thereby establishing a benchmark for this system. The wave functions are determined by imposing their continuity through $r = r_c$ and are also normalized.

They calculated the $1s$ state dipole polarizability $\alpha(v)$ at frequency v in the frame of perturbation theory (PT)

$$\alpha(v) = \sum_{n=2} \frac{f_{np}}{\left(E_{np} - E_{1s}\right)^2 - (hv)^2},$$

where f_{np}, is the oscillator strength for the $1s - np$ transitions,

$$f_{np} = \frac{2}{3}\left(E_{np} - E_{1s}\right)\left[\int_0^{r_c} R_{np}^{(i)} r R_{1s}^{(i)} r^2 dr + \int_{r_c}^{\infty} R_{np}^{(e)} r R_{1s}^{(e)} r^2 dr\right]^2.$$

Since the radial functions are power series, all integrals are obtained analytically. They showed that in order to calculate f_{np} it suffices to consider the discrete spectrum only.

Montgomery and Sen computed the static and dynamic polarizabilties for a few combinations of r_c and V_0. For finite potentials they found that the static polarizability is strongly dependent on r_c, which decreases as the cavity dimension diminishes. On the other hand, for a fixed value of r_c, the polarizability was found to decrease as V_0 grows. Their numerical results are considered benchmark calculations for this system.

Recently [13], the Ley-Koo-Rubinstein Hamiltonian was solved numerically by using the finite difference method, where the wave function is defined on a grid and the oscillator strength, together with transition probabilities, are calculated for a few states.

The endohedral fullerenes are systems in which atoms or small molecules are confined in the cage of the carbon structure $C_n (n \geq 20)$. The interest of studying these systems stems from a variety of applications they give rise to, from medicine to quantum computation. The study of the electronic structure of endohedral fullerenes is performed including all electrons treated via DFT or semi-empirical methods. Nascimento et al. considered the guest atom electrons only and they model the C_n by means of a short-range spherical Gaussian potential. They study the confined H atom in a cage of C_{30} and C_{60}, using the self-consistent finite-element method. The potential proposed by Nascimento et al. is given by

$$w(r) = -w_0 \exp\left[-(r - r_c)^2/\sigma^2\right],$$

where w_0 is the well depth, r_c is the radius of the center of the confinement shell and σ is defined as the half-width at the $w_0 e^{-1}$ amplitude. The r_c value is chosen so that it corresponds to the radius of the fullerene cage: 3.54 Å for C_{60} and 2.50 Å for C_{36}.

The other two parameters are obtained from theoretical and experimental information on fullerenes.

The Schrödinger equation for the H atom inside the fullerene is given by

$$\left[-\frac{1}{2}\nabla^2 - \frac{1}{r} + w(r)\right]\psi(\vec{r}) = E\psi(\vec{r}).$$

Katriel and Montgomery studied the virial for the hydrogen atom confined by various model potentials, penetrable and impenetrable, continuous and continuous to piece. The potential used by Ley-koo and Rubinstein becomes that of a hydrogen atom in a hard spherical box when V_0 goes to infinity. In this case the wave functions satisfy Dirichlet conditions. They have also solved the problem when the wave functions satisfy Neumann conditions. They also treated the problem of a hydrogen atom in a quantum dot that was proposed by Xiao and taken up by Varshni.

The Hamiltonian of the quantum dot atom is given by

$$H = -\nabla^2 - \frac{2}{r} + \omega r^2$$

Costa et al. added the Woods-Saxon potential

$$H = -\nabla^2 - \frac{2}{r} + \omega r^2 + \frac{2\lambda}{1 + epx[(R-r)/\eta]},$$

whereas Katriel and Montgomery modified the potential as

$$H = -\nabla^2 - \frac{2}{r} + \omega r^2 + \left(\frac{r}{R}\right)^k.$$

Zicovich-Wilson et al. studied the Hamiltonian

$$H = -\nabla^2 - \frac{2}{r} + \frac{1}{R}\cot\left(\frac{r}{R}\right)$$

In recent years, the following Hamiltonian has also been studied

$$H = -\nabla^2 - V_0 \exp\left[-\left(\frac{r}{R}\right)^2\right]$$

to model a quantum dot.

3.3 Variational and Perturbative Treatments of the Confined Hydrogen Atom with a Moving Nucleus

3.3.1 Introduction

The confined hydrogen atom has been treated considering hard and soft boxes of different geometrical shapes. In the case of an impenetrable spherical box the energy is known to be lowest when the nucleus is clamped at the origin, which increases as the nucleus is allowed to move toward the cavity surface. However, when the atom is in a real environment, this energy increase cannot be assumed to arise solely from the electron kinetic energy and its Coulomb interaction with the nucleus, but also from the latter interacting with the environment simulated by a particular confinement regime. As in the case of the particle in a box, we know that the nucleus cannot have zero energy and it should move because of its interaction with the surrounding cavity. Therefore, the fixed nucleus approach may not be the most realistic one to appropriately describe a compressed H atom, but rather, a model in which both the nucleus and the electron move within the box and are confined by the same boundary conditions.

We here calculate the ground state energy and other properties for a confined hydrogen atom where both electron and nucleus are allowed to move within an impenetrable spherical cavity, as a function of the box radius by using a variational method [26] and a perturbative approach. In the first treatment exponents and linear coefficients are variationally optimized via a generalized $\{r_e, r_n, r\}$-Hylleraas basis set that fulfills appropriate boundary conditions, whereas the second approach is based on an unperturbed exact solution for a pair of confined free particles. The variational results led to an increased kinetic energy and an enhanced Coulomb interaction arising from the nuclear motion, as compared to a variational description of the confined atom where the nucleus remains fixed. Throughout all box radii the variational energies are below those perturbatively obtained, however, the energy difference gets fairly reduced at the strong confinement region, which indicates that perturbation theory represents a physically consistent picture of the compressed atom due to the strongly free-particle behavior of the electron and nucleus at small cavity dimensions.

3.3.2 The Model

The Hamiltonian operator for a nonrelativistic hydrogen atom is

$$H = T + V = -\frac{\hbar^2}{2m_e}\nabla_e^2 - \frac{\hbar^2}{2m_n}\nabla_n^2 - \frac{e^2}{4\pi\varepsilon_0 r}, \tag{3.1}$$

where m_e and m_n are the masses of the electron and nucleus located at $\vec{r}_e$ and $\vec{r}_n$ with charges $-e$ and e, respectively, r = $|\vec{r}_e - \vec{r}_n|$ and ∇^2 denotes the Laplacian in the

coordinates indicated by the subscript. If the atom is confined to a spherical box of radius r_c with impenetrable walls then the states should vanish when either $|\vec{r}_e| = r_e = r_c$ or $|\vec{r}_n| = r_n = r_c$. In atomic units ($\hbar = m_e = e = 1$), the above Hamiltonian reads

$$H = -\frac{1}{2}\nabla_e^2 - \frac{1}{2m_n}\nabla_n^2 - \frac{1}{r} + U \tag{3.2}$$

where mass $m_n = 1836.15267261$ and the confining potential U is

$$U = \begin{cases} 0, & (r_e\,, r_n \leq r_c) \\ \infty, & (r_e\,, r_n > r_c). \end{cases} \tag{3.3}$$

3.3.3 Method of Calculation

3.3.3.1 Variational Treatment

Generalized Hylleraas basis sets expressed in $\{r_1 = r_e, r_2 = r_n, r_{12} = r\}$ coordinates

In Hylleraas $\{r_e, r_n, r\}$ coordinates, the Hamiltonian in Eq. (3.2) can be written as

$$\begin{aligned} H = &-\frac{1}{2}\left(\frac{\partial^2}{\partial r_e^2} + \frac{2}{r_e}\frac{\partial}{\partial r_e} + \frac{\partial^2}{\partial r^2} + \frac{2}{r}\frac{\partial}{\partial r} + 2\hat{r}_e \cdot \hat{r}\frac{\partial^2}{\partial r_e r}\right) \\ &-\frac{1}{2m_n}\left(\frac{\partial^2}{\partial r_n^2} + \frac{2}{r_n}\frac{\partial}{\partial r_n} + \frac{\partial^2}{\partial r^2} + \frac{2}{r}\frac{\partial}{\partial r} - 2\hat{r}_n \cdot \hat{r}\frac{\partial^2}{\partial r_n r}\right) \\ &-\frac{1}{r} + U \end{aligned} \tag{3.4}$$

where $\hat{r}_e$, $\hat{r}_n$ and $\hat{r}$ denote the unit vectors of the corresponding distances. Since $r^2 = |\vec{r}_e - \vec{r}_n|^2 = r_e^2 + r_n^2 - 2\vec{r}_e \cdot \vec{r}_n$, scalar product factors $\hat{r}_i \cdot \hat{r}$ $(i = e, n)$ yield

$$\begin{aligned} \hat{r}_e \cdot \hat{r} &= \frac{\vec{r}_e \cdot (\vec{r}_e - \vec{r}_n)}{r_e r} = \frac{r_e^2 - \vec{r}_e \cdot \vec{r}_n}{r_e r} = \frac{r_e^2 - r_n^2 + r^2}{2r_e r}; \\ \hat{r}_n \cdot \hat{r} &= \frac{\vec{r}_n \cdot (\vec{r}_e - \vec{r}_n)}{r_n r} = \frac{\vec{r}_n \cdot \vec{r}_e - r_n^2}{r_n r} = \frac{r_e^2 - r_n^2 - r^2}{2r_n r}. \end{aligned} \tag{3.5}$$

S symmetry wave functions expanded in Generalized Hylleraas (GH) basis sets [27–29] expressed in $\{r_1, r_2, r_{12}\}$ coordinates,

$$\psi_{GH} = \sum_k^N c_k\, r_1^{n_k}\, r_2^{m_k}\, r_{12}^{l_k}\, e^{-\alpha_k r_1 - \beta_k r_2 - \gamma_k r_{12}}, \tag{3.6}$$

have been utilized for the variational description of 3-body Coulomb systems, involving suitable optimization techniques depending on the required basis dimension and the desired level of accuracy. The explicitly correlated character of these functions ensures accurate energies for ground and low excited states of free two-electron atoms and three-body molecular species over relatively low expansions.

Since the particular system here analyzed refers to a confined hydrogen atom with a moving nucleus, the Hylleraas coordinates are to be identified as $\{r_1 = r_e, r_2 = r_n, r_{12} = r\}$. An earlier approach to this problem was based on the simple ansatz [30]

$$\phi(r_e, r_n, r) = A\left(1 - \frac{r_e}{r_c}\right)\left(1 - \frac{r_n}{r_c}\right)e^{-\gamma r}, \tag{3.7}$$

where γ is a variational parameter, A is an appropriate normalization factor and r_c denotes the confining spherical box radius. Since it exhibits the correct asymptotic behavior for the free atom, it yields accurate energies for large values of r_c. A natural improvement to such ansatz, allowing us to calculate ground and excited S states, would be given by a variational expansion of the form

$$\psi = \left(1 - \frac{r_e}{R}\right)\left(1 - \frac{r_n}{R}\right)e^{-\alpha r_e - \beta r_n - \gamma r}\sum_k^N c_k r_e^{n_k} r_n^{m_k} r^{l_k}, \tag{3.8}$$

where a cut-off function $(1 - r_e/r_c)(1 - r_n/r_c)$ is introduced in order to fulfill the boundary condition of a vanishing wave function whenever $r_e = r_c$ or $r_n = r_c$. Notice that toward the free atom regime ($r_c \to \infty$) the cut-off function goes to 1 and ψ becomes a variational ψ_{GH}-type wave function amenable for the description of an unconfined two-particle system. The optimized ansatz ψ contains a single set of nonlinear parameters $\{\alpha, \beta, \gamma\}$ and N linear expansion coefficients. This type of trial functions has recently been used to describe ground and excited states for confined helium and other compressed two-electron atoms [31–34].

Ground state energies correspond to expectation values of the Hamiltonian with respect to ψ,

$$E = \frac{\langle\psi|H|\psi\rangle}{\langle\psi|\psi\rangle}, \tag{3.9}$$

which leads to integrals in the spherical box of the form

$$\int_0^{r_c} dr_e \int_0^{r_c} dr_n \int_{|r_e - r_n|}^{r_e + r_n} dr\, r_e^N r_n^M r^L e^{-Ar_e - Br_n - Cr}. \tag{3.10}$$

These can be analytically evaluated where the differential volume is

$$dV = 8\pi^2 r_e r_n r\, dr_e\, dr_n\, dr. \tag{3.11}$$

For each trial function, E is minimized by varying three nonlinear parameters α, β, γ and N linear coefficients c_k through an algorithm based on a quasi-Newton method for multivariable functions. By using an analytical expression for the energy gradient, converged optimal values were attained within a gradient magnitude in the range $(10^{-6}, 10^{-4})$.

Energy calculations for each box radius r_c are performed by means of trial functions expressed via a (N = 4)-term GH basis set expansion for the ground state, spanned by powers $\{n, m, l\}$ commensurate with the condition $n + m + l \leq 1$, i.e., only up to linear terms in coordinates $\{r_e, r_n, r\}$ are considered.

For the sake of comparison ground state energies for a compressed hydrogen atom in the clamped or infinitely heavy nucleus approximation enclosed by a hard spherical cavity at a given radius, are also variationally obtained for each r_c. Accordingly, we have used 5-term S symmetry radial expansions in coordinate r including a cut-off factor,

$$\varphi = \left(1 - \frac{r}{r_c}\right) e^{-\delta r} \sum_{k=1}^{5} d_k r^{k-1}, \tag{3.12}$$

where parameter δ and linear coefficients d_k are optimized and φ vanishes at $r = r_c$, which is consistent with the description of one-electron systems spherically enclosed by impenetrable boxes ($V(r) = \infty$; $r > r_c$). The energies of the moving and fixed nucleus one-electron atoms are thus computed within the same variational scheme.

Calculation of total energies for spherically confined one-electron systems involves minimization of the expectation value

$$\varepsilon = \frac{\langle \varphi | H_{(fix\ nuc)} | \varphi \rangle}{\langle \varphi | \varphi \rangle};\ H_{(fix\ nuc)} = -\frac{1}{2}\nabla^2 + V;\ V = \begin{cases} -1/r, & (r \leq r_c) \\ \infty, & (r > r_c) \end{cases}, \tag{3.13}$$

by varying the corresponding parameters of φ where the same algorithm as for the electron + nucleus system is utilized. This leads to conventional integrals of the form

$$\int_0^{r_c} r^N e^{-Ar} dr. \tag{3.14}$$

Converged optimal values for the energy gradient were attained in the range $(10^{-6}, 10^{-5})$.

3.3.3.2 Perturbative Approach

As a first step we give a brief description of the free particle in a spherical cavity problem. The Hamiltonian for such a system in an impenetrable box of radius r_c is given by:

$$H = -\frac{\hbar^2}{2m}\nabla^2 + V(r) \tag{3.15}$$

where

$$V(r) = \begin{cases} 0, & (r \leq r_c) \\ \infty, & (r > r_c). \end{cases} \tag{3.16}$$

The eigenfunctions of the corresponding Schrödinger equations are

$$\chi(r, \theta, \phi) = R_{nl}(r)\, Y_{lm}(\theta, \phi) \tag{3.17}$$

where $R_{nl}(r)$ and $Y_{lm}(\theta, \phi)$ denote radial functions and spherical harmonics, respectively. The radial functions,

$$R_{nl}(r) = j_l(x_{nl} r / r_c) \tag{3.18}$$

correspond to spherical Bessel functions j_l of order l and x_{nl} is the nth root of j_l. The eigenergies are given by

$$E_{nl}(r) = \frac{\hbar^2 x_{nl}^2}{2m r_c^2}. \tag{3.19}$$

We consider the Hamiltonian $H = H_0 + V$, (see Eq. 3.2), expressed in atomic units, where the unperturbed operator and the perturbation are given by

$$H_0 = -\frac{1}{2}\nabla_e^2 - \frac{1}{2m_n}\nabla_n^2 \tag{3.20}$$

and

$$V = -\frac{1}{r}, \tag{3.21}$$

respectively.

The zeroth order solutions are products of the form

$$\psi^{(0)}_{nlm,n'l'm'}(\vec{r}_e, \vec{r}_n) = \chi_{nlm}(r_e, \theta_e, \phi_e)\, \chi_{n'l'm'}(r_n, \theta_n, \phi_n) \tag{3.22}$$

with eigenvalues

$$E^{(0)}_{nl,n'l'} = \frac{1}{2r_c^2}\left(x^2_{nl} + \frac{1}{m_n}x^2_{n'l'}\right) \tag{3.23}$$

The first order correction to the energies is given by

$$E^{(1)}_{nl,n'l'} = E^{(0)}_{nl,n'l'} - \left\langle \psi^{(0)}_{nlm,n'l'm'} \left| \frac{1}{r} \right| \psi^{(0)}_{nlm,n'l'm'} \right\rangle, \tag{3.24}$$

where S states ($n = n' = 1, l = l' = 0$) are only considered.

3.3.4 Results and Discussion

We here define the strong confinement region ($r_c \leq 1.0$ au) as that corresponding to spherical cavities smaller than the ground state average nucleus-electron distance for the free hydrogen atom with a fixed nucleus. Beyond this, intermediate and weak confinement regimes would extend throughout larger box radii ($r_c > 1.0$ au).

In Table 3.1 are shown the ground state perturbative and variational energies for the confined hydrogen with a moving and a fixed nucleus as obtained with the methods utilized in this report.

The perturbative energies for all box radii compiled in that table remain above the variational values calculated with the GH wave functions. It is interesting to note that this occurs due to an underestimated Coulomb attraction in the perturbative description rather than to an overestimate of the electron and nuclear kinetic energies, which, despite arising from the motion of a free and a "quasi-free" particles, they are found to be lower than those in the variational approach. In the strong confinement region the atomic total energy increases so dramatically under growing compression that the electron, and to a considerably lesser extent the nucleus (due to its heavier mass), can be regarded as a free and a quasi-free particles moving at high speed within the hard spherical walls, where the Coulomb interactions become very small as compared to the total kinetic energy. Since this feature is the underlying basis for applicability of the perturbation method, in such a region it is physically justified to estimate the energy accordingly. This interpretation is consistent with the fact of having comparable differences between the perturbation and variational (with a moving nucleus) energies and those occurring between the two variational schemes.

By comparing the variational results for the moving and fixed nucleus hydrogen atoms at each box radius, we can see that the full E and total kinetic energy $\langle T \rangle$ are expectedly higher when the nucleus is allowed to move. However, it should be noted that the electron kinetic energy $\langle T_e \rangle$ is systematically higher within the moving nucleus scheme for all r_c's, i.e., the electron increases its energy when in the presence of another moving particle where both are confined in the same cavity. Also, the Coulomb interaction between them increases slightly (it becomes less

Table 3.1 Perturbative and variational results (1st and 2nd row on each entry, respectively) for the confined hydrogen atom (CHA) with a moving nucleus as a function of the box radius r_c (au)

r_c	E	$\langle T\rangle$	$\langle T_e\rangle$	$\langle T_n\rangle$	$\langle V\rangle$
0.1	475.88825	493.74898	493.48022	0.26876	−17.86073
	473.84272	497.55784	495.52046	2.03739	−23.71513
	468.99313	493.59225	493.59225	0.0	−24.59911
0.2	114.50688	123.43724	123.37006	0.06719	−8.93037
	112.47785	124.54287	123.91907	0.62381	−12.06502
	111.07107	123.48629	123.48629	0.0	−12.41522
0.3	48.90742	54.86100	54.83114	0.02986	−5.95358
	47.28928	55.44914	55.13094	0.31820	−8.15987
	46.59279	54.94902	54.94902	0.0	−8.35623
0.4	26.39413	30.85931	30.84251	0.01680	−4.46518
	25.06003	31.26099	31.06244	0.19855	−6.20096
	24.63398	30.96278	30.96278	0.0	−6.32881
0.5	16.17781	19.74996	19.73921	0.01075	−3.57215
	15.03997	20.06358	19.92556	0.13802	−5.02361
	14.74805	19.86217	19.86217	0.0	−5.11412
1.0	3.15142	4.93749	4.93480	0.00269	−1.78607
	2.46468	5.13617	5.09161	0.04456	−2.67149
	2.37399	5.07314	5.07314	0.0	−2.69915
2.0	0.34134	1.23437	1.23370	0.00067	−0.89304
	−0.09946	1.43084	1.41801	0.01283	−1.53031
	−0.12500	1.41016	1.41016	0.0	−1.53515
4.0	−0.13793	0.30859	0.30843	0.00017	−0.44652
	−0.47520	0.59178	0.58854	0.00325	−1.06699
	−0.48327	0.58486	0.58486	0.0	−1.06813
6.0	−0.16053	0.13715	0.13708	0.00007	−0.29768
	−0.49615	0.51194	0.51064	0.00130	−1.00809
	−0.49928	0.50635	0.50635	0.0	−1.00563
8.0	–	–	–	–	–
	−0.49857	0.50256	0.50180	0.00075	−1.00113
	−0.49997	0.50032	0.50032	0.0	−1.00029
10.0	–	–	–	–	–
	−0.49916	0.50070	0.50013	0.00057	−0.99985
	−0.50000	0.50002	0.50002	0.0	−1.00002

Variational results for the CHA with a fixed nucleus are given in the 3rd row. Total energies (E) and average values for kinetic ($T = T_e + T_n$) and potential (V) energies, are given in hartrees

negative) for a varying nuclear position on a large portion of the confinement region r_c's ($r_c \leq 4.0$ au). This is in line with recent results [35] on perturbed energy calculations for confined helium with a moving nucleus, where it is found an important effect on the electrostatic interaction among all three particles under such conditions. We have verified that for most r_c's the variational energies for the

fixed-nucleus hydrogen atom coincide within the 5 digit values reported in Table 3.1 with those calculated via the two highly accurate methods utilized by Aquino et al. [36].

In Table 3.2 are given all variational parameters for the ansätze ψ and φ, as they evolve along the box radius. It should be pointed out that optimization of ψ leads systematically to a vanishing exponent α (associated with coordinate r_e) for all r_c's. This probably indicates a quantum mechanical tendency of the electron to remain mostly delocalized within the confining cavity ($\psi \approx e^{-\alpha r_e}$ where $\alpha \ll 1$). By contrast, exponent β of r_n, becomes very large for box radii ≤ 3.0 au (diminishing slightly for growing cavities), which shows precisely the opposite effect: the moving nucleus remains strongly localized near the origin within the confining sphere ($\psi \approx e^{-\beta r_n}$ where $\beta \gg 1$). On the other hand, exponent γ of relative distance r is also large—though not as much as β—throughout the strong confinement region $r_c \leq 1.0$ au thus displaying a lesser degree of localization of the electron as it moves around a shifting nucleus that is comparatively more constrained inside the spherical box. The mixed character of ansatz ψ can also be seen to change by looking at the contributions that coefficients c_i's yield as a function of r_c. Because of a remarkably increased kinetic energy experienced by the electron at the confinement interval $r_c \leq 1.0$ au the relevant polynomial contributions are associated with r and r_e, which leads to a wave function of the approximate form $\psi \approx c_2 r e^{-\gamma r} + c_4 r_e e^{-\gamma r}$. It then follows an intermediate r_c interval ($1.1 \leq r_c \leq 2.5$ au) where coefficient c_3 (associated with r_n) is largest in conjunction with a value of exponent β that continues to be sizable, perhaps enhancing the strongly localized character of the nuclear particle at a slightly farther distance from the origin. Finally, at the extended range of box radii ($r_c \geq 3.0$ au), i.e., as we relax the confinement strength, ψ clearly approaches the exact ground state wave function for a free fixed-nucleus hydrogen atom ($\psi \approx c_1 e^{-\gamma r}$ where $c_1 = 1.0$ and $\gamma \sim 1$).

Variational description of the confined clamped-nucleus atom through the r-dependent trial function φ, yields a large value of exponent δ at the strong confinement region, where the most important coefficients d_k ($\rightarrow r^{k-1}$) appear to favor those associated with powers $k - 1 \geq 1$. This probably indicates a localized character of the electron in such region, as well as its free particle behavior on account of an increased kinetic energy. However, for $r_c \geq 1.3$ au, φ follows a trend parallel to ψ, clearly approaching the exact ground state wave function for a free hydrogen atom ($\varphi \approx d_1 e^{-\delta r}$ where $d_1 = 1.0$ and $\delta \sim 1$).

In Table 3.2 are also given the average distances $\langle r_e \rangle$, $\langle r_n \rangle$ and $\langle r \rangle_{mov}$ ($\langle r \rangle_{fix}$), calculated with respect to ψ (φ), as a function of the box radius. It can be seen how very close to the origin the nucleus remains for most of r_c's, especially in the strong confinement region, on the other hand, the average values of r_e and r are located at $\approx r_c/2$ which is known to occur when a free particle is confined in an impenetrable cavity. The average relative positions $\langle r \rangle_{mov}$ and $\langle r \rangle_{fix}$ in both schemes yield very similar values throughout all box radii, approaching, for large r_c, the exact average electron-nucleus distance ($\langle r \rangle = 1.5$ au) for a free hydrogen atom ground state.

Table 3.2 Variational wave function parameters and average distances (au) with respect to the optimized ansatz for the CHA with a moving nucleus, $\psi = \left(1 - \frac{r_e}{r_c}\right)\left(1 - \frac{r_n}{r_c}\right) e^{-\alpha(=0) r_e - \beta r_n - \gamma r} (c_1 + c_2 r + c_3 r_n + c_4 r_e)$, for each box radius r_c (au)

r_c	β	γ	c_1	c_2	c_3	c_4		$\langle r_e \rangle$	$\langle r_n \rangle$	$\langle r \rangle_{mov}$
		δ	d_1	d_2	d_3	d_4	d_5			$\langle r \rangle_{fix}$
0.1	71.386	12.285	0.056	1.000	−0.210	0.446		0.050	0.017	0.052
	–	4.915	0.001	0.014	0.004	−1.154	2.836	–	–	0.050
0.2	40.494	6.305	0.120	1.000	−0.203	0.514		0.099	0.031	0.102
	–	1.068	0.095	0.531	−2.000	−1.603	−0.639	–	–	0.099
0.3	29.340	4.287	0.195	1.000	−0.203	0.588		0.148	0.044	0.152
	–	1.321	0.140	0.551	−0.946	−1.275	−0.567	–	–	0.147
0.4	23.400	3.267	0.286	1.000	−0.207	0.670		0.196	0.055	0.200
	–	1.267	0.261	0.767	−0.768	−1.127	−0.513	–	–	0.195
0.5	19.647	2.651	0.397	1.000	−0.214	0.767		0.243	0.066	0.248
	–	1.217	0.419	0.977	−0.593	−0.974	−0.437	–	–	0.242
1.0	11.365	1.393	0.954	0.551	−0.182	1.000		0.471	0.117	0.475
	–	1.011	0.972	0.980	0.073	−0.330	−0.033	–	–	0.468
2.0	10.303	0.510	0.056	−0.131	1.000	0.133		0.869	0.204	0.864
	–	1.348	1.000	0.841	0.385	0.062	0.045	–	–	0.859
4.0	2.974	0.642	1.000	−0.324	−0.015	0.319		1.391	0.449	1.320
	–	0.400	1.000	−0.350	0.086	−0.012	0.001	–	–	1.342
6.0	1.643	0.768	1.000	−0.200	−0.090	0.201		1.657	0.761	1.450
	–	0.465	1.000	−0.367	0.079	−0.010	0.001	–	–	1.481

(continued)

Table 3.2 (continued)

r_c	β	γ	c_1	c_2	c_3	c_4		$\langle r_e \rangle$	$\langle r_n \rangle$	$\langle r \rangle_{mov}$
		δ	d_1	d_2	d_3	d_4	d_5			$\langle r \rangle_{fix}$
8.0	1.043	0.851	1.000	−0.122	−0.126	0.139		1.887	1.106	1.480
	–	0.555	1.000	−0.319	0.057	−0.006	0.000	–	–	1.499
10.0	0.747	0.910	1.000	−0.067	−0.151	0.102		2.104	1.412	1.490
	–	0.935	1.000	0.032	0.009	−0.001	0.000	–	–	1.500

On the 2nd row for each entry are given the variational wave function parameters and the average distance $\langle r \rangle$ (au) corresponding to the optimized trial function for the CHA with a fixed nucleus, $\varphi = \left(1 - \frac{r}{r_c}\right) e^{-\delta r} \sum_{k=1}^{5} d_k r^{k-1}$, as a function of r_c

We consider the one-particle radial electron and nuclear densities of the compressed H atom with a moving nucleus, defined as

$$aligned\rho_{mov}(r_e)dr_n \int_{|r_e-r_n|}^{|r_e+r_n|} |\psi|^2 r\, dr; \rho(r_n)dr_e \int_{|r_e-r_n|}^{|r_e+r_n|} |\psi|^2 r\, dr; aligned \qquad (3.25)$$

and also the radial electron density for the confined H atom with a fixed nucleus, which simply corresponds to

$$\rho_{fix}(r) = \langle\varphi|\varphi\rangle^{-1} |\varphi|^2 r^2, \qquad (3.26)$$

where the subscripts in $\rho_{mov}(r_e)$ and $\rho_{fix}(r)$ refer to both schemes of atomic confinement.

The above densities are depicted in Figs. 3.1, 3.2 and 3.3 as a function of coordinates $\{r_e, r_n\}$ for the strong, intermediate and weak confinement regions. The following features emerge: The nucleus remains fairly close to the origin for the three box radii considered (r_c = 0.1, 1.0 and 5.0 au), as shown by the location of the nuclear density $[\rho(r_n)]$ maxima ($\approx$ at $r_c/10$) in the curves, which of course is entirely consistent with the fact of being the nucleus over three orders of magnitude more massive than the electron. The shape of the nuclear density in all cases

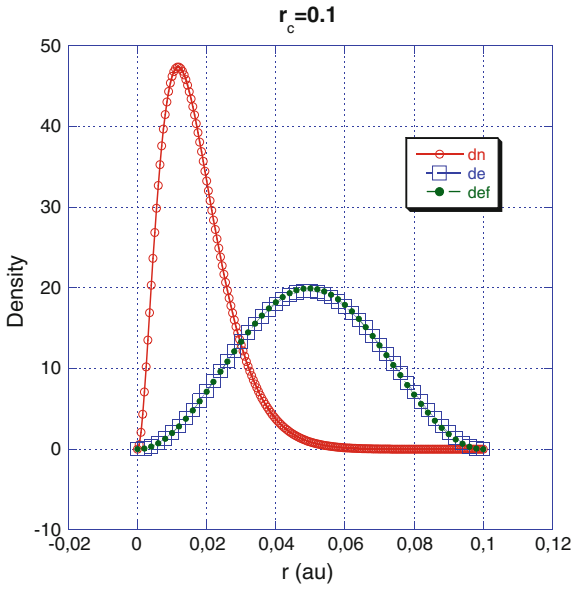

Fig. 3.1 Radial electron and nuclear densities for the CHA in the moving and fixed nucleus schemes as a function of coordinates $\{r_e, r_n\}$ for the cavity radius r_c = 0.1 au

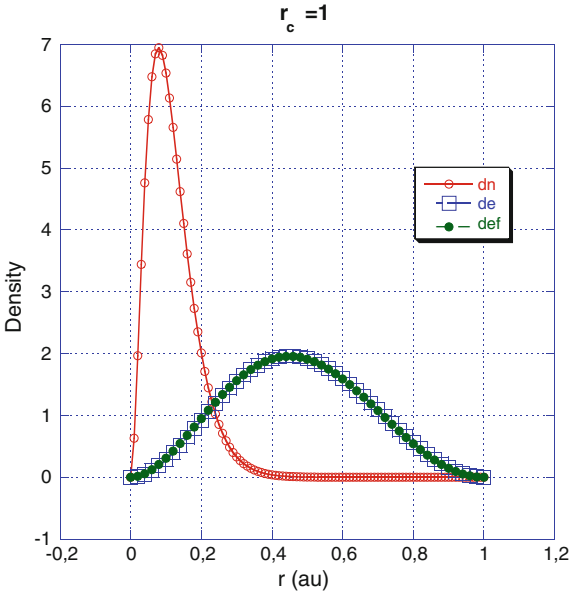

Fig. 3.2 Radial electron and nuclear densities for the CHA in the moving and fixed nucleus schemes as a function of coordinates $\{r_e, r_n\}$ for the cavity radius r_c = 1.0 au

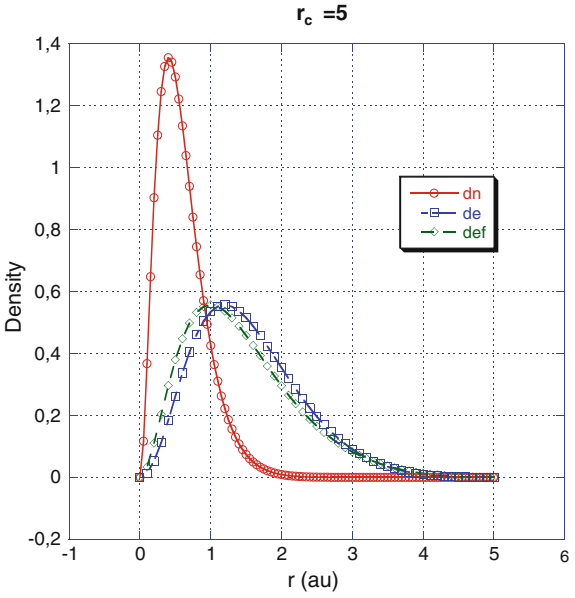

Fig. 3.3 Radial electron and nuclear densities for the CHA in the moving and fixed nucleus schemes as a function of coordinates $\{r_e, r_n\}$ for the cavity radius r_c = 5.0 au

corresponds to a localized rather than to a free particle, despite the strong confinement exerted within the smallest impenetrable cavities here considered. On the other hand, the electron densities in the moving and fixed nucleus schemes are quite similar to each other, as seen in those figures, displaying for the first two cases (r_c = 0.1 and 1.0 au) a symmetric shape, which indicates a free particle behavior for

the electron. It is interesting to note that the electron densities for the largest cavity radius (r_c = 5.0 au), where the curves are now closer to that corresponding to the free atom, our model consistently predicts an electron that can be found slightly farther away from the box center when the nucleus is allowed to move.

3.4 Shannon and Fisher Entropies for a Hydrogen Atom Under Soft Spherical Confinement

3.4.1 Introduction

In information theory, Shannon entropy is a measure of the uncertainty associated with a random variable, a concept introduced by Claude E. Shannon in his 1948 paper "A Mathematical Theory of Communication" [37]. Since its proposal this theory has led to a number of important applications in other areas, like statistical inference, cryptography, thermal physics, quantum computing, atomic and molecular structure and chemical reactivity, among others.

Shannon's entropy appears in the description of mean excitation energy [38] and it relates to certain features of the chemical bond [39]. Since the total entropy increases with the improvement of the basis, it has been used as a measure of basis quality in atomic and molecular calculations [40–42], and also to estimate the degree of correlation included in a wave function [43–45] as well as in several applications in physical chemistry [46, 47]. In chemistry, such entropy is closely related to electron delocalization which plays a crucial role in aromatic compounds [48]. There is a connection between Shannon entropy and the lowest ionization potential in atoms, as obtained by means of Koopman's theorem [49]. It has been used as a quantitative measure of spin polarization associated with the ground state of some atoms [50] and to describe the spreading of wave packets in fractal models [51], and also to analyze eigenstates and coherent states supported by a Poschl-Teller [52] potential and bound states for various systems [53].

Shannon entropy has been given an increasing attention [54] with regard to studies of atoms confined in impenetrable boxes, where the latter represents a simplified model to analyze how the atomic structure behaves under high pressure [1]. Shannon's quantum entropy has been interpreted as the uncertainty associated with the particle position, which in turn relates to the corresponding degree of localization (or delocalization) [43, 44]. Confined quantum systems like atoms and molecules trapped in impenetrable boxes, as well as quantum dots and quantum wells, are thus ideal systems to analyze that concept. The way Shannon entropy behaves has recently been studied for the ground state of one-, two- and three-electron atoms and ions in hard spherical boxes [54]. For several of these systems, local maxima and minima have been found along the curve of Shannon's total entropy as a function of the confinement radius. It has also been found that Shannon's entropy in the position space becomes negative for a strong confinement regime (very small cavity dimensions) in impenetrable boxes. In this connection, introducing a cavity of padded walls (soft

confinement) for an atomic or molecular system would represent a physically more realistic model, as discussed in this section, where the behavior of several quantum mechanical properties of the hydrogen atom confined by soft spherical walls of varying strength is analyzed as a function of the box radius r_c.

The Shannon entropies in the position and momentum space are defined as

$$S_r = -\int_0^\infty \rho(r)\,\ln[\rho(r)]\,d^3r; \tag{3.27}$$

$$S_p = -\int_0^\infty \gamma(p)\,\ln[\gamma(p)]\,d^3p; \tag{3.28}$$

whereas the total Shannon entropy is given by

$$S_t = S_r + S_p. \tag{3.29}$$

A quantity that more adequately describes the degree of delocalization of the electronic cloud in a system corresponds to the Shannon entropy power [37, 55]:

$$J_{r,p} = \frac{1}{2\pi e}\, e^{2S_{r,p}/3}. \tag{3.30}$$

The Fisher entropies [56] in the position and momentum space are given by

$$I_r = \int_0^\infty \frac{|\vec{\nabla}\rho(r)|^2}{\rho(r)} d^3r = \int_0^\infty 4\left[\frac{d\tilde{\psi}(r)}{dr}\right]^2 d^3r; \tag{3.31}$$

$$I_p = \int_0^\infty \frac{|\vec{\nabla}\gamma(p)|^2}{\gamma(p)} d^3p = \int_0^\infty 4\left[\frac{d\tilde{\phi}(p)}{dp}\right]^2 d^3p. \tag{3.32}$$

where ρ is the one-particle probability density of the system, measure the concentration (sharpness) of the electron density. These quantities fulfill a generalized uncertainty relation [55, 57]:

$$\frac{1}{3} I_{r,p} J_{r,p} \geq 1. \tag{3.33}$$

The *Fisher-Shannon information plane*, obtained by plotting $J_{r,p}$ versus $I_{r,p}$, provides us with a useful tool to systematically analyze the electron correlation in atoms [58].

Fisher's information measure has given rise to a broad spectrum of physical applications [59–65], for example, by minimizing such quantity one is led to a

Schrödinger-like equation for the probability amplitude, where the ground state describes equilibrium physics and the excited states take into account non-equilibrium situations [66]. By connecting Shannon entropy to disorder, Frieden et al. [67–69] have extensively studied the concept of order or complexity and have shown that it is associated with the Fisher entropy. Another measure of complexity is due to López-Ruiz, Mancini and Calbet (LMC) [70], which has been used in the context of electronic structure of atoms and molecules [71]. The Fisher-Shannon entropy power is a good descriptor of the complexity and it is related to the LMC complexity [72–76].

Calculations of Shannon entropies have been reported for one-electron atoms by Sen [54] and of Fisher-Shannon in conjunction with statistical complexity measures for two-electron atoms by Howard et al. [77], and also for the molecular ion H_2^+ by Montgomery and Sen [78]. Similar calculations for confined one-electron systems have been addressed in a review article by Sen et al. [79].

In this section, Shannon and Fisher entropies are calculated in the position (S_r, I_r) and momentum space (S_p, I_p) for the hydrogen atom spherically confined in soft and impenetrable (as a limiting case) boxes. For the latter, calculations for a free particle in a box are also included. For the atomic system and the free particle the evolution of these quantities is analyzed in terms of the cavity dimension r_c and strength U_0.

The densities

$$\rho(r) = |\tilde{\psi}(r)|^2; \tag{3.34}$$

$$\gamma(p) = |\tilde{\phi}(p)|^2, \tag{3.35}$$

are defined in terms of the one particle system wave functions $\tilde{\psi}(r)$, $\tilde{\phi}(p)$ in position and momentum coordinates, respectively.

In Sect. 3.4.2 we discuss the free particle in-a-box case and briefly review the variational method based on atomic wave functions expanded in Slater-type basis sets where, for soft confinement (finite U_0), the radial coordinate extends over the whole space (r goes from 0 to ∞). When $U_0 \to \infty$ (hard spherical confinement) the atomic wave function includes a cut-off factor to ensure correct fulfillment of Dirichlet boundary condition (vanishing wave function at the box edge, where the integral is performed from 0 to r_c). Section 3.4.3 is devoted to the presentation and discussion of results obtained by this method.

3.4.2 Method of Calculation

The eigenfunctions for a free particle in a spherical box of radius r_c are given by

$$\psi_{nlm}(r, \theta, \phi) = A_{nl} j_l(x_{nl}\, r/r_c)\, Y_{lm}(\theta, \phi), \tag{3.36}$$

with energies

$$E_{nl} = \frac{x_{nl}^2}{2r_c^2}, \tag{3.37}$$

where A_{nl} is a normalization constant, x_{nl} is the nth-root of the spherical Bessel function j_l and the Y_{lm}'s are the spherical harmonics.

Since we consider in particular the ground state, the corresponding wave function is

$$\psi_{100}(r,\theta,\phi) = A_{10} j_0(x_{10}\, r/r_c)\, Y_{00}(\theta,\phi) = \frac{A_{10}}{\sqrt{4\pi}} j_0(x_{10}\, r/r_c);\; j_0(\tau) = \mathrm{Sin}(\tau)/\tau. \tag{3.38}$$

The normalized ground state wave function for a spherically confined free particle in an impenetrable box is thus given by

$$\tilde{\psi}_{FP}(r) = \frac{1}{\sqrt{2\pi r_c}} \frac{\mathrm{Sin}(\pi r/r_c)}{r}; \tag{3.39}$$

$$\tilde{\phi}_{FP}(p) = \frac{1}{\sqrt{2\pi}} \frac{2}{p} \int_0^{r_c} \mathrm{Sin}(pr)\, \tilde{\psi}_{FP}(r) r\, dr = \frac{\sqrt{r_c}}{p} \frac{\mathrm{Sin}(pr_c)}{(\pi - pr_c)(\pi + pr_c)}, \tag{3.40}$$

where $\tilde{\phi}_{FP}(p)$ is the Fourier Transform of $\tilde{\psi}_{FP}(r)$.

For the H atom we consider the nonrelativistic one-electron Hamiltonian (given in atomic units) in the infinitely heavy nucleus approximation:

$$H = -\frac{1}{2}\nabla^2 - Z/r + V(r), \tag{3.41}$$

where $V(r)$ refers to a logistic potential here defined as

$$V(r) = \frac{U_0}{e^{w(1-r/r_c)} + 1}, \tag{3.42}$$

and where we have chosen a factor $w = 1{,}000$, which is sufficiently large so as to simulate a spherical penetrable barrier whose strength U_0 is nearly vanishing at $r < r_c$ and remains approximately constant in the range $r > r_c$, i.e.,

$$V(r) \cong \begin{cases} 0; & r \le r_c \\ U_0; & r > r_c \end{cases}. \tag{3.43}$$

Notice that, although $V(r)$ is very similar to the step potential $\tilde{V}(r)$, strictly defined as

$$\tilde{V}(r) = \begin{cases} 0; & r \leq r_c \\ U_0; & r > r_c \end{cases}, \tag{3.44}$$

it differs from it in one essential respect: while $V(r)$ is continuous in the entire radial coordinate domain, $\tilde{V}(r)$ is discontinuous at $r = r_c$. Hence, by using a logistic potential one avoids describing the problem in a scheme where the complete solution often depends on different trial wave functions at two separate spatial regions ($r \leq r_c$ and $r > r_c$) that are required to fulfill some appropriate boundary condition at $r = r_c$.

The hydrogen atom confined by $\tilde{V}(r)$ was studied previously [4–6, 9].

For soft confinement (finite U_0), the wave function is expanded in terms of radial functions of the form

$$\psi_{SC} = \sum_{i=1}^{5} C_i r^{n_i} e^{-\alpha r}, \tag{3.45}$$

whereas for impenetrable boxes ($U_0 \to \infty$), the wave function must include a cut-off factor that ensures fulfillment of Dirichlet boundary condition $\psi_{HC}(r_c) = 0$, i.e.,

$$\psi_{HC}(r) = \sum_{i=1}^{5} C_i r^{n_i} \left(1 - \frac{r}{r_c}\right) e^{-ar}. \tag{3.46}$$

(Labels *SC* and *HC* refer to soft and hard confinement, respectively.)

The parameter α and the linear coefficients C_i are optimized by minimizing the total ground state energy, given by the expectation value of the Hamiltonian with respect to ψ,

$$E = \frac{\langle \psi | H | \psi \rangle}{\langle \psi | \psi \rangle}. \tag{3.47}$$

The variational method for the latter case has previously been applied to the description of spherically compressed one and two-electron atoms [31, 32, 80] where the nucleus remains fixed at the center of the cavity. A comprehensive review on the subject has been reported by Aquino [9].

In order to obtain the corresponding wave functions in the momentum space, we calculate the Fourier Transform of the atomic functions,

$$\phi_A(p) = \frac{1}{\sqrt{2\pi}} \frac{2}{p} \int_0^\infty \mathrm{Sin}(pr)\, \psi_A(r) r\, dr. \tag{3.48}$$

(*A* refers to either label *SC* or *HC*.)

Functions $\tilde{\psi}_{FP}(r), \tilde{\psi}_A(r)$ and $\tilde{\phi}_{FP}(p), \tilde{\phi}_A(p)$ are normalized such that

$$\langle\tilde{\psi}|\tilde{\psi}\rangle = 4\pi \int_0^{r_c,\infty} |\tilde{\psi}(r)|^2 r^2 \, dr = 1; \tag{3.49}$$

$$\langle\tilde{\phi}|\tilde{\phi}\rangle = 4\pi \int_0^{\infty} |\tilde{\phi}(p)|^2 p^2 \, dp = 1, \tag{3.50}$$

where

$$\tilde{\psi}_A(r) = \frac{\psi_A(r)}{\sqrt{\langle\psi_A|\psi_A\rangle}}; \tag{3.51}$$

$$\tilde{\phi}_A(p) = \frac{\phi_A(p)}{\sqrt{\langle\phi_A|\phi_A\rangle}}. \tag{3.52}$$

3.4.3 Results and Discussion

In Fig. 3.4, both the ground state energy of the atom under hard and soft confinement and that of the free particle in an impenetrable box, are seen to increase at different rates, as we move toward the strong confinement region (small cavity radii). The almost parallel evolution (especially when the systems become strongly compressed) corresponding to the atom and free particle energies in a hard box, clearly confirms the near free particle behavior of the electron in that region. On the other hand, the atomic energies increase toward ever smaller cavities at gradually lower rates for penetrable boxes of correspondingly reduced strength (U_0 = 100, 50, 10, 1 hartrees). This behavior is consistent with the energy calculated by means of the potential $V(r)$, where such a trend naturally follows from having an electron trapped in cavity walls that exert less compression. For soft confinement and very small cavity radii ($r_c < 0.5$ au) $V(r) \sim U_0$; $r > r_c$, which leads to an effective free atom Hamiltonian approximately shifted by a constant value close to U_0, so that the optimized energies appear to flatten as we move to shorter box radii, approaching $U_0 + E_1$ (where $E_{n=1}$ is the H atom ground state energy).

For impenetrable boxes, our values for the confined H atom Shannon entropies, as given in Table 3.3, are in good agreement with those reported by Sen [54]. S_r and S_p values for the atom enclosed by soft and hard walls and the free particle in an impenetrable box are displayed in Fig. 3.5, as a function of r_c. Shannon entropies are associated with the degree of localization and delocalization in the position and momentum coordinates, respectively, evolving with the same rate but in opposite directions, so that, for a given confinement strength and cavity radius, the more spatially localized the electron the more delocalized in the momentum space. This

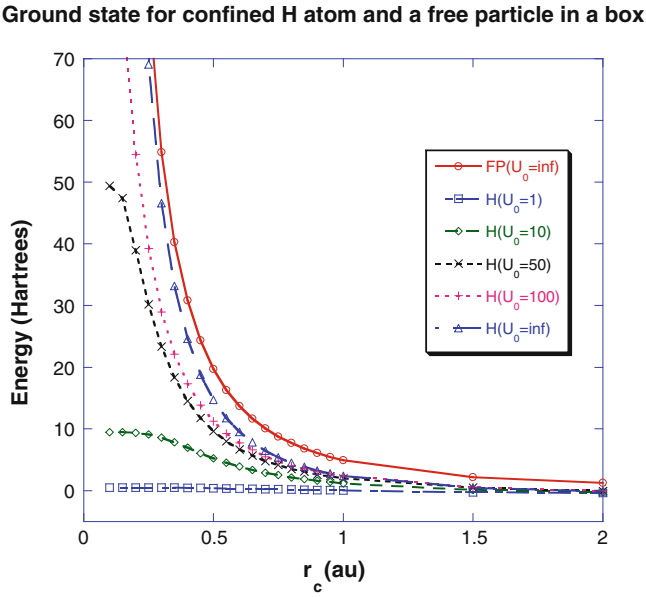

Fig. 3.4 Ground state energy of the H atom under hard and soft confinement and free particle energy in an impenetrable box, as a function of the cavity radius r_c

simultaneous behavior of both quantities (S_r and S_p), that closely relates to Heisenberg's uncertainty principle, is illustrated in Fig. 3.5, where the curves appear to be virtual mirror images from each other with respect to the horizontal reference line (drawn at ~ 3.3 in the vertical axis). Notice that only for impenetrable boxes the curves maintain the same trend all the way, growing in opposite directions as we move inward along r_c. By contrast, toward small cavity radii, the curves corresponding to penetrable boxes change their character in a pronounced way (especially for $U_0 = 100$ hartrees) where the finite potentials are unable to keep the electron localized within the box range, so that the S_r and S_p curves tend to approach each other, instead of moving away from one another. This behavior follows from having a charge cloud (given by the radial density $r^2|\psi(r)|^2$) that for $r_c = 0.1$ au and $U_0 = 100$ hartrees, for example, it extends out at a radial distance from the box center $r \sim 2.5$ au (far beyond r_c). Interestingly, this behavior is consistent with very recent results by Dolmatov and King [81] on a case study of a hydrogen atom under the pressure of a spherical penetrable confinement potential, where they find *atomic swelling effects upon compression*. In comparison to the case for $r_c = 1.0$ au, the radial density evolves in a similar way for $U_0 = \infty$ and 100 hartrees, which indicates that for cavity radii outside the critical range (strong confinement region) the system is less responsive to compression effects. Unlike the case for soft cavity walls, the radial density for the smallest impenetrable box radii here analyzed, are virtually identical when comparing the atomic electron and the free particle, which again confirms their nearly coincident behavior in the strong confinement region.

Table 3.3 Ground state energies E (hartrees), Shannon entropies (S_r, S_p, S_t) and Fisher information measures (I_r, I_p) for a compressed H atom enclosed by soft spherical walls of increasing values of U_0 (hartrees) and impenetrable boxes ($U_0 = \infty$), as well as for the free particle in a box ($U_0 = \infty^*$), as a function of the cavity radius r_c (au)

r_c	U_0	E	S_r	S_p	S_t	I_r	I_p
0.1	1	0.4988	4.1377	2.4295	6.5673	0.3204	0.9508
	10	9.4873	4.0662	2.5067	6.5729	0.3427	0.9083
	50	49.3829	3.4597	3.1589	6.6186	0.6209	0.6168
	100	98.3726	0.9440	5.8661	6.8102	4.9155	0.1371
	∞	468.9931	−6.2445	12.8536	6.6091	314.2306	0.0009
	∞^*	493.6082	−6.2322	12.8495	6.6173	314.1593	0.0009
0.2	1	0.4917	4.0955	2.4755	6.5711	0.3329	0.9264
	10	9.3620	3.4297	3.2025	6.6322	0.6106	0.6174
	50	38.9559	−1.6644	8.2041	6.5396	14.0952	0.0198
	100	54.5147	−2.7724	9.2284	6.4561	26.4911	0.0089
	∞	111.0711	−4.1777	10.7788	6.6011	78.6138	0.0035
	∞^*	123.4020	−4.1527	10.7701	6.6173	78.5398	0.0036
0.3	1	0.4744	3.9981	2.5810	6.5791	0.3615	0.8726
	10	8.6398	1.5249	5.1141	6.6391	2.0586	0.1750
	50	23.3259	−1.7611	8.1984	6.4373	13.2395	0.0173
	100	28.9483	−2.1916	8.6363	6.4447	17.7784	0.0130
	∞	46.5928	−2.9746	9.5676	6.5930	34.9816	0.0079
	∞^*	54.8454	−2.9363	9.5537	6.6173	34.9066	0.0081
0.5	1	0.3975	3.6147	2.9764	6.5910	0.4747	0.6801
	10	5.2456	0.3338	6.1505	6.4843	3.4552	0.0722
	50	9.6180	−0.8501	7.2976	6.4475	7.2936	0.0318
	100	11.2484	−1.0834	7.5446	6.4612	8.6342	0.0273
	∞	14.7480	−1.4702	8.0473	6.5771	12.6446	0.0214
	∞^*	19.7443	−1.4039	8.0212	6.6173	12.5664	0.0225
1.0	1	0.0285	2.8463	3.6859	6.5322	0.6982	0.3958
	10	1.1761	1.2005	5.2386	6.4390	1.8495	0.1246
	50	1.9496	0.7211	5.7336	6.4547	2.5853	0.0908
	100	2.3936	0.5438	5.9054	6.4492	2.9023	0.0806
	∞	2.3740	0.5290	6.0115	6.5405	3.2297	0.0806
	∞^*	4.9361	0.6756	5.9418	6.6173	3.1416	0.0900
5.0	1	−0.4985	4.0799	2.4704	6.5503	0.3251	0.9000
	10	−0.4947	3.9742	2.5567	6.5308	0.3390	0.8260
	50	−0.4898	3.8773	2.6397	6.5169	0.3540	0.7672
	100	−0.4870	3.8320	2.6794	6.5114	0.3617	0.7418
	∞	−0.4964	4.0174	2.5244	6.5418	0.3339	0.8547
	∞^*	0.1974	5.5039	1.1134	6.6173	0.1257	2.2494
∞	0	−0.5000	4.1447	2.4219	6.5666	0.3183	0.9549

Values for $r_c = \infty$ correspond to the free atom. Factor w in the logistic potential $V(r)$ was set to 1,000

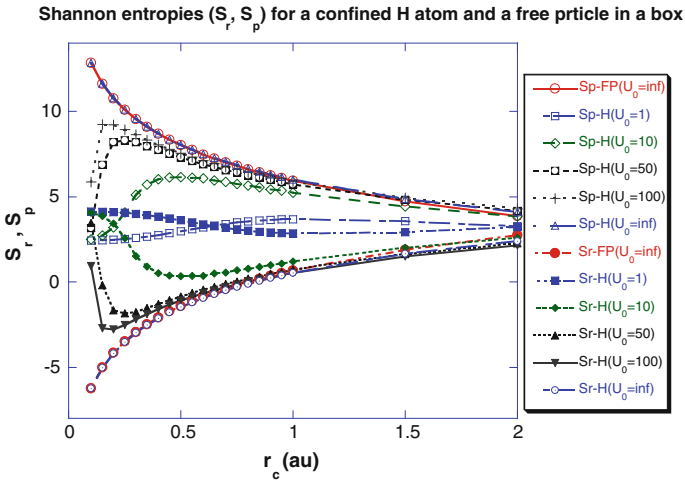

Fig. 3.5 Shannon entropies S_r and S_p for a compressed H atom and a free particle in a box, enclosed by spherical walls of selected values of U_0, as a function of the box radius r_c

The occurrence of negative values for the Shannon entropy in the position coordinate, S_r (see Table 3.3), can be explained due to the large density magnitude attained at those points, signaling a marked spatial localization of the electron/free particle, where $\rho_r = |\psi(r)|^2$ turns out to be $\gg 1$ [82], so that $-\rho_r \ln \rho_r < 1$, and since $S_r = -\int_0^{r_c} \rho_r \ln \rho_r d^3r$, S_r itself becomes negative.

In Fig. 3.6 are plotted the total Shannon entropies S_t for the systems here considered. It should be noted that they remain above the lower bound

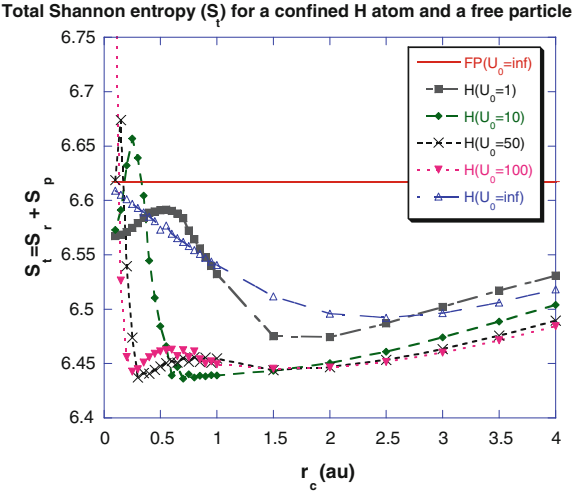

Fig. 3.6 Total Shannon entropy ($S_t = S_r + S_p$) for a compressed H atom and a free particle in a box enclosed by spherical walls of selected values of U_0, as a function of the box radius r_c

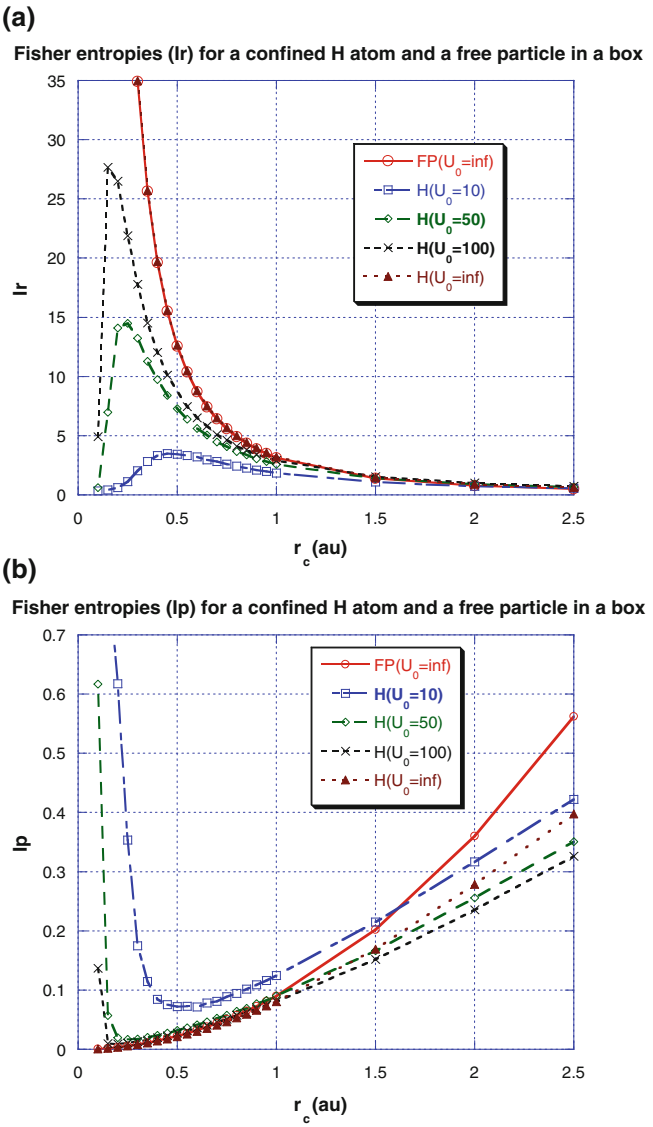

Fig. 3.7 Fisher information measures I_r (**a**) and I_p (**b**) for a compressed H atom in a box enclosed by spherical walls of selected values of U_0 and a free particle in impenetrable boxes, as a function of the cavity dimension r_c

corresponding to the entropy uncertainty principle as derived by Bialynicki-Birula and Mycielski [83],

$$S_t = S_r + S_p \geq 3(1 + \ln\pi) = 6.4342. \tag{3.53}$$

The evolution of this quantity as a function of r_c is determined by the smooth or changing nature of the S_r and S_p contributions, which relates to the above discussion in terms of the behavior of those curves along the strong, intermediate and weak confinement regions. Accordingly, we notice that the pronounced changes in S_t occur precisely for small cavity radii and soft compression regimes (finite U_0). In particular, for U_0 = 50 and 10 hartrees, the total entropy strongly fluctuates along boxes of radii $r_c < 1.5$ au, thus reflecting a situation where these spherical barriers are physically unable to contain the electron within cavities of such reduced dimensions.

In Fig. 3.7 are illustrated the position (I_r) and momentum (I_p) Fisher entropies as a function of r_c for the electron surrounded by hard and soft walls and a free particle confined in impenetrable boxes. The I_r and I_p curves follow opposite trends—in accordance with Heisenberg's uncertainty principle—thus behaving similarly to the Shannon entropies, S_r and S_p, i.e., while one increases (decreases), the other decreases (increases). For small cavity radii and penetrable boxes, the Fisher entropies noticeably change their character just as S_r and S_p do, due again to the extent the electron is localized in the strong confinement region when subjected to potentials of finite strength.

3.5 Conclusions

In Sect. 3.3 we have variationally calculated the ground state energy and some other properties for the spherically confined hydrogen atom in an impenetrable box of varying radius, where the system is described within two frameworks: in one, both electron and nucleus are allowed to move, whereas in the other the heavier of them remains fixed. In addition, a perturbative approach based on the unperturbed solution of two spherically confined free particles is utilized to calculate the moving nucleus hydrogen atom ground state energies. Through the variational method trial functions were constructed via Generalized Hylleraas basis sets that include up to linear terms in coordinates $\{r_e, r_n, r\}$ and radial expansions in relative distance r to describe the atom with a moving and a fixed nucleus, respectively. The variational ground state energies are found to be lower in comparison to those perturbatively obtained, however, the energy differences get reduced at the strong confinement region where the perturbative treatment of energies is physically justified due to the free- and quasi-free-particle behavior displayed by the electron and nucleus under pronounced compression. Our findings can be summarized as follows: The increase in kinetic energy due to addition of a moving nucleus is comparatively larger than the energy difference between the Coulomb interactions calculated for each scheme

along all box radii. The average nuclear position is found to be closer to the origin by a factor ranging from 34 % (at $r_c = 0.1$ au) up to 67 % (at $r_c = 10.0$ au), relative to the average electron position. As the confinement strength is relaxed the variational ansätze ψ, φ and average relative distances $\langle r \rangle_{mov}$, $\langle r \rangle_{fix}$ steadily approach the exact wave function and average electron-nucleus distance, respectively, corresponding to the free hydrogen atom. The radial densities show that the nucleus remains very close to the origin for all cavity radii considered, on account of its much greater mass, where the shape of the nuclear density corresponds to a localized rather than to a free particle. By comparison, the electron densities in the moving and fixed nucleus schemes are found to be very similar to each other, where a free particle behavior is clearly indicated toward the strong confinement region. On the other hand, as we approach the free atom limit, by letting the nucleus move, our model predicts an electron that can stray slightly farther away from the box center.

In Sect. 3.4, Shannon and Fisher entropies have been calculated in the position (S_r, I_r) and momentum space (S_p, I_p) for the hydrogen atom spherically confined in soft and impenetrable boxes, including the case of a free particle trapped by infinitely high walls, being all analyzed as a function of the cavity radius r_c and potential strength U_0. These quantities were found to evolve smoothly throughout the whole range of cavity radii r_c whenever the electron and free particle are confined by impenetrable boxes. On the other hand, for the atomic electron under soft compression regimes (finite U_0) they were found to importantly change over short radial intervals in the strong confinement region, a feature associated with the degree of spatial charge localization induced by potentials of finite strength. The occurrence of negative values for the Shannon entropy in the position coordinate is explained on grounds of a pronounced spatial localization of the electron or free particle, which leads to locally large density magnitudes.

Acknowledgments Financial support provided by *Sistema Nacional de Investigadores* (SNI, Mexico) is gratefully acknowledged.

References

1. Michels A, de Boer J, Bjil A (1937) Physica 4:981
2. Sommerfeld A, Welker H (1938) Ann Phys 32(5):56
3. deGroot SR, ten Seldam CA (1946) Physica 12:669
4. Ley-Koo E, Rubinstein S (1979) J Chem Phys 71:351
5. Ley-Koo E, Rubinstein S (1980) J Chem Phys 73:887
6. Marn JL, Cruz SA (1991) J Phys B: At Mol Opt Phys 24:2899
7. Marn JL, Cruz SA (1992) J Phys B: At Mol Opt Phys 25:4365
8. Aquino N (1995) Int J Quantum Chem 54:107
9. Aquino N (2009) Adv Quantum Chem 57:123 (and references therein)
10. Katriel J, Montgomery HE Jr (2012) J Chem Phys 137:114109
11. Le Sech C, Banerjee A (2011) J Phys B: At Mol Opt Phys 44:105003
12. Sarsa A, Le Sech C (2011) J Chem Theory Comput 7:2786
13. Cabrera-trujillo R, Cruz SA (2013) Phys Rev A 87:012502

14. Méndez-Fragoso R, Ley-Koo E (2011) Int J Quantum Chem 111:2882
15. Méndez-Fragoso R, Ley-Koo E (2010) Int J Quantum Chem 110:2765
16. Mateos-Cortés S, Ley-Koo E, Cruz SA (2002) Int J Quantum Chem 86:376
17. Ley-Koo E, Flores-Flores A (1998) Int J Quantum Chem 66:123
18. Garza J, Vargas R, Aquino N, Sen KD (2005) J Chem Sci (India) 117:379
19. Garza J, Hernn'andez-Pérez JM, Rámirez J, Vargas R (2012) J Phys B: At Mol Phys 45:015002
20. Garza J, Vargas R (2009) Adv Quantum Chem 57:241
21. Nascimento EM, Prudente FV, Guimaraes MN, Maniero AM (2011) J Phys B: At Mol Phys 44:1 (and references therein)
22. Sako T, Diercksen GHF (2003) J Phys B: At Mol Opt Phys 36:1433
23. Sako T, Diercksen GHF (2003) J Phys B: At Mol Opt Phys 36:1681
24. Aquino N, Granados VD, Yee-Madeira H (2009) Rev Mex Fis 55:125
25. Weyl JA (1979) J Chem Phys 71:2803
26. Fernández FM, Aquino N, Flores-Riveros A (2012) Int J Quantum Chem 112:823
27. Kolos W, Roothaan CCJ, Sack RA (1960) Rev Mod Phys 32:178
28. Szalewicz K, Monkhorst HJ, Kolos A, Scrinzi A (1987) Phys Rev A 36:5494
29. Froelich P, Flores-Riveros A (1993) Phys Rev Lett 70:1595
30. Fernández Francisco M (2010) Eur J Phys 31:285
31. Aquino N, Flores-Riveros A, Rivas-Silva JF (2003) Phys Lett A 307:326
32. Flores-Riveros A, Rodrguez-Contreras A (2008) Phys Lett A 372:6175
33. Flores-Riveros A, Aquino N, Montgomery HE Jr (2010) Phys Lett A 374:1246
34. Montgomery HE Jr, Aquino N, Flores-Riveros A (2010) Phys Lett A 374:2044
35. Fernández FM, arXiv:1004.2508v1 [quant-ph] 14 Apr 2010
36. Aquino N, Campoy G, Montgomery HE Jr (2007) Int J Quantum Chem 107:1548
37. Shannon CE (1948) Bell Syst Tech J 27(379):623
38. Hô M, Weaver DF, Smith VH Jr, Sagar RP, Esquivel RO (1998) Phys Rev A 57:4512
39. Karafiloglou P, Panos CP (2004) Chem Phys Lett 389:400
40. Maroulis G, Sana M, Leroy G (1981) Int J Quantum Chem 19:43
41. Simas AM, Thakkar AJ, Smith VH Jr (1983) Int J Quantum Chem 24:257
42. Grade SR, Sears SB, Chakravorty SJ, Bendale RD (1985) Phys Rev A 32:2602
43. Hô M, Sagar RP, Pérez JM, Smith VH Jr, Esquivel RO (1994) Chem Phys Lett 219:15
44. Tripathi AN, Smith VH Jr, Sagar RP, Esquivel RO (1996) Phys Rev A 54:1877
45. Nagy A, Parr RG (1996) Int J Quantum Chem 58:323
46. Grade SR (1984) Phys Rev A 30:620
47. Grade SR, Bendale RD (1985) Int J Quantum Chem 28:311
48. Chen Z, Wannere CS, Corminboeuf C, Puchta R, Schleyer PVR (2005) Chem Rev 105:3842
49. Hô M, Sagar RP, Schmider H, Weaver DF, Smith VH Jr (1994) Int J Quantum Chem 53:627
50. Fuentealba P, Melin J (2002) Int J Quantum Chem 90:334
51. Chataraj PK, Nath S (1995) Pramana. J. Phys. 45:545
52. Atre R, Kumar A, Kumar N, Panigrahi PK (2004) Phys Rev 69:052107
53. Das C, Bhattacharyya K (2009) Phys Rev A 79:012107
54. Sen KD (2005) J Chem Phys 123:074110
55. Dembo A, Cover TM, Thomas JA (1991) IEEE Trans Inf Theory 37:1501
56. Fisher RA (1925) Proc Cambridge Philos Soc 22:700
57. Pearson JM (1997) Proc Am Math Soc 125:3339
58. Romera E, Dehesa J (2004) J Chem Phys 120:8906
59. Frieden BR (1989) Am J Phys 57:1004
60. Frieden BR (1992) Phys Lett A 169:123
61. Frieden BR (1993) Phys A 198:262
62. Frieden BR, Hughes RJ (1994) Phys Rev E 49:2644
63. Frieden BR (1990) Phys Rev A 41:4265
64. Frieden BR, Soffer BH (1995) Phys Rev E 52:2274
65. Frieden BR (1991) Found Phys 21:757

66. Frieden BR, Plastino A, Plastino AR, Soffer BH (2002) Phys Rev E 66:046128
67. Frieden BR, Hawkins RJ (2010) Phys Rev E 82:066117
68. Frieden BR, Gatenbay RA (2011) Phys Rev E 84:011128
69. Frieden BR, Petri M (2012) Phys Rev E 86:032102
70. López-Ruiz R, Mancini HL, Calbet X (1995) Phys Lett A 209:321
71. Catalán RG, Garay J, López-Ruiz R (2002) Phys Rev E 66:011102
72. Romera E, López-Ruiz R, Sanudo J, Nagy A (2009) Int Rev Phys 3:207
73. López-Ruiz R, Nagy A, Romera E, Sanudo J (2009) J Math Phys 50:123528
74. Nagy A, Sen KD, Montgomery HE (2009) Phys Lett A 373:2552
75. Sanudo J, López-Ruiz R (2008) Phys Lett A 372:5283
76. Bouvrie PA, Angulo JC, Dehesa JS (2011) Phys A 390:2215
77. Howard IA, Sen KD, Borgoo A, Geerlings P (2008) Phys Lett A 372:6321
78. Montgomery HE Jr, Sen KD (2008) Phys Lett A 372:2271
79. Sen KD, Pupyshev VI, Montgomery HE Jr (2009) Adv Quantum Chem 57:25
80. Aquino N, Garza J, Flores-Riveros A, Rivas-Silva JF, Sen KD (2006) J Chem Phys 124:054311
81. Dolmatov VK, King VL (2012) J Phys B: At Mol Opt Phys 45:225003
82. Sam Trickey (private communication), 8 Sept 2011
83. Bialynicki-Birula I, Mycielski J (1975) Commun Math Phys 44:129

Chapter 4
Variational Perturbation Treatment for Excited States of Confined Two-Electron Atoms

H.E. Montgomery Jr. and K.D. Sen

4.1 Introduction

The numerical complications of confined system calculations have generally limited studies of these systems to calculation of ground state properties. Incorporation of Dirichlet boundary conditions as a cut-off function within the trial wavefunction significantly increases the number of integrals that must be calculated and has generally been considered a sufficient challenge. With the development of computer algebra systems such as Maple and Mathematica that facilitate matrix operations and evaluation of special functions and the porting of confined systems code to multiprocessor clusters, the confined systems community is now at a point where accurate treatment of excited state properties is a logical next step. In this work we report Hylleraas-Scherr-Knight variational perturbation theory (HSK-VPT) [1, 2] calculation of the energies of the $1s2s\,^1S$ and $1s2s\,^3S$ states of confined two-electron atoms and ions for $Z = 1$–4. These are the first two excited states of the two-electron system and serve as benchmarks for excited state calculations. The $1s2s\,^1S$ state is a challenge. While it can be calculated by the linear variational method using the Hylleraas-Undheim-MacDonald theorem [3–5], obtaining accurate energies for excited states while maintaining orthogonality to the $1s^2\ ^1S$ ground state requires inclusion of a large number of basis functions in the variational wavefunction, increases the computational time and introduces the possibility of linear dependence

H.E. Montgomery Jr. (✉)
Chemistry Program, Centre College, 600 West Walnut Street,
Danville KY 40422-1394, USA
e-mail: ed.montgomery@centre.edu

K.D. Sen
School of Chemistry, University of Hyderabad, Hyderabad, Telangana 500 046, India
e-mail: sensc@uohyd.ernet.in

K.D. Sen (ed.), *Electronic Structure of Quantum Confined Atoms and Molecules*,
DOI 10.1007/978-3-319-09982-8_4

of the basis functions. HSK-VPT provides a more direct path to excited state calculations and replaces solution of the secular determinant, with a process that is more akin to solution of simultaneous equations.

4.2 Variational Perturbation Theory

The derivation of Rayleigh-Schrödinger perturbation theory can be found in any introductory quantum theory text [6]. Only those parts required to develop variational perturbation theory are repeated here. The central idea is that for a system described by a Hamiltonian $\hat{H}$, with ground state eigenfunction Ψ and ground state eigenvalue E, a system can be found with Hamiltonian $\hat{H}_0$, ground state eigenfunction φ_0 and ground state eigenvalue ε_0 that satisfies the same symmetry and boundary conditions as $\hat{H}$. We thus require

$$\hat{H}_0\varphi_0 = \varepsilon_0\varphi_0 \tag{4.1}$$

$\hat{H}_0$ is the zero-order Hamiltonian and the Hamiltonian can now be written as

$$\hat{H} = \hat{H}_0 + \lambda\hat{H}_1, \tag{4.2}$$

where $\hat{H}_1$ is the first-order Hamiltonian and λ is called the perturbation parameter.

The Schrödinger equation is written as

$$\hat{H}\,\Psi = (\hat{H}_0 + \lambda\hat{H}_1)\Psi = E\,\Psi \tag{4.3}$$

Since $\hat{H}$ depends on λ, Ψ and E must also depend on λ and they can be expanded as power series in λ,

$$\Psi = \psi_0 + \lambda\psi_1 + \lambda^2\psi_2 + \lambda^3\psi_3 + \cdots, \tag{4.4}$$

$$E = E_0 + \lambda E_1 + \lambda^2 E_2 + \lambda^3 E_3 \; + \cdots, \tag{4.5}$$

and we set $\psi_0 = \varphi_0$ and $E_0 = \varepsilon_0 \cdot \psi_n$ is the nth order correction to the ground state wavefunction, while E_n is the nth order correction to the energy.

Substituting into the Schrödinger equation gives the Rayleigh-Schrödinger perturbation equations for E_0 and E_1

$$E_0 = \frac{\int \psi_0\hat{H}_0\psi_0\,d\tau}{\int \psi_0\psi_0\,d\tau}, \tag{4.6}$$

$$E_1 = \frac{\int \psi_0\hat{H}_1\psi_0\,d\tau}{\int \psi_0\psi_0\,d\tau} \tag{4.7}$$

The Rayleigh-Ritz variational principle,

$$\int U\left(\hat{H}-E\right)U\,d\tau \geq 0, \tag{4.8}$$

can be used to obtain approximate energies and wavefunctions. The variational wavefunction, U, is expanded as a power series in λ, analogous to (4.4), as

$$U = \varphi_0 + \lambda\varphi_1 + \lambda^2\varphi_2 + \lambda^3\varphi_3 + \cdots, \tag{4.9}$$

where for non-degenerate energy levels we take $\psi_0 = \varphi_0$. It is important to note that $\varphi_1, \varphi_2, \varphi_3, \ldots$ are approximate wavefunctions and need not be eigenfunctions of any operator. We restrict consideration to real φ_n and use the notation

$$\langle m|\Omega|n\rangle = \int \varphi_m\hat{\Omega}\varphi_n\,d\tau, \tag{4.10}$$

where $\hat{\Omega}$ is any operator.

Inserting the expansions for $\hat{H}$, U and E into (4.8) gives

$$\begin{aligned}&\langle 0|\hat{H}_0 - E_0|0\rangle + \left\{2\langle 1|\hat{H}_0 - E_0|0\rangle + \langle 0|\hat{H}_1 - E_1|0\rangle\right\}\lambda \\ &\quad + \left\{2\langle 1|\hat{H}_0 - E_0|0\rangle + \langle 1|\hat{H}_0 - E_0|1\rangle + 2\langle 1|\hat{H}_1 - E_1|0\rangle - E_2\langle 0|0\rangle\right\}\lambda^2 \\ &\quad + \left\{\begin{array}{l} 2\langle 0|\hat{H}_0 - E_0|3\rangle + 2\langle 0|\hat{H}_1 - E_1|2\rangle + 2\langle 1|\hat{H}_0 - E_0|2\rangle \\ +2\langle 1|\hat{H}_1 - E_1|1\rangle - E_2\langle 0 \mid 1\rangle - E_3\langle 0 \mid 0\rangle \end{array}\right\}\lambda^3 + \cdots \geq 0\end{aligned} \tag{4.11}$$

and in general,

$$\sum_{m=0}\sum_{n=0}\lambda^{m+n}\langle m|\hat{H}_0 + \lambda\hat{H}_1|n\rangle - \left\{\sum_{l=0}\lambda^l E_l\right\}\left\{\sum_{m=0}\sum_{n=0}\lambda^{m+n}\langle m \mid n\rangle\right\} \geq 0 \tag{4.12}$$

Expanding (4.12) gives a power series in λ. Since φ_0 is the unperturbed function in (4.1), the coefficients of λ^0 and λ^1 are zero and the term involving λ^2 must be the dominant term in the series. The term $\langle 1|\hat{H}_0 - E_0|0\rangle$ in the coefficient of λ^2 is zero by (4.6) and

$$E_2 \leq \langle 1|\hat{H}_0 - E_0|1\rangle + 2\langle 1|\hat{H}_1 - E_1|0\rangle, \tag{4.13}$$

provides a variational upper bound to E_2, the second-order energy, and an approximate first order wavefunction, φ_1. Equation (4.13) is the variational perturbation equation developed by Hylleraas [1] in 1930. To find E_2 and φ_1, φ_1 is expanded in a set of k trial functions, χ_i, as

$$\varphi_1 = \sum_{i=1}^{k} x_i \chi_i, \tag{4.14}$$

where the x_i are variational parameters and the χ_i must satisfy the same symmetry and boundary conditions as $\hat{H}$. The notation can be simplified by defining the two integrals

$$PB_i = \langle \chi_i | \hat{H}_1 - E_1 | \psi_0 \rangle, \tag{4.15}$$

$$T_{i,j} = \langle \chi_i | \hat{H}_0 - E_0 | \chi_j \rangle. \tag{4.16}$$

When the expansion for φ_1 is inserted into (4.13), we obtain

$$E_2 \leq 2 \sum_{i=1}^{k} x_i PB_i + \sum_{i=1}^{k} \sum_{j=1}^{k} x_i x_j T_{i,j}. \tag{4.17}$$

The x_i's are determined by minimizing E_2 with respect to each of the x_i's. This gives a set of k simultaneous linear equations that can be written as

$$\boldsymbol{Tx} = -\boldsymbol{PB}, \tag{4.18}$$

where $\boldsymbol{T}$ is a $k \times k$ symmetric matrix and $\boldsymbol{PB}$ is a k-element column vector. Inversion of $\boldsymbol{T}$ to find $\boldsymbol{T}^{-1}$ gives

$$\boldsymbol{x} = -\boldsymbol{T}^{-1}\boldsymbol{PB}. \tag{4.19}$$

Thus the wavefunction coefficients can be obtained by one call to the matrix inverse function of a Computer Algebra System (CAS) followed by a second call to a matrix multiplication function to multiply $\boldsymbol{T}^{-1}$ and $\boldsymbol{PB}$. Both Maple and Mathematica have linear algebra packages that include Gaussian elimination and linear solver functions that can solve (4.18) with a single function call.

Hylleraas [1] developed an efficient procedure for solving (4.18) subject to the requirement that E_2 be a minimum. A detailed outline of his method, which is similar to the Gauss exclusion algorithm for matrix inversion along with a numerical example of its application to the confined hydrogen atom were presented in [7].

Scherr and Knight [2] extended Hylleraas' work by showing that, to the extent that E_2 and $\varphi_1$are given accurately by (4.13), the coefficient of λ^2 vanishes and the coefficient of λ^3 provides an estimate of E_3. An upper bound to E_4 is given by the coefficient of λ^4 and in general E_n is given by the coefficient of λ^n. Note that a knowledge of φ_n allows calculation of E_{2n} and E_{2n+1}. This process can be continued to whatever order is desired.

A convenient aspect of HSK-VPT is that if the first-order and higher wavefunctions are composed of the same basis sets, the elements of the $\boldsymbol{T}$ matrix can be calculated

once and then reused. In similar fashion, all of the overlap terms $\langle \chi_i \mid \psi_0 \rangle$ and $\langle \chi_i \mid \chi_j \rangle$ and the interelectronic repulsion integrals $\langle \chi_i | \frac{1}{u} | \psi_0 \rangle$ and $\langle \chi_i | \frac{1}{u} | \chi_j \rangle$ need only be calculated once. This gives a very efficient way to carry the calculation to high order.

The φ_i calculated by the Hylleraas method do not satisfy the requirement that the total wavefunction be normalized. Since the lack of normalization does not affect the calculation of the E_n, we did not calculate the normalized wavefunction. The interested reader is referred to Sect. III of [2] for a detailed discussion of normalization.

Midtdal et al. [8] and Knight and Scherr [9] demonstrated that the higher order wavefunctions obtained from the variational perturbation equations satisfy the same orthogonality conditions as their exact first-order wavefunctions. This provides a straightforward path to calculation of excited state energies. The present work can be viewed as an extension of their work to helium confined at the center of an impenetrable sphere.

4.3 Calculational Details

4.3.1 Zero-Order Wavefunctions

The zero-order system was a one-electron atom/ion confined at the center of an impenetrable sphere of radius R. Although this system has an analytic solution in terms of the confluent hypergeometric function, evaluation of the integrals involving the confluent hypergeometrics imposed a severe time penalty. We therefore chose to solve the confined one-electron system variationally using a wavefunction of the form

$$\chi(r) = (R - r)e^{-\alpha r} \sum_{i=0}^{15} c_i r^i, \tag{4.20}$$

where $R - r$ is a cutoff function that insures that the wavefunction goes to zero at the surface of the sphere, and α and the c_is are variational parameters determined by minimizing the energy for the confined 1s wavefunction. The 1s wavefunction and energy correspond to the lowest root of the resulting secular determinant while the 2s wavefunction and energy were obtained from the second root. The variational energies were checked by comparison with the energy given by the confluent hypergeometric wavefunction and agreed to one part in 10^{12} or better.

The variational wavefunctions were then combined to give the zero-order singlet and triplet wavefunctions and transformed to the Hylleraas coordinates [10] defined by

$$s = r_1 + r_2; \quad t = -r_1 + r_2; \quad u = r_{12}. \tag{4.21}$$

4.3.2 Higher Order Wavefunctions

The higher order wavefunctions were expansions of the form

$$\varphi_n = \left[R - \frac{1}{2}(s-t)\right]\left[R - \frac{1}{2}(s+t)\right] e^{-\beta s} \sum_{k=1}^{N} c_k s^{l_k} t^{m_k} u^{n_k}, \tag{4.22}$$

and the factors $\left[R - \frac{1}{2}(s \pm t)\right]$ are cutoff functions. The wavefunctions included all terms with $l_k + m_k + n_k \leq 7$ subject to the requirement that m_k = even for the singlet state to ensure the required permutational symmetry of the spatial part of wavefunction. The triplet state wavefunction was obtained by multiplying each term of the singlet wavefunction by t. The resulting wavefunctions thus included 70 basis sets. β was found by variational minimization of E_2.

The variational perturbation equations were programmed using the Maple 17 CAS. The coding was a Maple version of the FORTRAN code originally provided to H.E.M. by R.E. Knight in 1969. Knight had used it in the work reported in [2, 9] and was quite proud that he was able to take Hylleraas' derivation [1] and convert it to FORTRAN by following the details of Hylleraas' arithmetic. Hylleraas' work is thus an interesting example of 83 years of "reused code".

4.4 Results and Discussion

The calculations were carried out to 31st order in the energy. A representative set of energy corrections for the $1s2s\,^1S$ and $1s2s\,^3S$ states of the helium atom for $R = 2\ a_0$ are shown in Table 4.1. Energy corrections for the $1s2s\,^3S$ state typically converged more rapidly than did the energies for the $1s2s\,^1S$ state.

The E_n for both states exhibit a periodic oscillation, similar to that observed in a previous HSK-VPT calculation [11] of one-electron wavefunctions. In that work we concluded that the oscillation resulted from a degeneracy in the complex plane caused by a square-root branch point singularity. We believe that we are seeing a similar effect here, but further work is required to fully understand the behavior of the energy corrections. In particular, it would be nice to quantify how changes in R and Z affect the period and amplitude of the oscillations in the E_n.

Energies were calculated for the $1s2s\,^1S$ and $1s2s\,^3S$ states over a range of confinement radii $R = 1$–$10\ a_0$ and for $Z = 1$–4. These data are shown in Table 4.2.

A discussion of the convergence of these HSK-VPT calculations must consider two different kinds of convergence. The first, termed perturbational convergence [9], deals with a consideration of how many E_n's must be incorporated in the perturbation expansion to give the desired accuracy. As mentioned above, the answer to this question depends on the nuclear charge, the confinement radius and the electronic state under consideration. In general, large nuclear charge converges

Table 4.1 Energy corrections in E_h for the helium atom confined in a sphere of radius 2 a_0

Order	$1s2s^3S$	$1s2s^1S$
0	−0.252118681457	−0.252118681457
1	0.825389375615	1.249788436512
2	−0.013546832372	−0.051963754504
3	0.000550205816	0.001902482589
4	−0.000023581149	−0.001221349851
5	0.000000756472	0.000213363982
6	−0.000000005409	−0.000009122421
7	−0.000000001474	−0.000003724051
8	0.000000000131	0.000001201274
9	−0.000000000006	−0.000000035819
10	0.000000000000	−0.000000011818
11		0.000000001005
12		−0.000000000399
13		0.000000000079
14		−0.000000000040
15		0.000000000001
16		0.000000000003
17		0.000000000000

more rapidly than small nuclear charge, tight confinement converges more rapidly than loose confinement and the triplet state converges more rapidly than the singlet.

The second kind of convergence, termed variational convergence, applies to the question of how well a given set of E_{2n}, E_{2n+1} and φ_n provide upper bounds to the energy corrections. This is a much more difficult question to answer since the calculations reported in this work are, to the best of our knowledge, the first perturbation theory calculations of confined excited states. In an effort to assess our calculated energies, we recently performed a variational calculation of the excited state energies for confined helium using a 125-term wavefunction in Hylleraas coordinates [10]. These data are shown in Table 4.3 and compared with other recent variational calculations.

The HSK-VPT energies for the triplet state reproduce the variational energies within 2.0×10^{-6} E_h and are lower than the variational energies of [12]. For the singlet state for $R \leq 6$ a_0 agreement among the HSK-VPT, 125-term variational and the 161-term variational energies of [13] is excellent. For $R > 6$ a_0, The HSK-VPT energies are lower than the 125-term variational energies but are quite close to the energies of [13]. This is consistent with our experience that variational calculations of the $1s2s^1S$ under moderate or low confinement require a large number of basis sets in the wavefunction to achieve accurate energies.

Table 4.2 $1s2s^3S$ and $1s2s^1S$ energies for confined two electron systems with Z = 1–4 and confinement radius R = 1–10

R/a_0	Z = 1		Z = 2		Z = 3		Z = 4	
	1^3S	2^1S	1^3S	2^1S	1^3S	2^1S	1^3S	2^1S
1					7.779717	8.513725	0.629026	1.439810
2			0.560251	0.946589	−3.508574	−3.121965	−8.410046	−8.092452
3	1.209495	1.406976	−1.370511	−1.114121	−4.771861	−4.583621	−9.178754	−9.019399
4	0.337130	0.510332	−1.874612	−1.717515	−5.027140	−4.915165	−9.297162	−9.160231
5	−0.026735	0.122490	−2.048044	−1.949761	−5.090062	−5.005498	−9.295587	−9.181753
6	−0.205016	−0.079197	−2.117816	−2.050700	−5.105964	−5.031362	−9.297024	−9.184517
7	−0.302371	−0.199761	−2.148564	−2.098069	−5.109726	−5.038499	−9.297151	−9.184789
8	−0.359992	−0.278374	−2.162783	−2.121503	−5.110529	−5.040280	−9.297162	−9.184809
9	−0.396331	−0.332059	−2.169479	−2.133440	−5.110683	−5.040646	−9.297163	−9.184810
10	−0.420466	−0.369824	−2.172625	−2.139594	−5.110711	−5.040701	−9.297163	−9.184809
∞	−0.499716	−0.499604	−2.175229	−2.145974	−5.110727	−5.040876	−9.297167	−9.184873

For $Z = 1$, $R = 1$ and $2a_0$ and for Z = 2, $R = 1a_0$, the perturbation expansions were unstable and those energies are not reported

Table 4.3 Comparison of HSK-VPT energies for confined helium with variational energies calculated using a 125-term wavefunction in Hylleraas coordinates

R/a_0	$1s2s^3S$		$1s2s^1S$	
	E_{VPT}	E_{VAR}	E_{VPT}	E_{VAR}
2	0.560251	0.560251	0.946589	0.946589
3	−1.370511	−1.370511	−1.114121	−1.114121
		−1.36799[a]		−1.114121[b]
4	−1.874612	−1.874612	−1.717515	−1.717517
5	−2.048044	−2.048044	−1.949761	−1.949762
		−2.04787[a]		−1.949761[b]
6	−2.117816	−2.117816	−2.050700	−2.050701
7	−2.148564	−2.148564	−2.098069	−2.097824
		2.14748[a]		−2.098084[b]
8	−2.162783	−2.162784	−2.121503	−2.120562
9	−2.169479	−2.169481	−2.133440	−2.129709
10	−2.172625	−2.172627	−2.139594	−2.133647
		−2.17146[a]		−2.139619[b]

Energies are in E_h

[a] Yakar et al. [12]

[b] Bhattacharyya et al. [13]

While the work reported here is an initial investigation into the applicability of HSK-VPT to confined systems, the data presented in Tables 4.2 and 4.3 support our hypothesis that it is a viable approach, particularly for excited states. Preliminary investigation of the $1s3s^1S$ and $1s4s^1S$ states indicates that our approach can be readily extended to higher excited states.

Another area of investigation with interesting possibilities is extension of Knight's work on 3-10 electron atoms [14] to confined atoms. While the evaluation of the required three-electron contributions presents significant numerical challenges, calculation of the energies of confined many-electron systems could provide an exciting insight into the effects of nanoscale confinement.

References

1. Hylleraas EA (1930) Uber den Grundterm der Zweielektronenprobleme von H^-, He, Be^{++} usw. Z Physik 65(3–4):209–225. Translated in Hettema H *Quantum Chemistry* (World Scientific: Singapore) 2000
2. Scherr CW, Knight RE (1963) Two-electron atoms III. A sixth-order perturbation study of the 1^1S ground state. Rev Mod Phys 35(3):436–442
3. Hylleraas EA, Undheim B (1930) Numerische Berechnung der 2 *S*-Terme von Ortho- und Par-Helium. Z Phys 65(11–12):759–772

4. MacDonald JKL (1933) Successive approximations by the Rayleigh-Ritz variation method. Phys Rev 43(10):830–833
5. Bacalis NC, Xiong Z, Karaoulanis D (2008) Hylleraas-Undheim-MacDonald higher roots, and minimization functionals at the excited states. J Comput Methods Sci Eng 8(4–6):277–285
6. Schiff LI (1955) Quantum mechanics, 2nd edn. McGraw Hill, New York
7. Montgomery HE (2011) Variational perturbation treatment of the confined hydrogen atom. Eur J Phys 32(5):1275–1284
8. Midtdal J, Aashamar K (1969) Variational perturbation theory calculations through 41st order of the non-relativistic energies of the states 1s2s $^{3,1}S$ and 1s2p $^{3,1}P$. Physica Norvegica 3 (3):163–178
9. Knight RE, Scherr CW (1963) Two-electron atoms II. A perturbation study of some excited states. Rev Mod Phys 35(3):431–436
10. Hylleraas EA (1929) Neue berechnung der energie des heliums im grundzustande, sowie des tiefsten terms von ortho-helium. Z Phys 54(5–6):347–366
11. Montgomery HE (1999) One-electron wavefunctions: variational perturbation theory. Chem Phys Lett 311(5):367–371
12. Yakar Y, Çakir B, Özmen A (2011) Computation of ionization and various excited state energies of helium and helium-like quantum dots. Int J Quant Chem 111(15):4139–4149
13. Bhattacharyya S, Saha JK, Mukherjee PK, Mukherjee TK (2013) Precise estimation of the energy levels of two-electron atoms under spherical confinement. Phys Scr 87(6):065305 (10 pp)
14. Knight RE (1969) Correlation energies of some states of 3-10 electron atoms. Phys Rev 183 (1)

Chapter 5
Confined Quantum Systems Using the Finite Element and Discrete Variable Representation Methods

Frederico V. Prudente and Marcilio N. Guimarães

5.1 Introduction

In atomic and molecular physics, confinement can not be considered as a recent problem, but the interest in quantum confined systems has increased considerably over the years [1–4]. Indeed, many physical and chemical phenomena can occur in environments that are considered cavities. As examples, the existence of atoms and molecules under high pressure, impurities in solids, chemical reactions in zeolite molecular sieves or fullerenes, etc. Furthermore, the advent of modern experimental techniques have enabled the fabrication of semiconductor nanostructures, such as quantum wells and quantum dots [5] providing additional motivation for the study of confined quantum systems. The spatial confinement is responsible for modifying the physical chemistry properties of the object relative to the free system due to interaction between the quantum mechanical properties of the confining cage and those of the enclosed object. These changes become more significant if the effective size of the object is of the same magnitude as the cavity size.

The determination of spectra is associated with the possibility of interpretation of experimental spectroscopic data for the confined systems, helping in a more detailed understanding of various physical and chemical phenomena. Therefore, an exact or approximate solution is useful for understanding some properties of these systems. The physical theory that provides the natural approach to describe these phenomena is quantum mechanics. However, difficulties in theoretical applications are found due to the complexity of the calculation for the precise determination of

F.V. Prudente (✉)
Instituto de Física, Universidade Federal Da Bahia, Salvador, BA 40170-115, Brazil
e-mail: prudente@ufba.br

M.N. Guimarães
Centro de Formação de Professores, Universidade Federal Do Recôncavo Da Bahia, Amargosa, BA 45300-000, Brazil
e-mail: marcilio@ufrb.edu.br

K.D. Sen (ed.), *Electronic Structure of Quantum Confined Atoms and Molecules*,
DOI 10.1007/978-3-319-09982-8_5

the most interesting properties of quantum systems. Thus, an important factor to be considered in these studies is the implementation of theoretical and computational methodologies for its implementation. A numerical methodology should, among other things, provide a good accuracy of the results and require less computational effort for its implementation. Accordingly, various theoretical approaches have been developed and/or employed for performing quantum-mechanical calculations of confined quantum systems. Indeed, there are several ways to find this solution numerically. Among them, the variational procedures have demonstrated to be a very powerful tool in the development of algorithms for problems involving bounded quantum systems. In this case the wave function is expanded in terms of known basis functions and the coefficients of expansion are determined by solving a set of linear algebraic equations. The success of variational calculus depends on the correct choice of the set of basis functions; if the basis functions are appropriate to the problem, then only a small number of them will be needed to obtain accurate results.

A quite accurate procedure that is applied to solve quantum mechanical problems within the variational formalism of the wave function expansion is the finite element method (FEM) [6]. The FEM is a general nomenclature for a set of procedures that are based on discretization technique of the space in elements and the use of polynomial basis functions defined in each of these elements. Another (quasi) variational procedure is the discrete variable representation (DVR) method which considers the discretized space and uses basis functions that diagonalize the matrix representation of the potential energy operator on the points of the discretized space [7, 8]. In this case, the matrix representation of the operator kinetic energy can be calculated analytically bringing great efficiency in the evaluation of the array elements. Together with the uses of global basis functions, the DVR and FEM are some of most utilized methods to solve quantum problems in molecular physics. Being variational approximations, they provide a means to systematically improve the accuracy of the calculations by increasing the number of basis functions.

In the actual chapter we present a review of Finite Element and Discrete Variable Representation methods to study typical confined quantum systems, discussing the advantages and disadvantages of each one of them. This chapter is organized as follows. In the Sect. 5.2 we establish the general theoretical problem to study confined quantum systems. In Sect. 5.3 we discuss the variational formalism, and presents the one-dimensional DVR and *p*-FEM methods for solving the time independent Schrödinger equation associated with the electronic structure problem of the confined systems. In the Sect. 5.4 is presented the applications to confined systems with one and two electrons. Specifically, results for the energy spectrum and other properties are presented for the bounded harmonic oscillator, the hydrogen atom confined spherically and endohedrally, hydrogenic ion confined in a plasma, and one and two electrons quantum dots. Finally, in the Sect. 5.5 we present our concluding remarks.

5.2 Confined Quantum Systems

The basic ingredients to the study of confined quantum systems are established in this section. We restrict the analyze only to electronic movement, but it can be extended easily for problems involving another particles (e.g., nuclei of atoms and molecules). In such a case, the time independent Schrödinger equation for N confined electrons is written as

$$\hat{H}\Psi(\mathbf{r}) = E\Psi(\mathbf{r}) \tag{5.1}$$

where the Hamiltonian operator, without any spin term, is given by

$$\hat{H} = \sum_{k=1}^{N} \hat{h}(\mathbf{r}_k) + \sum_{k=1}^{N} \sum_{l>k}^{N} \frac{e^2}{r_{kl}}, \tag{5.2}$$

$\mathbf{r} \equiv \{\mathbf{r}_1, \ldots, \mathbf{r}_N\}$ represents collectively the position vector of N electrons, $\mathbf{r}_k$ is the position vector of the kth electron, and r_{kl} is the kth and lth electrons distance. The one-electron Hamiltonian $\hat{h}(\mathbf{r}_k)$, including an external electromagnetic field, consists of

$$\hat{h}(k) = \frac{1}{2m_e}\left(-i\hbar\nabla_k - \frac{e}{c}\vec{A}(\mathbf{r}_k)\right)^2 + e\Phi(\mathbf{r}_k) - \sum_A \frac{Z_A e^2}{r_{kA}} + \hat{w}(\mathbf{r}_k), \tag{5.3}$$

being $Z_A e$ the charge of the nucleus A, r_{kA} the distance between the kth electron and Ath nucleus, $\vec{A}(\mathbf{r}_k)$ and $\Phi(\mathbf{r}_k)$ the vector and scalar potentials that define the electromagnetic field, and $\hat{w}(\mathrm{r}_k)$ the confinement potential term.

Of this way, the properties of an electronic confined system depend of many different issues as the way to simulate the spatial confinement and its geometric shape, the existence and the intensity of external electrical and/or magnetic field, the accuracy of the description of electron-electron interaction, the inclusion of spin dependent terms in Hamiltonian, and the quality of the calculations, among others. Some of them are discussed in the next subsections.

5.2.1 Spatial Confinement Models

Usually, the spatial confinement of a quantum system can be simulated by the imposition of the boundary conditions on the wave functions, by changing of the actual potential by a model one, and by introduction of a confinement potential (see Refs. [1, 3, 4] and references therein). The choice of these ways, as well as the shape of the model potential, will depend strongly on the nature of the confinement.

In particular, the potential models to treat confined electronic systems can be separated into at least three general categories. The first one represents the confinement by a repulsive potential barrier, which can be penetrable or impenetrable. These models are found, for example, in atoms under extreme pressure or inserted in cavities (such as in zeolites or impurities in solids) and in semiconductor nanostructures such as artificial atoms and molecules and quantum dots. Some examples of these potential models are:

- Infinite Spherical Box [9] $\hat{w}(r_k) = \begin{cases} 0 & \text{for} \quad r_k < r_k^c \\ \infty & \text{for} \quad r_k \geq r_k^c \end{cases}$
- Harmonic potential [10] $\hat{w}(r_k) = \frac{1}{2} m\omega^2 r_k^2$
- Wood-Saxon potential [11] $\hat{w}(r_k) = \frac{2\lambda}{1+\exp[(r_0 - r_k)/\eta]}$
- Gaussian confining potential [12] $\hat{w}(r_k) = -D\left[1 - \exp\left(-\gamma r_k^2\right)\right]$
- Anisotropic harmonic potential [13] $\hat{w}(r_k) = \frac{1}{2} m\left(\omega_x^2 x_k^2 + \omega_y^2 y_k^2 + \omega_z^2 z_k^2\right)$
- Quartic potential [14] $V(r_k) = \frac{m_e \omega_0^2}{2}\left(\frac{1}{4a^2}\left(x_k^2 - a^2\right)^2 + y_k^2\right)$

The second type is a confinement by an attractive enclosure, which is always penetrable, it is found, for example, in atoms inside fullerenes. Some examples of these potential models are:

- Attractive spherical shell [15] $\hat{w}(r_k) = \begin{cases} -U_0 & \text{if} \quad r_k^c \leq r_k \leq r_k^c + \Delta \\ 0 & \text{otherwise} \end{cases}$
- δ-potential [16] $\hat{w}(r_k) = -U_0 \delta(r_k - r_c)$
- Gaussian spherical shell [17] $\hat{w}(r_k) = -U_0 \exp\left(-\frac{(r_k - r_0)^2}{\sigma^2}\right)$

The third group aims to describe atoms embedded in neutral media (e.g., neutral plasma or liquid helium). Some examples of these potential models are:

- Debye screened potential [18] $\hat{w}(r_k) = -Ze^2 \frac{\exp(-\mu r_k)}{r_k}$
- Ion-sphere potential [19] $\hat{w}(r_k) = \begin{cases} \frac{(Z-1)e^2}{2r_k^c}\left[3 - \left(\frac{r_k}{r_k^c}\right)^2\right] & \text{for} \quad r_k \leq r_k^c \\ 0 & \text{for} \quad r_k > r_k^c \end{cases}$

Details of each one of these potential models and their constants can be found in the cited references. Note that each one of them has advantages and disadvantages for treating the confined systems that it is proposing to do. For example, the harmonic potential is convenient to represent electrons in a quantum dot close to the equilibrium geometry, but is not superiorly limited. An alternative for this case is the use of a Gaussian potential. In the case of attractive layer, the attractive spherical shell potential is easily implemented, but exhibits discontinuities, which can be overcome by Gaussian spherical shell. And the Debye screened and Ion-sphere potentials are indicated for different plasma regimes.

5.2.2 Levels of Many-Particle Interactions

Others indispensable ingredients to a precise determination of quantum effects in the few electrons quantum systems are the accuracy of the description of electron-electron interaction and the quality of the calculation. Various theoretical approaches have been used for this purpose. We can cite, among them, the Hartree approximation [20–22], the Hartree-Fock procedure [20, 23–26], the CI method [23, 26–28], the density functional theory [26, 29–32], the exact diagonalization [33, 34], the Green function [35], the Quantum Monte Carlo technique [26, 36, 37], the analytical approaches [38–40], the asymptotic iteration method [41], the perturbation theory [42, 43], the WKB treatment [44], and the Random Phase approximation [45]. Most of these methodologies are limited to calculate ground and few excited states properties [13, 46]. Due to the number of studies and interest, the two-electron quantum systems are attractive workbenchs for testing any new computational or theoretical procedure.

5.3 Variational Methods

5.3.1 Variational Formalism

Within the spirit of the Rayleigh-Ritz variational principle, the problem of determining the eigenenergies and eigenfunctions of a quantum problem as the Eq. (5.1) consists in finding stationary solutions of a functional of energy as follows

$$J[\Psi^*, \Psi] = \int_{\Omega} dv \Psi^*(\mathbf{r}) \left[\hat{H} - E\right] \Psi(\mathbf{r}), \tag{5.4}$$

where Ω is the accessible volume of system, the normalization condition of $\Psi(\mathbf{r})$ is added by the Lagrange multiplier E, dv is the volume element. In the case of a confined system, it is considered that the accessible volume is finite and the wave function should vanish at the closed surface which delimits Ω.

To obtain the solutions of problem (5.1), initially the wave function $\Psi(\mathbf{r})$ is expanded in terms of a finite basis functions set $\{f_j(\mathbf{r})\}$,

$$\Psi(\mathbf{r}) = \sum_j c_j f_j(\mathbf{r}), \tag{5.5}$$

where $\{c_j\}$ are the coefficients of expansion. This allows rewriting Eq. (5.4) in a matrix notation as follows

$$J[\mathbf{c}^\dagger, \mathbf{c}] = \mathbf{c}^\dagger (\mathbf{H} - E\mathbf{O})\mathbf{c}, \tag{5.6}$$

where **c** is a column vector with the expansion coefficients, and **H** and **O** are, respectively, the Hamiltonian and Overlap matrices whose elements are given by

$$H_{ij} = \int_{\Omega} dv f_i^*(\mathbf{r}) \hat{H} f_j(\mathbf{r}) \tag{5.7}$$

and

$$O_{ij} = \int_{\Omega} dv f_i^*(\mathbf{r}) f_j(\mathbf{r}). \tag{5.8}$$

The next step is to impose the stationarity condition on $J[\mathbf{c}^\dagger, \mathbf{c}]$ under variations of such coefficients. Using the calculus of variation and taking the functional variation on $\mathbf{c}^\dagger$, the stationary condition leads to

$$\mathbf{Hc} = E\mathbf{Oc}, \tag{5.9}$$

which is a generalized eigenvalue-eigenvector problem whose solutions are the energies and the respective wave functions of the quantum system. Taking the functional variation on **c**, equivalent result is obtained because **H** and **O** matrices are hermitian.

5.3.2 Discrete Variable Representation

The Discrete Variable Representation (DVR) method was originally proposed by Harris et al. [47] to calculate matrix elements of potential energy operator in one-dimensional problems, specifically of anharmonic oscillators ones. Later, Dickinson and Certain [48] showed that the method proposed by Harris et al. is equivalent to Gaussian quadrature when the basis is constructed of orthogonal polynomials. In 1985, Light and co-workers [49] generalized this method to calculate matrix elements of Hamiltonian operator of one-dimensional problems, furthermore they had discussed the extension of this method for multidimensional problems. From these original works, the DVR method has been widely used to determine the rovibrational excited states of polyatomic molecules and to describe processes of bimolecular reactions, among others (see Refs. [7, 8] and references therein). Only recently the DVR method began to be used for the study of quantum confined systems [11, 50–53] and electronic structure calculations [54].

Although the DVR method is not strictly variational, it presents formal and strong links with other variational methods (see, for example, Ref. [55]). Therefore, it can be employed to study problems using the formalism of Sect. 5.3.1. The DVR method considers the discretized space due to a Gaussian quadrature and uses basis

functions that diagonalize the matrix representation of the potential energy operator. An advantage of this method is that the matrix representation of kinetic energy operator can be generally calculated analytically.

In this subsection we describe the DVR method for a general Gaussian quadrature in a one-dimensional space and show its main features. Also we discuss the equally spaced DVR which is the simplest choice of quadrature points.

5.3.2.1 Methodology

Given a particular set of orthonormal functions $g_i(x), i = 1, \ldots, n$, which has the following property,

$$\sum_{i=1}^{n} |g_i\rangle\langle g_i| = \hat{1}, \tag{5.10}$$

we can construct a Gaussian quadrature, where the points $\{x_i\}$ are eigenvalues of the matrix $\mathbf{X}$ whose elements are given by

$$\{\mathbf{X}\}_{ij} = \langle g_i|\hat{x}|g_j\rangle = \int dx g_i^*(x) x g_j(x), \tag{5.11}$$

and their respective weights $\{w_i\}$ are obtained from the following relation:

$$w_i = \frac{1}{\sum_{j=1}^{n} g_j^*(x_i) g_j(x_i)}. \tag{5.12}$$

In particular, the functions $\{g_i(x)\}$ are known as primitive functions of the Gaussian quadrature.

Specifically, the DVR method consists to obtain a set of orthonormalized functions that satisfy the condition

$$f_i(x_j) = \frac{\delta_{ij}}{\sqrt{w_i}}, \tag{5.13}$$

and utilize it as a basis to expand the wave function of the system within the variational formalism. To obtain this basis set $\{f_i\}$, To get this set of basis functions $\{f_i\}$, we expand it in terms of primitive functions $\{g_i\}$,

$$f_i(x) = \langle x|f_i\rangle = \sum_{j=1}^{n} \langle x|g_j\rangle\langle g_j|f_i\rangle, \tag{5.14}$$

and evaluate the integral $\langle g_j|f_i\rangle$ by applying the quadrature rule

$$\langle g_j|f_i\rangle = \sum_{l=1}^{n} w_l g_j^*(x_l) f_i(x_l) = \sqrt{w_i} g_j^*(x_i), \tag{5.15}$$

where it is employed the property (5.13). Replacing the expression (5.15) in Eq. (5.14), the set of basis functions $\{f_i\}$ becomes

$$f_i(x) = \sum_{j=1}^{n} \sqrt{w_i} g_j^*(x_i) g_j(x). \tag{5.16}$$

Therefore, the discrete variable representation method consists in the expansion of the wave function using the basis set (5.16) and in the evaluation of the relevant integrals by quadratures, with the quadrature points obtained from the diagonalization of the matrix **X** (Eq. 5.11) and the weights shown in Eq. (5.12). Then the elements of potential and kinetic energy matrices, calculated by using the Gaussian quadrature rule, are, respectively,

$$V_{ij} = \langle f_i|\hat{V}|f_j\rangle = V(x_i)\delta_{ij} \tag{5.17}$$

and

$$T_{ij} = \sqrt{w_i w_j} \sum_{k,l=1}^{n} g_k^*(x_i) g_l(x_j) \langle g_k|\hat{T}|g_l\rangle. \tag{5.18}$$

Evidencing that the matrix representation of potential energy operator is diagonal and the matrix representation of kinetic energy operator is obtained analytically since, usually, the integral $\langle g_k|\hat{T}|g_l\rangle$ can be calculated analytically. In the literature, there is a great amount of DVR primitive functions which have been utilized to generate the DVR basis functions (see, for example, Ref. [56]), including numerically optimized DVR basis set [57, 58].

5.3.2.2 Equally Spaced DVR

In practice, the eigenvalues of position operator are not used in computation of matrix elements as quadrature points. In substitution are used the roots of the $(n+1)$th DVR primitive basis function. A simple primitive DVR functions are eigenfunctions of a particle in a one-dimensional box of range $[a, b]$ [59],

$$g_j(x) = \left(\frac{2}{b-a}\right)^{1/2} \sin\left[\frac{j\pi(x-a)}{b-a}\right], \quad j = 1, \ldots, n, \tag{5.19}$$

being $[a, b]$ the interval where the particle is confined. As the used quadrature points are the roots of $g_{n+1}(x)$ function, we have that

$$x_i = a + i\frac{b-a}{n+1}, \quad i = 1, \ldots, n.$$

Using Eq. (5.12), the weights are given by

$$w_i \equiv w = \frac{b-a}{n+1}.$$

Because it forms a quadrature where the points are uniformly distributed in interval, this implementation is named Equally Spaced DVR.

With this choice of DVR primitive basis functions we get orthonormalized functions in the integration region and, furthermore, each one satisfy conditions that are desired to the wave function $\Psi(x)$, i.e., they are vanishing on the interval limits. Figure 5.1 shows the complete set of basis functions, $\{f_i(x)\}$ $(i = 1, \ldots, 9)$ obtained

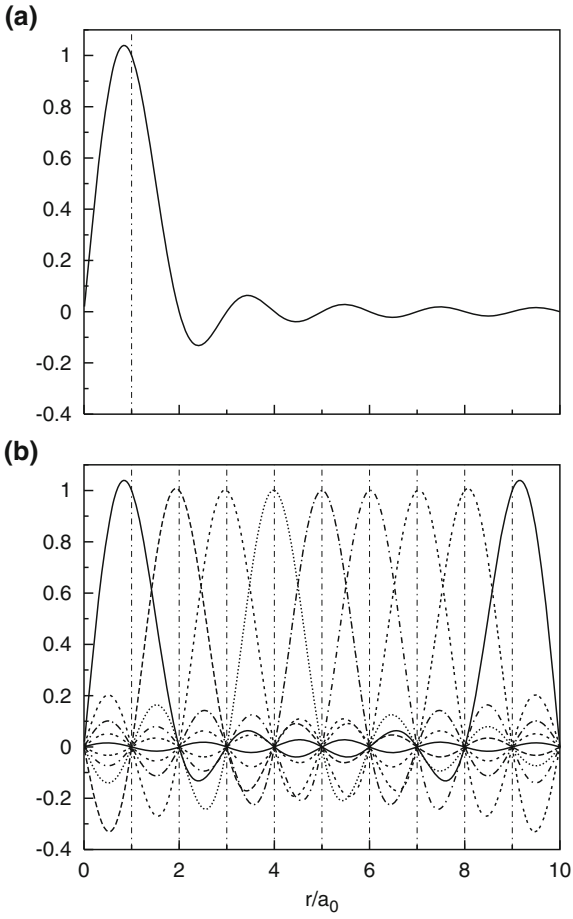

Fig. 5.1 The particle-in-box DVR basis eigenfunctions for $N = 9$, **a** $f_1(r)$ and **b** $f_i(r)$, $i = 1, \ldots, 9$. *Dot-dashed vertical lines* indicates the position of equally spaced grid points. Reproduced from Ref. [124]

from Eqs. (5.16) and (5.19). Thus, the kinetic energy matrix elements of Eq. (5.18) become

$$T_{ij} = -\frac{\hbar^2}{2\mu} w \sum_{k,l=1}^{N} g_k^*(x_i) g_l(x_j) \frac{2}{b-a} \int_a^b \mathrm{d}x \sin\left[\frac{k\pi(x-a)}{b-a}\right] \frac{d^2}{dx^2} \sin\left[\frac{l\pi(x-a)}{b-a}\right]$$
$$= \frac{\hbar^2}{2\mu} w \left(\frac{\pi}{b-a}\right)^2 \sum_{k=1}^{N} k^2 g_k^*(x_i) g_k(x_j),$$

where we use the fact that

$$\langle g_k | \hat{T} | g_l \rangle = -\frac{\hbar^2}{2\mu} \int dx g_k^*(x) \frac{d^2}{dx^2} g_l(x),$$

with μ being the mass, and

$$\frac{2}{b-a} \int_a^b \mathrm{d}x \sin\left[\frac{k\pi(x-a)}{b-a}\right] \sin\left[\frac{l\pi(x-a)}{b-a}\right] = \delta_{kl}.$$

We remember that the potential energy matrix is diagonal with elements given by Eq. (5.17).

5.3.3 *Finite Element Method*

The finite element method (FEM) is employed in quantum mechanics as a methodology based on the variational formalism for the expansion of the wave function in a finite basis set [6]. It is a general nomenclature for a set of procedures which are based on the technique of space discretization in elements and in the use of polynomial basis functions defined in each of these elements. The finite element method has been widely used in the analysis of engineering problems [60, 61], but in recent years has increased its application in the study of molecular dynamics and electronic structure for bounded systems [62–68], including in confined quantum systems [9, 69–71], as well as scattering processes [72–76].

The procedure for space discretization and the representation of the wave function by pieces of polynomials generate errors which can be minimized by strategies to converge the results toward the exact values. Based on this, several versions of the finite element method have been developed. The traditional version of FEM is the *h*-version in which the accuracy of the results is increased by decreasing the size, *h*, of the mesh elements due the increase of the number of elements. In the *p*-version remains the same number of elements and increases the order, *p*, of the polynomial. Already *hp*-version combines both approaches [77].

In this subsection we describe the one-dimensional p-version of the finite element method (p-FEM) and show its main features. Also we present the self-consistent FEM (SC-FEM) for construction of a optimized mesh of elements.

5.3.3.1 Methodology

The finite element method (FEM) consist of dividing the space into subregions (or elements) and expand the wave function in terms of basis functions defined in each of these elements. In the unidimensional case, the range of integration $[a, b]$ is divided into N_e elements, being the ith element defined in the range of x_{i-1} up to x_i with $x_0 = a$ and $x_{N_e} = b$, and the wave function is expanded as follows:

$$\Psi(x) = \sum_{i=1}^{N_e} \sum_{j=0}^{k_i} c_j^i f_j^i(x), \tag{5.20}$$

where the basis functions $\{f_j^i(x)\}$ satisfy the following property:

$$f_j^i(x) = 0 \ \text{ if } x \notin [x_{i-1}, x_i]. \tag{5.21}$$

The parameter k_i is the highest order of polynomials associated with ith element, $f_j^i(x)$ is the jth basis function of the same element and $\{c_j^i\}$ are the coefficients of expansion.

The p-version of the method of finite element (p-MEF) uses interpolant linear and shape functions that allow to employ polynomials of different orders in different elements. The two interpolant functions are defined as

$$\begin{aligned} I_1^i(x) \equiv f_0^i(x) &= \frac{x_i - x}{x_i - x_{i-1}} \\ I_2^i(x) \equiv f_{k_i}^i(x) &= \frac{x - x_{i-1}}{x_i - x_{i-1}} \quad x \in [x_{i-1}, x_i], \end{aligned} \tag{5.22}$$

while the $k_i - 1$ shape functions are defined as

$$S_j^i(x) \equiv f_j^i(x) = (4j + 2)^{-\frac{1}{2}} \left[P_{j+1}(y^i) - P_{j-1}(y^i) \right], \quad j = 1, \ldots, k_i - 1, \tag{5.23}$$

where $y^i = 2f_0^i(x) - 1$ e $P_j(y^i)$ are Legendre polynomials. In the Fig. 5.2 is shown the linear and shape functions until the third order, and in Fig. 5.3 we display pictorially the basis set for $N_e = 3$ and $k_i = k = 2$. These functions, defined in expressions (5.22) and (5.23), satisfies the following relationships at the edges of the elements:

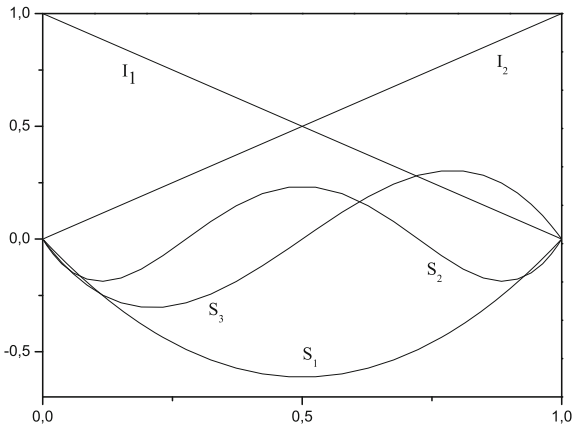

Fig. 5.2 Some local basis functions used in *p*-FEM

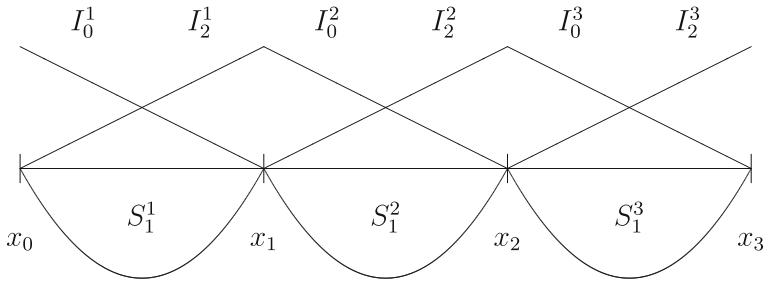

Fig. 5.3 Example of a *p*-FEM basis functions set with $N_e = 3$ and $k = 2$ used to expand the wave function

$$\begin{aligned} f_0^i(x_{i-1}) &= 1 = f_{k_i}^i(x_i) \\ f_0^i(x_i) &= 0 = f_{k_i}^i(x_{i-1}) \\ f_j^i(x_{i-1}) &= 0 = f_j^i(x_i) \quad j = 1, \ldots, k_i - 1. \end{aligned} \tag{5.24}$$

Note that, based on relations (5.24), the imposition of the continuity of the wave function in the nodes of elements yields the relationship $c_{k_i}^i = c_0^{i+1}$ between the coefficients of expansion, requiring that $f_{k_i}^i(x) + f_0^{i+1}(x)$ be considered the basis function that serves two elements. We then define a new set of independent coefficients $\{a_k\}$, whose relationship with the coefficients $\{c_j^i\}$ is given by

$$a_k = c_j^i \Leftrightarrow k = (i-1)k_i + j + 1.$$

Considering the wave function given by the expansion (5.20), whose the basis functions satisfies the properties (5.21) and (5.24), the matrix representation $\mathbf{B}$ of any local operator $\widehat{B}$ assumes the following block tridiagonal form:

$$\mathbf{B} = \begin{bmatrix} \mathbf{B}^1 & \mathbf{b}^1 & \mathbf{0} & \mathbf{0} & \cdots & \mathbf{0} \\ (\mathbf{b}^1)^\dagger & \mathbf{B}^2 & \mathbf{b}^2 & \mathbf{0} & \cdots & \mathbf{0} \\ \mathbf{0} & (\mathbf{b}^2)^\dagger & \mathbf{B}^3 & \mathbf{b}^3 & \ddots & \vdots \\ \mathbf{0} & \mathbf{0} & (\mathbf{b}^3)^\dagger & \ddots & \ddots & \mathbf{0} \\ \vdots & \vdots & \ddots & \ddots & \mathbf{B}^{N_e} & \mathbf{b}^{N_e} \\ \mathbf{0} & \mathbf{0} & \cdots & \mathbf{0} & (\mathbf{b}^{N_e})^\dagger & \mathbf{B}^{N_e+1} \end{bmatrix}, \tag{5.25}$$

where

$$\mathbf{B}^i = \begin{bmatrix} B^{i-1}_{k_i k_i} + B^i_{00} & B^i_{01} & \cdots & B^i_{0k_i-1} \\ B^i_{10} & B^i_{11} & \cdots & B^i_{1k_i-1} \\ \vdots & \vdots & \ddots & \vdots \\ B^i_{k_i-10} & B^i_{k_i-11} & \cdots & B^i_{k_i-1k_i-1} \end{bmatrix}, \quad \mathbf{b}^i = \begin{bmatrix} B^i_{0k_i} & 0 & \cdots & 0 \\ B^i_{1k_i} & 0 & \cdots & 0 \\ \vdots & \vdots & \ddots & \vdots \\ B^i_{k_i-1k_i} & 0 & \cdots & 0 \end{bmatrix}$$

with $i = 1, \ldots N_e$ and

$$\mathbf{B}^{N_e+1} = B^{N_e}_{k_{N_e} k_{N_e}}.$$

In these expressions, the non-zero elements of $\mathbf{B}$ matrix are

$$B^i_{jj'} = \int_{x_{i-1}}^{x_i} dx f^i_j(x) \widehat{B} f^i_{j'}(x) \ .$$

Note that when it is employed a p-FEM the $\mathbf{B}$ matrix is sparse, concentrated on the diagonal and also it is hermitian if $\widehat{B}$ is hermitian. Another important property is that only one basis function is different from zero in the last knot of mesh ($x = x_{N_e} = b$). Because of this, the spatial confinement on the wave function $\Psi(x)$ can be imposed easily employing a p-FEM just removing the basis function $f^{N_e}_{k_i}(x)$ of the expansion (5.20) [9].

5.3.3.2 Self-consistent FEM

An important point in p-FEM is the choice of size of each element of the unidimensional mesh or distribution of the nodes that define these elements. A simple

way to build the mesh is to get a equidistant discretization for the nodes, $\{x_i,\, i = 0, \ldots, N_e\}$, given by

$$x_i = a + i\frac{(b-a)}{N_e}. \tag{5.26}$$

However, in many cases it is necessary a optimized mesh to achieve better convergence of results with a smaller number of basis functions. In Ref. [17], Nascimento et al. introduced an amendment in the quantum mechanical procedure (QMP) to build optimized meshes for each potential, originally proposed by Prudente and Soares Neto [63]. The QMP is based on the rule of Gaussian quadratures, used in the Potential Optimized DVR method [57, 58, 78]. This method uses a set of orthonormal eigenfunctions of a particular Hamiltonian operator to build a Gaussian quadrature associated with them, where the points of the quadrature can be given as the eigenvalues of position operator on these orthonormal basis functions.

In that renewed procedure, which is called self-consistent finite element method (SC-FEM), initially is proposed an equidistant mesh and, after some self-consistent cycles, it is obtained a new FEM mesh optimized for the potential [17]. The basic steps of this procedure are:

1. It is estimated a set of eigenfunctions $\phi_i(x)$ of the quantum system in question using the p-FEM with a mesh which initially may be uniform.
2. Using the $N_e - 1$ first eigenfunctions, we build a matrix whose elements are

$$\{\mathbf{X}\}_{ij} = \int_a^b dx \phi_i^*(x) x \phi_j(x),$$

   where $\mathbf{X}$ is a representation matrix of the position operator $\widehat{X}$.
3. We diagonalize the matrix $\mathbf{X}$, and their $N_e - 1$ eigenvalues are $x_1, x_2, \ldots, x_{N_e-1}$ nodes that define the edges of the elements.
4. It is done a test of convergence comparing the eigenvalues of energy obtained with the new mesh with those obtained with the previous mesh. If the difference between them is out of a given tolerance it is returned to the stage 1 repeating the procedure with the new mesh. When it reaches the convergence the process is completed and the final mesh is obtained.

5.3.4 Commentary About Other Methods

The B-spline method refers to a representation of piecewise polynomial functions (or pp-functions), i.e., functions defined piecewise by polynomials. Such pp-functions in the B-form are often called spline functions which are expressed as a linear

combinations of B-spline functions. Hence B-splines generalize polynomials in the approximation of arbitrary functions. The B-splines was originally developed by Curry and Schoenberg in 1947 [79] and the term is an abbreviation for *basis splines*. Important contributions to the development of B-spline's theory was also given by De Boor [80]. B-spline method have been widely employed in atomic and molecular physics [81–86] including review articles on the its applications in this field [87, 88]. The Monte Carlo is a term that denote a set of stochastic methods, doing reference to gambling located in Monte Carlo city. Specifically, the correlation function quantum Monte Carlo (CFQMC) method [89–91] consists in a combination of a variational procedure based on the expansion of wave function by a finite basis set together with a stochastic methodology to compute the multidimensional integrals. The stochastic feature of method is due to generation of a random walk by Metropolis algorithm to evaluate the related integrals.

5.4 Applications

5.4.1 One-Dimensional Harmonic Oscillator

The one-dimensional harmonic oscillator (HO-1D) is one of the most extensively used systems for testing new methodologies in quantum mechanics. In particular, the confined HO-1D has been used in the literature to explain some experimentally observed deviations from the results predicted by calculations based on the free harmonic oscillator model. We can cite, for example, the emission spectra of the luminescence centers in crystals [92], the infrared stretching transition of the porphine [10] and confinement effect in the vibrational energies of point defects, impurities or luminescence centers in solids [1, 10, 93].

In this subsection we show results of the numerical calculation done with the equally spaced discrete variable representation (DVR) applied to the study of confined HO-1D. For this purpose, Costa et al. [11] proposed the Woods-Saxon potential to simulate spatial confinement. In this procedure it is introduced in the "free" Hamiltonian of the quantum system an additional modified Wood-Saxon potential so that $V(x) = \frac{1}{2}kx^2 + V_{MWS}(x;R)$ where

$$V_{MWS}(x;R) = \begin{cases} \frac{2\lambda}{1+\exp[(R+x)/\eta]} & x<0 \\ \\ \frac{2\lambda}{1+\exp[(R-x)/\eta]} & x>0 \end{cases} \tag{5.27}$$

whereas R defines the confinement barrier position, λ controls the barrier height and η controls its slope. Figure 5.4 shows the V_{MWS} for different values of η. The great advantage this methodology is that it enables the study of a wide range of systems and confinement regimes by varying two parameters in the model potential. This technique was employed to find numerical results in two different cases.

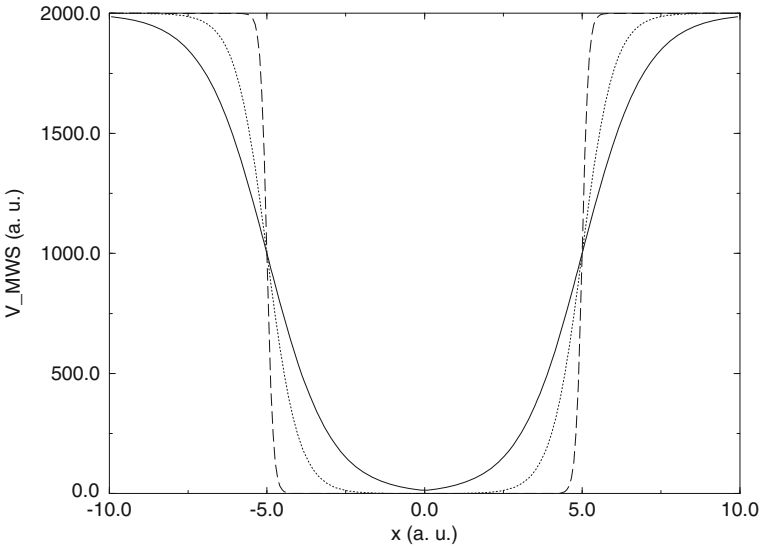

Fig. 5.4 General form of modified Woods-Saxon potential. Reproduced from Ref. [11]

5.4.1.1 Confinement with Zicovich-Wilson Model Potential

In order to simulate the Zicovich-Wilson et al. [10] confined potential given by

$$V(x) = \frac{1}{2}k\left(\frac{\tan \alpha x}{\alpha}\right)^2 \qquad \alpha = \frac{\pi}{2R}, \tag{5.28}$$

an optimization process is utilized to obtain the parameters η and λ. Then, the eigenenergies were calculated using 300 equally spaced points between -5.0 and 5.0 a.u. to build the DVR. Table 5.1 shows the energy eigenvalues for a few confinement radius values ($R = 0.5$, 1.0, 2.0, 3.0, 4.0) along with the exact values. It has used in the calculations $\hbar = m = k = 1$. The results are in very good agreement with results obtained by Zicovich-Wilson et al.

5.4.1.2 Confinement with Constant Infinite Barrier

The other system is the confined HO-1D with an infinite barrier. Again, it was utilized an optimization procedure to obtain the parameters η and λ. The eigenenergies were calculated utilizing 300 equally spaced points between -4.0 and 4.0 a.u. to build the DVR. Table 5.2 shows the energy eigenvalues for 5 confinement radius values ($R\sqrt{2} = 0.5$, 1.0, 2.0, 3.0, 4.0). The results obtained by Adams and Miller using the modified WKB method [94] and by Consortini and Frieden with an analytical quantum procedure [95] are presented for comparison. In these calculations

Table 5.1 Energy eigenvalues for confined one-dimensional harmonic oscillator using DVR method with Woods-Saxon model potential (V_{MWS}) and with Zicovich-Wilson method with their model potential (ZWPJ) ($\hbar = m = k = 1$)

State	R	V_{MWS}	ZWPJ [10]
0	0.5	4.97935	4.98463
0	1.0	1.39537	1.41056
0	2.0	0.67337	0.67745
0	3.0	0.58008	0.57321
0	4.0	0.54841	0.54004
1	0.5	19.88122	19.88835
1	1.0	5.44507	5.46495
1	2.0	2.33341	2.34079
1	3.0	1.85533	1.85672
1	4.0	1.69600	1.69722
2	0.5	44.66856	44.66101
2	1.0	12.00843	11.98583
2	2.0	4.63198	4.62097
2	3.0	3.40211	3.41438
2	4.0	2.98925	3.00861
3	0.5	79.32291	79.30261
3	1.0	21.03005	20.97307
3	2.0	7.54599	7.51800
3	3.0	5.24103	5.24620
3	4.0	4.45743	4.47422
4	0.5	123.80203	123.81313
4	1.0	32.40033	32.42660
4	2.0	11.01635	11.03189
4	3.0	7.361411	7.35218
4	4.0	6.10798	6.09404

Reproduced from Ref. [11]

$\hbar = m = 1$ and $k = \frac{1}{4}$. One sees that the DVR results are in quite good agreement with other results in the literature.

5.4.2 Confined Hydrogenic Atom/Ion

In this subsection we show application of theoretical and computational methodology based on variational formalism for bounded states and the p-version of finite element method (p-FEM) on more specifics situations involving hydrogenic atoms and ions. The Hamiltonian of the confined hydrogenic atom/ion assumes the same form of the free one, except the potential energy, $V(r)$. The variational solutions are

Table 5.2 Energy eigenvalues for confined HO-1D with constant infinite barrier using DVR method with Woods-Saxon potential (V_{MWS}), analytical quantum procedure (CF) and modified WKB (AM) ($\hbar = m = 1, k = \frac{1}{4}$)

State	$R\sqrt{2}$	CF [95]	AM [94]	V_{MWS}
0	0.5	9.87	9.88	9.87169
0	1.0	2.48	2.48	2.47645
0	2.0	0.65	0.67	0.64978
0	3.0	0.34	0.38	0.34373
0	4.0	0.27	0.30	0.26878
1	0.5	39.48	39.55	39.47954
1	1.0	9.89	9.90	9.89081
1	2.0	2.54	2.54	2.54007
1	3.0	1.25	1.26	1.24917
1	4.0	0.88	0.90	0.88269
2	0.5			88.80753
2	1.0			22.23399
2	2.0			5.63459
2	3.0			4.55298
2	4.0			1.70070
3	0.5			157.84127
3	1.0			39.51260
3	2.0			9.95907
3	3.0			7.01416
3	4.0			2.79291
4	0.5			246.54676
4	1.0			61.72734
4	2.0			15.51694
4	3.0			10.02051
4	4.0			4.18705

Reproduced from Ref. [11]

obtained after solving, for a particular angular momentum l, the generalized eigenvalue-eigenvector problem

$$\mathbf{H}^l\mathbf{c} = E\mathbf{O}^l\mathbf{c}, \tag{5.29}$$

where $\mathbf{c}$ is the coefficient vector. In such an equation the Hamiltonian and Overlap matrix elements are given by

$$\{\mathbf{H}^l\}_{ij} = \int_0^{r_c} dr \left\{ \frac{\hbar^2}{2\mu} \frac{df_i^{l*}}{dr} \frac{df_j^l}{dr} + f_i^{l*} V_l^{ef}(r) f_j^l \right\} \tag{5.30}$$

and

$$\{\mathbf{O}^l\}_{ij} = \int_0^{r_c} dr f_i^{l*}(r) f_j^l(r), \tag{5.31}$$

with $\{f_j^l\}$ being the finite basis set and $V_l^{ef}(r) = V(r) + [\hbar^2 l(l+1)/2\mu r^2]$.

We present applications concerning three problems. The first is the model of hydrogen atom under pressure showing some of its properties for various confinement radii. After we present results for the electronic structure of the hydrogen atom endohedrally confined by type C_{36} and C_{60} fullerenes using a model potential. Finally, we present the effect of plasma on the spectral properties of helium, aluminum and argon hydrogenic ions. Except when otherwise stated, all calculations are in atomic units and the element mesh was built using equidistant discretization and polynomials of same order for all elements ($k_i = k \; \forall \; i$).

5.4.2.1 Spherical Confinement

One of the first examples of confined quantum system, belonging to a small class of problems in atomic physics that can be solved exactly [96] is the hydrogen atom limited by an infinite spherical potential barrier. This model of compressed atom was introduced in 1937, when Michels et al. [97] proposed to simulate the effect of pressure on an atom. This work was followed by Sommerfeld and Welker [98] who performed calculations of ground state and recognized the importance of the model for astrophysics. Furthermore, several articles have studied this system including its use in the understanding of the interiors of giant planets [99, 100] and of atoms embedded in neutral media (e.g., neutral plasma or liquid helium [18, 101]).

We assume an infinite mass for the nucleus and putting it on the center of the hard sphere with radius r_c.[1] The potential energy becomes

$$V(r) = \begin{cases} -\frac{1}{r}, & r < r_c \\ \infty, & r \geq r_c \end{cases}, \tag{5.32}$$

where is included an impenetrable spherical barrier at $r = r_c$.

In Ref. [9] Guimarães and Prudente solved the problem given in Eq. (5.29) and calculated the energies for many states of confined hydrogen in various confinement

[1] Note that for a repulsive spherical cage the natural position of an atom is in the center, but for attractive potentials, this is not a general situation. However, even if the atom is off-center, it is reasonable first solve the problem with spherical symmetry, and then develop expansions that represent the effect of the displacement of the atom to some other position. Similarly, the surface of confinement need not be spherical, however, it is reasonable to start with a sphere, then consider how the system is modified by the distortion of the confining surface.

radii, using different numbers of basis functions, varying both the number of mesh elements, N_e, as the polynomials order, k. The convergence process for the energies was analyzed using the p-FEM with uniform mesh, given by expression (5.26), when N_e and k were increased, defining a convergence factor

$$|E(N_e, k) - E(N_e, k-1)| \leq 10^{-11}, \tag{5.33}$$

where $E(N_e, k)$ is the energy as function of the parameters of base (N_e and k). This study indicated that the eigenfunctions for the hydrogen atom are better approximated by high order polynomials. Hence, there should be a balance between the number of elements and the polynomial order to achieve a good convergence. This fact motivated the uses of $N_e = 5$ for calculations of energy levels while k was chosen in order to achieve a accuracy of at least 11 figures.

The very accurate results previously obtained by Aquino [102] and by Goldman and Joslin [103] were used as reference to evaluate the accuracy of p-FEM results. Aquino employed a numerical method which uses an approximation of wave function into Taylor series. On the other hand, Goldman and Joslin utilized an analytical solution of radial part of Schrödinger equation for the confined hydrogen atom, and, for each fixed l and r_c, searched numerically the zeros of confluent hypergeometric functions. The energies calculated by Aquino have precision of 10–11 figures, while Goldman and Joslin found results with accuracy of at least 7 figures. In Tables 5.3 and 5.4 are shown the energies for $1s$ and $3d$ states for various confinement radii and compared with the ones calculated by a variational method proposed by Varshni [104]. Moreover, in Table 5.3 the energies calculated by other variational method utilizing Gaussian basis set proposed by Zicovich-Wilson et al. [105] and the energies obtained by a time dependent variation perturbation calculations performed by Saha et al. [18] are shown for comparison.

The excellent precision of the p-FEM method to obtain eigenstates of confined hydrogen atom for ground and excited states for different values of l can be noted in these tables where the p-FEM results and the ones obtained by Aquino and Goldman and Joslin agree up to seven figures for any energy state independently of the confinement radius. Moreover, when compared with the other results shown in Tables 5.3 and 5.4 the p-FEM is the one that presents the best results. To obtain this precision, the value of highest order of polynomial basis functions associated with an element varied between $k = 4$ and $k = 9$ for small and larger confinement radii, respectively, representing small matrices with dimensions between 19×19 and 44×44. We also point out that the p-FEM basis are local functions, and, consequently, the integration is not performed over all region of space.

It is well known that not always an useful method for computing the energy spectrum is able for reproducing other electronic properties. In order to examine the efficiency of the p-FEM method on the calculation of such properties, the dipole polarizability (α) for the confined hydrogen atom in the $1s$ state for various confinement radii is shown in Table 5.5. They are compared with the values computed by Dutt et al. [106] obtained from an approximate formula using a numerical exact calculation, with the values calculated by Banerjee et al. [107] who utilized the

Table 5.3 Energy eigenvalue (in Hartree) for 1*s* state for a compressed hydrogen atom as a function of confinement radius (in Bohr); the *p*-FEM results are calculated using $N_e = 5$ and $k = 5$

r_c	Varshni[a]	Zicovich-Wilson et al.[b]	Saha et al.[c]	Goldman and Joslin[d]	*p*-FEM[e]	Aquino[f]
0.1	469.427			468.9930	468.993038659	
0.5	14.758			14.74797	14.7479700303	
0.81					4.39164157091	4.39164157090
1.0	2.3749		2.38187	2.373991	2.37399086610	
1.3	0.9173				0.91703708068	
1.6	0.27135				0.27131231264	
2.0	−0.12500		−0.12210	−0.1250000	−0.12500000000	−0.12500000000
3.0	−0.42255	−0.423949			−0.42396728773	
4.08671					−0.48533085511	−0.48533085511
5.0	−0.4947[g]	−0.496275	−0.49240		−0.49641700659	
7.0	−0.4993[g]	−0.499794	−0.49871		−0.49986257755	−0.49986257755
10.0		−0.499981	−0.499810	−0.4999993	−0.49999926328	−0.49999926328
14.0					−0.49999999950	−0.49999999949

[a] Ref. [104]; [b] Ref. [105]; [c] Ref. [18]; [d] Ref. [103]; [e] Ref. [9]; [f] Ref. [102]; [g] Dutt et al. [106]
Reproduced from Ref. [9]

Table 5.4 Energy eigenvalue (in Hartree) for $3d$ state for a compressed hydrogen atom as a function of confinement radius (in Bohr); the p-FEM results are calculated using $N_e = 5$

r_c	Varshni[a]	Goldman and Joslin[b]	p-FEM[c]	Aquino[d]
0.1		1644.530	1644.52992240	
0.5		63.16018	63.1601844674	
1.0	14.990	14.96746	14.9674640862	
1.5	6.294		6.28481943532	
2.0	3.3320	3.327509	3.32750915650	
3.0	1.2944		1.29280327199	
4.0	0.6220	0.6513558	0.62135577618	
5.0	0.32943		0.32911714297	
7.0	0.09666		0.09658964090	0.09658964089
8.0			0.04605824738	0.04605824737
10.0	−0.00709	−0.007092784	−0.00709278397	−0.00709278397
14.0			−0.04311347041	−0.04311347041
20.0			−0.05396756442	−0.05396756442

[a] Ref. [104]; [b] Ref. [103]; [c] Ref. [9]; [d] Ref. [102]
Reproduced from Ref. [9]

Table 5.5 Polarizability α (in atomic units) for the $1s$ state as function of confinement radius r_c; The p-FEM results are calculates using $N_e = 6$ and $k = 6$

r_c	Dutt et al.[a]	Banerjee et al.[b]	Saha et al.[c]	Laughlin[d]	p-FEM[e]
0.4	0.00085				0.000853148792
1.0	0.02868	0.03	0.0291		0.0287920226
1.4	0.09857				0.0990912992
2.0	0.34016	0.35	0.3344	0.342558	0.342558109
2.5	0.69490				0.700675176
3.0	1.02432	1.20			1.19170606
4.0	2.35782	2.39		2.377982333	2.37798233
5.0	3.40294	3.43	3.2176	3.422454224	3.42245422
7.0	3.51298	4.35	3.8079	4.347638027	4.34763803
9.0		4.49		4.487413391	4.48741338
12.0				4.499828228	4.49982819

[a] Ref. [106]; [b] Ref. [107]; [c] Ref. [18]; [d] Precise numerical values from Ref. [108]; [e] Ref. [9]
Reproduced from Ref. [9]

variational perturbation procedure, with the values calculated by Saha et al. [18] which also utilized variation perturbation calculations and with the precise numerical values extracted from Laughlin [108]. Note that the p-FEM results are

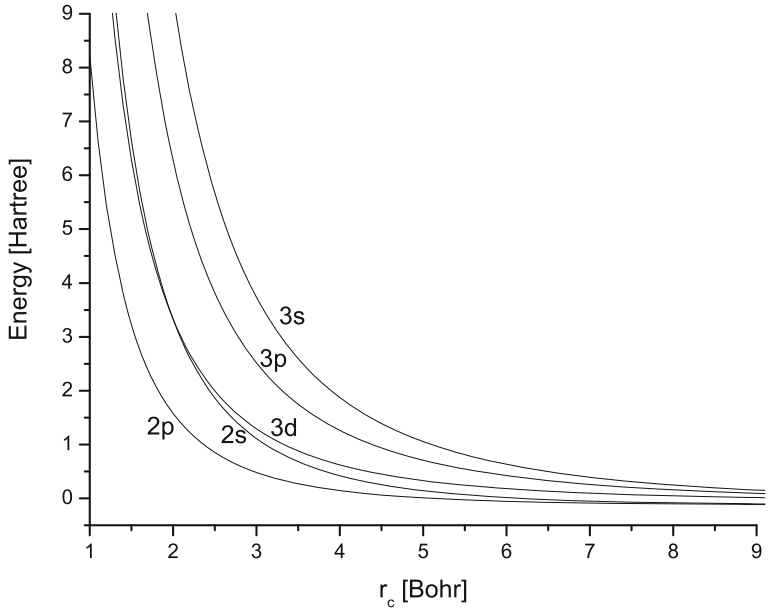

Fig. 5.5 Energy values (in Hartree) as function of confinement radius (in Bohr) for $2s$, $2p$, $3s$, $3p$ and $3d$ states of the compressed hydrogen atom. Reproduced from Ref. [9]

identical to precise numerical values of Laughlin, which it indicates that the wave function obtained within the p-version of the finite element method is enough accurate.

In Fig. 5.5 it is plotted the energy levels of $2s$, $2p$, $3s$, $3p$ and $3d$ states as function of confinement radius, r_c. It can be noted the splitting of the degeneracy observed in the free hydrogen atom for the levels $n\,l$, with $0 \neq l \leq n-1$, due to isotropic compression. Also, it can be observed accidental degeneracy between $2s$ and $3d$ levels at $r_c = 2.0$ bohr and the inversion of the energy values for $r_c > 2.0$ bohr.

5.4.2.2 Endohedral Confinement

Systems involving endohedral fullerenes, where atoms and small molecules are confined in a cage of carbon with $C_n (n \geq 20)$, have attracted much interest because their applications in nanoscience and nanotechnology [109]. Usually, the studies of electronic structure of endohedral fullerenes are performed considering all electrons by using ab initio, DFT and semi-empirical methods. However, it may be interesting to substitute all electrons description by models where the electrons of the guest atom or molecule are affected by an attractive spherical potential that simulate the C_n cage. This strategy has been utilized with success to describe the essential

features of the experimental results [2, 110]. The most employed models are the short-range potential shell of inner radius r_c and thickness Δ

$$V_{sr}(r) = \begin{cases} -U_0 & \text{for } r_c \leq r \leq r_c + \Delta, \\ 0 & \text{otherwise,} \end{cases} \tag{5.34}$$

and the δ-potential

$$V_{\delta}(r) = \begin{cases} -U_0 \delta(r) & \text{for } r = r_c, \\ 0 & \text{otherwise.} \end{cases} \tag{5.35}$$

In order to avoid numerical instability due to the sharp forms of potentials (5.34) and (5.35) and provide a more realistic description of the physical behavior of the confinement environment. Nascimento et al. [17] proposed to simulate the environment of a fullerene cage by an attractive short-range spherical Gaussian type potential given by

$$\hat{w}(r) = -w_0 \exp[-(r - r_c)^2/\sigma^2]. \tag{5.36}$$

Therewith, the fullerenes can be modeled by the adjustment of the radius of confinement shell, r_c, the thickness, given by σ, and the well depth, w_0. For the specific case of endohedrally confined hydrogen atom at the center of C_n cage, the potential will be described by $V(r) = -\frac{1}{r} + \hat{w}(r)$.

Here are presented results of Ref. [17] concerning the use of the p-FEM to perform electronic structure calculations of hydrogen atom inside C_{60} and C_{36} fullerenes modeled by the Gaussian shell potential (5.36). All p-FEM calculations were performed using $N_e = 20$, $k = 8$, totalizing 139 local basis functions, and $r_{\max} = 200.0\ a_0$; this assert an accuracy of, at least, four figures in the energy levels. The self consistent finite element method (SC-FEM) was also utilized to make the optimization process of element mesh. The Fig. 5.6 displays the equidistant and the optimized mesh, jointly with the effective (Coulombic + Gaussian confinement + centrifugal) potential, $V_l^{ef}(r)$, for $w_0 = 0.647$ Ryd, $\sigma = 0.57$ Å, $r_c = 3.54$ Å and $l = 0$. As expected, in the Figure it can be seen clearly that the node points of the optimized mesh are more concentrated in the regions where the potential reach a minimum. The consequence in the energy values is great: for the 1s energy level, the equidistant mesh gives a value of -0.4987 Hartree, while it is found the accurate value of -0.5006 Hartree for the optimized one.

In order to compare the Gaussian shell model with the previous one, Eq. (5.34), proposed by Connerade et al. [15], the energy levels of ns, $n = 1, \ldots, 4$, electronic states for H@C_{60} were calculated as a function of the confining well depth, w_0. The choice of r_c was taken equal to the characteristic (or experimental) radius of the fullerene cage; it was utilized $r_c = 3.54$ Å [111]. The value of σ of the Gaussian model was adjusted to satisfy the condition

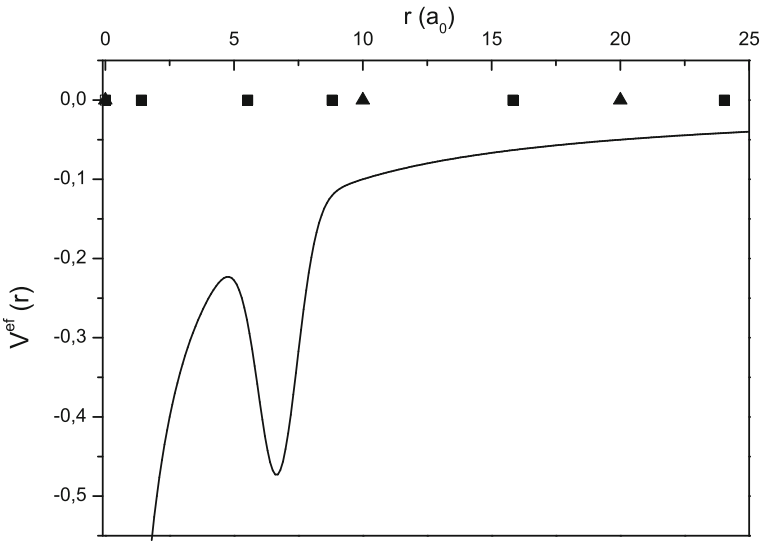

Fig. 5.6 The effective (Coulombic + Gaussian confinement) potential $V_0^{ef}(r)$ (*full line*), the equidistant (*triangle up*) mesh and optimized one (*square*) obtained using the SC-FEM; distance in bohr and potential energy in Hartree. Reproduced from Ref. [17]

$$\int_0^{\infty} w(r)dr = U_0\Delta \tag{5.37}$$

where U_0 is the well depth of the square well and Δ is the thickness of Eq. (5.34), while it is assumed that $w_0 = U_0$. Following Connerade et al. [15], it is assumed that $\Delta = 1$ Å, leading $\sigma = 0.57$ Å to the C_{60} cage. The results of the spherical Gaussian shell are shown in Fig. 5.7, where they are compared with those obtained by Connerade et al. [15]. There we can see a good agreement among both results, and the observed differences are due to the functional differences among the confinement potentials. For example, the 2s state is strongly modified even for small values of w_0, while the other states remain practically unchanged. However, the avoided crossings between ns and $(n+1)$s states remain in the Gaussian shell model, but their localizations are slightly differents; the 1–2s, 2–3s and 3–4s avoided crossings occur approximately at 1.5, 5.4 and 11.6 Ryd, respectively, for the present potential while for the Connerade et al. potential these crossings occur approximately at 1.4, 5.0, and 13.5 Ryd, respectively.

The potential depth w_0 to simulate a real cage can be obtained from experimental or theoretical data. A simple procedure is by fitting the calculated energy of an electron placed inside the Gaussian attractive shell (5.36) to the experimental value of the electron affinity [2]. Performing the evaluation of the potential depth w_0 to

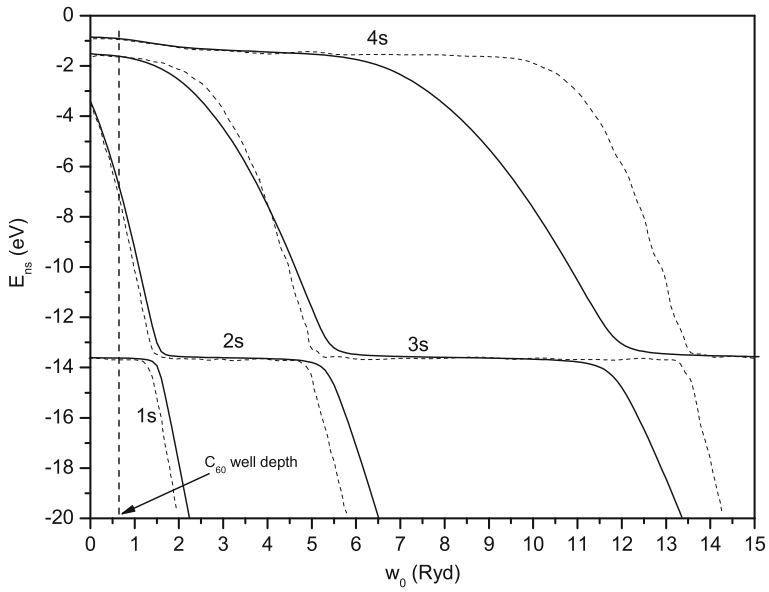

Fig. 5.7 Energies of 1s to 4s levels of H@C_{60}. *Solid lines*, *p*-FEM results; *dashed lines*, Connerade et al. Reproduced from Ref. [17]

simulate a real C_{36} cage, it was found $w_0 = 9.29$ eV $= 0.683$ Ryd considering the value of 2.8 eV for the experimental electron affinity of C_{36} [112]. Indeed, the quality of the *p*-FEM calculations enables to show clearly that, at this typical value of w_0 for the C_{36}, all states feel the influence of the confinement well. For this, in Fig. 5.8 we display the 1s to 4d wave functions calculated at this w_0, plotted with the effective potential (Coulombic + confinement). The choice of r_c was again taken equal to the characteristic (or experimental) radius of the fullerene cage; it was utilized $r_c = 2.50$ Å [113]. The states 2s, 2p, 3d have most of their amplitudes in the confinement region and remain bond in the outer well. The 3s, 4s, 3p, 4p and 4d states appears partially bound in the outer confining well. The 1s state has most of its amplitude in the inner Coulomb well but a significant amount of it in the outer well also, so that its energy is decreased by one amount nearly equal to the confining well depth.

Figure 5.9 displays the $1s$ to $4d$ energy levels of H@C_{60} as a function of w_0 calculated using the Gaussian shell. As well as in the spherical confinement (see Fig. 5.5), it can be noted the splitting of the degeneracy observed in the free hydrogen atom due to confinement potential. The *nl* states more affected by the fullerene cage are the ones with $l = n - 1$. Also the accidental degeneracy can be observed more clearly than in the spherical confinement as we can see between the $2s$ and $3d$ states.

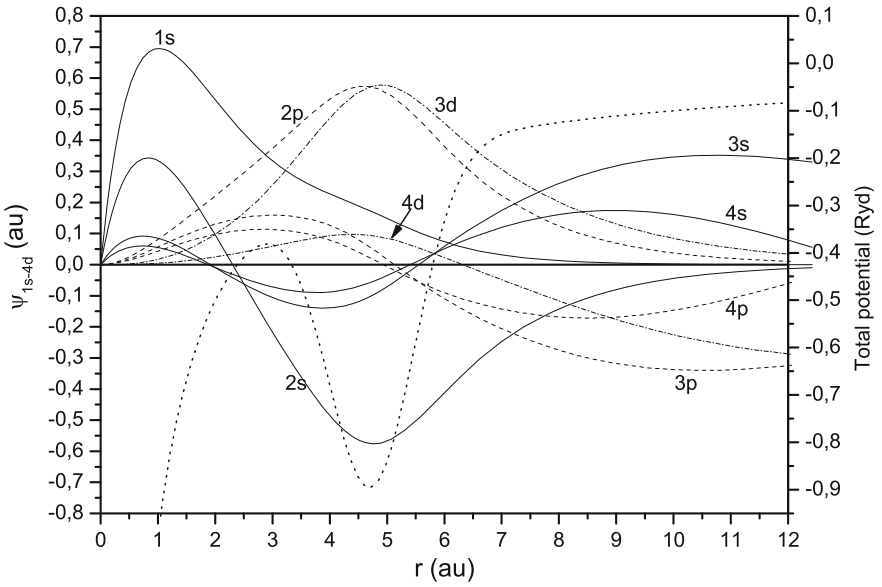

Fig. 5.8 The 1*s* to 4*d* radial wave functions for H@C_{60} at $w_0 = 0.683$ Ryd and the effective potential. *Solid lines*, *s* states; *dashed lines*, *p* states; *dashed dot lines*, *d* states; *dotted line*, effective potential (Coulombic + confinement). Reproduced from Ref. [17]

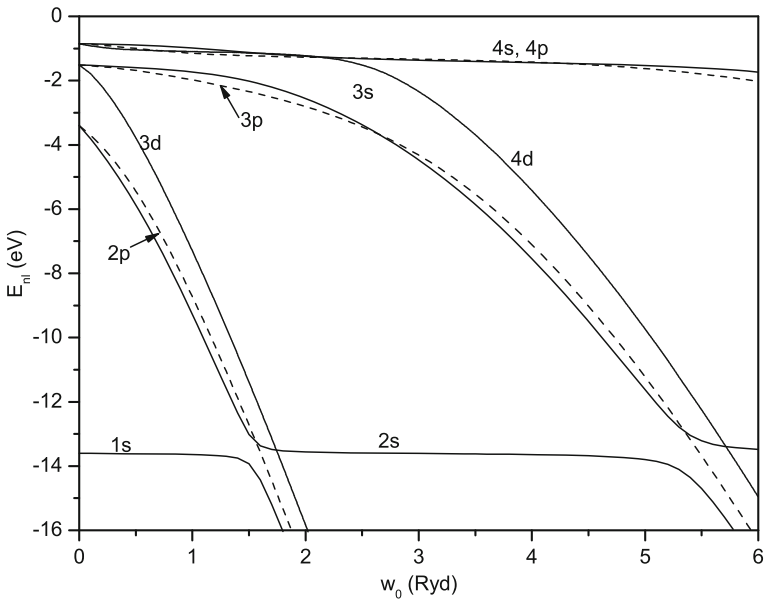

Fig. 5.9 The 1*s* to 4*d* energy levels of H@C_{60}. Reproduced from Ref. [17]

5.4.2.3 Plasmatic Confinement

The properties of the plasma environment and its effect on atomic systems has been subject of theoretical and experimental investigations for several years in many areas such as plasma physics, astrophysics, chemistry and so on [114, 115]. The interaction between the quantum mechanical properties of the plasma at a given temperature and those of the bound electrons from the embedded ions produces an external pressure on the system which modifies its spectral properties such as energy levels, polarizabilities, etc. To study the behavior of atomic systems in plasmas is necessary to understand their interaction with the plasma environment and find the effective interaction potential which is the sum of the interaction potential produced by strange electric charge in the plasma with the extra potential produced by the disturb of spatial distribution of charged particles in the plasma.

The coupling constant of a plasma, Γ, is defined as the ratio between the average Coulomb interaction energy and the average kinetic energy. For a weakly coupled plasma ($\Gamma \ll 1$) the *Debye-Hückel model* is very useful. Using this model, the plasma is considered as a neutral fluid of high electrical conductivity wherein we introduce an ion of electric charge Ze, where Z is the atomic number and e is the electron charge. For a hydrogenic ion this results in the modification of the Coulomb potential energy for the following (in Gaussian units)

$$V(r) = -Ze^2 \frac{e^{-\mu_D r}}{r}, \tag{5.38}$$

where μ_D is the Debye parameter. The Debye screening radius is given by

$$r_D = \frac{1}{\mu_D} = \left[\frac{k_B T}{4\pi(1+Z)ne^2}\right]^{\frac{1}{2}}.$$

where n is the density of ions and electrons in regions of null potential, k_B is the Boltzmann constant and T is the plasma absolute temperature.

In the case of one component spatially homogeneous strongly coupled plasma ($\Gamma > 1$), the *ion-sphere model* [116] is introduced as a useful concept replacing the Debye-Hückel model. O Ion sphere consists of a single ion of charge Ze and its neutralizing sphere negatively charged that surrounds it canceling its charge. This sphere represents the territorial domain of ion influence, in which other particles, having been repelled, are not likely to be found. Considering a hydrogenic ion with nuclear charge Ze having a single bound electron immersed in a homogeneous plasma with electronic charge density n within a sphere of radius R such that exactly $Z-1$ of the central positive charge is neutralized, under this condition the interaction potential energy is

$$V(r) = \begin{cases} -\frac{Ze^2}{r} + \frac{(Z-1)e^2}{2R}\left[3 - \left(\frac{r}{R}\right)^2\right] & , \quad \text{(for)} \quad r \leq R \\ 0 & , \quad \text{(for)} \quad r > R \end{cases}, \tag{5.39}$$

where,

$$R = \left[\frac{Z-1}{4\pi n/3}\right]^{\frac{1}{3}}.$$

In the Table 5.6, are presented results of ground state energy from Al^{12+} ion in a dense plasma for various ion-sphere radii calculated utilizing a optimized mesh by the SC-FEM performed by Guimarães and Prudente [117]. They are compared with others results calculated by a variational method which utilizes combination of Slater type orbitals proposed by Bhattacharyya et al. [19]. On the other hand, in Table 5.7, are presented results of ground state energy from Ar^{17+} ion for different Debye parameter and screening radius also calculated utilizing the SC-FEM. They are compared with results calculated by a variational method proposed by the same former authors. We note in both tables that almost all results with FEM and the ones obtained by Bhattacharyya et al. [19] agree in practically all decimals independently of the confinement radius. To get this accuracy, the number of mesh elements and the value of higher order polynomial basis functions associated with a mesh element were $N_e = 4$ and $k = 7$, respectively. These values for N_e and k represent matrices **H** and **O** (see Eqs. 5.30 and 5.31) with size 27×27. However, if we analyze the accuracy achieved in the calculations, the FEM has the feature of the computation be fast because of the sparse characteristic of matrices generated (see Eq. 5.25).

To demonstrate that the FEM is also effective in the calculation of excited states, in Fig. 5.10 it is shown the behavior of $1s$, $2s$, $2p$, $3s$, $3s$, $3p$ and $3d$ energies, as a function of ion-sphere radius, for the He^+ hydrogenic ion. When the confinement

Table 5.6 Ground state energy ($-E_{1s}$), in Hartree, for the Al^{12+} in different plasma electronic densities

Ion-sphere radius (a.u.)	Plasma density (/cc)	Bhattacharyya et al. [19]	SC-FEM [117]
9.9	1.99(22)	82.6819	82.6819
3.38146	5.0(23)	79.1796	79.1796
3.0227	7.0(23)	78.5489	78.5489
2.7798	9.0(23)	78.0297	78.0297
2.13018	2.0(24)	76.0610	76.0610
1.86089	3.0(24)	74.8437	74.8437
1.3419	8.0(24)	71.1306	71.1303

Notation $(x) \equiv 10^x$

The results obtained with SC-FEM use $N_e = 4$ and $k = 7$. Reproduced from Ref. [117]

Table 5.7 Ground state energy ($-E_{1s}$), in Hartree, for the Ar^{17+} in different Debye parameters and screening radius

Plasma density (/cc)	Temp. (eV)	Debye parameter (a.u.)	Screening radius (a.u.)	Bhattacharyya et al. [19]	SC-FEM [117]
1.0(23)	1,000	0.3103	3.2230	156.4865	156.4860
5.0(23)	1,000	0.6938	1.444	149.8640	149.8638
1.0(24)	1,000	0.9812	1.0192	145.0367	145.0360
5.0(24)	1,000	2.1939	0.4558	125.8566	125.8588

The results with SC-FEM utilize $N_e = 4$ and $k = 7$. Reproduced from Ref. [117]

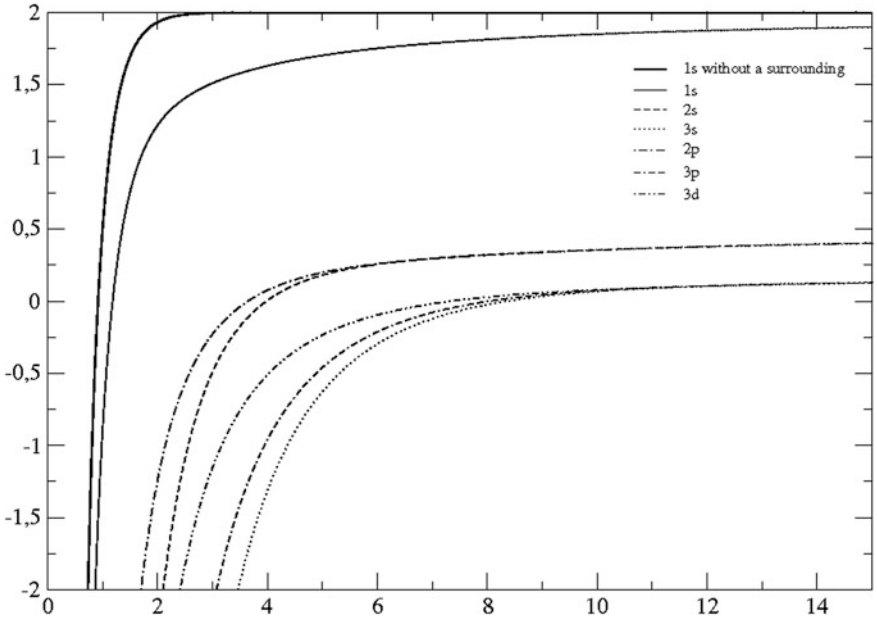

Fig. 5.10 Energy levels, $-E$, against the ion-sphere radius, R, for the hydrogenic ion, He^+. Also it is shown the 1*s* state with spherical confinement only, without the plasma surrounding. Values in atomic units. Reproduced from Ref. [117]

radius of ion-sphere tends towards zero the energy levels increase due to the increased plasma density, then the degeneracy break, observed in free hydrogenic ions, occurs, and the *s-p* competition tends to disappear. This common result occurs for the three hydrogenic systems studied in this section (see Figs. 5.5 and 5.9).

5.4.3 Quantum Dots

Another situation quite similar to the confinement of atoms is the quantization of electrons energy confining them in a quantum dot (semiconductor crystal having a diameter of few nanometers). Indeed, the Hamiltonian of a quantum dot is essentially the same as that of a confined atom, except that confinement is usually modeled by enclosing the system by a harmonic potential, being apparently somewhat good approximation for large radii. As quantum dots are similar to atoms, they are often referred as artificial atoms or quantum dot atoms. Comparisons have been made, for example, between the properties of the two-electron quantum dot, the helium atom, and the negative hydrogen ion, confined by a harmonic potential [46].

What draws attention to quantum dots is the possibility of controlling their shapes, their dimensions, their structures of energy levels and the number of confined electrons. Since quantum dots absorb and emit light in a very narrow spectral range, which is controlled, for example, by an external magnetic field, they might have applications in the construction of controllable semiconductor lasers more efficient and precise. Also is very promising the possibility of the quantum dots to be used as quantum "bit" in a new generation of computers.

In this subsection we show results of energy spectrum for two different types of quantum dot atoms: an impurity located in a parabolic quantum dot, and, a two-electron quantum dot. This spectrum is computed using the discrete variable representation (DVR) method.

5.4.3.1 Impurity in a Parabolic Quantum Dot

In the Ref. [11], Costa et al. considered the problem of a hydrogenic impurity in the center of a parabolic quantum dot using the DVR method and, even as in the Sect. 5.4.1, introducing the Woods-Saxon potential into the Hamiltonian so that, within framework of effective-mass approximation and using atomic units,

$$H = -\nabla^2 - \frac{2}{r} + \gamma_p^2 r^2 + V_{WS}(r;R). \tag{5.40}$$

where $\gamma_p = \frac{\hbar\omega_p}{2Ry}$ and

$$V_{WS}(x;R) = \frac{2\lambda}{1+\exp[(R-x)/\eta]} \tag{5.41}$$

Table 5.8 shows, for various confinement radius and three values of γ_p, the binding energies (defined by Varshini [118]) and the optimized Woods-Saxon parameters (η and λ) obtained by DVR method. Also is shown the Varshni's numerical results [118] obtained by integration of the Schrödinger equation using

Table 5.8 Optimized Woods-Saxon parameters and binding energy values for an impurity in a parabolic quantum dot using DVR method (V_{WS}), and Varshni's exact values (Vars)

R	$1/\eta$	2λ	V_{WS}	Vars [118]	γ_p
1.0	86.754759	2993.473288	5.152486	5.152486	0.2
1.0	88.340541	2993.466669	5.153915	5.153915	0.3
1.0	88.342176	2993.465715	5.155917	5.155917	0.4
2.0	95.675910	2993.399842	2.732638	2.732638	0.2
2.0	95.696075	2993.429949	2.745262	2.745262	0.3
2.0	95.722799	2993.423707	2.762897	2.762897	0.4
3.0	105.602453	2994.562167	1.982281	1.982281	0.2
3.0	105.993863	2994.448853	2.026906	2.026906	0.3
3.0	106.701360	2994.595237	2.087713	2.087713	0.4
4.0	127.355689	2993.460078	1.670637	1.670637	0.2
4.0	126.181523	2994.322813	1.770142	1.770142	0.3
4.0	211.185350	2995.657302	1.892868	1.892868	0.4
5.0	47.274217	445.1123830	1.545602	1.545602	0.2
5.0	2451.832229	268.9006551	1.700058	1.700058	0.3
5.0	2455.073658	1.841043423	1.861207	1.861207	0.4
6.0	393.531103	19.94505925	1.505747	1.505747	0.2
6.0	105.814563	2994.595237	1.689308	1.689316	0.3
6.0	91.105971	2993.419025	1.859172	1.859181	0.4
7.0	471.792157	2.362595237	1.497086	1.497088	0.2
7.0	471.814563	2.362595237	1.688523	1.688530	0.3
7.0	472.597096	2.9934190255	1.859125	1.859134	0.3

Reproduced from Reference [11]

Numerov's method and a logarithmic mesh. These values can be considered as exact binding energy and is utilized for comparison. One sees that DVR results reproduce the exact energy with a great precision for all values of confinement radius R and γ_p parameter considered. These results together with those obtained in the study of confined one-dimensional harmonic oscillator demonstrate the strength of the methodology of combining the Woods-Saxon model potential with the DVR method to study confined quantum systems.

5.4.3.2 Two-Electron Quantum Dot

Finally, we present the system of interest, namely, a two interacting electrons of effective mass m^* in a quantum dot with an anisotropic harmonic confinement potential whose Hamiltonian is

$$H = \sum_{j=1}^{2}\left\{-\frac{1}{2m^*}\left(\nabla_j^2\right) + V_{dot}\left(\vec{r}_j\right)\right\} + \frac{e^2}{\varepsilon|\vec{r}_1 - \vec{r}_2|} \tag{5.42}$$

where $\vec{r}_j$ is the position of the jth electron and

$$V_{dot}(\vec{r}_j) = \left(\frac{m^*}{2}\right)[\omega_\perp^2(x_j^2 + y_j^2) + \omega_z^2 z_j^2]$$

is the confinement potential of the quantum dot. The effective atomic units are used unless otherwise stated, i.e. $\hbar = m^* = \frac{e}{\sqrt{\epsilon}} = 1$.

It can be introduced the relative motion (RM) and the center-of-mass (CM) coordinates in Eq. (5.42) so that the Hamiltonian splits like $H = H_{CM} + H_{RM}$ [5]. Thus the total energy (E) of this system is the sum of the center-of-mass (E_{CM}) and relative motion (E_{RM}) eigenenergies. The center-of-mass part can be solved analytically and its solution is a planar oscillator with angular frequency $\omega_\perp$ and a Z-direction harmonic oscillator with frequency ω_z; in consequence the center-of-mass eigenenergy can be written as

$$E_{CM} = (2N + |M| + 1)\omega_\perp + \left(N_Z + \frac{1}{2}\right)\omega_z \tag{5.43}$$

where N and M are the radial and the azimuthal quantum numbers associated with the planar oscillator, respectively, and N_Z is the quantum number associated with the Z-direction harmonic oscillator.

The relative motion problem has not an analytical eigenfunction due to the Coulomb interaction. In Ref. [50], Prudente et al. developed a strategy to solve the relative motion Schrödinger equation employing a variational scheme based on the DVR method to expand the radial direction wave function, $\{\chi_j(r)\}$, while that for the angular directions the spherical harmonics, $Y_{lm}(\Omega)$, were employed. Thus, the relative motion problem turns to be the solution of a generalized eigenvalue problem, which in matrix notation is the following equation,

$$\mathrm{H}_{RM} c^{\sigma m} = E_{RM}^{\sigma m} O c^{\sigma m} \tag{5.44}$$

where $c^{\sigma m}$ is the coefficient vector, σ is the parity of the relative motion wave function with relation of interchange of the two electrons, and m is associated with the eigenvalue of the z-component of the angular momentum operator l_z. The Hamiltonian matrix elements are given by

$$\begin{aligned}\{\mathrm{H}_{RM}\}_{jj',ll'} = &\int \chi_j^*(r)\left\{-\frac{d^2}{dr^2} + \frac{l(l+1)}{r^2} + \frac{1}{4}\omega_\perp^2 r^2 + \frac{1}{r}\right\}\chi_{j'}(r)dr\delta_{ll'} \\ &+ \frac{\Delta\omega^2}{4}A_{l'}^{lm}\int \chi_j^*(r) r^2 \chi_{j'}(r)dr\end{aligned} \tag{5.45}$$

with $\Delta\omega^2 = \omega_z^2 - \omega_\perp^2$ and

$$A_{l'}^{lm} = \int Y_{lm}^*(\Omega)\cos^2\theta Y_{l'm}(\Omega)d\Omega \tag{5.46}$$

while

$$\{\mathbf{O}_{RM}\}_{jj',ll'} = \int \chi_j^*(r)\chi_{j'}(r)dr\delta_{ll'} \tag{5.47}$$

are the overlap matrix elements.

The energy spectra is presented for different confining parameters ($\omega_\perp$ and ω_z). The calculations were done expanding the relative motion wave function by using 30 spherical harmonics with a particular symmetry relative to singlet or triplet states (odd or even l's) and 100 $\{\chi_i(r)\}$ basis functions. The solutions $\{\chi_i(r)\}$ were obtained employing 2500 DVR basis functions equally spaced in an appropriate interval for each pair of parameters $\omega_\perp$ and ω_z. Thus, the energy spectra presented here have precision at least 6 significant digits.

Isotropic Case

The isotropic situation ($\omega_\perp = \omega_z$) is analyzed and calculations of the relative motion eigenenergies (E_{RM}) are presented. Due to the isotropy of the confinement potential, the expression (5.43) indicates that the results can be labels using only the radial, n, and angular momentum, l, quantum numbers. On the other hand, the expression (5.43) for the center of mass eigenenergies (E_{CM}) is reduced to

$$E_{CM} = \left(2N + L + \frac{3}{2}\right)\omega \tag{5.48}$$

where N and L denote, respectively, the radial and angular momentum quantum numbers related with the center-of-mass motion.

The complete spectrum ($E = E_{CM} + E_{RM}$) for a small set of (N, L, n, l) states are presented in Table 5.9 in order to compare with the ones obtained previously in Refs. [119] and [120]. These total energies of two electron quantum dot were determined in Ref. [120] solving the Hartree-Fock, Kohn-Sham and Schrödinger equations by using the shift-$1/N$ [121] and Schwartz numeric [122] methods, while in Ref. [119] the ones are calculated by using the orbital integration method [123]. A comparison between the results shown in Table 5.9 indicates that the procedure based on the DVR method gives results with a great precision, and that the use of methodologies that completely compute the correlation effects is very important.

Table 5.9 Three-dimensional two-electron quantum dot energies for select values of the confinement parameter ω

ω	(N, L, n, l)	HF-$1/N$[a]	HF-numa[b]	KS-$1/N$[c]	KS-num[d]	Exact-$1/N$[e]	Exact-num[f]	OIM[g]	DVR[h]
0.25	(0, 0, 0, 0)	1.1163	1.1241	1.1644	1.1742	1.0858	1.08926		1.089262
1.0	(0, 0, 0, 0)	3.7673	3.7717	3.8711	3.8791	3.7217	3.73012	3.9632	3.730120
	(0, 0, 0, 1)							4.7167	4.515101
	(0, 0, 0, 2)							5.5867	5.418156
	(0, 0, 0, 3)							6.5075	6.360638
	(0, 0, 0, 4)							7.4532	7.321609
4.0	(0, 0, 0, 0)	13.5693	13.5693	13.7902	13.7928	13.5057	13.5232		13.523214

[a] Hartree-Fock solutions by using the shifted-$1/N$ method; Ref. [120]
[b] Hartree-Fock solutions by using the accurate numerical technique; Ref. [120]
[c] Kohn-Sham solutions by using the shifted-$1/N$ method; Ref. [120]
[d] Kohn-Sham solutions by using the accurate numerical technique; Ref. [120]
[e] Exact Schrödinger solutions by using the shifted-$1/N$ method; Ref. [120]
[f] Exact Schrödinger solutions by using the accurate numerical technique; Ref. [120]
[g] Exact Schrödinger solutions by using the Orbital Integration Method; Ref. [120]
[h] Results by using the Discrete Variable Representation method
Energies are in effective atomic units. Reproduced from Ref. [50]

The spectrum with the lowest 245 energies of (N, L, n, l) states relative to the quantum dot parameter (i.e., E/ω) are displayed in Fig. 5.11 for different ω's and for non-interacting electron problem. In the last case, relative motion eigenenergies satisfy a similar expression of E_{CM} (Eq. 5.48), i.e., $E_{RM} = \left(2n + l + \frac{3}{2}\right)\omega$. In this Figure, the band structure clearly appears for $\omega \geq 0.5$, and when the values of quantum dot parameter increase, the bands go sharpening and the interacting two-electron spectrum move toward to the non-interacting ones. However, for weak confinement ($\omega \to 0$) it is observed a more diffuse spectrum. Since the energy gaps that occur between the $(N + 2L + n + 2l + 3)$-fold degenerate states of the non-interacting two-electron quantum dot is due to the spectrum associated with two harmonic oscillator, Fig. 5.11 indicates that for stronger quantum dot parameters (larger values of ω) the motion of the electrons is mainly governed by the confinement potential, while for a weak confinement the electron-electron interaction plays an important and essential role.

Anisotropic Case

The anisotropic situation ($\omega_\perp \neq \omega_z$) was analyzed and calculations of the relative motion eigenenergies (E_{RM}) associated with (n, m, n_z) states are presented. The first 42 relative motion energy levels for each pair of ω_z and $\omega_\perp$ are shown in Fig. 5.12 together with the non-interacting energy levels, which are given by $E_{RM}^{non} = (2n + m + 1)\,\omega_\perp + (n_z + 0.5)\,\omega_z$. From this figure we can observe that when it is considered the electron-electron interaction, differently from the isotropic case, the electronic states in the band structure do not present a general rule. Furthermore, we can observe that the error obtained to calculate the non-interacting triplet ground state is smaller than the one obtained to calculate the non-interacting singlet ground state. This indicates that the electron-electron interaction is more important for singlet states than triplet ones.

In order to analyze the degeneracies that happens in the energy spectrum, selected total energy levels ($E = E_{CM}$+E_{RM}) associated with (N, M, N_Z, n, m, n_z) states with up to two excitations for different ω_z's are displayed in Fig. 5.13 as function of ω_z parameter. We can see a splitting on the degenerate total energy levels for $\omega_\perp = \omega_z = 0.5$ when ω_z varies. Moreover, other crossings of states happens for different ω_z's as, for example, it can be seen in the Fig. 5.13 for $\omega_z = 1.0$ and for $\omega_z \approx 0.38$. We can note that these crosser of energy levels are of two types: one is due a symmetry of the confinement potential to particular ω parameters (as with $\omega_z = 1.0$), while the other is due an accidental degeneracy which occurs between excited relative motion states and excited center-of-mass ones (as with $\omega_z \approx 0.38$). The last one is result of the electron-electron interaction and the vertical deformation. Furthermore, it can be seen that the energy of a excited relative motion state, $(0, 0, 0, n, m, n_z)$, is always smaller than the one of the similar excited center-of-mass state, $(N, M, N_Z, 0, 0, 0)$ with $N = n$, $M = m$ and $N_Z = n_z$. This can indicate that the effect of the electron-electron interaction is more

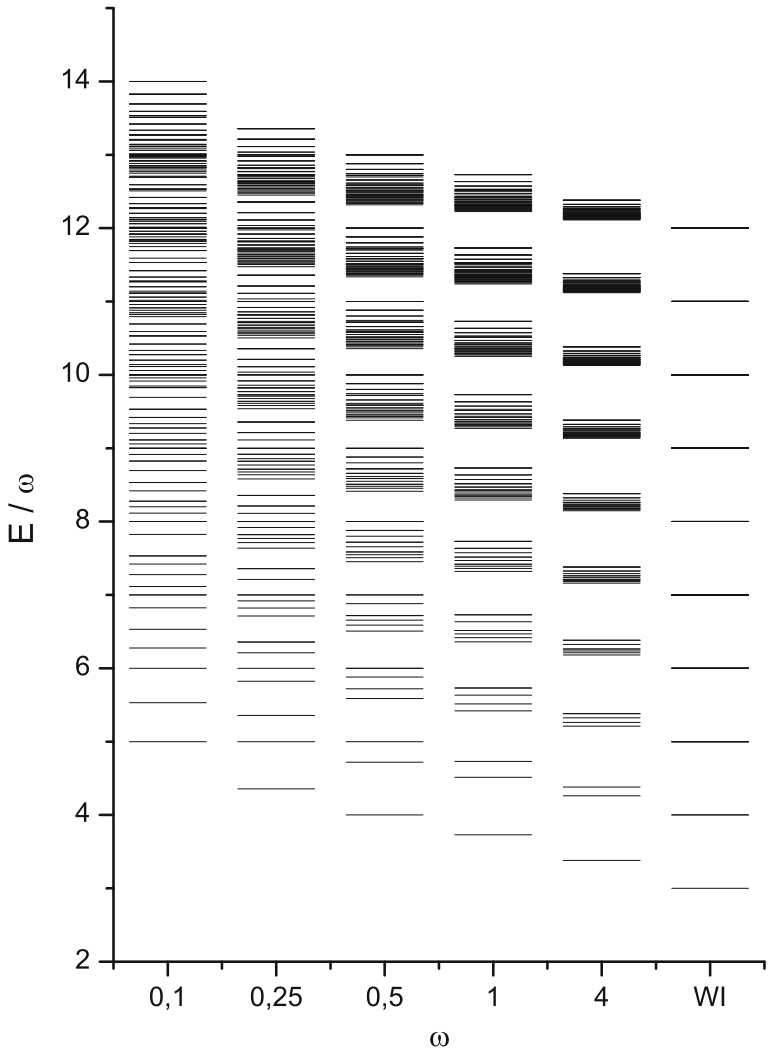

Fig. 5.11 Relative spectrum of isotropic two electron quantum dot with respect to confinement parameter ($E_{N,L,n,l}/\omega$) for five ω's (0.1, 0.25, 0.5, 1.0 and 4.0) and for non-interacting (WI) case. Reproduced from Ref. [50]

accentuated, as the isotropic case, to low-lying states than the highly excited (remembering that the center-of-mass eigenenergy is equal to the relative motion one when the electron-electron interaction is taken off).

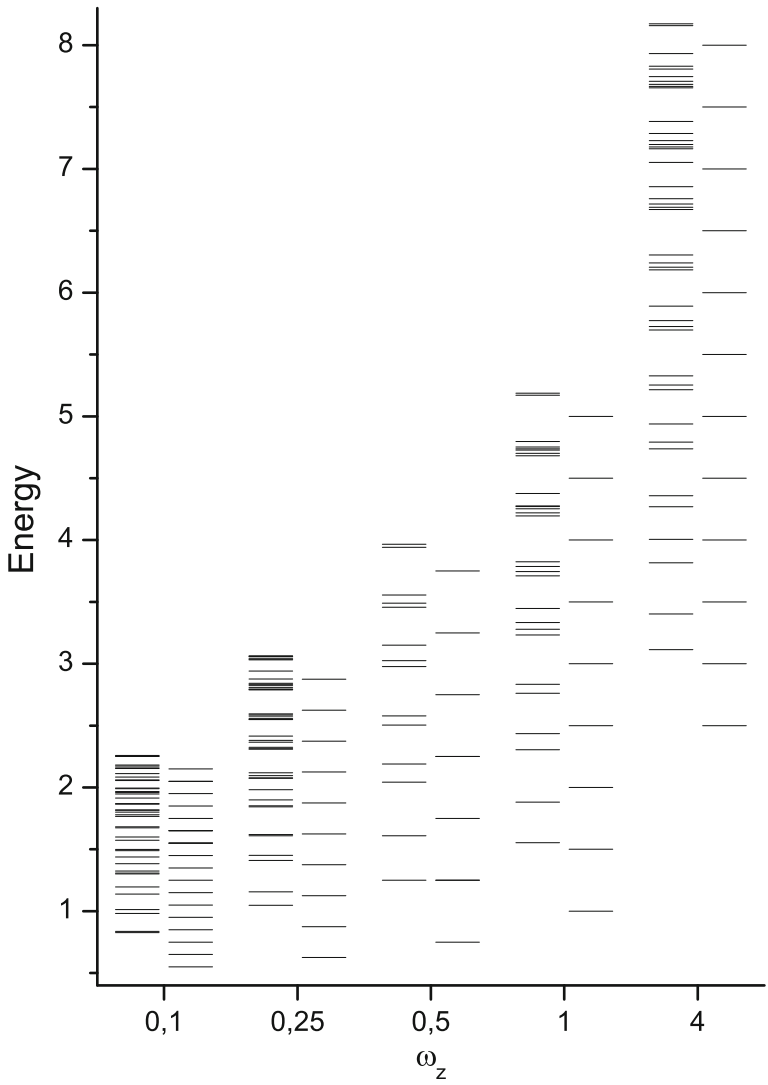

Fig. 5.12 Relative motion energy levels of anisotropic two electron quantum dot for $\omega_z = 0.1$, 0.25, 0.5, 1.0 and 4.0 with $\omega_\perp = 0.5$. The first entry of each ω_z is associated with the interacting problem while the second entry is related with the non-interacting one. Reproduced from Ref. [50]

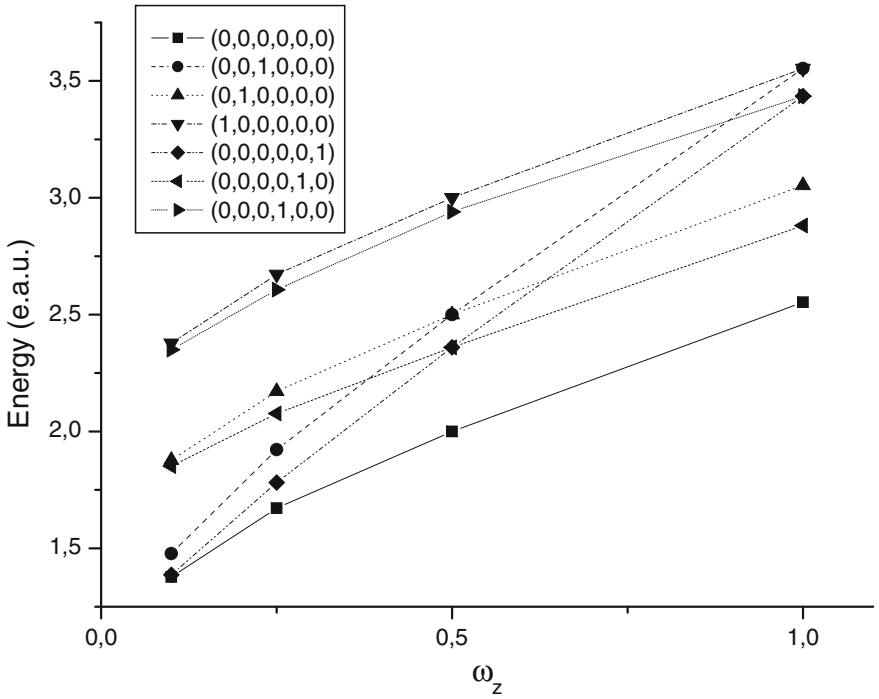

Fig. 5.13 Selected total energy levels as a function of ω_z parameter for the anisotropic two-electron quantum dot system with $\omega_\perp = 0.5$. Reproduced from Ref. [50]

5.5 Concluding Remarks

We have reviewed the theory of two variational numerical methodologies used to determine properties of confined quantum systems: the finite element method (FEM) and discrete variable representation (DVR) method. Applications of these methodologies also were reviewed concerning the study of confinement effects in some quantum systems. The first one was the one-dimensional harmonic oscillator in two different confinement regimes, namely, confined by a model potential, and confined between infinite rectangular walls. The second system was the hydrogenic atom/ion under three different confinement regimes, namely, atom confined by an infinite spherical potential barrier, atom confined endohedrally by fullerenes using a model potential, and ion confined in a plasma environment. The last system was regarding quantum dots, namely, the parabolic quantum dot-atom in presence of an impurity, and the two electron quantum dot using a three-dimensional anisotropic harmonic potential. We observed, in general, that the results agreed with others fairly accurate previously published.

We point out some important aspects of this review paper. First, we observe that in the present methodologies the basis functions are not modeled so as to be

restricted to the calculation of few states, thus providing any energy level, within a finite number of basis functions. Second, we note that the procedures are sufficiently accurate for any extension of the confinement region. Another consideration is that many methods use trial basis functions modeled to describe specific problems and such functions have to be modified if one wishes to study a different or more complex system. However, the FEM and DVR method can be applied to a variety of systems without the requirement of new trial basis functions. In particular, the use of the self-consistent FEM for optimization of elements mesh provides a reduction of the dimensions of the matrices involved in the problem, allowing a reduction of the computational time involved in the diagonalization. Also the DVR method has been widely applied in literature to study problems in molecular and chemical physics being a well established numerical method to treat three-dimensional systems.

Finally we note that in this paper the DVR and FEM were compared with several methodologies such as analytical methods, numerical variational methods using global basis functions, perturbation methods, Numerov's method, etc. However, no direct comparison between them has been made in the study of confined systems, so it is necessary a work in this direction. Nevertheless, we conclude that the procedures focusing on the FEM and DVR method are in general very efficient and we hope to have shown the feasibility of implementing these methods in the study of confined quantum systems.

Acknowledgments This work has been supported by the following Brazilian National Research Councils: Conselho Nacional de Desenvolvimento Científico e Tecnológico (CNPq), Fundação de Amparo à Pesquisa do Estado da Bahia (FAPESB) and Coordenação de Aperfeiçoamento de Pessoal de Nível Superior (CAPES).

References

1. Jaskólski W (1996) Phys Rep 271:1
2. Dolmatov VK, Baltenkov AS, Connerade J-P, Manson ST (2004) Rad Phys Chem 70:417
3. Sabin J, Brandas E, Cruz SA (2009) Advances in quantum chemistry, vol 57. Academic, Oxford
4. Sabin J, Brandas E, Cruz SA (2009) Advances in quantum chemistry, vol 58. Academic, Oxford
5. Jacak L, Hawrylak O, Wojs A (1998) Quantum dots. Springer, Berlin
6. Ram-Moham LR (2002) Finite element and boundary element applications in quantum mechanics. Oxford University Press, New York
7. Bacic Z, Light JC (1999) Ann Rev Phys Chem 40:469
8. Light JC, Carrington T Jr (2000) Adv Chem Phys 114:263
9. Guimarães MN, Prudente FV (2005) J Phys B At Mol Opt Phys 38:2811
10. Zicovich-Wilson C, Planelles JH, Jaskólski W (1994) Int J Quant Chem 50:429
11. Costa LS, Prudente FV, Acioli PH, Soares Neto JJ, Vianna JDM (1999) J Phys B At Mol Opt Phys 32:2461
12. Adamowski J, Sobkowicz M, Szafran B, Bednarek S (2000) Phys Rev B 62:4234
13. Sako T, Diercksen GHF (2003) J Phys Condens Matter 15:5487

14. Carvalho CR, Jalbert G, Rocha AB, Brandi HS (2003) J Appl Phys 94:2579
15. Connerade JP, Dolmatov VK, Lakshmi PA, Manson ST (1999) J Phys B At Mol Opt Phys 32:L239
16. Amusia MY, Baltenkov AS, Becker U (1998) Phys Lett A 243:99
17. Nascimento EM, Prudente FV, Guimarães MN, Maniero AM (2011) J Phys B At Mol Opt Phys 44:015003
18. Saha B, Mukherjee PK, Diercksen GHF (2002) Astron Astrophys 396:337
19. Bhattacharyya S, Sil AN, Fritzsche S, Mukherjee PK (2008) Eur Phys J D 46:1
20. Pfannkuche D, Gudmundsson V, Maksym PA (1993) Phys Rev B 47:2244
21. Creffield CE, Jefferson JH, Sarkar S, Tipton DLJ (2000) Phys Rev B 62:7249
22. Yao W, Yu Z, Liu Y, Jia B (2010) J Nanosci Nanotech 10:7612
23. Thompson DC, Alavi A (2005) J Chem Phys 122:124107
24. De Giovannini U, Cavaliere F, Cenni R, Sassetti M, Kramer B (2008) Phys Rev B 77:035325
25. Yakar Y, Cakir B, Ozmen A (2011) Int J Quantum Chem 111:4139
26. Odriazola A, Ervasti MM, Makkonen I, Delgado A, Gonzalez A, Rasanen E, Harju A (2013) J Phys Cond Matt 25:505504
27. Bryant GW (1987) Phys Rev Lett 59:1140
28. Jung J, Alvarellos JE (2002) J Chem Phys 118:10825
29. Jiang TF, Tong X, Chu S (2001) Phys Rev B 63:045317
30. Räsänen E, Harju A, Puska MJ, Nieminen RM (2004) Phys Rev B 69:165309
31. Jung J, García-González P, Alvarellos JE, Godby RW (2004) Phys Rev A 69:052501
32. Akyuz GB, Akgungor K, Sakiroglu S, Siddiki A, Sokmen I (2011) Physica E 43:1514
33. Avali A (2000) J Chem Phys 113:7735
34. Xie W (2006) Phys Rev B 74:115305
35. Cipriani G, Rosa-Clot M, Taddei S (2000) Phys Rev B 61:7536
36. Harting J, Mülken O, Borrmann P (2000) Phys Rev B 62:10207
37. Moreira NL, Cândido L, Rabelo JNT, Marques GE (2009) Semicond Sci Technol 24:075009
38. Taut M (1993) Phys Rev A 48:3561
39. Kestner NR, Sinanoglu O (1962) Phys Rev 128:2687
40. Dineykhan M, Nazmitdinov RG (1997) Phys Rev B 55:13707
41. Barakat T, Al-Rawaf AS (2011) Phys Scr 83:055001
42. Cantele G, Ninno D, Iadonisi G (2001) Phys Rev B 64:125325
43. Shi L, Yan Z (2011) J Appl Phys 110:024306
44. Klama S, Mishchenko EG (1998) J Phys Condens Matter 10:3411
45. Serra L, Nazmitdinov RG, Puente A (2003) Phys Rev B 035341
46. Sako T, Diercksen GHF (2003) J Phys B At Mol Opt Phys 36:1681
47. Harris DO, Engerholm GG, Gwinn WD (1965) J Chem Phys 43:1515
48. Dickinson AS, Certain PR (1968) J Chem Phys 49:4209
49. Light JC, Hamilton IP, Lill JV (1985) J Chem Phys 82:1400
50. Prudente FV, Costa LS, Vianna JDM (2005) J Chem Phys 123:224701
51. Kubota Y, Nobusada K (2007) Phys Lett A 369:128
52. Xu M, Sebastianelli F, Gibbons BR, Bacic Z, Lawler R, Turro NJ (2009) J Chem Phys 130:224306
53. Lin CY, Ho YK (2013) Few Body Syst 54:425
54. Parrish RM, Hohenstein EG, Martinez TJ, Sherrill CD (2013) J Chem Phys 138:194107
55. Lombardi M, Barletta P, Kievsky A (2004) Phys Rev A 70:032503
56. Szalay V (1993) J Chem Phys 99:1978
57. Echave J, Clary DC (1992) Chem Phys Lett 190:225
58. Bitencourt ACP, Prudente FV, Vianna JDM (2007) J Phys B At Mol Opt Phys 40:2075
59. Colbert DT, Miller WH (1992) J Chem Phys 96:1982
60. Jin J (1993) The finite element method in electromagnetics. Wiley, New York
61. Zienkiewicz OC (1971) The finite element method in engineering science. McGraw-Hill, New York
62. Soares Neto JJ, Prudente FV (1994) Theor Chim Acta 89:415

63. Prudente FV, SoaresNeto JJ (1999) Chem Phys Lett 302:43
64. Pask JE, Klein BM, Sterne PA, Fong CY (2001) Comput Phys Commun 135:1
65. Pask JE, Sterne PA (2005) Model Simul Mater Sci Eng 13:R71
66. Salci M, Levin S, Elander N, Yarevsky E (2008) J Chem Phys 129:134304
67. Alizadegan R, Hsia K, Martinez T (2010) J Chem Phys 132:034101
68. Guimarães MN, Ragni M, Bitencourt ACP, Prudente FV (2013) Eur Phys J D 67:253
69. Qu F, Alcalde AM, Almeida CG, Dantas NO (2003) J Appl Phys 94:3462
70. Ramírez HY, Santana A (2012) Comp Phys Commun 183:1654
71. Jurczak G, Young TD (2012) Appl Surf Sci 260:59
72. Linderberg J, Padkjær SB, Öhrn Y, Vessal B (1989) J Chem Phys 90:6254
73. Jaquet R, Schnupf U (1992) Chem Phys 165:287
74. Prudente FV, Soares Neto JJ (1999) Chem Phys Lett 309:471
75. Chuluunbaatar O, Gusev AA, Kaschiev MS, Kaschieva VA, Amaya-Tapia A, Larsen SY, Vinitsky SI (2006) J Phys B At Mol Opt Phys 39:243
76. Guimarães MN, Prudente FV (2011) Eur Phys J D 64:287
77. Babuška I, Guo BQ (1992) Adv Eng Softw 15:159
78. Soares Neto JJ, Costa LS (1998) Braz J Phys 28:1
79. Curry HB, Schoenberg IJ (1947) Bull Am Math Soc 53:1114
80. de Boor C (1978) A practical guide to splines. Springer, New York
81. Ndengué SA, Motapon O (2008) J Phys B At Mol Opt Phys 41:045001
82. Kang S, Li J, Shi T (2006) J Phys B At Mol Opt Phys 39:3491
83. Bhatti ML, Coleman KD, Perger WE (2003) Phys Rev A 68:044503
84. Xi J, Wu L, He X, Li B (1992) Phys Rev A 46:5806
85. Johnson WR, Sapirstein J (1986) Phys Rev Lett 57:1126
86. Shore BW (1973) J Chem Phys 58:3855
87. Bachau H, Cormier E, Decleva P, Hansen JE, Martín F (2001) Rep Prog Phys 64:1815
88. Martín F (1999) J Phys B At Mol Opt Phys 32:R197
89. Prudente FV, Acioli PH (1999) Chem Phys Lett 302:249
90. Prudente FV, Costa LS, Acioli PH (2000) J Phys B At Mol Opt Phys 33:R285
91. Costa LS, Prudente FV, Acioli PH (2000) Phys Rev A 61:012506
92. Grinberg M, Jaskólski W, Kopke C, Plannelles J, Jnowicz M (1994) Phys Rev B 50:6504
93. Goodfriend PL (1990) J Phys B At Mol Opt Phys 23:1373
94. Adams JE, Miller WH (1977) J Chem Phys 67:5775
95. Consortini A, Frieden BR (1976) Nuovo Cimento B 35:153
96. Almeida MM, Guimarães MN, Prudente FV (2005) Rev Bras Ens Fís 27:395
97. Michels A, de Boer J, Bijl A (1937) Physica 4:981
98. Sommerfeld A, Welker H (1938) Ann Phys (Leipzig) 32:56
99. Guillot T (1999) Space Sci 47:1183
100. Guillot T (2005) Annu Rev Earth Planet Sci 33:493
101. Tabbert B, Günther H, Zu Putlitz G (1997) J Low Temp Phys 109:653
102. Aquino N (1995) Int J Quantum Chem 54:107
103. Goldman S, Joslin C (1992) J Phys Chem 96:6021
104. Varshni YP (1997) J Phys B At Mol Opt Phys 30:L589
105. Zicovich-Wilson C, Jaskólski W, Planelles JH (1995) Int J Quant Chem 54:61
106. Dutt R, Mujherjee A, Varshni YP (2001) Phys Lett A 280:318
107. Banerjee A, Sen KD, Garza J, Vargas R (2002) J Chem Phys 116:4054
108. Laughlin C (2004) J Phys B At Mol Opt Phys 37:4085
109. Dillon AC, Jones KM, Bekkedahl TA, Kiang CH, Bethune DS, Heben MJ (1997) Nature 386:377
110. Dolmatov VK (2009) In: Sabin JR, Brändas E, Cruz SA (eds) Advances in quantum chemistry: theory of confined quantum systems, vol 58. Academic Press, Oxford, p 13
111. Xu YB, Tan MQ, Becker U (1996) Phys Rev Lett 76:3538
112. Yuan L, Yang J, Deng K, Zhu Q (2000) J Phys Chem A 104:6666
113. Piskoti C, Yarger J, Zettl A (1998) Nature 393:771

114. Ichimaru S (1982) Rev Mod Phys 54:1017
115. Sil AN, Canuto S, Mukherjee PK (2009) In: Sabin JR, Brändas E, Cruz SA (eds) Advances in quantum chemistry: theory of confined quantum systems, vol 58. Academic Press, Oxford, p 115
116. Ichimaru S (1992) Statistical plasma physics, volume I: basic principles. Addison-Wesley Publishing Company, New York
117. Guimarães MN, Prudente FV (2012) In: Apduhan B, Ragni M, Misra S, Gervasi O, Taniar D, Murgante B (eds) Proceedings of the 12th international conference on computational science and its applications, IEEE Computer Society's Conference Publishing Services, Los Alamitos, p 167
118. Varshni YP (1998) Superlattices Microstruct 23:145
119. Lee WC, Lee TK (2002) J Phys Condens Matter 14:1045
120. Pino R, Villalba VM (2001) J Phys Condens Matter 13:11651
121. Imbo T, Pagnamenta A, Sukhatme U (1984) Phys Rev D 29:1669
122. Schwartz C (1985) J Math Phys 26:411
123. Friedberg R, Lee TD, Zhao WQ (1999) Nuovo Cimento A 112:1195
124. Prudente FV, Riganelli A, Varandas AJC (2001) Rev Mex Fis 47:568

Chapter 6
Bound and Resonant States in Confined Atoms

L.G. Jiao and Y.K. Ho

6.1 Introduction to the QD Confinement

With the fast development of experimental technology in the design and fabrication of nanoscale electronic devices, a great deal of effort has been devoted to the investigation of quantum confined systems, such as the atoms confined in hard [1–3] or soft spherical cavities [4, 5], atoms encapsulated in fullerence cages [6–8], and electrons or impurities confined in semiconductor quantum dot (QD) [9, 10]. The quantum dots, which are often described as artificial atoms, have attracted considerable interest in recent years due to their not only fundamental importance in theoretical researches but also practical significance in designing new functional devices.

The theoretical investigation of the electronic structures and optical properties of the QD is an active research area. Abundant phenomena have been discovered by authors assuming the multi-electron systems with different model confinement potentials. The rectangular potential, which has the form of

$$V_{RECT}(r) = \begin{cases} -V_0 & r < R, \\ 0 & r \geq R, \end{cases} \tag{6.1}$$

has been widely used to describe the quantum dots built of a narrow-gap semiconductor nanocrystal of radius R, surrounded by a wide-gap dielectric medium with the conduction band off-set equal to V_0. The energy spectra [11] including the relativistic effects [12], fine structures [13] and electric-filed Stark effects [14] for

L.G. Jiao · Y.K. Ho (✉)
Institute of Atomic and Molecular Sciences, Academia Sinica,
PO Box 23-166, Taipei 106, Taiwan
e-mail: ykho@pub.iams.sinica.edu.tw

K.D. Sen (ed.), *Electronic Structure of Quantum Confined Atoms and Molecules*,
DOI 10.1007/978-3-319-09982-8_6

one-electron QD have been calculated accurately by many authors. The bound state and quantum capacity for many-electron QD have also been investigated [15]. The recent research by Bylicki et al. [16] has shown that the two-electron quantum dots have very rich spectrum for resonant states. A new phenomenon of the transformation from Feshbach to shape characters with changing the dot size has been observed. The investigation of the quantum entanglement of the resonant states in QD has also become increasingly interest in recent years [17].

Although the rectangular potential has simple form and good numerical feasibility, it is unphysical due to the non-parabolic shape at the center of the quantum dot. Another widely used model potential has the harmonic oscillator (HO) form which fulfills such requirement in small region

$$V_{HO}(r) = \frac{1}{2}\omega_0^2 r^2. \tag{6.2}$$

The Schrödinger equation of the two-electron quantum dot confined in HO potential has analytical solutions for a particular, denumerably infinite sets of oscillator frequency [18, 19]. Some numerical methods have also been developed to calculate the energies for the two- and many-electron QD in HO potential [20–22]. However, because of the infinite depth and range of the harmonic oscillator potential, it is inappropriate for the description of the experimentally measured quantum dots by finite number of excess electrons. For example, it automatically excludes the possibility of autoionizing resonant states and also forbids the electron exchanges between the QD and its surroundings. To circumvent these problems, somewhat relatively weak confining models are warranted in favor of experiments.

The Gaussian attractive confining potential of the form

$$V_G(r) = -V_0 \exp\left(\frac{-r^2}{R^2}\right), \tag{6.3}$$

has been suggested by several authors to study the properties of finite excess electrons in QD. Such potential possesses finite depth and range, and it can be approximated by the parabolic potential in the vicinity of the dot center. The bound state energies and photoionization processes of one- and two-electron quantum dots have been investigated in different confining radius and potential depth [23–26]. Recently, it has been observed by Sajeev and Moiseyev [26] that the singly excited states of two-electron QD can become resonant states for appropriately chosen confining potential parameters. Further investigations by Genkin and Lindroth [27] demonstrate that the impurity placed in the vicinity of the dot would significantly influence the autoionizing resonant states. The impurity can lead to bound-resonant transitions and avoided-crossing behaviors in the energy spectrum when the impurity charge is varied.

An alternative weakly confining potential is the finite oscillator (FO) potential given as

$$V_{FO}(r) = -V_0(1 + Rr)\exp(-Rr). \tag{6.4}$$

Such potential has the r^2-dependence near the center of QD, which is typical for the harmonic oscillator, but necessarily deviates from it with increasing the confinement distance. The FO potential shows large similarities in profile as the Gaussian type and, at the same time, it allows for much simple and closed form matrix elements in computation, especially when the Slater-type orbitals are used in constructing the system wave functions. The FO potential has been used by Winkler [28] to study the two-electron bound and resonant states in QD. However, the author calculated some bound and resonant states of the two-electron system using the wave functions optimized without the electron-electron interaction. Even the interaction was included back in the subsequent calculations with full Hamiltonian, the final results are subject to certain uncertainties. Later, Kimani et al. [29] applied the restricted Hartree-Fock method to estimate the ground states of many-electron close-shell quantum dots with the electron correlations included approximately. It should also be noted that, the impurity effect was not taken into account in their investigations. As mentioned in the Gaussian potential, the Coulomb field generated by impurity ions would have large effects on the various properties of QD [30]. Most recently, Chakraborty and Ho [31] have investigated the two-electron resonances of QD with He^{2+} impurity by using the stabilization method. The resonance parameters for the $2s^2\ ^1S^e$ state was calculated for a wide variety of confining potential radius. It has been shown that the resonance width has an oscillatory behavior when the size of the dot changes, which is a direct evidence of the interferences between the QD potential and resonance wave functions.

In this work, we present a detailed investigation of the bound and autoionizing resonant states of two-electron QD with He^{2+} impurity (i.e. the He atom confined in QD) by employing the Rayleigh-Ritz variational method and the complex-scaling method, respectively. The emphasis is placed on the FO model potential. The impurity charge was fixed to 2 so that a comparison with the free He atom can be made. Two types of trial basis sets, the configuration-interaction (CI) basis built from the product of Slater-type orbitals and the correlated Hylleraas-type basis are used in the expansion of system wave functions. The present paper is organized as follows. In Sect. 6.2, we describe the general problems of one- and two-electron QD with impurity. The construction of the trial wave functions and the procedure of the complex-scaling calculations are also introduced in Sect. 6.2. The results and discussions of the energy spectra for one- and two-electron QD systems are presented in Sect. 6.3. Concluding remarks are made in Sect. 6.4. The traditional atomic unit notations are used throughout the work to label the effective atomic units based on the effective-mass approximation, in which the energy and length units are denoted by effective Hartree and effective Bohr radius, respectively [11, 15–17, 27].

6.2 Theoretical Method

6.2.1 One-Electron QD

The Hamiltonian describing a one-electron QD system confined in the FO potential is

$$H = -\frac{1}{2}\nabla^2 - \frac{Z}{r} + V_{FO}(r), \tag{6.5}$$

where Z is the impurity charge. The FO potential in spherical symmetry is suggested by [28, 29, 31, 32]

$$V_{FO}(r) = -A\left(1 + \frac{B}{\sqrt{A}}r\right)\exp\left[-\left(\frac{B}{\sqrt{A}}r\right)\right], \tag{6.6}$$

where A and $1/B$ have length dimensions and characterize the depth and width of the FO confining potential. In Fig. 6.1, we show the profiles of the FO potential for a particular depth ($A = 0.5$ a.u.) and different radii ($1/B = 0.1, 1, 10$ and 100 a.u.) as well as the pure Coulomb potential for $Z = 2$. The limit $1/B \to 0$ represents the confining potential V_{FO} approaches to 0 except at the original point, i.e. only the Coulomb interaction exists; whereas the limit $1/B \to \infty$ refers to a rectangle potential well with infinite width, i.e. the pure Coulomb plus a constant potential $-A$. In other cases, the QD confinement would interact with the Coulomb potential and

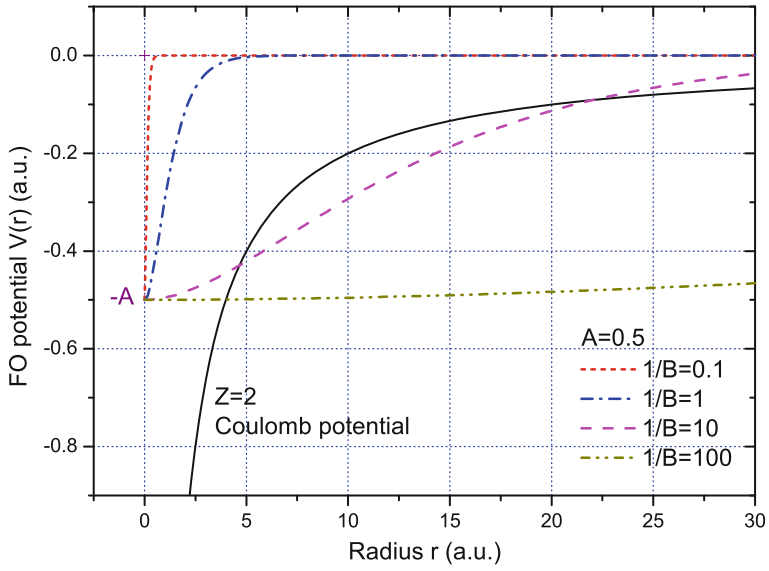

Fig. 6.1 Comparison of the pure Coulomb potential for He^+ ion and the FO potentials with $A = 0.5$ a.u. and $1/B = 0.1, 1, 10$ and 100 a.u.

such problem has no analytic solutions. In a variational treatment, one can expand the system radial wave function in the Slater orbitals

$$\Psi(r) = \sum_i C_i r^{n_i} \exp(-\xi_i r). \tag{6.7}$$

The one-electron energies can then be calculated, such as, in the framework of Rayleigh-Ritz variational principle.

6.2.2 Two-Electron QD: CI Basis

The Hamiltonian for the two-electron QD inside a FO potential cavity is expressed by

$$H = -\frac{1}{2}\nabla_1^2 - \frac{1}{2}\nabla_2^2 - \frac{Z}{r_1} - \frac{Z}{r_2} + V_{FO}(r_1) + V_{FO}(r_2) + \frac{1}{r_{12}}, \tag{6.8}$$

where r_1 and r_2 are the radial coordinates of the two electrons and r_{12} is their relative distance. In the CI representation of the two-electron wave functions, it is useful to employ the product of Slater-type orbitals to construct the basis

$$\Psi(r_1, r_2) = A \sum_{l_a, l_b} \sum_{i,j} C_{a_i, b_j} \eta_{a_i}(r_1) \eta_{b_j}(r_2) Y^{LM}_{l_a, l_b}(\hat{r}_1, \hat{r}_2) S(\sigma_1, \sigma_2), \tag{6.9}$$

where A is the anti-symmetrization operator

$$A = \left(1 + (-1)^S \hat{P}_{12}\right), \tag{6.10}$$

and C's are the coefficients to be determined. In Eq. 6.10, $\hat{P}_{12}$ is the permutation operator and S is the total spin of the system. In Eq. 6.9, η's are the single-electron Slater orbitals

$$\eta_{a_i}(r) = r^{n_{a_i}} \exp(-\alpha \xi_{a_i} r), \tag{6.11}$$

in which α is an overall scaling parameter. Y is the eigenfunction of the two-electron total angular momentum L

$$Y^{LM}_{l_a, l_b}(\hat{r}_1, \hat{r}_2) = \sum_{m_{l_a}} \sum_{m_{l_b}} C(l_a, l_b, L; m_{l_a}, m_{l_b}, M) Y_{l_a, m_{l_a}}(\hat{r}_1) Y_{l_b, m_{l_b}}(\hat{r}_2) \tag{6.12}$$

with C the Clebsch-Gordan coefficients. S is the two-electron spin eigenfunction. Such CI-type wave functions have limitations to accurately calculate the lower-lying intrashell states with small total angular momentum, due to the omission of

r_{12} coordinate in the system wave functions. A strategy to improve the convergence of calculations is employing multiple ξ for Slater orbitals with same l. Such a choice of basis set corresponds to an extensive representation of the wave functions in both the close- and far-range space sectors.

6.2.3 Two-Electron QD: Hylleraas Basis

Due to the electron-electron coordinate is not included explicitly in the CI-type wave function, an alternative choice of the basis is the Hylleraas-type wave function, which introduces powers of the interelectronic distance r_{12} to take into account the electron correlation effects explicitly. For two-electron systems, we use the following form to build up the system wave function

$$\Psi(r_1, r_2) = A \sum_{l_a, l_b} \sum_{p} C_{l_a, l_b, p} \chi_p(\alpha, \beta) r_1^{l_a} r_2^{l_b} Y_{l_a, l_b}^{LM}(\hat{r}_1, \hat{r}_2) S(\sigma_1, \sigma_2), \tag{6.13}$$

where

$$\chi_p(\alpha, \beta) = r_1^i r_2^j r_{12}^k \exp(-\alpha r_1 - \beta r_2), \tag{6.14}$$

with $(i + j + k) \leq \omega$ and $(l_a + l_b) \leq L$. In Eq. 6.14, p is the index labeling the three nonnegative integer values $\{i, j, k\}$. A, Y and S have same expressions as those in CI basis. For the lower-lying S-wave states of a two-electron atom, Eq. 6.13 reduces to a more simpler form

$$\Psi(r_1, r_2) = \sum_{i,j,k} C_{i,j,k} r_{12}^k \left[r_1^i r_2^j + (-1)^S r_1^j r_2^i \right] \exp[-\alpha(r_1 + r_2)], \quad i \geq j. \tag{6.15}$$

In computation, the Hamiltonian of the system must be written in the Hylleraas coordinate $\{r_1, r_2, r_{12}, \Omega_1, \Omega_2\}$

$$\begin{aligned} H = & -\frac{1}{2} \sum_{i=1}^{2} \left[\frac{\partial^2}{\partial r_i^2} + \frac{2}{r_i} \frac{\partial}{\partial r_i} - \frac{l_i(l_i+1)}{r_i^2} \right] - \left[\frac{\partial^2}{\partial r_{12}^2} + \frac{2}{r_{12}} \frac{\partial}{\partial r_{12}} \right] \\ & - \frac{1}{2} \left[\frac{r_1^2 - r_2^2 + r_{12}^2}{r_1 r_{12}} \frac{\partial^2}{\partial r_1 \partial r_{12}} + \frac{r_2^2 - r_1^2 + r_{12}^2}{r_1 r_{12}} \frac{\partial^2}{\partial r_2 \partial r_{12}} \right] \\ & + \left[(\vec{r}_2 \cdot \nabla_1^Y) \frac{1}{r_{12}} \frac{\partial}{\partial r_{12}} + (\vec{r}_1 \cdot \nabla_2^Y) \frac{1}{r_{12}} \frac{\partial}{\partial r_{12}} \right] \\ & - \frac{Z}{r_1} - \frac{Z}{r_2} + V_{FO}(r_1) + V_{FO}(r_2) + \frac{1}{r_{12}}, \end{aligned} \tag{6.16}$$

where ∇_i^Y corresponds to the angular part of the gradient operator. The calculation details are available in the literatures [33–35] and will not be presented here.

6.2.4 Complex-Scaling Method

The ground and bound-excited states of the two-electron QD can be calculated via the Rayleigh-Ritz variational procedure as in the one-electron system. However, the calculations of the doubly-excited resonant states are more complicated due to the asymptotic divergence of the wave functions. There are two simple ways to calculate atomic resonances using the bound-state-type wave functions, the complex-scaling method [36, 37] and the stabilization method [37, 38]. The stabilization method diagonalizes the real Hamiltonian matrix with different box sizes. A resonance exists when the eigenvalues exhibit stationary behavior in the stabilization plateau, which reveals the localization of resonant scattering wave functions at short range. Such a method shows particular simplicity in calculating the lower-lying resonant states and has been extensively used in investigating the resonances in many atomic systems [31, 38].

In the complex-scaling approach, the radial coordinates of the system are transformed by

$$r \rightarrow re^{i\theta}, \tag{6.17}$$

so that the resonance wave function becomes asymptotically convergent and then can be calculated by using the L^2-type basis functions. The Hamiltonian of the system is transformed to

$$H(\theta) = Te^{-2i\theta} + V_C e^{-i\theta} + V_{FO}(r_1 e^{i\theta}) + V_{FO}(r_2 e^{i\theta}), \tag{6.18}$$

where T is the kinetic energy operator and V_C the Coulomb potential operator. In the present calculations, the complex FO potential matrix elements are calculated by scaling the potential parameter

$$B' = Be^{i\theta}. \tag{6.19}$$

Due to the fact that both the CI-type and Hylleraas-type trial wave functions are non-orthogonal basis, the generalized complex eigenvalue problem is solved with

$$\sum_j C_j^{\lambda}(H_{ij} - E^{\lambda}N_{ij}) = 0, \tag{6.20}$$

in which the Hamiltonian matrix elements are

$$H_{ij} = \langle \psi_i | H(\theta) | \psi_j \rangle, \tag{6.21}$$

and the overlapping matrix elements

$$N_{ij} = \langle \psi_i | \psi_j \rangle. \tag{6.22}$$

In the above equations, ψ_i represents a single basis function of the type defined in Eqs. 6.9 or 6.13. The resonance poles are determined by finding the positions where the complex eigenvalues exhibit the most stabilized characters with respect to the changes of rotation angle θ and scaling parameter α [39]

$$\left.\frac{|\partial E_{res}|}{\partial \theta}\right|_{\alpha=\alpha_{opt}} = \min, \quad \left.\frac{|\partial E_{res}|}{\partial \alpha}\right|_{\theta=\theta_{opt}} = \min . \tag{6.23}$$

Once the position of the resonance pole is determined, the corresponding energy (E_r) and total width (Γ) are given by [36, 37]

$$E_{res} = E_r - \frac{1}{2} i\Gamma. \tag{6.24}$$

6.3 Results and Discussions

6.3.1 One-Electron QD State

The energy levels of the He^+ QD confined by FO potential are calculated by using Eq. 6.7. In most situations, the employing of 20 Slater orbitals is accurate enough to obtain the low- and intermediate-lying hydrogen-like states. The $He^+(n = 1 - 4, l = 0 - 3)$ bound state energies are listed in Table 6.1 and displayed in Fig. 6.2 with potential depth $A = 0.5$ a.u. and radius $1/B$ varying from 0.1 to 100 a.u. Since $1/B \to 0$ and ∞ correspond to a free atom and a free atom plus a negative constant potential $-A$, respectively, the energy levels with same principal quantum numbers n are nearly degenerate at these two limits. For intermediate values of $1/B$, the hydrogenic states with same n and different l quantum numbers split separately and cross with each other forming a much complicated pattern. Although there is no rigorous rule about the sequence of the energy levels, it can be empirically concluded from these figures that (a) for relatively small confinement radius, the $l = n - 1$ states are always higher than others with same n and (b) for relatively large radius, the states in the same n shell have descending orders with increasing l.

The one-electron QD confined in the FO potential exhibits the energy spectrum which is very similar to those in other weakly confining potentials. Lin and Ho [25] have compared the bound state energies of the hydrogen impurity in a spherical QD confined by FO and Gaussian potentials, and similar confinement effects have been

Table 6.1 Bound state energies of the one-electron He^+ ion confined in QD modeled by FO potential with depth $A = 0.5$ a.u.

$1/B$	$1s$	$2s$	$2p$	$3s$	$3p$	$3d$	$4s$	$4p$	$4d$	$4f$
0	−2.00000	−0.50000	−0.50000	−0.22222	−0.22222	−0.22222	−0.12500	−0.12500	−0.12500	−0.12500
0.1	−2.01810	−0.50211	−0.50008	−0.22284	−0.22225	−0.22222	−0.12526	−0.12501	−0.12500	−0.12500
0.1667	−2.05104	−0.50542	−0.50064	−0.22379	−0.22244	−0.22223	−0.12565	−0.12509	−0.12500	−0.12500
0.25	−2.10071	−0.50958	−0.50293	−0.22495	−0.22315	−0.22225	−0.12613	−0.12540	−0.12502	−0.12500
0.4	−2.18509	−0.51659	−0.51376	−0.22691	−0.22613	−0.22258	−0.12694	−0.12662	−0.12519	−0.12500
0.6667	−2.29004	−0.53742	−0.55425	−0.23188	−0.23446	−0.22590	−0.12893	−0.12985	−0.12675	−0.12513
1	−2.36356	−0.58258	−0.62146	−0.24071	−0.24620	−0.24007	−0.13229	−0.13418	−0.13187	−0.12623
1.6667	−2.42986	−0.68411	−0.73517	−0.27090	−0.28480	−0.30391	−0.14179	−0.14546	−0.14740	−0.13965
2.5	−2.46187	−0.77689	−0.82151	−0.33155	−0.35392	−0.39381	−0.16209	−0.16943	−0.18061	−0.19113
4	−2.48247	−0.86795	−0.89821	−0.43571	−0.45936	−0.50337	−0.22758	−0.24150	−0.26653	−0.29932
6.6667	−2.49293	−0.93398	−0.95044	−0.54649	−0.56392	−0.59735	−0.34138	−0.35585	−0.38241	−0.41791
10	−2.49667	−0.96469	−0.97387	−0.61357	−0.62523	−0.64808	−0.42962	−0.44096	−0.46222	−0.49124
16.667	−2.49874	−0.98511	−0.98912	−0.66862	−0.67475	−0.68698	−0.51512	−0.52202	−0.53533	−0.55413
25	−2.49943	−0.99283	−0.99479	−0.69371	−0.69709	−0.70388	−0.56043	−0.56463	−0.57288	−0.58485
40	−2.49977	−0.99702	−0.99785	−0.70937	−0.71094	−0.71411	−0.59271	−0.59488	−0.59919	−0.60559
66.667	−2.49992	−0.99889	−0.99920	−0.71713	−0.71776	−0.71905	−0.61102	−0.61199	−0.61392	−0.61683
100	−2.49996	−0.99950	−0.99964	−0.71985	−0.72015	−0.72076	−0.61817	−0.61865	−0.61962	−0.62107

The rows of $1/B = 0$ represent the free He^+ ion

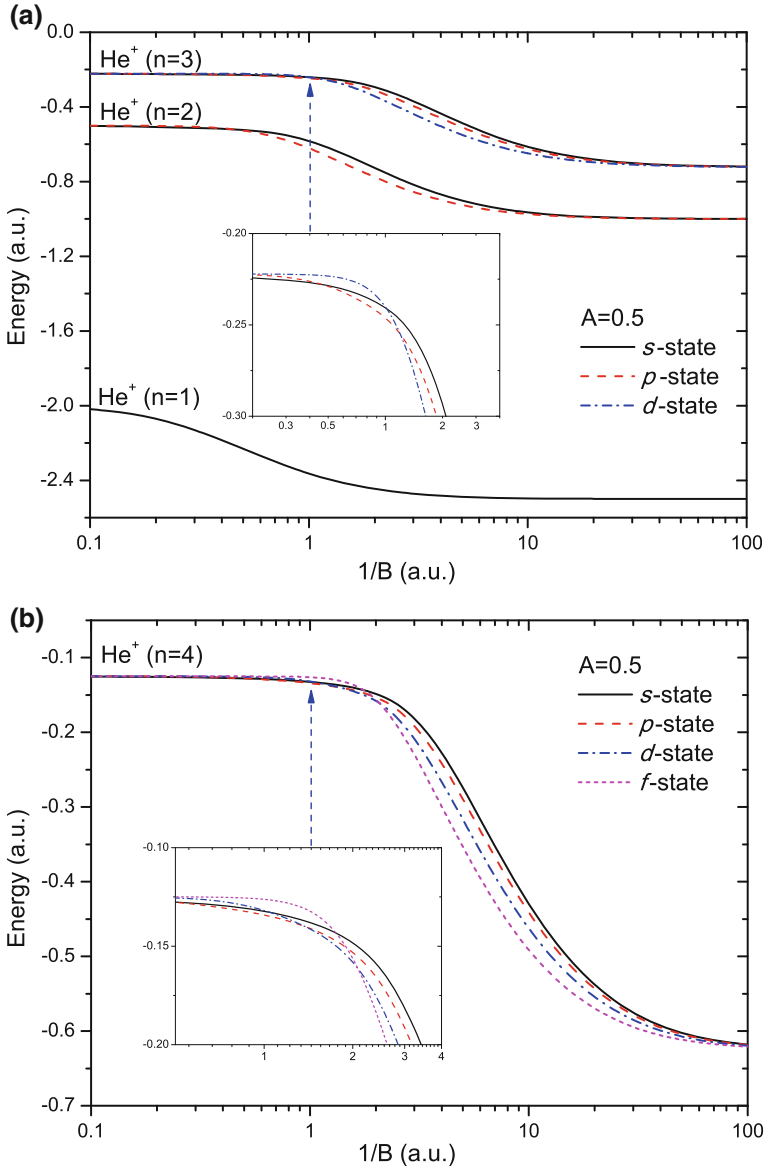

Fig. 6.2 Energy levels of the He^+ QD states as functions of potential radius $1/B$ with $A = 0.5$ a.u. **a** He^+ $(n = 1 - 3)$ states and, **b** He^+ $(n = 4)$ states

found. In addition, Yang et al. [13] have also shown the one-electron QD in finite rectangle potential well has a similar energy level splitting and ordering sequence as shown in Fig. 6.2.

6.3.2 Two-Electron QD Bound States

The $^1S^e$ bound states of the two-electron He QD confined in FO potential are investigated in the variational framework by using the two types of basis set mentioned above. For the CI-type wave functions, we construct the basis by using two groups of Slater orbitals. The first group contains 10 *s*-, 9 *p*-, 8 *d*-, 7 *f*-, 6 *g*-, 5 *h*-, 4 *i*-, 3 *k*-, 2 *l*-, 1 *m*-type Slater orbitals of Eq. 6.11 with all $\xi = 1.0$, the second group contains 5 *p*-, 4 *d*-, 3 *f*-, 2 *g*-, 1 *h*-type orbitals with $\xi = 0.4$. These two groups would couple to a total of 385 terms in the expansion of system wave functions. Here we use the notation $l_{\max} = 9 - 4$ to represent such basis. We also construct an enlarged CI basis of $l_{\max} = 10 - 5$, which couples to 538 terms, to check the calculation convergence. For the Hylleraas-type wave functions, we use one-group functions of Eq. 6.15 with $\omega = 16$, and the total number of terms in the basis is 525. All the calculation results are shown in Fig. 6.3 for $A = 0.2$ and 0.5 a.u., and displayed in Table 6.2 for $A = 0.5$ only. In Table 6.2, we also include the state-of-the-art He $^1S^e$ free-atom bound states calculated by Drake [40, 41] who uses a multi-group Hylleraas-type basis set.

As we can see from Table 6.2, the convergence of the CI calculations is quite good with only small discrepancies in the last decimal point. However, for the $1s^2$ ground state, the Hylleraas results are expected to be more accurate than those obtained by CI due to the explicit inclusion of r_{12} coordinate in the wave functions. The overall discrepancy between these two kinds of basis sets is about 0.00007 a.u. For the higher-lying excited states, such as $1s4s$, the CI calculations are more reliable than the Hylleraas results due to the fact that we use only one-group basis in the latter. The calculations by multiple-group Hylleraas basis are worthwhile to try in the future.

The variations of the He QD bound states with the dot size are illustrated in Fig. 6.3 and their changes are quite interesting. The ground state energy decreases monotonously with increasing the confining radius $1/B$, due to the two electrons are simultaneously trapped into a closer region near the center of QD which would lead to a lower energy. For the singly-excited states, the energies first decrease rapidly, then show a flat "plateau" at moderate values of potential radius, and then continuously decrease as $1/B$ increases. Such phenomenon is closely related to the different radial distributions of the two electrons. When the radius is relatively small, the confining potential affects mostly on the inner electron and the overall QD confinement effects on the two-electron states are dominated by the inner-electron trapping. As a result, the energy variation of the He QD system is very similar to its ionization threshold (He^+ ($1s$) state), as we can see from Fig. 6.3. When the dot radius increases to larger values, the confinement effects of the potential move to the outer electron. The overall energy continuously decreases to lower energies, which corresponds to the second fast decrease in the energy spectrum. This can also be understood from the right-shift of the "plateau" from $1s2s$ to $1s4s$ states. The movement of the plateau to larger values for higher excited states reflects the increased distance of the outer electron with respect to the center

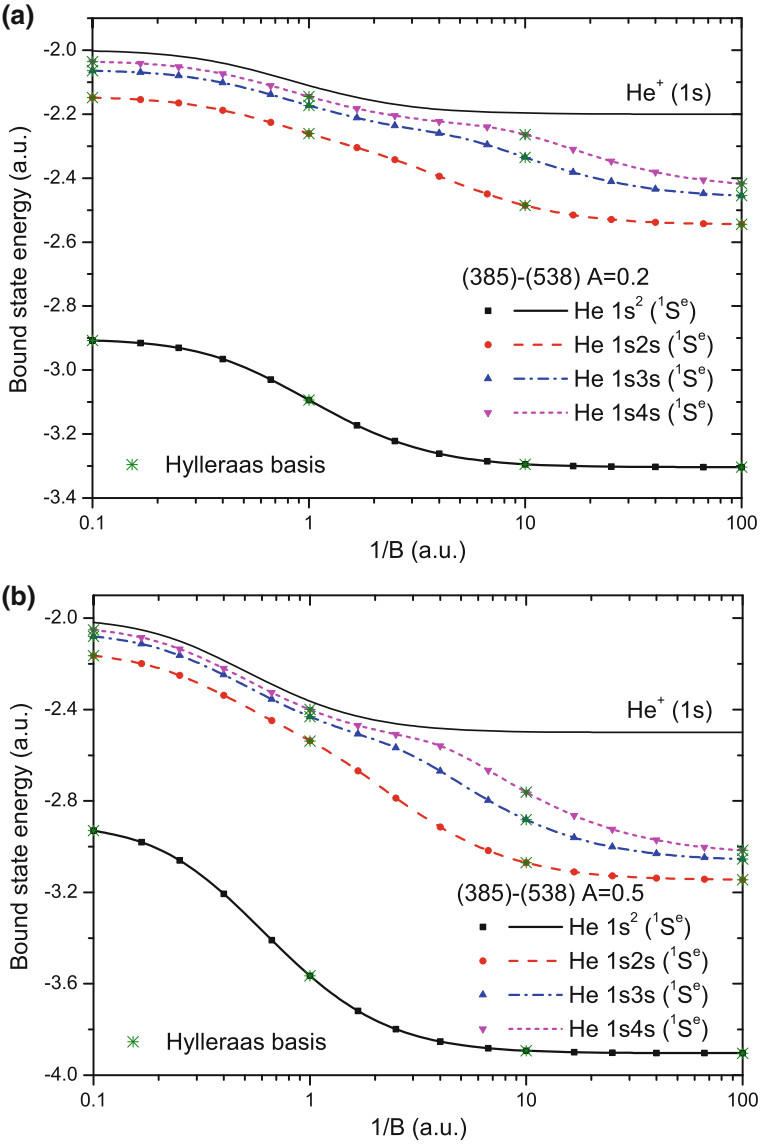

Fig. 6.3 Energy levels of the He QD bound-excited $^1S^e$ states as functions of potential radius $1/B$. 385 and 538 represent the number of terms in CI basis in the calculations and their results are demonstrated by dots and lines, respectively. The *green* stars refer to the results using Hylleraas-type basis. **a** $A = 0.2$ a.u. and **b** $A = 0.5$ a.u.

of QD. The variations of the energies for the triplet and higher angular momentum states against the confining radius are similar to the trends as shown in Fig. 6.3, and they will not be shown here.

Table 6.2 The $^1S^e$ bound state energies of the two-electron He QD with FO potential depth $A = 0.5$ a.u.

$1/B$	*Basis*	$1s^2$	$1s2s$	$1s3s$	$1s4s$
0	*a*	−2.90362	−2.14595	−2.06125	−2.03357
	b	−2.90364	−2.14596	−2.06126	−2.03358
	c	−2.90372	−2.14597	−2.06127	−2.03331
	d	−2.90372	−2.14597	−2.06127	−2.03359
0.1	*a*	−2.92995	−2.16459	−2.07950	−2.05172
	b	−2.92997	−2.16460	−2.07951	−2.05173
	c	−2.93004	−2.16461	−2.07952	−2.05141
0.25	*a*	−3.05937	−2.24985	−2.16282	−2.13460
	b	−3.05939	−2.24986	−2.16283	−2.13463
0.4	*a*	−3.20593	−2.33703	−2.24794	−2.21929
	b	−3.20594	−2.33703	−2.24794	−2.21931
1	*a*	−3.56480	−2.53712	−2.43113	−2.39958
	b	−3.56482	−2.53713	−2.43114	−2.39959
	c	−3.56490	−2.53715	−2.43115	−2.39947
2.5	*a*	−3.79809	−2.78686	−2.56669	−2.50800
	b	−3.79811	−2.78687	−2.56670	−2.50801
4	*a*	−3.85292	−2.91402	−2.66961	−2.55870
	b	−3.85293	−2.91403	−2.66962	−2.55870
10	*a*	−3.89344	−3.06988	−2.88199	−2.76116
	b	−3.89346	−3.06989	−2.88200	−2.76117
	c	−3.89353	−3.06990	−2.88201	−2.76118
25	*a*	−3.90184	−3.12730	−3.00103	−2.92321
	b	−3.90186	−3.12731	−3.00103	−2.92322
40	*a*	−3.90292	−3.13769	−3.03030	−2.97058
	b	−3.90293	−3.13770	−3.03031	−2.97059
100	*a*	−3.90352	−3.14445	−3.05431	−3.01606
	b	−3.90353	−3.14446	−3.05432	−3.01606
	c	−3.90361	−3.14448	−3.05433	−3.01605

The rows of $1/B = 0$ represent the free He atom. The notations *a* and *b* label the CI-type basis with $l_{\max} = 9 - 4$ and $l_{\max} = 10 - 5$, respectively, and *c* refers to the Hylleraas-type basis with $\omega = 16$. *d* represents the most accurate results calculated by Drake [40, 41] for the free-atom case

6.3.3 Two-Electron QD Resonant States

In the present work, we employ the complex-scaling method described in Sect. 6.2.3 to investigate the resonant states of He QD confined in FO potential. The basis sets used here are $l_{\max} = 10 - 5$ for CI-type and $\omega = 16$ for Hylleraas-type wave functions. The calculations are performed in varying the parameters α and θ in a wide range to make sure that the stationary conditions of Eq. 6.23 can be fulfilled. In Fig. 6.4 we demonstrate the general procedure of extracting the resonance parameters for the lowest resonance state at $A = 0.5$ and $1/B = 10$ a.u. The rotational paths near the resonance pole for a group of α are displayed with different θ. In each curve, the movement of the complex eigenvalues with increasing θ slows down when θ approaches θ_{opt}. The cusp positions are calculated by using Eq. 6.23. With further examination of the changes of eigenvalues with respect to α at θ_{opt}, the value of α_{opt} can be obtained. Finally, the complex eigenvalue at θ_{opt} and α_{opt} is used in Eq. 6.24 to determine the resonance parameters.

Following the above procedure, the lowest five $^1S^e$ resonance states ($2s^2$, $2p^2$, $2s3s$, $2p3p$ and $2s4s$) are calculated for $A = 0.2$ and 0.5 a.u. with $1/B$ varying from 0.1 to 100 a.u. or to 1000 a.u. All the results are shown in Fig. 6.5 for resonance energy and Figs. 6.6, 6.7, 6.8, 6.9 and 6.10 for width. Some selected values for $A = 0.5$ a.u. are listed in Tables 6.3 and 6.4 for energy and width, respectively. In the free-atom situation, several methods have been applied to investigate the

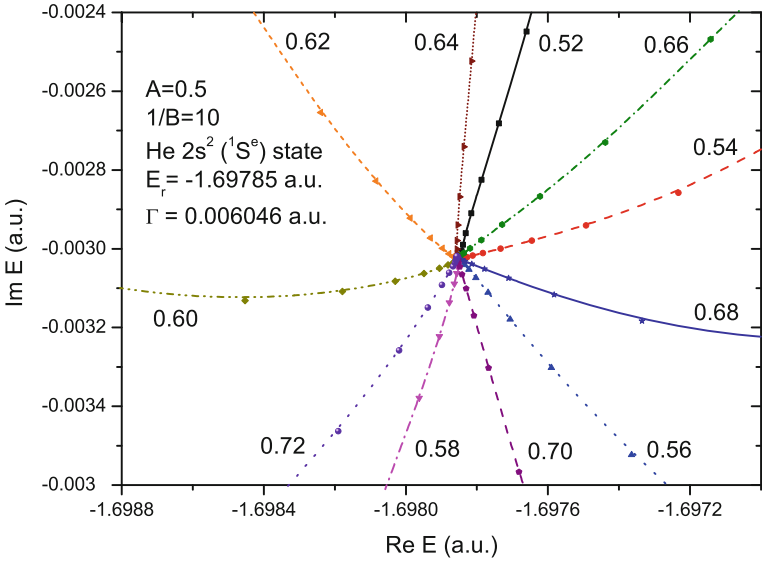

Fig. 6.4 Rotational paths for the He QD $2s^2$ ($^1S^e$) resonant state at $A = 0.5$ and $1/B = 10$ a.u. by using the CI-type basis functions. Each line represents the trajectory with a single value of α and different rotational angle θ. The resonance parameters are obtained by using Eq. 6.24

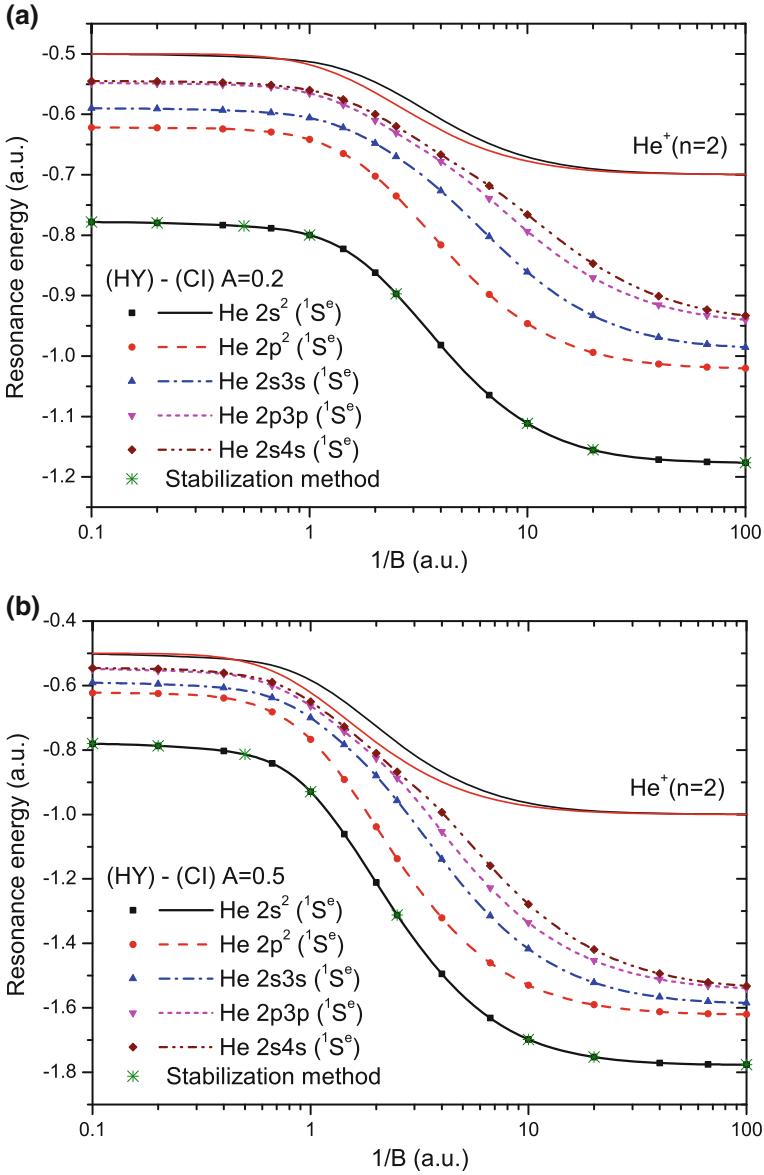

Fig. 6.5 Resonant state energies of the He QD in ${}^1S^e$ symmetry as functions of potential radius $1/B$. HY and CI represent the Hylleraas-type and CI-type basis sets and the corresponding results are demonstrated by dots and lines, respectively. The green stars refer to the results from stabilization calculations [31]. **a** $A = 0.2$ a.u. and **b** $A = 0.5$ a.u.

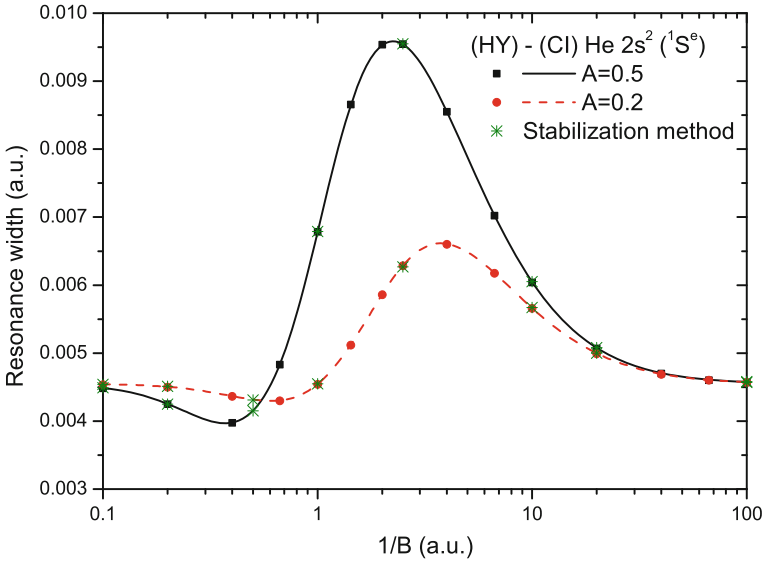

Fig. 6.6 Resonance width for the He QD $2s^2\ ^1S^e$ resonant state at $A = 0.2$ and 0.5 a.u. The notations are same as Fig. 6.5

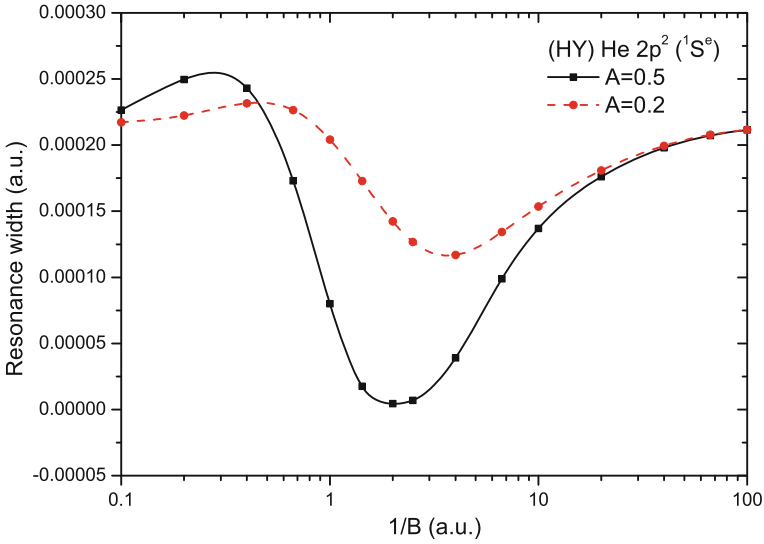

Fig. 6.7 The same as Fig. 6.6 but for the $2p^2\ ^1S^e$ resonant state. Only the Hylleraas results are included. Lines are used to guide the eyes

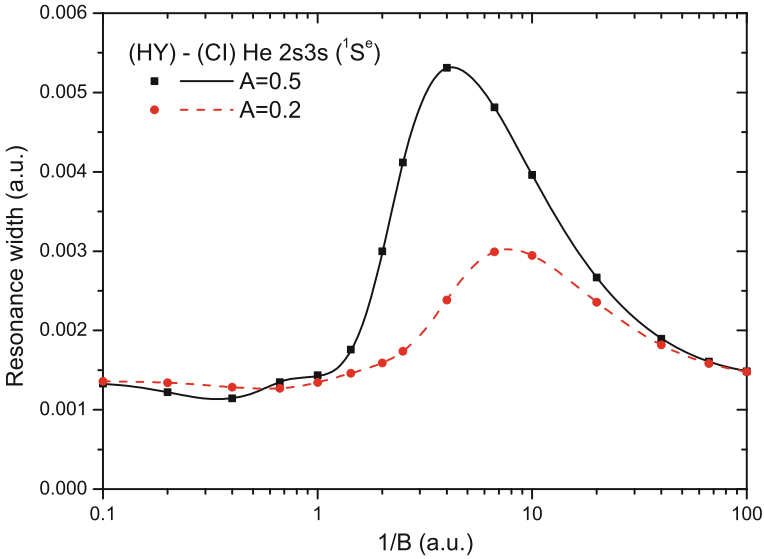

Fig. 6.8 The same as Fig. 6.6 but for the $2s3s\ ^1S^e$ resonant state

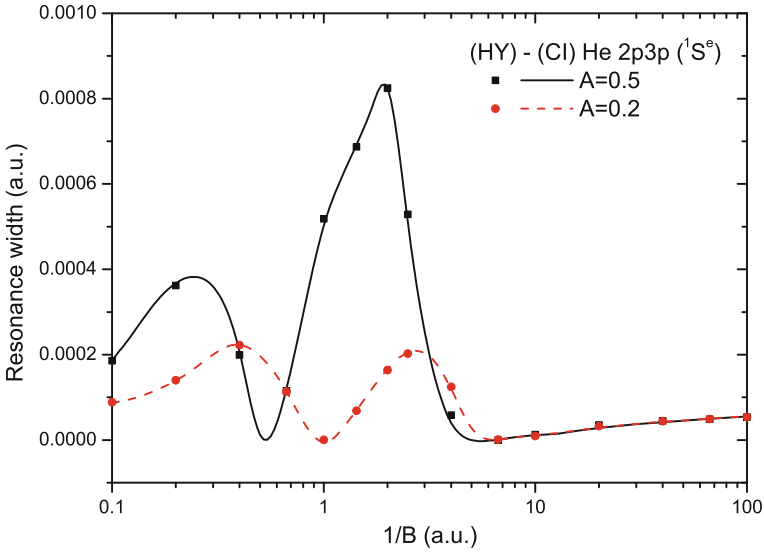

Fig. 6.9 The same as Fig. 6.6 but for the $2p3p\ ^1S^e$ resonant state

resonance phenomena in atomic systems, such as the Feshbach projection method [42, 43], the close-coupling approximation [44], multi-configuration Hartree-Fock method [45], hypersphercial close-coupling method [46, 47], stabilization method

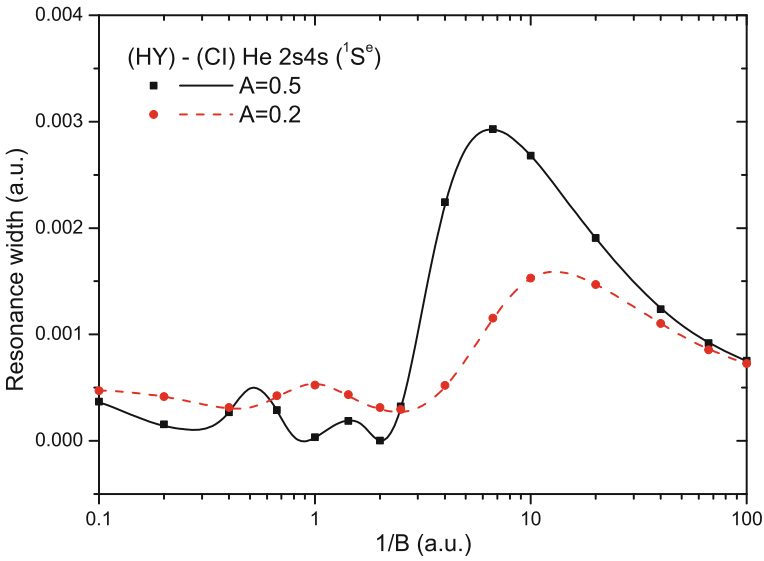

Fig. 6.10 The same as Fig. 6.6 but for the $2s4s\ ^1S^e$ resonant state

[48–50] and the complex-scaling method [51–53]. In Tables 6.3 and 6.4, we also include the results of Bürgers et al. [53] by using the complex-scaling method with the Sturmian-type basis. It can be seen that the results calculated by Hylleraas basis are more accurate than those by CI for the $npn'p$ resonances, especially for the $2p^2$ state. It has long time been recognized that [53, 54] the angle θ_{12} between the two electron position vectors for $nsn's$ resonance states has values larger than 90°. In the limit of $n' \to \infty$ these states have a collinear configuration $X - Y - X$ with the two electrons are localized on the opposite sides of the nucleus ($\theta_{12} \approx 180°$). However, for $npn'p$ resonance states in $^1S^e$ symmetry, θ_{12} is generally smaller than 90°, and the limit $n' \to \infty$ corresponds to a collinear configuration $Y - X - X$ with both electrons on the same side the nucleus ($\theta_{12} \approx 0°$). It is expected that the electron correlation effects in $npn'p$ states are quite important and, therefore, the inclusion of r_{12} factor in the system wave function is necessary.

When the He atom is confined in the QD, only the stabilization method calculation was performed by Chakraborty and Ho [31] for the lowest-lying resonance state. The comparisons in Figs. 6.5 and 6.6 show that the present complex-scaling calculations with both basis sets are in excellent agreement with the previous results. Figure 6.5 depicts the variations of the resonance energies of He QD along with the corresponding He^+ ($n = 2$) threshold states when the potential radius changes. Although the energies continuously decrease with increasing the dot size, no "plateau" patterns are visible for the doubly-excited resonant states as compared to the singly-excited bound states displayed in Fig. 6.3. It should be noticed that even though the resonant state is denoted by the products of single-electron orbitals, $2s^2$ for example, it actually has components of all those products that can couple to

Table 6.3 The $^1S^e$ resonant state energies of the two-electron He QD with FO potential depth $A = 0.5$ a.u.

$1/B$	*Basis*	$2s^2$	$2p^2$	$2s3s$	$2p3p$	$2s4s$
0	*a*	−0.77787	−0.62193	−0.58989	−0.54809	−0.54488
	b	−0.77786	−0.62182	−0.58989	−0.54806	−0.54488
	c	−0.77787	−0.62193	−0.58989	−0.54809	−0.54488
0.1	*a*	−0.78051	−0.62258	−0.59151	−0.54925	−0.54598
	b	−0.78050	−0.62246	−0.59151	−0.54923	−0.54598
0.4	*a*	−0.80257	−0.63835	−0.60704	−0.56404	−0.56045
	b	−0.80256	−0.63823	−0.60704	−0.56402	−0.56044
0.6667	*a*	−0.84176	−0.68169	−0.63750	−0.59976	−0.58983
	b	−0.84174	−0.68154	−0.63749	−0.59975	−0.58980
1	*a*	−0.92896	−0.76689	−0.70009	−0.66370	−0.64983
	b	−0.92894	−0.76669	−0.70008	−0.66372	−0.64982
2	*a*	−1.21136	−1.03822	−0.88034	−0.82562	−0.81020
	b	−1.21131	−1.03799	−0.88032	−0.82562	−0.81016
2.5	*a*	−1.31169	−1.13749	−0.95735	−0.88707	−0.86767
	b	−1.31164	−1.13721	−0.95733	−0.88702	−0.86763
4	*a*	−1.49484	−1.32089	−1.13860	−1.05314	−0.99368
	b	−1.49481	−1.32062	−1.13857	−1.05305	−0.99366
6.6667	*a*	−1.63186	−1.46037	−1.31474	−1.22809	−1.15959
	b	−1.63184	−1.46014	−1.31473	−1.22800	−1.15958
10	*a*	−1.69787	−1.52964	−1.41769	−1.33566	−1.27821
	b	−1.69785	−1.52944	−1.41768	−1.33558	−1.27820
20	*a*	−1.75265	−1.59042	−1.52205	−1.45321	−1.41945
	b	−1.75263	−1.59027	−1.52205	−1.45315	−1.41945
40	*a*	−1.77076	−1.61243	−1.56685	−1.51089	−1.49345
	b	−1.77074	−1.61230	−1.56685	−1.51085	−1.49345
66.667	*a*	−1.77518	−1.61823	−1.58033	−1.53099	−1.52051
	b	−1.77517	−1.61810	−1.58033	−1.53096	−1.52050
100	*a*	−1.77665	−1.62022	−1.58533	−1.53933	−1.53214
	b	−1.77664	−1.62010	−1.58532	−1.53931	−1.53213

The rows of $1/B = 0$ represent the free He atom. The notations *a* and *b* label the Hylleraas-type basis with $\omega = 16$ and CI-type basis with $l_{\max} = 10 - 5$, respectively. *c* represents the resonant states of free He atom calculated by Bürgers et al. [53]

Table 6.4 The same as Table 6.2 but for the resonance widths of the two-electron He QD modeled by FO potential

$1/B$	*Basis*	$2s^2$	$2p^2$	$2s3s$	$2p3p$	$2s4s$
0	*a*	0.004541	0.000216	0.001363	0.000075	0.000492
	b	0.004546	0.00017	0.001361	0.00006	0.000491
	c	0.004541	0.000216	0.001363	0.000075	0.000492
0.1	*a*	0.004483	0.000226	0.001329	0.000186	0.000368
	b	0.004488		0.001329	0.00018	0.000363
0.4	*a*	0.003976	0.000243	0.001146	0.000200	0.000270
	b	0.003980		0.001145	0.00020	0.000271
0.6667	*a*	0.004830	0.000173	0.001350	0.000115	0.000290
	b	0.004832		0.001349	0.00011	0.000285
1	*a*	0.006785	0.000080	0.001435	0.000518	0.000036
	b	0.006781		0.001423	0.00049	0.000029
2	*a*	0.009538	0.000004	0.002997	0.000825	0.000002
	b	0.009531		0.002973	0.00081	0.000001
2.5	*a*	0.009544	0.000007	0.004119	0.000529	0.000325
	b	0.009541		0.004111	0.00050	0.000307
4	*a*	0.008551	0.000039	0.005311	0.000059	0.002243
	b	0.008554		0.005309	0.00003	0.002215
6.6667	*a*	0.007022	0.000099	0.004813	0.000001	0.002931
	b	0.007028		0.004813	0.00000	0.002926
10	*a*	0.006039	0.000137	0.003960	0.000012	0.002682
	b	0.006046		0.003962	0.00001	0.002680
20	*a*	0.005070	0.000176	0.002667	0.000035	0.001906
	b	0.005076		0.002668	0.00002	0.001905
40	*a*	0.004700	0.000198	0.001898	0.000045	0.001239
	b	0.004706		0.001899	0.00003	0.001240
66.667	*a*	0.004603	0.000207	0.001608	0.000049	0.000919
	b	0.004609		0.001608	0.00003	0.000921
100	*a*	0.004570	0.000211	0.001486	0.000054	0.000755
	b	0.004575		0.001487	0.00004	0.000751

the final $^1S^e$ configuration, such as the $nsn's$, $npn'p$, $ndn'd$ etc. Such configuration interactions are stronger for higher-lying resonances. As a results, the radial distribution of the resonant state is more complicated than the bound states and no "plateau" exists.

The widths of the $2s^2$, $2p^2$, $2s3s$, $2p3p$ and $2s4s$ resonances are shown in Figs. 6.6, 6.7, 6.8, 6.9 and 6.10, respectively. The oscillatory behavior of the resonance width was firstly predicted by Chakraborty and Ho [31] for the lowest resonant state. The present complex-scaling calculations confirm this phenomenon and, in addition, it has been found that the oscillatory frequency increases for higher-lying resonant states. Such character arises from the strong interferences between the QD confining potential and the resonance wave functions. For two-electron systems, the wave functions of a doubly excited autoionizing state has large amplitude in the inner region and oscillator character in the outer region. The radial distribution of the two electrons in r_1 and r_2 contour plot show nodal and antinodal structures resulting from the electron correlations and configuration interactions. When the He atom is confined in a QD cavity, the node or antinode of the resonance wave function lies on the edge of the potential cavity, destructive or constructive interferences would take place inside the cavity, leading to shortening or prolonging of the autoionization lifetime. As a result, the resonance width exhibits oscillatory behavior when the size of the QD changes. For an extremely small ($1/B \to 0$) or large ($1/B \to \infty$) dot size, the resonance width approaches to the free-atom values in both cases, as we can see from Figs. 6.6, 6.7, 6.8, 6.9 and 6.10. The higher-lying resonant states have more nodal and antinodal structures [55] and therefore show more oscillatory characters between these two limits. From these Figures, one can also observe that the deepening of the confinement potential increases the oscillatory amplitude, which can be understood as the enhancement of the interference effects by the QD cavity.

Another interesting phenomenon is the nearly opposite effects of the QD cavity on the width for different resonant states. In Fig. 6.11, we categorize the $2s^2$, $2s3s$ and $2p^2$ in one group and $2s4s$ and $2p3p$ in another. It is found that the resonant states with $nsn's$ and $npn'p$ configurations in each group show nearly opposite changes against $1/B$. The different angular correlations (approximate $X-Y-X$ structure for $nsn's$ states and $Y-X-X$ structure for $npn'p$ ones) and the nearly degenerate energies between the $nsNs$ and $np(N-1)p$ states [53] are responsible to such interesting phenomenon. Last but not least, we would like to mention the possible interferences existing between the resonant states in strong confinement. In Fig. 6.11d for $A = 0.5$, the $2s4s$ and $2p3p$ states show additional structures in the region of $1/B = 1$ to 2 a.u., whereas in Fig. 6.11b for $A = 0.2$ they do not. Such phenomenon may also become severer for higher-lying resonances and in deeper confining potentials.

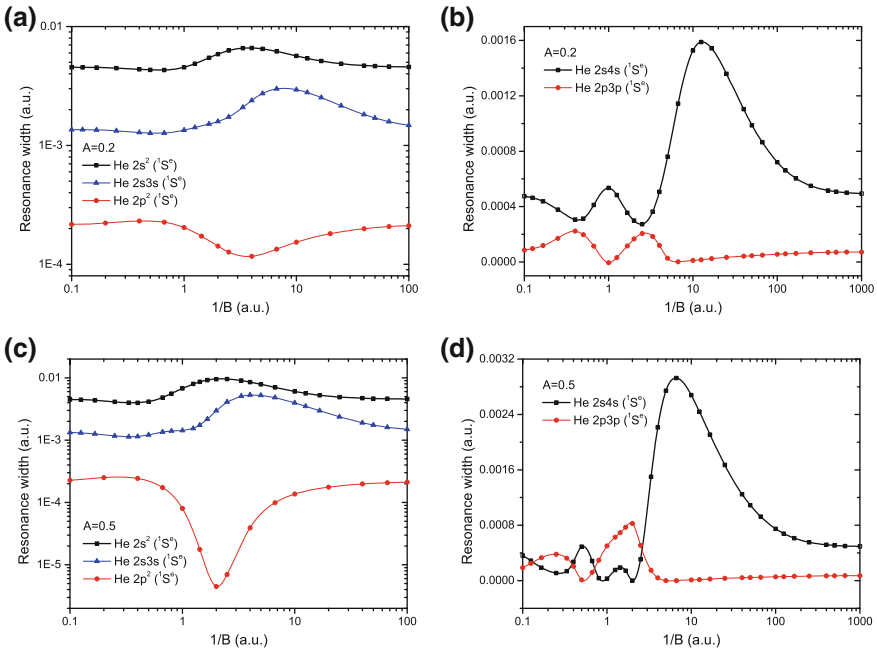

Fig. 6.11 Categories of the resonance width for He QD resonant states in ${}^1S^e$ symmetry. **a** $2s^2$, $2s3s$ and $2p^2$ resonances for $A = 0.2$ a.u., **b** $2s4s$ and $2p3p$ resonances for $A = 0.2$ a.u., **c** the same as (**a**) but for $A = 0.5$ a.u. and **d** the same as (**b**) but for $A = 0.5$ a.u.

6.4 Concluding Remarks

In this work, we investigate the confinement effects of the quantum dots modeled by finite oscillator potential on atomic systems. The bound states of the one- and two-electron QD with He^{2+} impurity are calculated in the variational approach. The degeneracies of the one-electron hydrogen-like energy levels are destroyed when the confinement potential is introduced. The two-electron bound states show some interesting "plateaus" in the energy spectrum arising from the different radial distributions of the two electrons in singly excited states. The doubly-excited resonant states of He QD are calculated by using the complex-scaling method. The system wave functions are represented by the configuration interaction-type and Hylleraas-type basis sets. The resonance energies decrease monotonously with increasing the dot radius, but no "plateau" patterns exist due to the strong configuration interactions. In the extremely small or large QD radii, the system approaches to a free atom situation or to a free atom plus a constant potential with infinite radius. Between these two limits, the resonance widths show oscillatory characters against the dot size, which is a result of the constructive and destructive interferences between the confining potential and the nodal structures of the resonance wave functions. The oscillatory behaviors are also manifestations of the radial and angle correlations of

the two electrons in autoionizing resonant states. The properties of the bound and resonant states of QD systems with impurities are very different with those containing only excess electrons, and there may still be other interesting phenomena that have not been discovered and fully understood. It is hoped that our work would encourage further investigations on the confinement effects in the QD systems.

Acknowledgment Financial support from the Ministry of Science and Technology of Taiwan (Republic of China) is gratefully acknowledged.

References

1. Sabin JR, Brandas E (2009) Advances in quantum chemistry, vol 57. Academic Press, New York
2. Laughlin C (2004) J Phys B 37:4085
3. Montgomery HE (2002) Chem Phys Lett 352:529
4. Montgomery HE, Sen KD (2012) Phys Lett A 376:1992
5. Cabrera-Trujillo R, Cruz SA (2013) Phys Rev A 87:012502
6. Kilcoyne ALD, Aguilar A, Müller A, Schippers S, Cisneros C, Alna'Washi G, Aryal NB, Baral KK, Esteves DA, Thomas CM, Phaneuf RA (2010) Phys Rev Lett 105:213001
7. Lin CY, Ho YK (2012) J Phys B 45:145001
8. Lin CY, Ho YK (2013) Few-Body Syst 54:425
9. Maksym PA, Chakraborty T (1990) Phys Rev Lett 65:108
10. Kastner MA (1996) Comments Condens Matter Phys 17:349
11. Buczko R, Bassani F (1996) Phys Rev B 54:2667
12. Huang YS, Yang CC, Liaw SS (1999) Phys Rev A 60:85
13. Yang CC, Liu LC, Chang SH (1998) Phys Rev B 58:1954
14. Sahoo S, Ho YK (2004) Phys Rev B 69:165323
15. Bednarek S, Szafran B, Adamowski J (1999) Phys Rev B 59:13036
16. Bylicki M, Jaskólski W, Stachów A, Diaz J (2005) Phys Rev B 72:075434
17. Ferrón A, Osenda O, Serra P (2009) Phys Rev A 79:032509
18. Taut M (1993) Phys Rev A 48:3561
19. Kandemir BS (2005) Phys Rev B 72:165350
20. Merkt U, Huser J, Wagner M (1991) Phys Rev B 43:7320
21. Pederiva F, Umrigar CJ, Lipparini E (2000) Phys Rev B 62:8120
22. Sako T, Diercksen GHF (2005) J Phys: Condens Matter 17:5159
23. Adamowski J, Sobkowicz M, Szafran B, Bednarek S (2000) Phys Rev B 62:4234
24. Adamowski J, Sobkowicz M, Szafran B, Bednarek S (2000) Phys Rev B 62:13233
25. Lin CY, Ho YK (2011) Phys Rev A 84:023407
26. Sajeev Y, Moiseyev N (2008) Phys Rev B 78:075316
27. Genkin M, Lindroth E (2010) Phys Rev B 81:125315
28. Winkler P (2004) Int J Quantum Chem 100:1122
29. Kimani P, Jones P, Winkler P (2008) Int J Quantum Chem 108:2763
30. Kwon YD (2006) Phys Rev B 73:165210
31. Chakraborty S, Ho YK (2011) Phys Rev A 84:032515
32. Lin CY, Ho YK (2012) Fingerprints in the optical and transport properties of quantum dots, Chap. 7. In Tech, Croatia
33. Drake GWF (1978) Phys Rev A 18:820
34. Cardona JC, Sanz-Vicario JL (2008) J Phys B 41:055003
35. Ordóñez-Lasso AF, Cardona JC, Sanz-Vicario JL (2013) Phys Rev A 88:012702

36. Reinhardt WP (1982) Ann Rev Phys Chem 33:223
37. Ho YK (1983) Phys Rep 99:1
38. Kar S, Ho YK (2005) New J Phys 7:141
39. Moiseyev N, Friedland S, Certain PR (1981) J Chem Phys 74:4739
40. Drake GWF (1996) Atomic molecular and optical physics handbook, Chap. 11. AIP Press, New York
41. Drake GWF, Cassar MM, Nistor RA (2002) Phys Rev A 65:054501
42. Bhatia AK, Temkin A (1975) Phys Rev A 11:2018
43. Bhatia AK, Temkin A (1984) Phys Rev A 29:1895
44. Oza DH (1986) Phys Rev A 33:824
45. Fischer CF, Idrees M (1990) J Phys B 23:679
46. Lin CD (1995) Phys Rep 257:1
47. Tang J, Watanabe S, Matsuzawa M (1992) Phys Rev A 46:2437
48. Mandelshtam VA, Ravuri TR, Taylor HS (1993) Phys Rev Lett 70:1932
49. Müller J, Yang X, Burgdörfer J (1994) Phys Rev A 49:2470
50. Kar S, Ho YK (2005) Chem Phys Lett 402:544
51. Ho YK (1986) Phys Rev A 34:4402
52. Chakraborty S, Ho YK (2008) Eur Phys J D 49:59
53. Bürgers A, Wintgen D, Rost JM (1995) J Phys B 28:3163
54. Wintgen D, Richter K, Tanner G (1992) Chaos 2:19
55. Tanner G, Richter K, Rost JM (2000) Rev Mod Phys 72:497

Chapter 7
Spatial and Shell-Confined One Electron Atomic and Molecular Systems: Structure and Dipole Polarizability

S.A. Ndengué and O. Motapon

7.1 Introduction

The idea of confined quantum system originates from the pioneering work of Michels et al. [1] who used an impenetrable cavity to simulate the effect of pressure on the static polarizability of a hydrogen atom. Later on, the concept of confinement was used to model atomic systems subjected to different types of traps. Under special constraints—spatial restriction (of various geometries) under pressure, trapping inside a hollow cage (fullerene cage) or an attractive potential—atoms have been found to undergo numerous changes in their properties (orbitals, energy levels, localization of electrons, polarizability, filling of shells, photon induced ionization and absorption, etc.) compared to the free atoms. In the past two decades, confined atoms have known a rising interest owing to the whole bunch of potential applications: hydrogenic impurities in semiconductors/nanostructures (quantum dots, quantum well, quantum well wires), atoms emprisoned in zeolite traps, atoms trapped in fullerene cages, etc. Detailed discussions of these applications are available on several review articles [2–4]. Recently, two consecutive volumes of *Advances in Quantum Chemistry* [5, 6] provided state-of-the-art advances in the study of confined atoms and molecules. The principal idea one may consider for the attractivity of this study is the inadequacy of standard quantum chemistry programs to obtain adequate results, that is most of the time, new (or modified standard) codes and approaches have to be proposed to tackle issues related to confinement.

It is currently admitted that the spherical cage [7–9] can be an ideal representation of the endohedral confinement, as well as the spherical cavity proposed by Michels et al. [1] and used by several authors [10–15] is an ideal description of the pressure effect in an ionized medium. This situation is adequate for analytical or

S.A. Ndengué · O. Motapon (✉)
Laboratoire de Physique Fondamentale, UFD Mathématiques, Informatique Appliquée et Physique Fondamentale, University of Douala, P.O. Box 24157, Douala, Cameroon
e-mail: omotapon@univ-douala.com

K.D. Sen (ed.), *Electronic Structure of Quantum Confined Atoms and Molecules*,
DOI 10.1007/978-3-319-09982-8_7

numerical treatment due to the separability of the Schrödinger equation as well as it is interesting for modelling spherical atomic trapping. The effect of such an environment on the energy levels, the shell filling and other properties of atoms were described [8, 16–18], and the wavefunctions used to account for the redistribution of oscillator strengths and the so-called confinement resonances that appear in the photoionization cross section of endohedrally confined atoms [9, 18–20].

The cavity can have a deformed shape. This is why prolate spheroidal cavity can be used to generalize the spherical one, and this is natural in the molecular context. A less ideal situation for numerical computations would be to consider the atom confined in a cylindrical cavity. This could happen if one imagines an atom trapped in a nanotube, a nanowire or any other type of cylindrical potential. In this situation, the Schrödinger equation is no longer completely separable (except for some special types of potentials [21]) and we therefore have to deal with a multidimensional equation with a Coulomb potential.

Molecules can also experience spatial or endohedral confinement. Experiments [22] have reported the encapsulation of molecules in fullerene cages. Ab initio and semi-empirical computations have been devoted to the characterization of the stabilization—equilibrium distance and energy—of some basic molecules trapped inside the C_{60} cage [23, 24] or inside nanotubes [25]. The study of hydrogen molecular ion inside a penetrable prolate spheroidal box was addressed by the group of Cruz [26–28] where spatial confinement was obtained at the infinite limit of the confining potential. A similar work, based on H_2, was carried out by Pang [29] using a diffusion quantum Monte Carlo method. Tayebirad et al. [30] used the same method to study slightly varying equilibrium position of hydrogen molecule and hydrogen molecular ion inside a fullerene cage. Those works were limited to the description of the energy curve and spectroscopic properties of the electronic ground state.

This contribution revisits the structure and electric dipole polarizability of one electron atoms and molecular systems. It proceeds in a first step through a description of spherical one-electron basis sets, indicated for one electron atoms in spherically symmetric potentials. In a second step, a two-center spheroidal basis set approach, appropriate for the description of one-electron molecular systems is developed. Results for both the ground and excited electronic states of H_2^+, since we are interested in the polarizability, under spatial confinement, are presented. We also report an investigation of the same states submitted to a confinement within a fullerene cage $\left(H_2^+@C_{60}\right)$. Such a system constitutes a benchmark for the study of the properties of simple molecules confined in an endohedral cage, and represents a starting point for the theoretical study of the storage of small molecules in this kind of device as experimentally realized recently in nanotubes [31, 32]. Finally, the atomic limit of the confined H_2^+ can be obtained by taking adequate electric charges at the two centers and an appropriate limit for the internuclear distance. This has enabled us to revisit the so-called centered and off-centered hydrogen atom spatially confined (previously studied by Ting-Yun et al. [33] and Neek-Amal et al. [34]) or endohedrally confined [35, 36]. In a third step, we present the case of the cylindrical

confinement of the H atom, indicated to model trapping in quantum nanowires and nanotubes. After the initial works of Yurenev et al. [37] and Yurenev et al. [38] who studied the energy and stability of the hydrogen atom confined in a perfect cylinder, we revisit previous calculations of the non-relativistic energies of cylindrically centered confined atom and follow our current interest on confined systems [39, 40] in computing the static and dynamic dipole polarizability. An implemented fit approach consisting in expressing the potential as an expansion of product form is found to be efficient in saving computation time [41].

This contribution is organized as follows. The theoretical method is presented in Sect. 7.2. It deals with the methods of solutions of the Schrödinger equation in different confinement situations, as well as the polarizability computation. In Sect. 7.3, we present the results of the developed models. We conclude this chapter by presenting the future directions that those initial works can initiate.

7.2 Theoretical Method

The Schrödinger equation is the starting ground for the study of microsystems. In our works, we approximate it with the variational Galerkin approach, expanding the wavefunctions on a B-Splines basis set. This section gives a brief description of the mathematical tools used to solve the Schrödinger equation. Also the forms of the Schrödinger equation in the various types of confinement investigated, the methods for their solutions, and the operational forms for the static and dynamic electric dipole polarizability of the corresponding systems will be developed.

7.2.1 B-Splines Basis Set and Variational Galerkin Approach

7.2.1.1 B-Splines Basis Set

A B-Splines basis set is a set of piecewise polynomials represented in a finite interval. That interval is divided into segments, the endpoints of which are given by a knot sequence $\{t_i\}, i = 1, 2, \ldots, n + k$, where n is the number of B-splines and k their order. Following the notation of de Boor [42] the B-Splines of order $k, B_{i,k}(r)$, are defined in this knot sequence by the relations:

$$B_{i,1}(r) = \begin{cases} 1 & t_i \leq r \leq t_{i+1} \\ 0 & otherwise \end{cases} \tag{7.1}$$

and

$$B_{i,k}(r) = \frac{r - t_i}{t_{i+k-1} - t_i} B_{i,k-1}(r) + \frac{t_{i+k} - r}{t_{i+k} - t_{i+1}} B_{i+1,k-1}(r) \tag{7.2}$$

They satisfy the relations

$$\begin{cases} \int_0^{r_{\max}} B_{i,k}(r) B_{j,k}(r) dr = 0 \quad for \quad |i-j| > k \\ \sum_{i=1}^{k} B_{i,k}(r) = 1 \end{cases} \tag{7.3}$$

The functions $B_{i,k}(r)$ are piecewise polynomials of degree $k-1$ in the interval $t_i \leq r \leq t_{i+k}$ and vanish out of this interval. The points defining our sequence have a multiplicity of k at $r = 0$ and $r = r_{\max}$, i.e. $t_1 = t_2 = \cdots = t_k = 0$ and $t_{n+1} = t_{n+2} = \cdots = t_{n+k} = r_{\max}$. These points can be distributed at our convenience linearly, geometrically, exponentially or even sinusoidally. They can also be adjusted so as to describe non differentiable conditions of the wavefunctions at some regions of the space. The Spline $B_{i,k}(r)$, defined in the range $[t_i, t_{i+k}]$ is differentiable of order $k - m - 1$ on the knots of its range, where m is the multiplicity of the particular knot [43, 44]. The exponential knot sequence is suitable in atomic physics in general because it concentrates points at the small radii where the wavefunctions oscillate. In this work, a linear sequence has been preferred to insure a correct description of the wavefunctions at the boundaries of the shell potential i.e. at r_c and $r_c + \Delta$.

The B-splines are reliable for their flexibility and have drawn a great interest during the last 25 years. They provide a good alternative to the finite difference methods for the solution of differential equations. Their definition and properties have been presented by de Boor [42] and have been widely reviewed or used in a number of papers of interest in atomic and molecular physics among which one can mention several references [45–49]. They have been used to solve the Schrödinger equation in one or several dimensions, for two or many body problems, in spherical or spheroidal coordinates.

7.2.1.2 Variational Galerkin Approach

In order to solve with the variational Galerkin approach the Schrödinger equation:

$$\hat{H}\psi = E\psi \tag{7.4}$$

we expand the radial wavefunction as:

$$\psi_{nl}(r) = \sum_{i=1}^{N} c_i B_{i,k}(r) \tag{7.5}$$

where $B_{i,k}$ is the ith B-Spline function of order k.

When studying a free atom, an atom confined in fullerene (modelled as a shell), an atom in a plasma (modelled by a Debye potential), or an atom under an infinite range potential, the infinite space is restricted to a finite one in order to make computations numerically affordable. This is done by defining a parameter $r_{\max}$ that controls our domain and chosen sufficiently great so that most of the low-lying levels wavefunctions are evanescent at $r_{\max}$. For systems under hard wall confinements, $r_{\max}$ would represent the confinement radius and thus suits well with this type of studies. However, since the method is approximate and the basis functions are not eigenfunctions of our system, in all the mentioned cases, convergence is achieved by increasing the B-Splines basis size.

The transformation of the radial Schrödinger Eq. (7.4) through the variational Galerkin procedure [50] with respect to the c_i coefficients leads to an $N \times N$ generalized eigenvalue problem:

$$Av = \varepsilon Sv \tag{7.6}$$

v being the column matrix of the c_i coefficients, A the hamiltonian matrix, S the overlapping matrix and ε the variational energies. Solving this generalized eigenvalue equation gives the eigenvalues ε^{λ} which are energy levels and eigenvectors v^{λ} which are used to generate the eigenfunctions.

At this point it is important to note that the variational Galerkin procedure employed here does not include the conditions at the boundaries of the shell potential (Eq. 7.13). Nevertheless we are able to solve accurately the problem taking advantage of the integration which is not perturbed much by the discontinuity at the shell boundary for any function (continuous or not). The major problem comes from the derivative of B-Splines which may have extremely high (or infinite) values at the shell boundary due to the discontinuity of their (discontinuous) primitive counterpart function. This problem is overcome by either using a relatively high (more than a hundred) number of B-Splines functions to obtain correct results or increasing the multiplicity of the knots at the non differentiable points of the domain as stated in the previous section.

7.2.2 Schrödinger Equation in Spherical Representation: Solutions and Dipole Polarizability

7.2.2.1 Wavefunctions and Energy Levels

The radial wavefunction $\phi_{nl}(r) = \frac{\psi_{nl}(r)}{r}$ and the eigenenergies E_{nl} of a hydrogen like system confined or trapped in a potential $U(r)$ can be obtained, in the non relativistic case, by solving the radial Schrödinger equation which reads (after the common transformation) in atomic units ($m = \hbar = e = 1$):

$$\left\{\frac{-1}{2}\left[\frac{d^2}{dr^2}-\frac{l(l+1)}{r^2}\right]-\frac{Z}{r}+U(r)\right\}\psi_{nl}(r)=E_{nl}\psi_{nl}(r) \tag{7.7}$$

In the case of a spatial confinement, $U(r)$ is represented by:

$$U(r)=\begin{cases}0 & r\leq R_{\max}\\ \infty & otherwise\end{cases} \tag{7.8}$$

The endohedral environment can be modelled, in the case of a single-walled cage, by a potential of the form [7, 8]:

$$U(r)=\begin{cases}-U_0 & r_c\leq r\leq r_c+\Delta\\ 0 & otherwise\end{cases} \tag{7.9}$$

where U_0 is positive, r_c is the inner radius of the shell and Δ the difference between the inner and the outer radii. For r_c and Δ, we used the values proposed by Xu et al. [7] for a fullerene C_{60} molecule, that is $r_c \simeq 5.75$ a.u., and $\Delta \simeq 1.89$ a.u.

In the case of a multi-walled cage (buckyonion), the endohedral environment can be modelled by a potential of the form:

$$U(r)=\sum_{i=1}^{n} a_i U_i(r) \tag{7.10}$$

with $a_i = 0$ or 1, and:

$$U_i(r)=\begin{cases}-U_0^{(i)} & r_c^{(i)}\leq r\leq r_c^{(i)}+\Delta^{(i)}\\ 0 & otherwise\end{cases} \tag{7.11}$$

where $U_0^{(i)}, r_c^{(i)}$ and $\Delta^{(i)}$ stand for the depth, the inner radius and the distance between the inner and the outer radii for the *i*th shell. For the three-shell case modelling H@C_{60}@C_{240}@C_{540} for example, the values for these constants are taken to be [40, 51] $U_0^{(i)} = 0.302$ a.u. for C_{60}, 0.367 for C_{240}, and 0.441 for C_{540}; $r_c^{(i)}$ is 5.75 a.u. for C_{60}, 12.60 for C_{240}, and 18.85 for C_{540}; and $\Delta^{(i)}$ is the same (1.89 a.u.) for C_{60}, C_{240}, and C_{540}, because the thickness is largely determined by the extent of the carbon atom.

The radial wavefunctions $\psi_{nl}(r)$, which are part of the total wavefunctions $\Psi_{nlm}(\mathbf{r}) = \frac{1}{r}\psi_{nl}(r)Y_{lm}(\theta,\phi)$ where the $Y_{lm}(\theta,\phi)$'s are spherical harmonics, satisfy to the boundary conditions:

$$\psi_{nl}(0)=\psi_{nl}(\infty)=0 \tag{7.12}$$

and

$$\frac{\psi'_{nl}(r_<^{(i)})}{\psi_{nl}(r_<^{(i)})} = \frac{\psi'_{nl}(r_>^{(i)})}{\psi_{nl}(r_>^{(i)})} \tag{7.13}$$

at each wall where the prime denotes a derivative with respect to $r, r_<^{(i)}$ and $r_>^{(i)}$ corresponding to two regions separated by a wall located at $r^{(i)}$ or $r^{(i)} + \Delta^{(i)}$.

In the case of simple space confinement, $U(r)$ is taken to be zero, and the pressure effect comes from vanishing wave functions at $R_{\max}$. To solve the Schrödinger Eq. (7.7), we apply the variational Galerkin procedure [50] with B-Splines functions as the expanding set.

7.2.2.2 Electric Dipole Polarizability

When the atom in the state $n_0 l_0$ is submitted to a uniform electric field directed along the z axis, the electric static dipole polarizability, that materializes the atomic second order response, reads:

$$\alpha_{n_0 l_0} = 2 \sum_{nlm \neq n_0 l_0 m_0} \frac{|\langle \Psi_{nlm}(\mathbf{r}) | r \cos\,\theta | \Psi_{n_0 l_0 m_0}(\mathbf{r}) \rangle|^2}{E_{nl} - E_{n_0 l_0}} \tag{7.14}$$

Replacing the functions $\Psi_{nlm}(\mathbf{r})$ and $\Psi_{n_0 l_0 m_0}(\mathbf{r})$ by their expression, one finds:

$$\alpha_{n_0 l_0} = 2 \sum_{nlm \neq n_0 l_0 m_0} \frac{1}{E_{nl} - E_{n_0 l_0}} \left(\mathscr{R}^{nl}_{n_0 l_0}\right)^2 \left(\mathscr{A}^{lm}_{l_0 m_0}\right)^2 \tag{7.15}$$

or

$$\alpha_{n_0 l_0} = 2 \sum_{nlm \neq n_0 l_0 m_0} \frac{\left(\mathscr{R}^{nl}_{n_0 l_0}\right)^2}{E_{nl} - E_{n_0 l_0}} (2l+1)(2l_0+1) \begin{pmatrix} l & 1 & l_0 \\ 0 & 0 & 0 \end{pmatrix}^2 \begin{pmatrix} l & 1 & l_0 \\ -m & 0 & m_0 \end{pmatrix}^2 \tag{7.16}$$

where

$$\mathscr{R}^{nl}_{n_0 l_0} = \int_0^{r_{\max}} r \psi_{nl}(r) \psi_{n_0 l_0}(r) dr \tag{7.17}$$

and

$$\mathscr{A}^{lm}_{l_0 m_0} = \int d\boldsymbol{\Omega} (-)^m Y_{l,-m}(\boldsymbol{\Omega}) Y_{10}(\boldsymbol{\Omega}) Y_{l_0 m_0}(\boldsymbol{\Omega}) \tag{7.18}$$

$\begin{pmatrix} a & b & c \\ d & e & f \end{pmatrix}$ being a Wigner $3j$ symbol.

For an atom initially in the ground state ($n_0 l_0 = 1s$), one has

$$\alpha_{1s} = \frac{2}{3} \sum_{np, n \neq 1} \frac{\left(\mathscr{R}^{np}_{1s}\right)^2}{E_{np} - E_{1s}} \tag{7.19}$$

7.2.3 Schrödinger Equation in the Prolate Spheroidal Representation: Solutions and Dipole Polarizability

7.2.3.1 One Electron Schrödinger Equation

Let us consider the Hydrogen molecular ion in the Born-Oppenheimer approximation. The two atoms are positioned in A and B separated by a distance R. This approach can then be extended to atomic systems, by considering half atoms centered on A and B with $R \rightarrow 0$ (nearly centered case), or a full atom centered on either A or B (off-center case). For such systems it is natural to use prolate-spheroidal coordinates:

$$(\xi \in [1, \infty); \eta \in [-1, 1]; \phi \in [0, 2\pi]), \tag{7.20}$$

with:

$$\xi = \frac{r_A + r_B}{R} \quad and \quad \eta = \frac{r_A - r_B}{R}, \tag{7.21}$$

where r_A (resp. r_B) is the distance from center A (resp. B) to the electron and ϕ is the angle around the internuclear axis.

We follow the description proposed by Vanne and Saenz [52] of which we will just present the main steps in this text, and invite the interested reader to report to this reference.

The One Electron Schrödinger Equation (OESE) is written as:

$$\hat{h}\psi = \varepsilon\psi \tag{7.22}$$

with

$$\hat{h} = -\frac{1}{2}\nabla^2 + V(\xi, \eta) + U(\xi, \eta). \tag{7.23}$$

where

$$\nabla^2 = \frac{1}{R^2}\frac{1}{\xi^2-\eta^2}\left[\frac{\partial}{\partial\xi}\left(\xi^2-1\right)\frac{\partial}{\partial\xi}+\frac{\partial}{\partial\eta}\left(1-\eta^2\right)\frac{\partial}{\partial\eta}+\frac{\xi^2-\eta^2}{\left(\xi^2-1\right)\left(1-\eta^2\right)}\frac{\partial^2}{\partial\varphi^2}\right] \tag{7.24}$$

$V(\xi,\eta)$ is the Coulomb potential, written as follows:

$$V(\xi,\eta) = -\frac{2}{R^2\left(\xi^2-\eta^2\right)}\left\{(Z_B+Z_A)R\xi+(Z_B-Z_A)R\eta\right\}, \tag{7.25}$$

and U the confinement potential.

The wave functions are searched in the form:

$$\psi(\xi,\eta,\varphi) = \left(\xi^2-1\right)^{|m|/2}B_{i,k_\xi}(\xi)\left(1-\eta^2\right)^{|m|/2}B_{j,k_\eta}(\eta)\frac{1}{\sqrt{2\pi}}e^{im\varphi} \tag{7.26}$$

To solve Eq. (7.22), two sets of B-Splines are introduced. The first set comprises n_ξ B-Splines $B_r(\xi)(r=1,\ldots,n_\xi)$ of order k_ξ for variable ξ. The knot sequence $\left\{\xi_i^b\right\}$ is chosen according to:

$$1=\xi_i^b=\cdots=\xi_{k_\xi}^b<\xi_{k_\xi+1}^b<\cdots<\xi_{n_\xi+1}^b=\cdots=\xi_{n_\xi+k_\xi}^b=\xi_{\max}, \tag{7.27}$$

Similarly, the second set comprises n_η B-Splines $B_r(\eta)\left(r=1,\ldots,n_\eta\right)$ of order k_η for variable η, but now using the knot sequence $\left\{\eta_i^b\right\}$ according to:

$$-1=\eta_i^b=\cdots=\eta_{k_\xi}^b<\eta_{k_\xi+1}^b<\cdots<\eta_{n_\xi+1}^b=\cdots=\eta_{n_\xi+k_\xi}^b=1. \tag{7.28}$$

This OESE can be used to treat both centered and off-centered situations of hydrogen-like systems. In the centered case, we place 1/2 charges on each center and let the intercenter distance $R\to 0$ and $\xi\to\infty$ [35]. In the off-centered case, we place a charge on one center and let the other center free of charge. The off-centered displacement will then be half the intercenter distance R.

7.2.3.2 Spatial Confinement in the Spheroidal Description

Referring to the approach described above for the OESE, we *easily* implement the spatial confinement on the system. The basis parameter $\xi_{\max}$ defines the size of the ellipsoidal box in which the OESE is solved. It is related to the semi-major axis of the elliptical box $(2R_c)$ by the relation:

$$\xi_{\max} = \frac{2R_c}{R} \tag{7.29}$$

Working with a particular value of the spatial confinement (R_c) is then equivalent to studying the system for a value of $\xi_{\max}$ dependent of R_c and the intercenter distance, as the previous equation shows. The same formalism applies to Hydrogen and Hydrogen-like systems. In this case, having $\xi \to \infty$ and $R \to 0$ is used to ensure that the the semi-major axis of the ellipsoidal box $(2R_c)$ will be sufficiently large so that the wavefunctions of the system shall not feel a spatial confinement in a free atom case. In the situation of spatial confinement, we just have to let $R \to 0$ and impose a value of R_c. We deduce then the value of $\xi_{\max}$.

7.2.3.3 Shell Potential Confinement in the Spheroidal Description

The endohedral shell potential is modelled according to two methods which give the same results in a particular case. The first approach consists in writing the shell potential as:

$$U(\xi) = \begin{cases} -U_0 & \xi_s \leq \xi \leq \xi_s + \Delta_s \\ 0 & otherwise \end{cases} \tag{7.30}$$

In this approach the endohedral shell has a shape homothetically similar to the box, that is the shell will exhibit the same deformation than the ellipsoidal box. Hence, if the box is strongly deformed from a sphere, it will be the same for the shell potential.

The second approach consists in writing the shell potential as:

$$U(\xi, \eta) = \begin{cases} -U_0 & inside\ the\ shell \\ 0 & otherwise \end{cases} \tag{7.31}$$

where the shell is located between two ellipsoids [35] of revolution with principal diameters A_{in}, B_{in} and A_{out}, B_{out} given by:

$$A_{in} = \left(\frac{2+\delta}{2-\delta}\right)^{2/3} R_s, \quad A_{out} = \left(\frac{2+\delta}{2-\delta}\right)^{2/3} [R_s + \Delta_s] \tag{7.32}$$

$$B_{in} = \left(\frac{2-\delta}{2+\delta}\right)^{2/3} R_s, \quad B_{out} = \left(\frac{2-\delta}{2+\delta}\right)^{2/3} [R_s + \Delta_s] \tag{7.33}$$

R_s being the inner radius of the shell and Δ_s the difference between the inner and the outer radii. For R_s and Δ_s, we used the values proposed by Xu et al. [7] for a fullerene C_{60} molecule, that is $R_s \simeq 5.75$ a.u., and $\Delta_s \simeq 1.89$ a.u.

The ellipsoidal potential shell region of non-zero potential is defined by the following system of two equations:

$$\frac{d^2}{4}\frac{\left(\xi^2-1\right)(\eta^2-1)}{B_{in}^2}+\frac{d^2}{4}\frac{\xi^2\eta^2}{A_{in}^2}\geq 1 \tag{7.34}$$

$$\frac{d^2}{4}\frac{\left(\xi^2-1\right)(\eta^2-1)}{B_{out}^2}+\frac{d^2}{4}\frac{\xi^2\eta^2}{A_{out}^2}\leq 1 \tag{7.35}$$

where d is the focal distance defining the family of spheroidal coordinates.

7.2.3.4 Electric Dipole Static and Dynamic Polarizability

The polarizability of the H_2^+ as any molecular system consists of an electronic contribution and a nuclear contribution which can be both described simultaneously in a non adiabatic approach or separately in a Born-Oppenheimer approach. In the present work, we deal with the latter approach. In this case, the electronic part of the electric dipole polarizability can be separated into two components:

(i) A transversal component

$$\alpha_{e\perp}=2\sum_{ex}\frac{\left|\langle\psi_0|d_x|\psi_{ex}\rangle\right|^2}{E_{ex}-E_0}, \tag{7.36}$$

where

$$d_x=-r\cos\varphi=\frac{-\sqrt{2r_1^2r_2^2+2r_1^2R^2+2r_2^2R^2-r_1^4-r_2^4-R^4}}{2R}\cos\varphi. \tag{7.37}$$

(ii) A longitudinal component

$$\alpha_{e\parallel}=2\sum_{ex}\frac{\left|\langle\psi_0|d_z|\psi_{ex}\rangle\right|^2}{E_{ex}-E_0}, \tag{7.38}$$

where

$$d_z=-\frac{r_1^2-r_2^2}{2R}. \tag{7.39}$$

In the above equations, the subscript 0 and *ex* are used for the initial (ground) state and the excited states respectively.

The weighted electronic polarizability is:

$$\alpha_e = (\alpha_{e\parallel} + 2\alpha_{e\perp})/3. \tag{7.40}$$

In spheroidal coordinates, the wave functions can be put in the forms:

$$\psi_0(r;R) \equiv \psi_0(\xi,\eta,\varphi) = \frac{1}{\sqrt{2\pi}}\phi_0(\xi,\eta)e^{im_0\varphi} \tag{7.41}$$

and

$$\psi_{ex}(r;R) \equiv \psi_{ex}(\xi,\eta,\varphi) = \frac{1}{\sqrt{2\pi}}\phi_{ex}(\xi,\eta)e^{im_{ex}\varphi} \tag{7.42}$$

and the electric dipole moment component in the form:

$$d_x = -r\cos\varphi = -\frac{\cos\varphi}{2R}\sqrt{-R^4\xi^2\eta^2 - R^4 + R^4\left(\xi^2+\eta^2\right)}, \tag{7.43}$$

that is

$$d_x = -\frac{R\cos\varphi}{2}\sqrt{(1-\eta^2)\left(\xi^2-1\right)}, \tag{7.44}$$

and

$$d_z = -\frac{r_1^2 - r_2^2}{2R} = -\left(\frac{R}{2}\right)\xi\eta. \tag{7.45}$$

In this case, the transversal electronic polarizability is given by:

$$\begin{aligned}\alpha_{e\perp} = \frac{R^8}{256}\sum_{ex}\frac{\left(\int\int \phi_0\cdot\phi_{ex}\sqrt{(1-\eta^2)\left(\xi^2-1\right)}\left(\xi^2-\eta^2\right)d\xi d\eta\right)^2}{(E_{ex}-E_0)} \\ \times\frac{1}{2\pi}\left(\int e^{-im_0\varphi}e^{im_{ex}\varphi}\cos\varphi d\varphi\right)^2\end{aligned} \tag{7.46}$$

Note that $\frac{1}{2\pi}\int e^{-im_0\varphi}e^{im_{ex}\varphi}\cos\varphi d\varphi = \frac{1}{2}$ if and only if $m_{ex} = m_0 \pm 1$.

For $m_0 = 0, m_{ex}$ is ± 1 is, which means that transitions are from σ to π and vice versa. One will then have:

$$\alpha_{e\perp} = \frac{R^8}{512}\sum_{ex}\frac{\left(\int\int \phi_0\cdot\phi_{ex}\sqrt{(1-\eta^2)\left(\xi^2-1\right)}\left(\xi^2-\eta^2\right)d\xi d\eta\right)^2}{(E_{ex}-E_0)}. \tag{7.47}$$

The longitudinal electronic polarizability gives:

$$\alpha_{e\parallel} = \frac{2R^8}{256}\sum_{ex}\frac{\left(\int\int \phi_0 \cdot \phi_{ex}\xi\eta\left(\xi^2-\eta^2\right)d\xi d\eta\right)^2}{E_{ex}-E_0} \times \frac{1}{2\pi}\left(\int e^{-im_0\varphi}e^{im_{ex}\varphi}d\varphi\right)^2. \tag{7.48}$$

$\frac{1}{2\pi}\int e^{-im_0\varphi}e^{im_{ex}\varphi}d\varphi = 1$ if and only if $m_{ex} - m_0 = 0$ which implies a transition from a σ to a σ state. When this condition is satisfied, the longitudinal electronic polarizability is:

$$\alpha_{e\parallel} = \frac{R^8}{128}\sum_{ex}\frac{\left(\int_{-1}^{1}\int_{1}^{+\infty}\phi_0 \cdot \phi_{ex}\xi\eta\left(\xi^2-\eta^2\right)d\xi d\eta\right)^2}{E_{ex}-E_0}. \tag{7.49}$$

The integrals involved in the transversal and longitudinal polarizabilities can be expressed as sums of products of integral expressions involving B-splines which can be evaluated accurately by a Gauss-Legendre quadrature. It is to be reminded that $\alpha_{e\perp}$ and $\alpha_{e\parallel}$ are functions of the internuclear distance R. In the Born-Oppenheimer approximation, the total polarizability at the equilibrium distance $\alpha(R_e)$, including the nuclear part, is obtained by averaging $\alpha_e(R)$ over the rovibronic state $f_{J,v}(\mathbf{R})$. For the ground state polarizability, the clamped nucleus approximation [53] gives:

$$\alpha_g = \int f_{0,0}(\mathbf{R})\alpha_e(R)f_{0,0}(\mathbf{R})d\mathbf{R}. \tag{7.50}$$

7.2.4 Schrödinger Equation in the Cylindrical Representation: Solutions and Dipole Polarizability

The hydrogen atom experiencing a cylindrical confinement can be described as a one electron atom fixed at the geometric center of an impenetrable wall cylinder of length $z_{\max}$ and radius $\rho_{\max}$. The Schrödinger Eq. (7.4) obeyed by our system then reads:

$$\left[-\frac{1}{2\rho}\frac{\partial}{\partial\rho}\left(\rho\frac{\partial}{\partial\rho}\right) - \frac{1}{2\rho^2}\frac{\partial^2}{\partial\phi^2} - \frac{1}{2}\frac{\partial^2}{\partial z^2} - \frac{Z}{\sqrt{z^2+\rho^2}}\right]\Psi = \varepsilon\Psi \tag{7.51}$$

with $0 \le \rho \le \rho_{\max}$, $\frac{-z_{\max}}{2} \le z \le \frac{+z_{\max}}{2}$ and $0 \le \phi \le 2\pi$. The wavefunction, solution to Eq. (7.51) is written as:

$$\Psi(\rho, z, \phi) = \psi(\rho, z)\frac{e^{im\phi}}{\sqrt{2\pi}} \tag{7.52}$$

and satisfies the following boundary conditions:

$$\psi(\rho, z_{\max}/2) = \psi(\rho, -z_{\max}/2) = \psi(\rho_{\max}, z) = 0 \tag{7.53}$$

That is the wavefunction vanishes on the walls of our cylinder. This is equivalent to solving the Schrödinger equation with a potential having the Coulomb type inside the cylinder domain, but infinite outside.

Equation (7.51) is solved by expanding the wavefunction on B-Splines, like in the two previous cases, but with a different approach.

7.2.4.1 Variational Method for the Cylindrical Problem

The non angular part of the wavefunction is expanded as a linear combination of products of functions in ρ and z:

$$\psi(\rho, z) = \sum_{i=1}^{N} C_i f_i(\rho) g_i(z) \tag{7.54}$$

with N being the number of functions and C_i the real coefficients of the expansion to be determined. The functions f and g are B-splines functions:

$$f_i(\rho) = B_\alpha^{k_\rho}(\rho); g_i(z) = B_\beta^{k_z}(z) \tag{7.55}$$

The i index is expressed as:

$$i = (\alpha - 1)\tilde{\eta}_u + \beta; \alpha = 1, \tilde{\eta}_\rho; \beta = 1, \tilde{\eta}_u. \tag{7.56}$$

$$\tilde{\eta}_\rho = \eta_\rho - 1; \tilde{\eta}_u = \eta_u - 2. \tag{7.57}$$

The -1 and -2 in Eq. (7.57) come from the exclusion of the edge splines, following our boundary conditions. This happens since the first and last B-Splines are non-zero on the boundaries of the domain they span.

When the atom is placed at the center of the cylinder, the system has a $D_{\infty h}$ symmetry [38] and the confined states are defined by the quantum number m, the absolute value of the projection of angular momentum onto the z axis of the cylinder. Also, the parity of the states with respect to inversion is denoted by $\mathscr{P}$ taking values +1 and −1, corresponding to *gerade* and *ungerade* states. Taking advantage of those elements we reduce by four (selectively computing *gerade* or *ungerade* states) the size of our basis by conveniently defining our wavefunctions [52]. The f and g functions change to:

$$f_i(\rho) = B_{\alpha}^{k_\rho}(\rho); g_i(z) = B_{\beta}^{k_z}(z) + (-1)^m \mathscr{P} B_{\eta_u+1-\beta}^{k_z}(z), \tag{7.58}$$

Hence, with

$$\tilde{\eta}_\rho = \eta_\rho - 1; \tilde{\eta}_u = (\eta_u - 2)/2, \tag{7.59}$$

the variational transformation of the Schrödinger Eq. (7.51) leads to a set of $N \times N$ generalized eigenvalue equation on the energies ε and the coefficients C_i.

$$Hv = \varepsilon S v \tag{7.60}$$

where H is the Hamilltonian matrix and S the overlapping matrix. v is the vector of C_i coefficients.

Following a recently proposed fit approach [41], the Coulomb potential is expressed as a linear combination of product of functions depending on ρ and z.

$$V(\rho, z) = \frac{-Z}{\sqrt{\rho^2 + z^2}} = \sum_{j=1}^{M} D_j B_{\gamma}^{k_{f_\rho}}(\rho) B_{\zeta}^{k_{f_z}}(z) \tag{7.61}$$

where the $D's$ are the coefficients of the expansion and the B's are B-Splines functions of order k_{f_ρ} and k_{f_z} (generally low—cubic or quartic—in order to reduce the Runge phenomenon [54]).

The fit of the Coulomb potential is performed using the *regrid* subroutine of the Dierckx package [55–57] from the NETLIB repository. The routine allows a fast and adjustable calculation of the expansion coefficients and produce accurate results except at the center of the cylinder $(\rho = 0, z = 0)$ due to the Runge phenomenon. This situation is inconvenient since (at least) the ground state wavefunction and energy relies on the accuracy of the potential close to the center, as the principal structure of the wavefunction is localized in that region. However, this issue could be overcome by having more B-Splines functions located in the problematic region so as to better describe it.

The calculation of the polarizability proceeds by the sum-over-states method. As the numerical approach is very similar to the calculation of the electronic component of the hydrogen molecular ion polarizability and has been detailed elsewhere [41], we shall not repeat it here.

7.3 Computations and Results

The methods presented in the previous section are implemented in Fortran codes. In this section the energies and polarizabilities obtained for one electron systems in the three different types of confinement (prolate spheroidal, spherical and cylindrical) will be presented and discussed. We will then present successively the study of the

hydrogen molecular ion in prolate spheroidal coordinates and the hydrogen atom in spherical, prolate spheroidal and cylindrical coordinates.

7.3.1 *Electronic Energies and Polarizabilities of Spatially and Endohedrally Confined One Electron Molecular Systems*

The hydrogen molecular ion is the simplest and thus a benchmark system for the study of molecules. It has been studied with different approaches, using adiabatic as well as non adiabatic computations. However, it is only until about 10 years that the group of Cruz [26–28] and others ([29, 30] to mention few) started comprehensive work on the confinement of hydrogen molecular ion and hydrogen molecule. In this section, we will extend previous known results on the hydrogen molecular ion under spheroidal confinement. We will then consider the hydrogen molecular ion under spatial confinement but also under endohedral confinement and compute the electronic energies as well as the polarizability.

The theoretical methods developed in Sect. 7.2.3 were used to compute the electronic energies and generate the Potential Energy Curves (PECs). In Table 7.1, we compare the electronic ground state potential energy at equilibrium distance R_e, for various confinement radii $R_{\max}$, with the results of Mateos-Cortés et al. [26] for H_2^+. This table shows a good agreement with those computations and confirms the good accuracy of our computations. The last value reported in this table, i.e. −0.602634, which corresponds to the case of the free hydrogen molecular ion, agrees very well with other values found in the literature in the Born-Oppenheimer approximation [58, 59].

We also present in Figs. 7.1 and 7.2 the effect of spatial confinement on some Potential Energy Curves (PECs). Whereas Fig. 7.1a represents the five lowest Σ_g^+

Table 7.1 Comparison of the ground state energy of H_2^+ with that of Mateos-Cortés et al. [26] at equilibrium distance R_e for various confinement radii $R_{\max}$

R_e (a.u.)	$R_{\max}$ (a.u.)	Ref. [26]	This work
0.588	1.0	2.291855	2.292825
0.902	1.5	0.293301	0.293721
1.193	2.0	−0.271120	−0.270893
1.450	2.5	−0.472430	−0.472292
1.660	3.0	−0.551622	−0.551531
1.815	3.5	−0.583451	−0.583389
1.912	4.0	−0.595851	−0.595805
1.997	∞	−0.602634	−0.602634

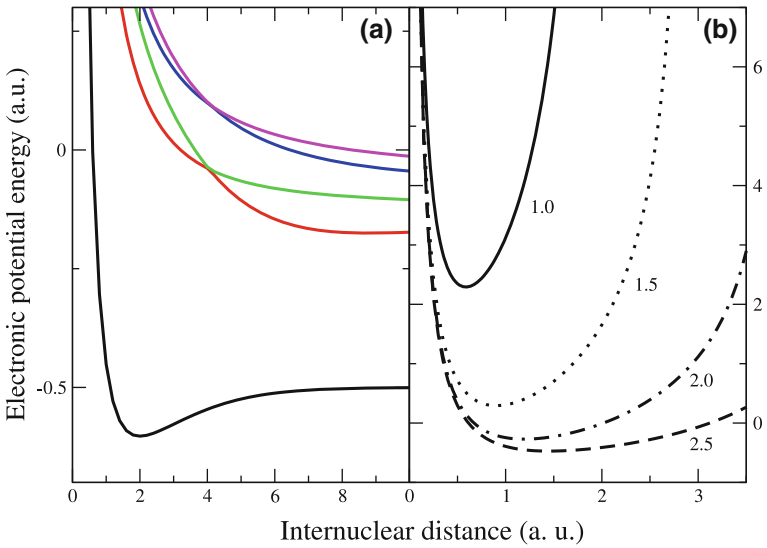

Fig. 7.1 **a** PECs of the first five Σ_g^+ states in the absence of confinement; **b** Ground state potential energy curve of the electronic ground state for various confinement radii. In case (**b**), the number near each curve is the radius $R_{\max}$ of the confining cavity

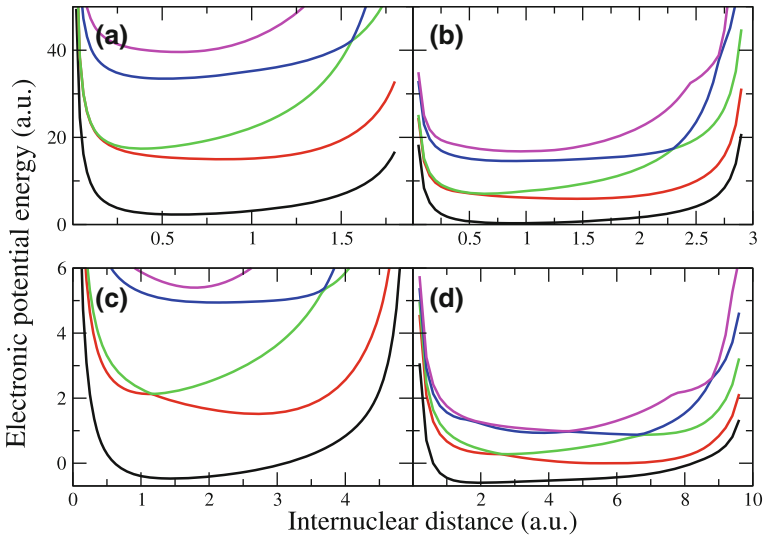

Fig. 7.2 PECs of the first five Σ_g^+ states under spatial confinement of values: **a** $R_{\max}$ = 1 u.a.; **b** $R_{\max}$ = 1.5 u.a.; **c** $R_{\max}$ = 2.5 u.a.; **d** $R_{\max}$ = 5 u.a

states of H_2^+ in the absence of confinement, Fig. 7.1b, illustrating various confinement cases of the ground state PEC, is found to reproduce well the graphs of Fig. 7.1e of the paper by Mateos-Cortés et al. [26].

The spatial confinement has a number of effects on the PECs. The first one is the bending experienced by the PECs, clearly due to the effect of the box pressure. This wall pressure leads to an increase of the energy value, as can be seen from Fig. 7.1. With decreasing R_{max}, the equilibrium distance is shifted leftward and the bending structure of the PECs is increased to such a point that they may allow to obtain vibrational states with high energy values and higher frequencies. The energy increase is in analogy to what can be observed with hydrogen atom [13] in an impenetrable cavity: that is positive energy ground state, because the electron could not escape from the potential barrier. In Fig. 7.2, we can see, in addition to the bending structure of the PECs, that spatial confinement *keeps symmetry* since the avoided crossings remain. All levels have the *potential* to possess vibrational states because of the shape exhibited by PECs. This proves that the spectroscopy of the molecule in such a confinement will exhibit a richer spectrum than free molecular hydrogen.

The study of the endohedral confinement of H_2^+ is reported in Figs. 7.3 and 7.4. To the best of our knowledge, the only report made on this system is that of Tayebirad et al. [30] which was devoted to the study of the ground state near the equilibrium position ($R = 2$ a.u.) as a function of the shell potential. We cannot make relevant comparison since we are—much more—interested in the behaviour

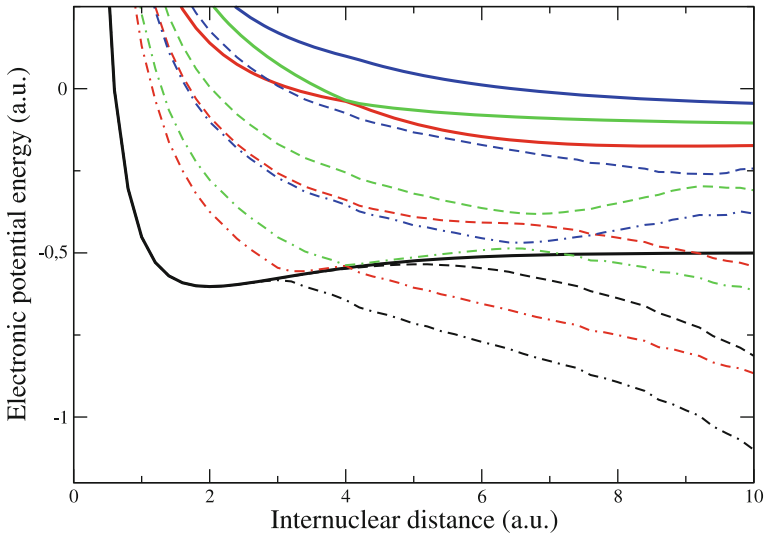

Fig. 7.3 PECs of the first four Σ_g^+ states under endohedral confinement: *full lines* U_0 = 0 u.a.; *dashed lines* $U_0 = 0.6$ u.a.; *dashed-dotted lines* $U_0 = 1.0$ u.a

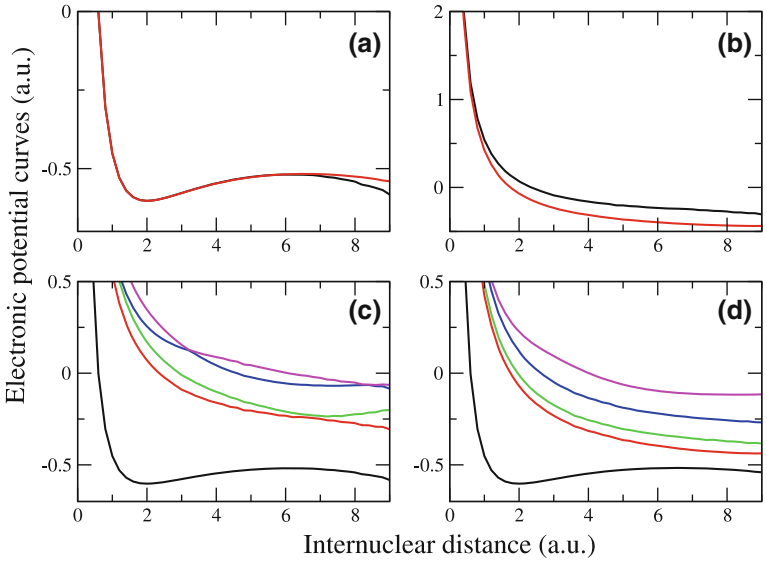

Fig. 7.4 Deformation effects on the lower electronic curves with Σ_g^+ within the endohedral confinement with $U_0 = 0.302$ a.u. **a–b**: in *black* $\delta = 0.0$ and in *red* $\delta = 0.5$, **a** ground state; **b** $2\Sigma_g^+$. **c–d**: five lowest Σ_g^+ states when $\delta = 0.0$ (**c**) and $\delta = 0.5$ (**d**)

of the PECs under the shell confinement at various U_0 and for different cage deformations. However we may discuss some features presented in that paper.

The endohedral confinement of H_2^+ molecule acts on it differently from the pure spatial confinement. Here, the ground state's curve is progressively bent downward at high values of R as U_0 increases, hence exhibiting a shoulder. The Coulomb barrier that appears is canceled with increasing U_0, and the potential is expected to be totally repulsive at high values of U_0 with a strong slope. As for the excited states, they experience avoided crossings—as a consequence of the Wigner and Von Newmann's rule [60]—at very different positions than that in the cage free case, and present various wells that may justify a rich vibrational structure above $R = 3$ a.u. With increasing value of U_0, lower states become one after the other totally repulsive. Usually, the next upper level after a state that has just become repulsive may possess vibrational states as we can see from Fig. 7.3. We may see it as the *new ground state* of the system when the potential well value U_0 increases. This is quite similar to the effect observed on the hydrogen atom [39]. We observed shell potential (well) levels dominating Coulomb levels and going below those levels. This mechanism has here the additional effect to create a displacement of the equilibrium position of the *new ground states* as the PECs structure vary with the value of U_0. These *new states* have the further advantage that we may observe vibrational states on highly *excited states* which were dissociative in the free molecule case. One further remark is the observation of avoided crossings, the shell potential has as only effect to shift them slightly. Moreover, where they appear,

seems to be the equilibrium position of the corresponding *new state*. A similarity can be made with the paper of Tayebirad et al. [30]. In Fig. 7.3, we can see that till the value $U_0 = 1.0$ a.u. the equilibrium position is not modified by the effect of the cage though, as the graph shows, the entire structure of the PEC of the ground state is modified. We thus expect, as it was pointed out in Ref. [30], that at the value $U_0 = 1.3$ a.u the structure of the state may feel the effect of the well depth (and that is indeed the results we obtain in calculations not shown here). This can be explained, considering similarities with the H-atom case [39], by the fact that we have reached at this particular value of R a level of the system consisting of an electron inside a potential well. In Fig. 7.4 we have represented the effects of the deformation on the lower electronic curves with Σ_g^+ symmetry within the endohedral confinement with $U_0 = 0.302$ a.u. The shell deformation has values $\delta = 0.0$ and 0.5. Some of the values used to represent those curves are reported in Table 7.2. The increase of the deformation is found to decrease the electronic energy values. Furthermore, the avoided crossings are found to be removed by the deformation of the cavity, which means that the deformation reduces the configuration interaction.

The situation depicted here as a *hard box confinement* is an extreme (ideal) case of confinement that is not often observed in real-life systems. More realistic potentials would be a penetrable potential as presented in [26] or even shell potential such as those used to model fullerene [7]. Those potentials globally move the equilibrium positions of the system and modify the energy values which result in an increase of the vibrational energy. This could then lead to an enhancement of the nuclear tunneling through Coulomb barrier which, added to other actions, may increase fusion rates significantly, as revealed by Segal et al. [61].

Accurate computations of the electronic ground and excited states, as we presented above, give the possibility to express the electronic but also total polarizability of the hydrogen molecular ion (that is incuding the nucleus contribution) and its symmetric isotopologues (D_2^+ and T_2^+). As a matter of fact, computations reported in previous works for H_2^+ and D_2^+, using the adiabatic and/or the clamped

Table 7.2 Electronic energies of the ground and first two gerade excited states Σ_g^+ of H_2^+ in an endohedral potential well value of $U_0 = 0.302$ a.u. with deformation δ having values ≈0.0 and 0.5

R (a.u.)	$1\sigma_g$		$2\sigma_g$		$3\sigma_g$	
	$\delta \to 0.0$	$\delta \to 0.5$	$\delta \to 0.0$	$\delta \to 0.5$	$\delta \to 0.0$	$\delta \to 0.5$
1.0	−0.4518	−0.4518	0.5411	0.4232	0.6696	0.4842
2.0	−0.6026	−0.6027	0.0698	−0.0681	0.1695	−0.0094
3.0	−0.5777	−0.5780	−0.0897	−0.2321	−0.0101	−0.1739
4.0	−0.5467	−0.5474	−0.1609	−0.3154	−0.1014	−0.2563
5.0	−0.5266	−0.5277	−0.2039	−0.3649	−0.1640	−0.3050
6.0	−0.5187	−0.5185	−0.2319	−0.3972	−0.2086	−0.3358
7.0	−0.5234	−0.5177	−0.2490	−0.4194	−0.2327	−0.3561
8.0	−0.5414	−0.5250	−0.2728	−0.4327	−0.2242	−0.3718

nucleus approach, give polarizabilities that are very close to those obtained experimentally from the non adiabatic treatment [53, 62]. Contrary, the correct description of asymmetric isotopologues like HD^+ require a full account of non adiabatic effects that enhances significantly the corresponding polarizabilities. The contribution of the nuclear motion to the total polarizability of H_2^+ has been obtained using the development presented in Sect. 7.2.3.4. The calculation of the electronic energies under various confinements leads to the PECs which are used as inputs in relations (7.47)–(7.49). Here, the electric potential is replaced by the potential energy curve and the confinement or endohedral potential is disregarded since it is already being taken into account in the calculation of the PEC.

Table 7.3 presents the electronic and total static dipole polarizabilities of H_2^+ experiencing a spatial confinement. We can see that our computations agree well with the previous studies and that the nuclear contribution to the electric dipole polarizability at equilibrium distance decreases with space confinement. It varies from 10.71 % for $R_{max} = \infty$ to 5.06 % for $R_{max} = 3.5$ and less than 0.2 % for $R_{max} = 1$. In Table 7.4, the static dipole polarizabilities of D_2^+ and T_2^+ are presented in comparison with previous works whenever available. This exhibits the effect of isotropic substitution on the electric static dipole polarisability of H_2^+.

The ground state dynamic dipole polarizability of H_2^+ at equilibrium distance R_e is represented in Figs. 7.5, 7.6 and 7.7 for the three confinement radii $R_{max} = 1$, 3 and 6 a.u. respectively. In each graph, the transversal and longitudinal components of the polarizability are plotted as well as the total polarizability. Resonant structures are observed, starting at low frequencies for the high R_{max} case, and at high frequencies for the low R_{max} cases. In fact, as we have seen, in the presence of pressure, the energy levels are shifted upward, and the energy differences between electronic states are increased, resulting in high resonance frequencies. The differences between the resonance positions resulting from the longitudinal and transversal component is a consequence of the selection rules of the transitions between electronic states.

The study of the hydrogen molecular ion could be connected to the study of the hydrogen atom inside a prolate spheroidal cavity. This is possible through the atomic limit of the model, and will be presented in Sects. 7.3.3 and 7.3.4, where the spatial and endohedral confinements are studied separately.

7.3.2 *Energies and Polarizabilities of Endohedrally Confined Centered Hydrogen Atom*

For the endohedrally confined hydrogen atom, the energy levels are combinations of the Coulomb potential energy levels and the potential well energy levels. As a matter of fact, for a particular value of U_0, the energy levels come either from the Coulomb potential problem or the potential well problem. Considering $N = 160$ B-Splines of order $k = 12$ and $R_{max} = 80$ a.u., energies and polarizabilities of a single-

Table 7.3 Comparison of the electric dipole polarizability (electronic part and total) of the ground state energy of H_2^+ at equilibrium distance R_e for various confinement radii R_{max}, with other computations

R_e (a.u.)	R_{max} (a.u.)	References	$\alpha_{e\parallel}$	$\alpha_{e\perp}$	α_e	α_g
0.588	1.0	This work	0.032674021	0.021745237	0.025388164	0.025422149
		Ref. [26]	0.031998	0.021564	0.025042	
0.902	1.5	This work	0.16151798	0.091085539	0.11456302	0.11518771
		Ref. [26]	0.158429	0.090445	0.113107	
1.193	2.0	This work	0.48756678	0.23645037	0.32015584	0.32395005
		Ref. [26]	0.4766987	0.23474	0.315397	
1.450	2.5	This work	1.0961524	0.46624140	0.67621174	0.69028822
		Ref. [26]	1.070265	0.461576	0.664472	
1.660	3.0	This work	1.9827796	0.76142154	1.1685410	1.20841228
		Ref. [26]	1.934183	0.749521	1.144408	
1.815	3.5	This work	2.9988196	1.0756733	1.7167221	1.80359646
		Ref. [26]	2.923839	1.049882	1.674534	
1.912	4.0	This work	3.8905283	1.3495811	2.1965635	2.34920126
		Ref. [26]	3.794213	1.303753	2.133907	
1.997	∞	This work	5.0776490	1.7576486	2.8643155	3.171241
		Ref. [26]	4.918180	1.644148	2.735492	
		Ref. [73]	5.0776490	1.7576486	2.8643154	
		Ref. [74]	5.07765	1.75765	2.86431	
		Ref. [75]				3.1713
		Refs. [76, 77]				3.1681
		Ref. [78]				3.178 303
		Ref. [79]				3.168 725
		Ref. [53]				3.1682

$\alpha_{e\parallel}$ and $\alpha_{e\perp}$ stand for the parallel and the longitudinal components of the electronic part of the ground state electric dipole polarizability, and α_g is the total molecular ground state dipole polarizability

shell confined H atom have been computed, as a function of the shell potential. Figure 7.8 shows the behaviour of energies of the atom in the endohedrally confined potential as a function of U_0. Starting from $U_0 = 0$ Ry when the energy levels are purely due to the Coulomb potential, the increase of the shell potential depth (U_0) induces a progressive appearance of new bound states (around U_0 = 1.5 Ry, U_0 = 5 Ry, U_0 = 13.5 Ry, etc.), hence modifying the position of the initial 1*s* level in the classification which then becomes 2*s*, 3*s*, 4*s* and so on. This shift accounts for the avoided crossings observed around the 1*s*-energy level and the permanent existence of that *s* state around −1.0 Ry justifies a stabilization zone around this

Table 7.4 Total molecular ground state dipole polarizability of D_2^+ and T_2^+

R_e (a.u.)	R_{max} (a.u.)	References	$\alpha_g(D_2^+)$	$\alpha_g(T_2^+)$
0.588	1.0	This work	0.02540922	0.02540414
0.902	1.5	This work	0.11498836	0.11490263
1.193	2.0	This work	0.32281123	0.32231329
1.450	2.5	This work	0.68607061	0.68421745
1.660	3.0	This work	1.19663937	1.19145879
1.815	3.5	This work	1.77755320	1.76614925
1.912	4.0	This work	2.30309463	2.28302384
1.997	∞	This work	3.07386246	3.03160831
		Ref. [80]	3.07198869	3.03062032
		Ref. [75]	3.0731	
		Refs. [76, 77]	3.0712	
		Ref. [79]	3.071988	

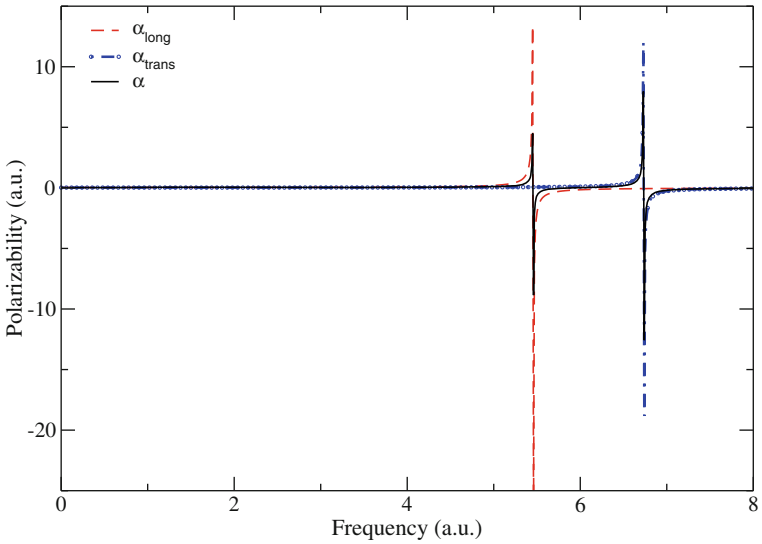

Fig. 7.5 Dynamic polarizability of the H_2^+ molecular ion at equilibrium distance R_e confined in a sphere with $R_{max} = 1$ a.u

energy value. Figure 7.9 represents the wavefunctions of 1*s*, 2*s*, 3*s*, 2*p*, 3*p* and 4*p* for different values of U_0. For the considered values of U_0 (0.0, 0.4, 1.7 and 5 Ry for *s* states and 0.0, 0.2, 1.4 and 7 Ry for *p* states), the wavefunctions are subjected to significant changes. For very low and high values of U_0, 1*s* and 2*s* on one hand, and 2*p* and 3*p* on the other hand, vary between from pure Coulomb potential

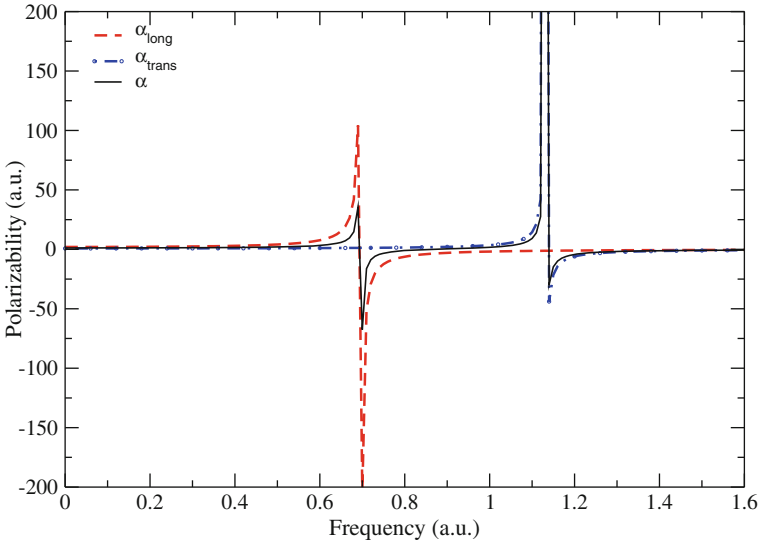

Fig. 7.6 Dynamic polarizability of the H_2^+ molecular ion at equilibrium distance R_e confined in a sphere with $R_{max} = 3$ a.u

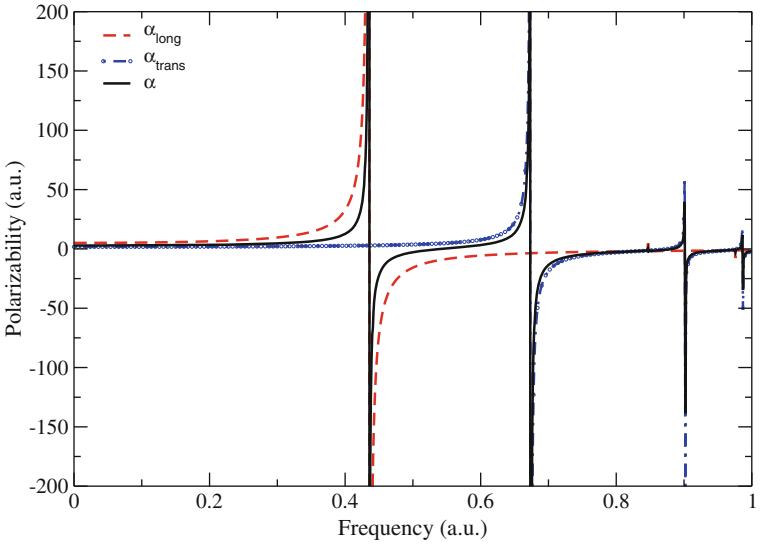

Fig. 7.7 Dynamic polarizability of the free H_2^+ molecular ion at equilibrium distance

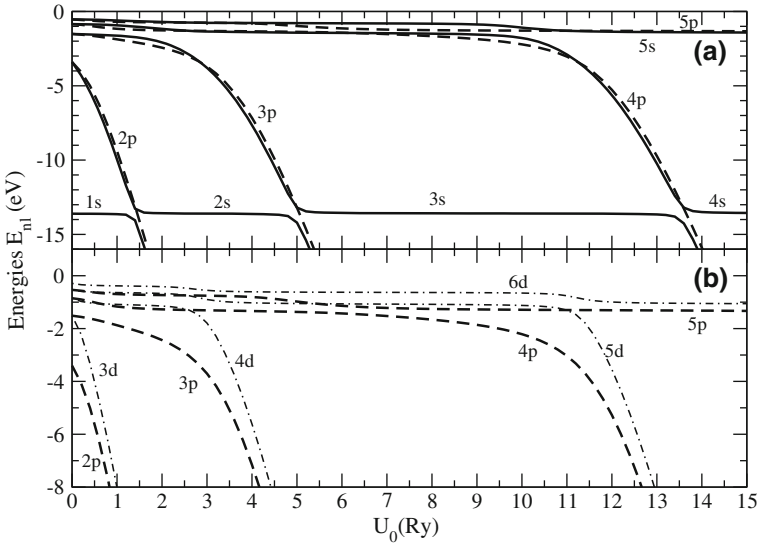

Fig. 7.8 Energies of the lowest *ns*, *np* and *nd* states versus the confining potential U_0: **a** *s* (*full lines*) and *p* (*dashed lines*) states; **b** *p* (*dashed lines*) and *d* (*dashed-dotted lines*) states (from Ref. [39]. © IOP Publishing. Reproduced with permission. All rights reserved)

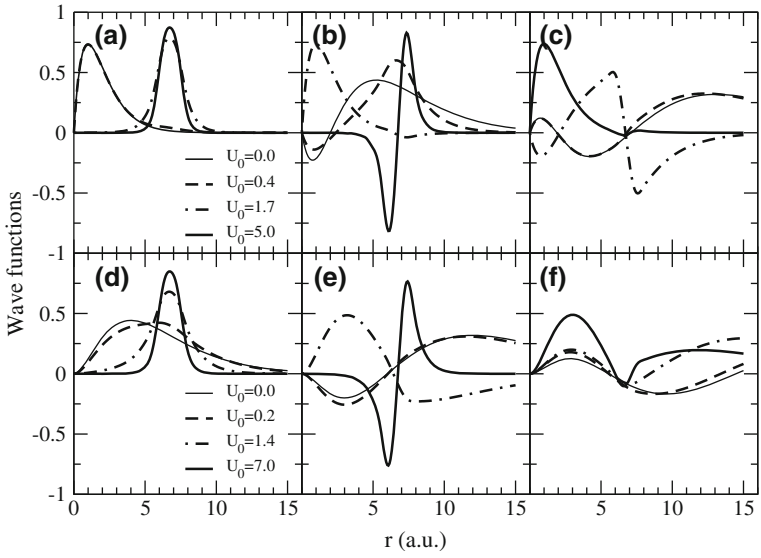

Fig. 7.9 Wavefunction change of the: **a** 1*s*, **b** 2*s*, **c** 3*s* for different values of U_0 (0, 0.4, 1.7, 5.0 Ry); **d** 2*p*, **e** 3*p*, **f** 4*p* for different values of U_0 (0.0, 0.2, 1.4, 7.0 Ry). Graphs (**b**), (**c**) and (**e**), (**f**) have same legend than (**a**) and (**d**) respectively (from Ref. [39]. © IOP Publishing. Reproduced with permission. All rights reserved)

functions and pure shell potential functions. For intermediate values of U_0 or for $3s$ and $4p$ levels, the wavefunctions are superpositions of Coulomb potential and shell potential eigenfunctions. Furthermore, the $1s$ function appears, with increasing U_0 as a $2s$ and a $3s$ wavefunction. This is a signature of the avoided crossings mentioned above, as the energy levels follow the same evolution. That is not the case for the p states for which the centrifugal potential compensates the Coulomb potential at short radial distances, such that the potential well barrier is much easily crossed than for low s states. The features observed here can be analyzed from the probability for finding the electron in the shell potential, as it is closely related to the behaviour of the wavefunction. This probability can be used more generally to describe the localization of electrons between the Coulomb and shell potential for endohedrally confined atoms, as described for $He@C_{60}$ [44].

The polarizabilities of the $1s$, $2s$ and $3s$ levels of the hydrogen atom, as well as the contributions of the $2p \rightarrow ns$ and $2p \rightarrow nd$ transitions to the polarizability of the $2p$ state, subjected to single shell confinement, are reported in Table 7.5. The first row of this table gives the well known values of the polarizabilities of these states in the free H atom. When increasing U_0, singularities occur at the values of U_0 for which the state that dominates the contributions to the polarizabilities (see Eq. 7.16) is close to the initial state, and negative values occur when this state lies lower in energy than the initial state.

The effects of additional shell confinement (buckyonions) have also been investigated. Considering a one-shell $\left(U_0^{(1)} \neq 0.0,\ U_0^{(2)} = 0.0,\ U_0^{(3)} = 0.0\right)$, two-shell $(U_0^{(1)} \neq 0.0, U_0^{(2)} = 0.367, U_0^{(3)} = 0.0)$ and three-shell $\left(U_0^{(1)} \neq 0.0, U_0^{(2)} = 0.367, U_0^{(3)} = 0.441\right)$ fullerene, the static polarizabilities have been calculated as a function of the confining potential of the first shell $U_0^{(1)}$, for various initial states. A representative case is shown on Fig. 7.10 for the $3p \rightarrow nd$ transition. It has been clearly found that except for the 1s case, the addition of the second shell increases the static polarizability significantly and that the addition of the third shell increases it much more. More generally, the multiwall endohedral confinement may lead to very large values of the static polarizability of the encapsulated atom. It can be also observed that the significant enhance due to the second- and third-shells vanishes when $U_0^{(1)}$ exceeds a critical value. This increase is due to the proximity of the initial state with the dominant contributing state.

The dynamic polarizabilities have been computed for $H@C_{60}$, $H@C_{60}@C_{240}$, and $H@C_{60}@C_{240}@C_{540}$ corresponding to a single-walled, two-walled, and a three-walled fullerene cage. Sample results obtained are reported in Figs. 7.11 and 7.12, respectively, for $2p \rightarrow ns$ and $2p \rightarrow nd$ transitions. The polarizabilities present a rich singularities structure, the positions of which correspond to transition frequencies between the initial state and all the relevant accessible states. Many more poles appear in some cases than others, especially, when there are several states close to the initial state. This is a consequence of the removal of the degeneracy in the energy spectrum when there are several potential shells.

Table 7.5 Static dipole polarizabilities of the endohedrally confined hydrogen atom in the first three *ns* states and the 2*p* state, as a function the shell confining potential U_0

U_0 (a.u.)	1*s*	2*s*	3*s*	$2p \rightarrow ns$	$2p \rightarrow nd$
0	4.500	120.000	1,012.498	8.000	208.000
0.1	4.595	2,636.408	−95,543.641	−2,568.169	276.005
0.2	4.749	1,715.888	−29,038.680	−1,680.189	347.036
0.3	5.034	1,478.299	−10,292.068	−1,460.100	406.040
0.4	5.678	1,405.290	−2,751.142	−1,396.314	447.728
0.5	7.731	1,396.158	498.472	−1,393.505	475.097
0.6	21.527	1,435.350	1,647.143	−1,448.713	492.848
0.7	521.961	1,964.075	1,638.302	−2,479.098	504.586
0.8	1,165.974	−6.841	1,024.757	−1,152.912	512.604
0.9	1,249.389	3.265	211.806	−1,246.876	518.279
1	1,279.378	4.069	−548.688	−1,277.951	522.437
1.2	1,306.122	4.323	−2,065.306	−1,305.248	528.022
1.4	1,319.417	4.447	−211.225	−1,318.768	531.544
1.6	1,327.669	4.623	3,240.817	−1,327.151	533.944
1.8	1,333.356	4.957	1,854.034	−1,332.924	535.679
2	1,337.531	5.791	1,539.245	−1,337.159	536.989
2.2	1,340.732	9.220	1,472.435	−1,340.404	538.014
2.4	1,343.268	64.744	1,605.082	−1,342.974	538.837
2.6	1,345.329	1,024.975	−31.688	−1,345.062	539.514
2.8	1,347.039	1,208.999	2.943	−1,346.794	540.081
3	1,348.483	1,254.207	3.841	−1,348.255	540.564
3.2	1,349.720	1,275.782	3.961	−1,349.507	540.980
3.4	1,350.793	1,289.034	4.000	−1,350.593	541.342
3.6	1,351.734	1,298.226	4.024	−1,351.544	541.662
3.8	1,352.567	1,305.056	4.045	−1,352.387	541.947
4	1,353.311	1,310.363	4.066	−1,353.138	542.202
4.2	1,353.980	1,314.619	4.088	−1,353.815	542.432
4.4	1,354.586	1,318.116	4.112	−1,354.427	542.641
4.6	1,355.138	1,321.044	4.139	−1,354.984	542.833
4.8	1,355.643	1,323.536	4.171	−1,355.495	543.008
5	1,356.108	1,325.686	4.210	−1,355.964	543.171
5.5	1,357.127	1,329.971	4.377	−1,356.993	543.528
6	1,357.985	1,333.193	4.903	−1,357.859	543.830
6.5	1,358.722	1,335.725	11.228	−1,358.602	544.091

(continued)

Table 7.5 (continued)

U_0 (a.u.)	1*s*	2*s*	3*s*	$2p \rightarrow ns$	$2p \rightarrow nd$
7	1,359.365	1,337.784	1,136.654	−1,359.251	544.320
7.5	1,359.934	1,339.505	1,270.063	−1,359.825	544.523
8	1,360.443	1,340.975	1,299.589	−1,360.338	544.706
8.5	1,360.904	1,342.254	1,314.346	−1,360.802	544.872
9	1,361.323	1,343.384	1,323.595	−1,361.225	545.024
9.5	1,361.708	1,344.395	1,330.103	−1,361.612	545.164
10	1,362.063	1,345.308	1,335.041	−1,361.970	545.293

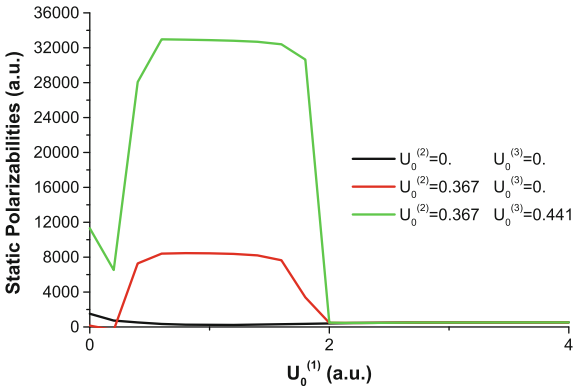

Fig. 7.10 $3p \rightarrow nd$ static polarizability as a function of the confining potential. $U_0^{(1)}$, $U_0^{(2)}$ and $U_0^{(3)}$ have values shown in the graph. (from Ref. [40]. Copyright © 2010 Wiley Periodicals, Inc. Reproduced with permission. All rights reserved)

7.3.3 *Energies of Spatially Confined Centered Hydrogen Atom*

We have computed energy values of centered H atom within a prolate spheroidal spatial confinement, reported in Table 7.6 on one hand, and within a prolate spheroidal endohedral confinement, reported in Table 7.7 on the other hand. In Table 7.6, A and B represent respectively the semi-minor and semi-major axis values in an elliptical case. They are used to deduce the confinement radius value in the spherical situation according to the formula $R_c = \sqrt{[3]A^2B}$. Our approach uses a prolate spheroidal two-center study, putting half charge on each center and letting the intercenter distance turn to zero. Imposing $R \rightarrow 0$ and a semi-minor or semi-major axis value leads to a quasi-spherical system (and not a perfectly spherical one). Hence, comparison with results of Neek-Amal et al. [34] could not be

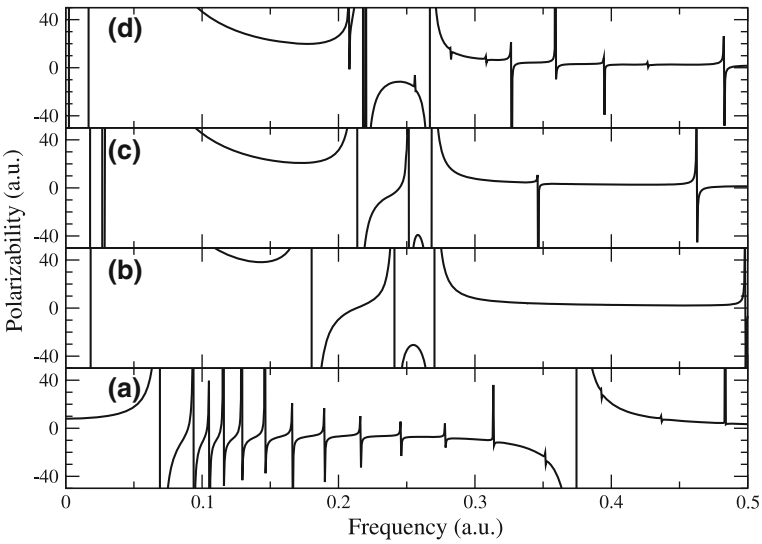

Fig. 7.11 $2p \rightarrow ns$ dynamic polarizability as a function of the confining potential. **a** $U_0^{(1)} = 0.0, U_0^{(2)} = 0.0, U_0^{(3)} = 0.0$. **b** $U_0^{(1)} = 0.302, U_0^{(2)} = 0.0, U_0^{(3)} = 0.0$. **c** $U_0^{(1)} = 0.302$, $U_0^{(2)} = 0.367, U_0^{(3)} = 0.0$. **d** $U_0^{(1)} = 0.302, U_0^{(2)} = 0.367, U_0^{(3)} = 0.441$. (from Ref. [40]. Copyright © 2010 Wiley Periodicals, Inc. Reproduced with permission. All rights reserved)

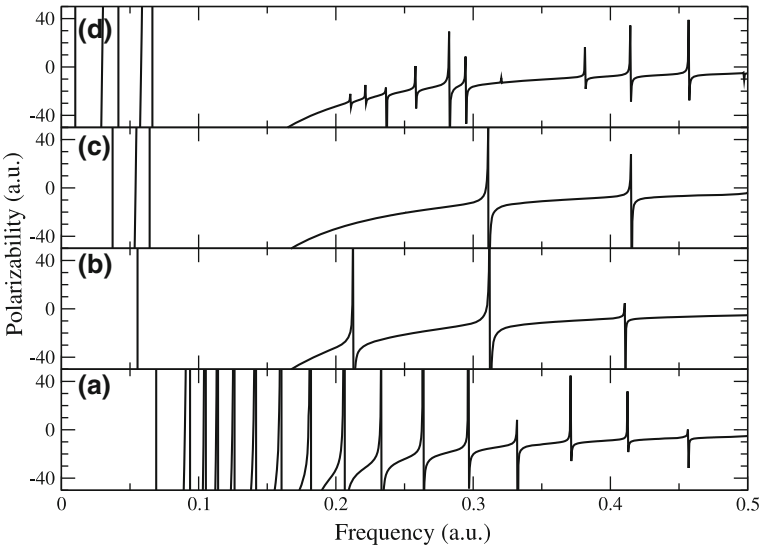

Fig. 7.12 $2p \rightarrow nd$ dynamic polarizability as a function of the confining potential. **a** $U_0^{(1)} = 0.0, U_0^{(2)} = 0.0, U_0^{(3)} = 0.0$. **b** $U_0^{(1)} = 0.302, U_0^{(2)} = 0.0, U_0^{(3)} = 0.0$. **c** $U_0^{(1)} = 0.302$, $U_0^{(2)} = 0.367, U_0^{(3)} = 0.0$. **d** $U_0^{(1)} = 0.302, U_0^{(2)} = 0.367, U_0^{(3)} = 0.441$. (from Ref. [40]. Copyright © 2010 Wiley Periodicals, Inc. Reproduced with permission. All rights reserved)

Table 7.6 Comparison of the ground state energy (in atomic units) of centered spherically confined H atom with a prolate spheroidally confined H atom from Neek-Amal et al. [34]

A	B	R_c	Ref. [34]	Sphere	Spheroid
1.0	1.1	1.0323	1.8321	2.1458	2.1485
2.0	2.2	2.0646	−0.1843	−0.1640	−0.1634
3.0	3.3	3.0968	−0.4343	−0.4344	−0.4341
4.0	4.4	4.1291	−0.4823	−0.4862	−0.4861
5.0	5.5	5.1614	−0.4937	−0.4972	−0.4971
1.0	1.5	1.1447	1.4607	1.5111	1.5132
2.0	3.0	2.2894	−0.2578	−0.2685	−0.2680
3.0	4.5	3.4341	−0.4522	−0.4606	−0.4604
4.0	6.0	4.5789	−0.4946	−0.4931	−0.4930
5.0	7.5	5.7236	−0.5008	−0.4989	−0.4988

Sphere and spheroid stand respectively for the spherical and spheroidal representation. A and B are semi-minor and semi-major axis for the prolate spheroidally confined case and R_c is *corresponding* spherical confinement radius

Table 7.7 Comparison of the 15 lowest H energy states with those of Connerade et al. [35] in the prolate spheroidal centered case. Energies are in eV

nl	Connerade et al. [35]		This work	
	Confined H	Free H	Confined H	Free H
1s	−13.6160	−13.6057	−13.6158	−13.6057
2s	−6.78244	−3.40143	−6.77138	−3.40133
2p	−6.28502	−3.40143	−6.27453	−3.40133
3d	−4.73846	−1.51174	−4.72910	−1.51165
4f	−2.83312	−0.85036	−2.82788	−0.85026
3p	−1.68030	−1.51174	−1.68088	−1.51165
3s	−1.57282	−1.51174	−1.57262	−1.51165
4d	−1.05907	−0.85036	−1.05858	−0.85026
4p	−1.04016	−0.85036	−1.04045	−0.85026
4s	−0.88192	−0.85036	−0.88186	−0.85026
5f	−0.76559	−0.54423	−0.76519	−0.54413
5g	−0.72233	−0.54423	−0.72132	−0.54413
5p	−0.65131	−0.54423	−0.65126	−0.54413
5d	−0.62804	−0.54423	−0.62756	−0.54413
5s	−0.56613	−0.54423	−0.56607	−0.54413

coherent as they used a perfect sphere for their computations. Still we compared those results with the ones that would have been obtained for equivalent values of the volume when a deformation of spatial confinement is taken into account. They are reported in Table 7.6. We can see that they are globally in good agreement with those of Neek-Amal et al. [34]. This shows that the action of a spatial spheroidal confinement on the Hydrogen atom is nearly comparable to that of to the spherical one when the confinement pressure is not too great. Comparisons made with similar results from Connerade et al. [35] show also a good agreement.

7.3.4 Energies of Spatially and Endohedrally Confined Off-centered Hydrogen Atom

Table 7.8 reports the effects of spatial confinement in an off-centered case on the H atom with comparison made with papers from Ting-Yun et al. [33] and Neek-Amal et al. [34]. In this table, the *deformation ratio* represents the ratio between the semi-

Table 7.8 Comparison of the ground state energy (in atomic units) with those of Ting-Yun et al. [33] and Neek-Amal et al. [34] in the off center case for various confinement radii R_{max} and displacement distances D

R_{max} (a.u.)	D (a.u.)	Deformation ratio	Ref. [33]	Ref. [34]	This work
2	0.1	1.00125	−0.12285	–	−0.12158
	0.5	1.03226	−0.06888	–	−0.03778
	1.0	1.14354	0.12760	–	0.32165
3	0.1	1.00055	−0.42358	–	−0.42337
	0.3	1.00504	–	−0.39980	−0.41881
	0.5	1.01406	−0.41388	–	−0.41029
	0.6	1.02062	–	−0.38560	−0.40348
	0.9	1.04829	–	−0.38430	−0.37387
	1.0	1.05887	−0.37835	–	−0.36009
	1.2	1.09108	–	−0.37130	−0.32231
	1.5	1.15470	–	−0.29650	−0.23414
4	0.1	1.00031	−0.48317	–	−0.48311
	0.5	1.00787	−0.48105	–	−0.48045
	1.0	1.03226	−0.47337	–	−0.47057
5	0.5	1.00504	–	−0.48810	−0.49569
	1.0	1.02062	–	−0.49470	−0.49360
	1.5	1.04829	–	−0.48640	−0.48883
	2.0	1.09108	–	−0.49080	−0.47865
	2.5	1.15470	–	−0.47160	−0.45682

major axis and the semi-minor axis, which are determined by the spheroidal cavity. We can see that our results are closed to those of the above mentioned authors results [33, 34] when this ratio is close to one as expected (our case corresponds to an ellipsoidal cavity and in such situations values may have been taken as reference).

Calculations made gave as value for the ground state energy under endohedral confinement with parameters $U_0 = -0.4$ a.u. and $D = 0.25$ a.u. (the displacement from the center), the value −0.50069 a.u., consistent with the value of Connerade et al. [35] of −0.5004 a.u. in a centered case with $U_0 = -0.302$ a.u. but rather inconsistent with the value of −0.5072 a.u. given by Neek-Amal et al. [63] in the same conditions. This is also the case when we look at the value of the energy when $U_0 = 0.0$ a.u. and $D = 0.25$ a.u. for instance we obtain −0.5000 a.u. when Neek-Amal et al. [63] obtain −0.5010 a.u. This has a sense since when $U_0 = 0.0$ there is indeed no interaction potential between the shell and the Hydrogen atom and energy is supposed to be the free H-atom ground state energy. Though the approach presented here is able to achieve a complete study of prolate spheroidal off-centered H-atom ground and excited states with and without deformation, we rather skipped it as it was not the major scope of our work, and it requires much more computational effort than that needed for the H_2^+ molecule.

7.3.5 Dynamic Polarizabilities of Spatially Confined Centered and Off-centered Hydrogen Atom

In Tables 7.9 and 7.10, we report dynamic polarizabilities of the 1*s* state of free and confined Hydrogen, using three different representations: the spherical representation and the two atomic limits (symmetric and asymmetric) of the spheroidal representation. The polarizability of the H atom has been widely studied using a variety of methods and approximations [11–13, 15, 36, 64–72]. The comparison has been done only between our results and those of Cohen et al. [64] and Montgomery [36] which almost agree with former investigations. The agreement we obtain is excellent. In particular, the two spherical limits (symmetric and asymmetric) of the spheroidal description lead to the same polarizabilities. This code can be used to calculate the polarizabilities of ground and excited states of off-centered atom as well its isoelectronic atomic systems, in a variety of confinement situations, with a good accuracy.

7.3.6 Energies and Polarizabilities of Cylindrically Confined Hydrogen Atom

The B-Splines based variational method using the sum of products for the representation of the Coulomb potential has been recently used to compute the polarizability of the hydrogen atom in a cylindrical potential [41]. The energies obtained

Table 7.9 Dynamic polarizabilities $\alpha(\omega)$ for the 1s state of the free H atom

ω $(a.u.)$	S.R. (Ref. [40])	Ref. [64]	Ref. [36]	S.S.R.	S.A.R.
0.00	4.5000000	4.5000000	4.50000	4.5000000	4.5000000
0.05	4.5675530	4.5675530	4.56755	4.5675530	4.5675530
0.10	4.7843004	4.7843003	4.78430	4.7843003	4.7843003
0.15	5.2009678	5.2009678	5.20097	5.2009678	5.2009678
0.20	5.9416749	5.9416749	5.94167	5.9416747	5.9416747
0.25	7.3351730	7.3351730	7.33517	7.3351731	7.3351731
0.30	10.563890	7.3351730	10.56389	10.563890	10.563889
0.35	25.935844	25.935849	25.93585	25.935850	25.935848
0.40	−16.822640	−16.822645		−16.822645	−16.822645
0.45	−17.646880	−17.646935		−17.646935	−17.646935
0.50	1.9150256			1.9150272	1.9150272

In the two last columns we have the dynamic polarizabilities computed from the code on H_2^+ in some limits cases. B-splines parameters are $n_\xi = 61, k_\xi = 7, n_\eta = 18, k_\eta = 6$. *S.R.* stands for Spherical Representation, *S.S.R.* for Spheroidal Symmetric Representation and *S.A.R.* for Spheroidal Asymmetric Representation

Table 7.10 Same as Fig. 7.10 for the 1 s state of spatially-confined H ($R_{\max} = 6$ u.a.)

ω $(a.u.)$	S.R. (Ref. [40])	Ref. [64]	Ref. [36]	S.S.R.	S.A.R.
0.00	4.0581405	4.0581402	4.05814	4.0581405	4.0581405
0.05	4.1080867	4.1080867	4.10809	4.1080867	4.1080867
0.10	4.2658656	4.2658655	4.26587	4.2658656	4.2658656
0.15	4.5587057	4.5587056	4.55871	4.5587057	4.5587057
0.20	5.0463858	5.0463857	5.04639	5.0463858	5.0463858
0.25	5.8585577	5.8585574	5.85856	5.8585577	5.8585577
0.30	7.3124756	7.3124749	7.31248	7.3124752	7.3124752
0.35	10.409677	10.409677	10.40968	10.409677	10.409677
0.40	20.743222	20.743216		20.743220	20.743220
0.45	−134.30635	−134.30689		−134.30674	−134.30674
0.50	−13.910520	−13.910522		−13.910520	−13.910520

are very accurate as compared to previous computations [37, 38]. Obviously, at large cylinder dimensions, the free H atom values are recovered. The ground state polarizabilities for the perfect cylinder ($L = 2R$) and the infinitely long cylinder ($L \geq 10R$) are presented in Fig. 7.13 for different cylinder radii.

The static dipole polarizability for the Hydrogen atom confined in a perfect cylinder reduces with the confinement radius, less however, than in a sphere with the same confinement radius. Similar in symmetry to the hydrogen molecular ion,

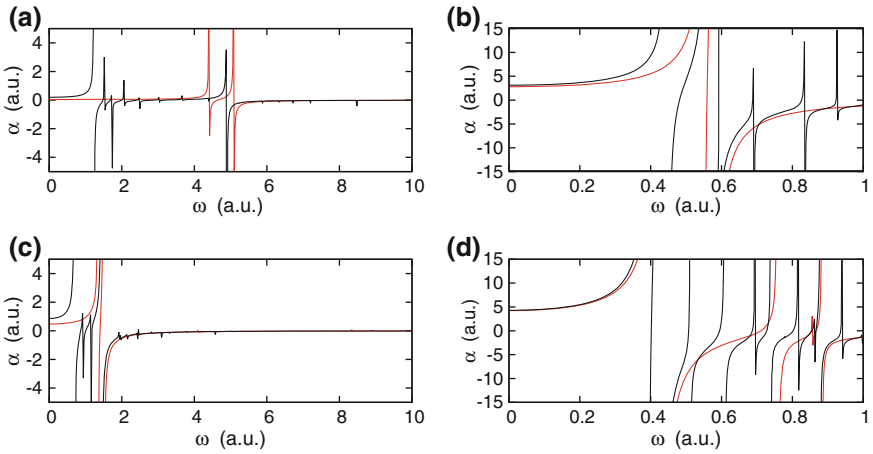

Fig. 7.13 Ground state dynamic dipole polarizability of perfect (*red*) and infinitely long (*black*) cylinder for $\rho_{max} = 1$ (**a**), 2 (**c**), 4 (**b**) and 6 a.u. (**d**)

the cylindrically confined hydrogen atom has selection rules and the dipole polarizability is split in two components: a parallel and an orthogonal component. The singularities on Fig. 7.13 identify either $\Delta m = 0$ or $\Delta m = +1$. The Figure also presents comparison of the perfect to infinitely long confinement of the atom. We see that the infinitely long cylinder presents many more structures than the perfect cylinder as one would have expected.

7.4 Conclusion

Coupled to the variational procedure, the finite basis methods offer a powerful tool for the study of confined quantum systems, for which the boundary conditions do not allow obvious analytical solutions. These methods lead to eigenenergies, eigenfunctions and other properties quite systematically. Many features depending on the shell potential depth like the avoided crossings pointed out by Connerade [8] and their impact on the polarizability can be explained easily. Based on finite basis expanded solutions, the prolate spheroidal approach is a suitable and efficient way to determine energies and polarizabilities of spatially and endohedrally confined H-atom and H_2^+ molecule. The present works describe and explain numerous structures observed on the PECs of H_2^+ subjected to spatial and endohedral confinements such as the removal of avoided crossings with increasing shell deformation or the modification of equilibrium position and vibrational energy.

Several aspects developed in this contribution may be an interesting object of investigation on bigger systems, that is, many electrons systems, in which electron

correlation may play a significant role on the effects of confinement. Our future works will be devoted to such systems trapped in various type of confinements (endohedral and others).

Acknowledgment The authors are grateful to R. L. Melono Melingui for fruitful discussions.

References

1. Michels A, de Boer J, Bijl A (1937) Physica 4:981–994
2. Dolmatov VK, Baltenkov AS, Connerade JP, Manson ST (2004) Radiat Phys Chem 70:417–433
3. Jaskólski W (1996) Phys Rep 271:1–66
4. Connerade JP, Kengkan P (2003) In: Proceedings of idea-finding symposium Frankfurt Institute for advanced studies, pp 35–46
5. Sabin JR, Brãndas E, Cruz SA (eds) (2009) Theory of confined quantum systems: part one, advances in quantum chemistry. Academic Press, New York, vol 57, 334 pp
6. Sabin JR, Brãndas E, Cruz SA (eds) (2009) Theory of confined quantum systems: part two, advances in quantum chemistry. Academic Press, New York, vol 58, 297 pp
7. Xu YB, Tan MQ, Becker U (1996) Phys Rev Lett 76:3538–3541
8. Connerade JP, Dolmatov VK, Lakshmi PA, Manson ST (1999) J Phys B: At Mol Phys 32: L239–L246
9. Kilcoyne ALD, Aguilar A, Müller A, Schippers S, Cisneros C, Alna'Washi G, Aryal NB, Baral KK, Esteves DA, Thomas CM, Phaneuf RA (2010) Phys Rev Lett 105:213001
10. Dutt R, Mukherjee A, Varshni Y (2001) Phys Lett A 280:318–324
11. Patil SH (2002) J Phys B: At Mol Phys 35:255–266
12. Laughlin C, Burrows BL, Cohen M (2002) J Phys B: At Mol Phys 35:701–716
13. Laughlin C (2004) J Phys B: At Mol Phys 37:4085–4100
14. Goldman S, Joslin C (1992) J Phys Chem 96:6021–6027
15. De Groot SR, Ten Seldam CA (1946) Physica 12:669–682
16. Connerade JP, Dolmatov VK, Manson ST (1999) J Phys B: At Mol Phys 32:L395–L404
17. Connerade JP, Dolmatov VK, Lakshmi PA (2000) J Phys B: At Mol Phys 33:251–264
18. Connerade JP, Dolmatov VK, Manson ST (2000) J Phys B: At Mol Phys 33:2279–2285
19. Dolmatov VK, Manson ST (2000) J Phys B: At Mol Phys 33:165001
20. Amusia MY, Baltenkov AS, Dolmatov VK, Msezane AZ, Manson ST (2004) Phys Rev A 70:023201
21. Eisenhart LP (1948) Phys Rev 74:87–89
22. Komatsu K, Murata M, Murata Y (2005) Science 307:238–240
23. Cioslowski J (1991) J Am Chem Soc 113:4139–4141
24. Ren YX, Ng TY, Liew KM (2006) Carbon 44:397–406
25. Ma Y, Xia Y, Zhao M, Ying M (2002) Chem Phys Lett 357:97–102
26. Mateos-Cortés S, Ley-Koo E, Cruz SA (2002) Int J Quantum Chem 86:376–389
27. Cruz SA, Colin-Rodriguez R (2009) Int J Quantum Chem 109:3041–3054
28. Colin-Rodriguez R, Diaz-Garcia C, Cruz SA (2011) J Phys B: At Mol Phys 44:241001
29. Pang T (1994) Phys Rev A 49:1709–1713
30. Tayebirad G, Molayem M, Neek-Amal M (2008) J Comp Theo Nanosci 5:366–374
31. Nikitin A, Li X, Zhang Z, Ogasawara H, Dai H, Nilsson A (2008) Nano Lett 8:162–167
32. Liu C, Fan YY, Liu M, Cong HT, Cheng HM, Dresselhaus MS (1999) Science 5442:1127–1129
33. Ting-Yun S, Hao-Xue Q, Bai-Wen L (2000) J Phys B: At Mol Phys 33:L349–L356
34. Neek-Amal M, Tayebirad G, Molayem M, Foulaadvand ME, Esmaeili-Sereshki L, Namiranian A (2008) Sol State Com 145:594–599

35. Connerade JP, Lyalin AG, Semaoune R, Semenov SK, Solov'yov AV (2001) J Phys B: At Mol Phys 34:2505–2511
36. Montgomery HE (2002) Chem Phys Lett A 352:529–532
37. Yurenev PV, Scherbinin AV, Pupyshev VI (2006) Int J Quantum Chem 106:2201–2207
38. Yurenev PV, Scherbinin AV, Pupyshev VI (2008) Int J Quantum Chem 108:2666–2677
39. Ndengué SA, Motapon O (2008) J Phys B: At Mol Phys 41:045001–045008
40. Motapon O, Ndengué SA, Sen KD (2011) Int J Quant Chem 111:4425–4432
41. Ndengué SA, Motapon O, Melingui Melono RL, Etindele AJ (2014) J Phys B: At Mol Phys 47(1):015002
42. de Boor C (1978) A practical guide to splines. Springer, New York, 345 pp
43. Hao-Xue Q, Ting-Yun S, Bai-Wen L (2002) Comm Theor Phys 37:221–224
44. Ndengué SA, Motapon O (2009) Eur Phys Jour D 55:43–51
45. Johnson WR, Blundell SA, Sapirstein J (1988) Phys Rev A 37:307–315
46. Sapirstein J, Johnson WR (1996) J Phys B: At Mol Phys 29:5213–5225
47. Martín F (1999) J Phys B: At Mol Phys 32:R197–R231
48. Qiu Y, Froese Fischer C (1999) J Comp Phys 156:257–271
49. Bachau H, Cormier E, Decleva P, Hansen JE, Martin F (2001) Rep Prog Phys 64:1815–1943
50. Fletcher WA (1984) Computational Galerkin methods. Springer, New York, p 309
51. Dolmatov VK, Brewer P, Manson ST (2008) Phys Rev A 78:013415–013415.6
52. Vanne YV, Saenz A (2004) J Phys B: At Mol Phys 37:4101–4118
53. Shertzer J, Greene CH (1998) Phys Rev A 58:1082–1086
54. Runge C (1901) Zeitschrift für Mathematik und Physik 46:224–243
55. Dierckx P (1980) A fast algorithm for smoothing data on a rectangular grid while using spline functions. Report TW53, Department of Computer Science, K.U
56. Dierckx P (1982) Siam J Num Anal 19:1286–1304
57. Dierckx P (1993) Curve and surface fitting with splines, monographs on numerical analysis. Oxford University Press, Oxford
58. Laaksonen L, Pyykkö P, Sundholm D (1983) Int J Quantum Chem 23:309–317
59. Madsen MM, Peek JM (1971) At Data 2:171–204
60. Von Neuman J, Wigner EP (1927) Z Phys 30:465–467
61. Segal D, Seideman T, Kurizki G, Shapiro M (2006) Chem Phys Lett 420:241–244
62. Moss RE, Valenzano L (2002) Mol Phys 100:1527–1535
63. Neek-Amal M, Tayebirad G, Asgari R (2007) J Phys B: At Mol Phys 40:1509–1521
64. Cohen M, Themelis SI, Sen KD (2008) Int J Quant Chem 108:351–361
65. Aquino NA (1999) Int J Quantum Chem 54:107–115
66. Buckingham R (1937) Proc Roy Soc A 160:94–113
67. Guimarães MN, Prudente FV (2005) J Phys B: At Mol Phys 38:2811–2825
68. Kirkwood JG (1932) Phys Z 33:57–60
69. Ley-Koo E, Rubinstein S (1979) J Chem Phys 71:351–357
70. Saha B, Mukherjee PK, Diercksen GHF (2002) Astron Astrophys 396:337–344
71. Sen KD, Garza J, Vargas T, Aquino NA (2002) Phys Lett A 295:299–304
72. Unsöld A (1927) Z Phys 43:563
73. Tsogbayar Ts (2009) J Phys B: At Mol Opt Phys 42:165007
74. Bishop DM, Cheung LM (1978) J Phys B: At Mol Phys 11:3133–3144
75. Bishop DM, Lam B (1988) Mol Phys 65:679–688
76. Jacobson PL, Fischer DS, Fehrenback CW, Sturrus WG, Lundeen SR (1998) Phys Rev A 56:R4361–R4364 (1997)
77. Jacobson L, Fischer DS, Fehrenback CW, Sturrus WG, Lundeen SR (1998) Phys Rev A 57:4065–4065
78. Moss RE (2000) Phys Rev A 61:040501(R)
79. Taylor JM, Dalgarno A, Babb JF (1999) Phys Rev A 60:R2630–R2632
80. Yan ZC, Zhang JY, Li Y (2003) Phys Rev A 67:062504

Chapter 8
Density Functional Theory Applied on Confined Many-Electron Atoms

Jorge Garza and Rubicelia Vargas

8.1 Density Functional Theory and Confinement Imposed by Rigid Walls

The density functional theory (DFT) has been applied on atoms, molecules, solids and surfaces, where the electrons are under the influence of external potentials that impose boundary conditions on the electron density [1–3]. For atoms, spatial restrictions have been considered to modeling spatial confinements, which give additional contributions to the external potential [4–7]. In particular, one restriction used for the study of confined atoms is represented by a spherical potential, $\upsilon_R(\mathbf{r})$, which is defined as

$$\upsilon_R(\mathbf{r}) = \begin{cases} 0 & for \quad r < R_c \\ h & for \quad r \geq R_c \end{cases} \tag{8.1}$$

where h is a constant. If $h = 0$ we have a non-confined atom but if $h \neq 0$ we have an atom spatially confined. In particular, in this report we discuss the confined imposed by $h = \infty$, such that the atom is confined by rigid walls. Naturally, we must take care of the conditions imposed on the electron density at the boundary R_c. In 2009, Advances in Quantum Chemistry devoted two volumes, 57 and 58, to confined systems, the reader is encouraged to read carefully these volumes.

By its nature, the DFT has several ways to estimate the total energy of an electronic system. The starting point of this theory is given by the first theorem of Hohenberg and Kohn [8] where the total energy is written as

J. Garza (✉) · R. Vargas
Departamento de Química, Universidad Autónoma Metropolitana-Iztapalapa,
San Rafael Atlixco 186, Col. Vicentina, CP 09340 México, D.F., México
e-mail: jgo@xanum.uam.mx

K.D. Sen (ed.), *Electronic Structure of Quantum Confined Atoms and Molecules*,
DOI 10.1007/978-3-319-09982-8_8

$$E[\rho] = F[\rho] + \int d\mathbf{r}\rho(\mathbf{r})\upsilon(\mathbf{r}). \tag{8.2}$$

In this equation $F[\rho]$ is the universal functional which contains the kinetic energy, T, the electron-electron interaction, V_{ee}, and the last term in Eq. 8.2 represents the nuclear-electron interaction. Precisely, in the universal functional is where many approximations are involved since this quantity is unknown.

In this report, we discuss two forms of the universal functional that have been discussed in different contexts and that have been applied on confined atoms. In particular we treat the Thomas-Fermi model, [9, 10] which was used even before of the Hohenberg and Kohn theorems were reported. Additionally, we also deal with the Kohn-Sham model, [11] which is the most popular version of the DFT, and that it has been applied successfully on confined many-electron atoms.

8.2 Thomas-Fermi Model Applied on Confined Atoms

One simple model to the kinetic energy and the electron-electron interaction is represented by the proposal made independently by Thomas [10] and Fermi [9] where, in the context of the universal functional,

$$F[\rho] = C_F \int d\mathbf{r}\rho^{5/3}(\mathbf{r}) + \frac{1}{2}\iint d\mathbf{r}d\mathbf{r}' \frac{\rho(\mathbf{r})\rho(\mathbf{r}')}{|\mathbf{r}-\mathbf{r}'|}. \tag{8.3}$$

The first term in Eq. 8.3 represents the kinetic energy, with $C_F = \frac{3}{10}\left(3\pi^2\right)^{2/3}$, and the second one the electron-electron interaction, estimated as the Coulomb contribution of a charge distribution named many times as $J[\rho]$. The minimum of the energy is reached when the method of Lagrange multipliers is used to incorporate the restriction

$$N = \int d\mathbf{r}\rho(\mathbf{r}). \tag{8.4}$$

Thus, the electron density that minimize the total energy must satisfy

$$\mu = \frac{5}{3}C_F\rho^{2/3}(\mathbf{r}) + \upsilon(\mathbf{r}) + \int d\mathbf{r}' \frac{\rho(\mathbf{r}')}{|\mathbf{r}-\mathbf{r}'|}, \tag{8.5}$$

where μ represents a Lagrange multiplier. For atoms

$$\upsilon(\mathbf{r}) = -\frac{Z}{r}, \tag{8.6}$$

and consequently the Euler-Lagrange equation is

$$\mu = \frac{5}{3} C_F \rho^{2/3}(\mathbf{r}) - \frac{Z}{r} + \int d\mathbf{r}' \frac{\rho(\mathbf{r}')}{|\mathbf{r} - \mathbf{r}'|}. \tag{8.7}$$

Recognizing that the electrostatic potential is

$$\Phi(\mathbf{r}) = \frac{Z}{r} - \int d\mathbf{r}' \frac{\rho(\mathbf{r}')}{|\mathbf{r} - \mathbf{r}'|}, \tag{8.8}$$

then

$$\rho(\mathbf{r}) = \left(\frac{3}{5C_F}\right)^{3/2} [\mu + \Phi(\mathbf{r})]^{3/2}. \tag{8.9}$$

By using the Poisson equation

$$\nabla^2 \Phi = 4\pi\rho(\mathbf{r}) - 4\pi Z\delta(\mathbf{r}), \tag{8.10}$$

and the function Q defined from

$$\mu + \Phi(\mathbf{r}) = \frac{Z}{r} Q(r), \tag{8.11}$$

in Eq. 8.9, it is obtained that

$$\frac{d^2 Q}{dr^2} = 4\pi \left(\frac{3}{5C_F}\right)^{3/2} \left(\frac{Z}{r}\right)^{1/2} Q^{3/2}(\mathbf{r}), \tag{8.12}$$

or

$$\frac{d^2 Q(x)}{dx^2} = \frac{Q^{3/2}(x)}{x^{1/2}}, \tag{8.13}$$

with $x = \left(\frac{128}{9\pi^2}\right)^{1/3} Z^{1/3} r$, and the condition on $Q(0) = 1$.

Equation 8.13 does not admit an analytic solution and consequently there are several proposals to get an approximated solution. In particular, Slater and Krutter used this model to estimate the pressure on an atom. Such an approach implies necessarily a spatial confinement. In their work, Slater and Krutter proposed an atom enclosed by a spherical potential, which mimics a polyhedral cell in a metal [12]. Thus, by integrating Eq. 8.10 within a sphere of radius R_c we obtain

$$R_c^2 \left.\frac{d\Phi}{dr}\right|_{r=R_c} = N_c - Z, \tag{8.14}$$

or in terms of Q

$$R_c \left.\frac{dQ}{dr}\right|_{r=R_c} - Q(R_c) = \frac{N_c}{Z} - 1. \tag{8.15}$$

In Eqs. 8.14 and 8.15, N_c represents the number of electrons enclosed by the sphere of radius R_c.

In their original proposal, Slater and Krutter studied neutral systems and the working equation is obtained from Eq. 8.15, which gives

$$R_c \left.\frac{dQ}{dr}\right|_{r=R_c} = Q(R_c), \tag{8.16}$$

or in terms of x

$$x_c \left.\frac{dQ}{dr}\right|_{x=x_c} = Q(x_c). \tag{8.17}$$

This condition has a direct implication on the electron density because from 8.9 and 8.11

$$\rho(\mathbf{r}) = \left(\frac{3}{5C_F}\frac{Z}{r}\right)^{3/2} Q(r)^{3/2}, \tag{8.18}$$

and using the condition 8.16 it is obtained for neutral atoms that

$$\left.\frac{d\rho}{dr}\right|_{r=R_c} = 0. \tag{8.19}$$

Thus, in the Thomas-Fermi model we can confine a neutral atom within a sphere of radius R_c where the density is different than zero and its derivative is cancelled. The solution of Eq. 8.13 is obtained by using numerical techniques, for this purpose it is convenient to use the variable $x = \omega^2/2$ giving as result

$$\frac{d^2Q}{d\omega^2} = \frac{1}{\omega}\frac{dQ}{d\omega} + \sqrt{2}\omega Q^{3/2}. \tag{8.20}$$

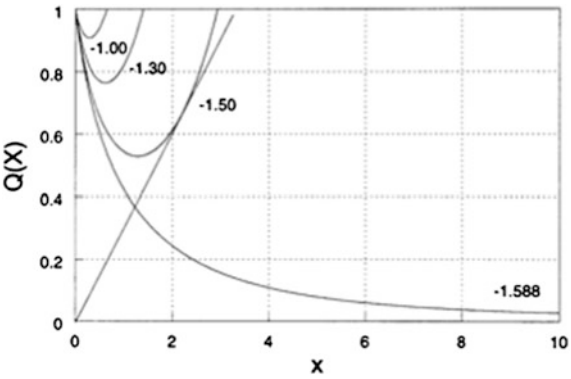

Fig. 8.1 $Q(x)$ for several values of a_2. The intersection of $Q(x)$ with a line of the form $f = mx$ is presented for $a_2 = -1.5$

For $\omega \approx 0$ the solution is

$$Q(\omega) = 1 + \frac{1}{2}a_2\omega^2 + \frac{2^{1/2}}{3}\omega^3 + \cdots \tag{8.21}$$

For this case the solution is expressed exclusively in terms of the coefficient a_2. With the information around $\omega \approx 0$ we can use any numerical technique to solve the corresponding differential equation. The algorithm to solve Eq. 8.13 under the restriction of Eq. 8.17 is as follows: (1) A value for a_2 must be proposed. (2) Apply a numerical technique to solve Eq. 8.20. (3) Find the intersection of the solution with the straight line $f = mx$ with $m = {}^{dQ}/_{dx}\Big|_{x=x_c}$ Following this algorithm, we found $Q(x)$ for several values of a_2. The corresponding solutions are depicted in Fig. 8.1.

Naturally, with the solution we can evaluate the total energy, the electron density, or any property that depends explicitly on the density. In particular, the pressure can be found from

$$P = -\left(\frac{\partial E}{\partial V}\right)_N. \tag{8.22}$$

For atoms in the Thomas-Fermi model it is found that [13]

$$P = \frac{2}{3}C_F\rho(R_c)^{5/3}. \tag{8.23}$$

From Eq. 8.23 it is clear the role of the density evaluated at the boundary where it is evident that in the limit of $\rho(R_c) \to 0$ the pressure will be null.

For non-neutral atoms the confinement on atoms within the Thomas-Fermi model must be analyzed carefully. Suppose that

$$Q(R_c) = 0 \tag{8.24}$$

on Eq. 8.15. If $N_c \neq Z$ and R_c is arbitrary then Eq. 8.15 is transformed in

$$\left.\frac{dQ}{dr}\right|_{r=R_c} = \frac{1}{R_c}\left(\frac{N_c}{Z} - 1\right). \tag{8.25}$$

Depending on the values assigned for N_c and Z we see three possibilities:

1. N_c = Z. For this case, the derivative is equal to zero. Thus, the solution and its derivative are equal to zero. This condition is reached just for $R_c \to \infty$, in conclusion: the electron density for neutral atoms in the Thomas-Fermi model cannot be cancelled for an arbitrary r.
2. $N_c < Z$. For this case, $\left.{}^{dQ}/_{dr}\right|_{r=R_c} < 0$. According to Fig. 8.1, this condition is reached when $Q(x)$ intercepts the abscises axis. Thus, in the Thomas-Fermi model the atoms with positive charge have finite size.
3. $N_c > Z$. For this case, $\left.{}^{dQ}/_{dr}\right|_{r=R_c} > 0$. This possibility is unacceptable by the behavior exhibited in Fig. 8.1. Thus, anions in the Thomas-Fermi model cannot be confined.

In summary, just atoms with positive charge allow confinement with rigid walls in the Thomas-Fermi model neutral atoms and anions do not exist under such a circumstance.

8.3 Modified Thomas-Fermi model

The Thomas-Fermi model exhibits several problems, between these problems we want to mention the behavior of the electron density close to the origin. For this model, the electron density at the nucleus diverges and evidently shows a wrong behavior. In order to correct such a deficiency Parr and Gosh [14] proposed

$$M = \int d\mathbf{r}\nabla^2\rho(r)e^{-2kr}, \tag{8.26}$$

as restriction on the minimization process. In the same way than the previous section and imposing the cusp condition [15]

$$\left.\frac{d\rho(r)}{dr}\right|_{r=0} = -2Z\rho(0), \tag{8.27}$$

it is obtained that

$$\rho(\mathbf{r}) = \left(\frac{3}{5C_F}\right)^{3/2}\left[\mu - \int d\mathbf{r}'\,\frac{\rho(\mathbf{r}')}{|\mathbf{r}-\mathbf{r}'|} + kZe^{-2kr} + \frac{Z}{r}\left(1-e^{-2kr}\right)\right]^{3/2}, \tag{8.28}$$

with

$$k = \left(\frac{5}{6}C_F\right)^{1/2}\rho^{1/3}(0). \tag{8.29}$$

Parr and Ghosh solved Eq. 8.28 by using an iterative procedure. However, in this report we solve this equation numerically following the ideas of Feynman, Metropolis and Teller [16]. On this way, by using the definition for $Q(r)$, in Eq. 8.11, and scaling r by α

$$x = \alpha r, \tag{8.30}$$

with

$$\alpha = \left(\frac{128}{9\pi^2}\right)^{1/3} Z^{1/3}, \tag{8.31}$$

Equation 8.28 is written as

$$\rho(x) = \left(\frac{3Z\alpha}{5C_F x}\right)^{3/2}\left[Q(x) + \left(\frac{kx}{\alpha} - 1\right)e^{-2kr/\alpha}\right]^{3/2} \tag{8.32}$$

The variable ω is more convenient to use, in order to analyze the behavior near to the origin of $\rho(r)$, thus

$$\rho(\omega) = \left(\frac{6Z\alpha}{5C_F\omega^2}\right)^{3/2}\left[Q(\omega) + \left(\frac{k\omega^2}{2\alpha} - 1\right)e^{-k\omega^2/\alpha}\right]^{3/2}. \tag{8.33}$$

If

$$Q(\omega) = \sum_{n=0}^{\infty} c_n\omega^n \tag{8.34}$$

then

$$\rho(\omega) = \left(\frac{6Z\alpha}{5C_F}\right)^{3/2}\left[\frac{c_0 - 1}{\omega^2} + \frac{c_1}{\omega} + \left(c_2 + \frac{3k}{2\alpha}\right) + O(\omega)\right]^{3/2}. \tag{8.35}$$

By using this equation, if $\rho(0) \neq \infty$ when $\omega \to 0$ then $c_0 = 1$ and $c_1 = 0$. Consequently

$$Q(\omega) = 1 + c_2\omega^2 + \cdots \tag{8.36}$$

and

$$\rho(0) = \left(\frac{6Z\alpha}{5C_F}\right)^{3/2}\left[c_2 + \frac{3k}{2\alpha}\right]^{3/2} \tag{8.37}$$

by using Eq. 8.29 it is found that

$$c_2 = \frac{3k}{2\alpha}\left(\frac{k}{Z} - 1\right). \tag{8.38}$$

If we use the Poisson equation (Eq. 8.10) and $Q(0) = 1$ then Eq. 8.32 is written as

$$\frac{d^2Q}{dx^2} = \frac{1}{x^{1/2}}\left[Q + \left(\frac{kx}{\alpha} - 1\right)e^{-2kr/\alpha}\right]^{3/2}. \tag{8.39}$$

Comparing this equation with Eq. 8.13 we can see that they are very similar and the difference is imposed by the exponential function. In terms of ω we have

$$\frac{d^2Q}{dw^2} = \frac{1}{w}\frac{dQ}{dw} = 2^{1/2}w\left[Q + \left(\frac{kw^2}{2\alpha} - 1\right)e^{-kw^2/\alpha}\right]^{3/2}. \tag{8.40}$$

Inserting Eq. 8.34 in 8.40 we obtain a recurrence relation for the coefficients c_l. The first twelve coefficients c_l are reported in Table 8.1.

With this analysis, the solution is known for the range $0 \leq \omega < \omega_i$. For the whole domain we applied the Runge-Kutta method of fourth order where it is needed a mesh with a step = h. In Table 8.2, the results obtained with this approach ($h = 0.04$, $\omega_i = 0.26$ and 16 terms for the polynomial expansion) are compared with those reported by Parr and Ghosh [14].

From Table 8.2 it is evident that the iterative approach to solve Eq. 8.28 and the numerical solution give the same results.

In order to estimate the pressure according to the Slater and Krutter proposal, the Poisson equation is sufficient, thus for the function $Q(\omega)$ we have

Table 8.1 First twelve coefficients of Eq. 8.33 to satisfy Eq. 8.41

$c_2 = \frac{3k}{2\alpha}\left(\frac{k}{Z} - 1\right)$	$c_4 = 0$
$c_6 = \frac{\left(k/\alpha + c_2\right)^{3/2}}{12\sqrt{2}}$	$c_8 = -\frac{\left(k/\alpha + c_2\right)^{1/2}}{16\sqrt{2}}\left(\frac{k}{\alpha}\right)^2$
$c_{10} = \frac{3}{320\sqrt{2}\left(k/\alpha + c_2\right)^{1/2}}\left(\frac{k}{\alpha}\right)^4 + \left(\frac{3\left(k/\alpha + c_2\right)^{1/2}}{160\sqrt{2}}\right)\left(\frac{k}{\alpha}\right)^3 + \frac{\left(k/\alpha + c_2\right)^2}{640}$	
$c_{12} = \frac{1}{960\sqrt{2}\left(k/\alpha + c_2\right)^{3/2}}\left(\frac{k}{\alpha}\right)^6 - \frac{1}{160\sqrt{2}\left(k/\alpha + c_2\right)^{1/2}}\left(\frac{k}{\alpha}\right)^5 - \frac{\left(k/\alpha + c_2\right)^{1/2}}{240\sqrt{2}}\left(\frac{k}{\alpha}\right)^4 - \frac{\left(k/\alpha + c_2\right)}{768}\left(\frac{k}{\alpha}\right)^2$	

Table 8.2 $\rho(0)$, $\rho(0)/Z^3$ for noble gases

Z	$\rho(0)$	$\rho(0)/Z^3$	
	This work		Parr and Ghosh
2	1.8184	0.2273	0.2274
10	367.1735	0.3672	0.3672
18	2,343.9946	0.4019	0.4020
36	20,175.8832	0.4324	0.4325
54	70,214.2495	0.4459	0.4460
86	291,401.9354	0.4581	0.4581

$$\omega_c \left.\frac{dQ}{d\omega}\right|_{\omega=\omega_c} = 2Q(\omega_c). \tag{8.41}$$

With this condition it is possible to evaluate the density at the surface of the sphere. In Fig. 8.2, this quantity is depicted as a function of the confinement radius for noble gases.

This plot gives an idea about of the atomic size. For example, for a fixed confinement radius (vertical line at $R_c = 0.5$ a.u.) clearly the Rn atom has the biggest value of the density on the surface of the sphere and the helium the smallest one. Because the Rn atom has more electrons than the helium atom, its electron density is rapidly touched by the surface of the sphere. Additionally, for a fixed value of the density on the surface of the sphere, in this example the horizontal line at $\rho(R_c) = 1$, the helium needs smaller R_c values to reach this value than other atoms. Naturally, these results are in accord with the physical intuition.

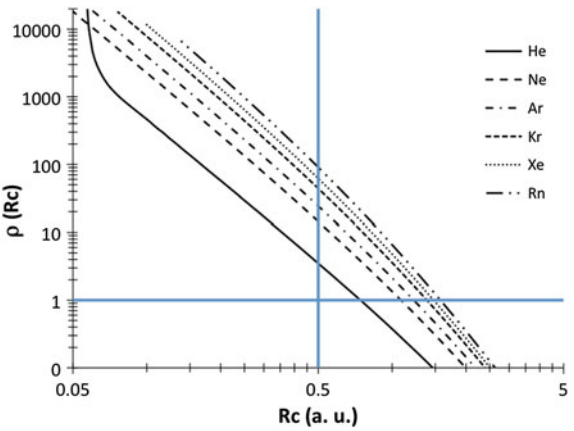

Fig. 8.2 Electron density at R_c as a function of R_c

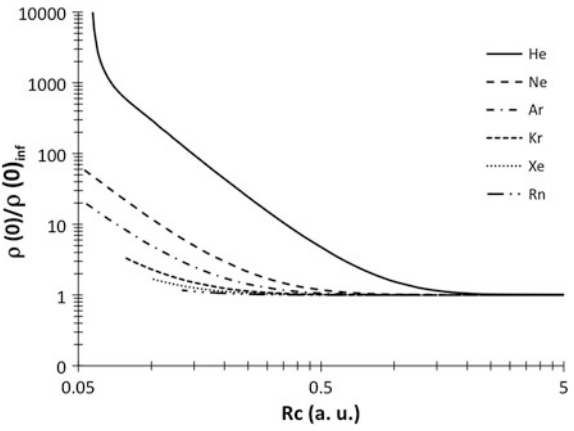

Fig. 8.3 Electron density evaluated at the nuclei of noble gases atoms

The proposal by Parr and Ghosh to determine the density at the origin allows a study of this quantity as a function of the confinement radius. The behavior of the density at the origin divided by its value at the infinity, $\rho(0)/\rho(0)_{\text{inf}}$, is depicted in Fig. 8.3.

The electron density evaluated at the origin is a local property, which is corroborated in Fig. 8.3 where all noble gases, except the helium, response to pressure effects for small confinement radii. In particular, the Rn atom shows important deviation for quite small confinement radii. By other side, the helium atom is the atom that exhibits a pronounced response when the confinement radius is reduced.

In these two sections we have discussed the Thomas-Fermi model and its connection with confined atoms, where the energy is minimized with regard to the electron density. Naturally, there is a vast literature around the Thomas-Fermi model. In recent years, Díaz-García and Cruz have tackled the confined atoms problem under the Thomas-Fermi model by a different strategy [17, 18].

8.4 Kohn-Sham Model

The Kohn-Sham model is the most successful approach within the DFT, [11] in this approach the universal functional of Hohenberg and Kohn is written as

$$F[\rho] = T_s + \frac{1}{2}\iint d\mathbf{r}d\mathbf{r}' \frac{\rho(\mathbf{r})\rho(\mathbf{r}')}{|\mathbf{r}-\mathbf{r}'|} + E_{xc'} \tag{8.42}$$

where

$$T_s = \sum_{i=1}^{N} \left\langle \varphi_i \middle| -\frac{1}{2}\nabla^2 \middle| \varphi_i \right\rangle \tag{8.43}$$

and the exchange-correlation functional, Exc, is defined as

$$E_{xc} = T - T_s + V_{ee} - J. \tag{8.44}$$

By its definition, E_{xc} contains small contributions to the total energy and consequently it is hard to be modeled. Currently, there are many approximations to this quantity and depending on the problem to be solved is the E_{xc} to be used.

We see from Eq. 8.43 that the energy has an explicit dependence on a set of orbitals. The orbitals that minimize to the total energy must satisfy the Kohn-Sham equations

$$\left(-\frac{1}{2}\nabla^2 + \int d\mathbf{r}' \frac{\rho(\mathbf{r}')}{|\mathbf{r}-\mathbf{r}'|} + \frac{\delta E_{xc}}{\delta\rho(\mathbf{r})}\right)\varphi_i(\mathbf{r}) = \varepsilon_i\varphi_i(\mathbf{r}), \tag{8.45}$$

and the electron density is build with these orbitals from

$$\rho(\mathbf{r}) = \sum_{i=1}^{N} \varphi_i^*(\mathbf{r})\varphi_i(\mathbf{r}). \tag{8.46}$$

For confined atoms there are several reports where rigid walls are used [19–21]. This kind of walls implies that the solution of Eq. 8.45 must be found by imposing Dirichlet boundary conditions. One way to solve Eq. 8.45 with these boundary conditions has been reported by Garza et al. [21]. In this approach the radial Kohn-Sham equations are solved numerically in a mesh with a fixed step, this procedure is carried out over three steps and the results are extrapolated according to a Richardson extrapolation. Details of the implementation can be found in Ref. [21]. In the original paper of Garza et al. few exchange-correlation functionals were implemented, fortunately there is a library where many exchange-correlation functionals are available, such a library has been linked with the original numerical code of Garza et al. [22]. The results presented in the next sections have been obtained with this library.

Table 8.3 Total energy and $\Delta E/\Delta R_c$ for Na ([Ne]$1s^1$) and K ([Ar]$4s^1$)

R_c (a. u.)	Na		K	
	TE	$\Delta E/\Delta R_c$	TE	$\Delta E/\Delta R_c$
1.0	−118.937095		−475.747431	
1.2	−138.349633	−97.06	−531.531071	−278.92
1.4	−148.079988	−48.65	−559.589815	−140.29
1.6	−153.322850	−26.21	−574.814123	−76.12
1.8	−156.311764	−14.94	−583.562278	−43.74
2.0	−158.098476	−8.93	−588.818996	−26.28
3.0	−160.988374		−597.140863	
4.0	−161.525124		−598.442127	
5.0	−161.687817		−598.766797	

The results were obtained with the PBE exchange-only functional. All quantities are in atomic units

8.4.1 Electronic Transitions Induced by Spatial Confinement

In Table 8.3 we are presenting the total energy as a function of the confinement radius for two atoms, Na and K, by using the PBE exchange-only functional [23, 24]. The change rate $\Delta E/\Delta R_c = (E_{i+1} - E_i)/0.2$ for few values of R_c is also reported in Table 8.3. We have used the electronic configuration that corresponds to the non-confined atom for this table.

From this table we can appreciate large changes on the total energy when many-electron atoms are confined under small confinement radii. The non-confined atom corresponds to that R_c where changes on the total energy are not observed.

Naturally, the confinement impact is observed also on orbital energies and not just on the total energy. In Fig. 8.4, we are presenting the highest orbital energies for the K atom.

The Fig. 8.4 shows several important results about the confinement effect on the electronic structure of atoms. The first effect we want to stress is the orbital energies crossing. Let us suppose that the K atom starts to be confined, in this figure $R_c = 8$ a. u. represents the beginning of the confinement. Clearly, when the confinement is increased the orbital energies increase their values, although with different rate. In particular, the 4s energy grows up faster than the 3d energy and therefore there is a point (around 4.5 a. u) where these energies have the same value. For this electronic configurations we impose that the 4s orbital is occupied, however after the crossing point the 3d energy is below of the 4s orbital suggesting that now the configuration is [Ar]$3d^1$ instead of [Ar]$4s^1$. This effect in solid state physics is know as *s-d* transition and is observed for many atoms where the valence shell is not totally occupied. If this is true then the total energy of the configuration [Ar]$3d^1$ must be deeper than the [Ar]$4s^1$ when the crossing between orbital energies is presented. In Table 8.4 the total energy for the [Ar]$4s^1$ configuration is contrasted with the

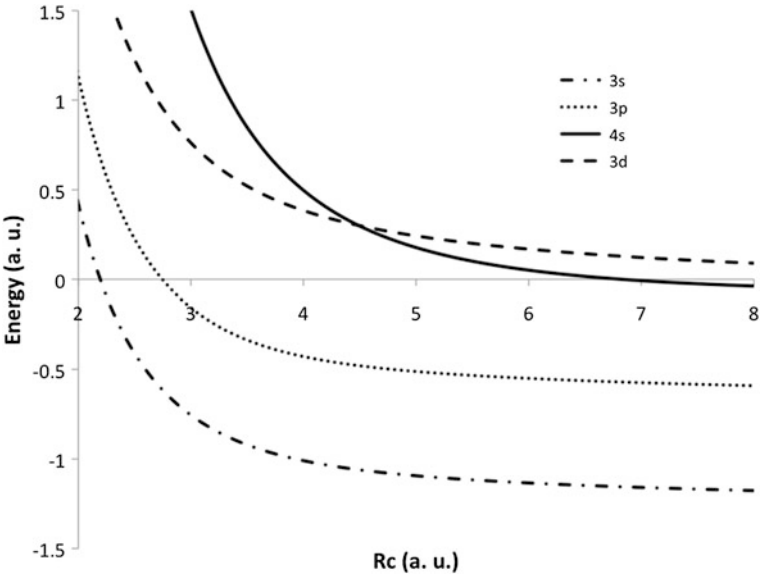

Fig. 8.4 Orbital energies for the K atom as functions of the confinement radius

corresponding energy for the $[Ar]3d^1$ configuration. Clearly, there is a crossing between the total energies of these configurations, around 4.6 a. u. Thus, for R_c greater than the crossing point the $[Ar]4s^1$ is the most stable configuration and for R_c less than that point the $[Ar]3d^1$ is the most stable configuration.

It is evident from these results that the pressure, obtained numerically from Eq. 8.22, will be different for each configuration since the response to the confinement on each electronic configuration is different. In Fig. 8.5, we are presenting the dependence of the energy on the pressure.

Figure 8.5 is important because shows the pressure where the transition is observed. In fact, we have made estimations for *s-d* transitions for two families in the periodic table and our results are acceptable with respect to the experimental data [25, 26]. The amazing result we have found with this simple model is the volume change observed for this transition since for the pressure where both electronic configurations give the same energy the confinement radii are different predicting in this way different volumes for each electronic configuration.

8.4.2 Ionization Potential for Confined Atoms

An additional effect we can extract from Fig. 8.4 is that all orbital energies are increased when the confinement radius is reduced, in fact the 4s orbital energy has positive values before of the crossing point. The radius where the 4s orbital energy

Table 8.4 Total energy for the K atom for two electronic configurations

R_c (a. u.)	[Ar]4s^1	[Ar]3d^1	[Ar]3d^1 − [Ar]4s^1
4.0	−598.442127	−598.577197	−0.1351
4.2	−598.541390	−598.620407	−0.0790
4.4	−598.618504	−598.653297	−0.0348
4.6	−598.679245	−598.678994	0.0003
4.8	−598.727701	−598.699610	0.0281
5.0	−598.766797	−598.716561	0.0502

All quantities are in hartrees

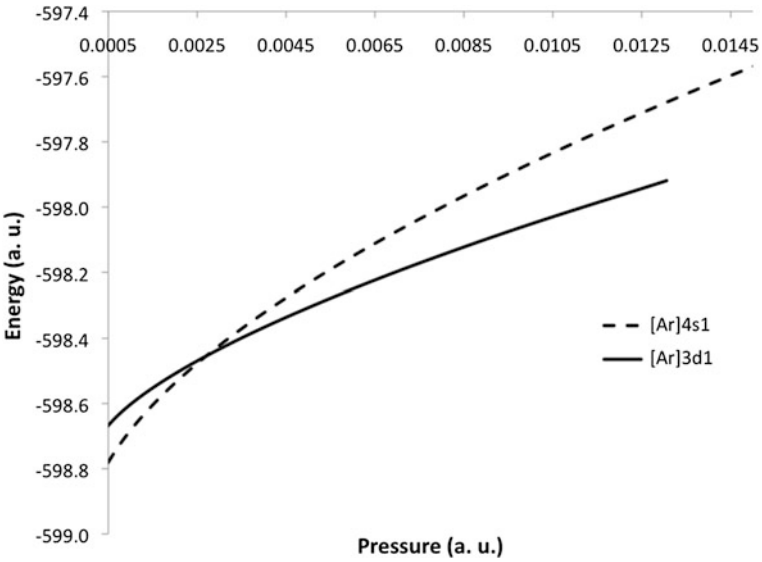

Fig. 8.5 Total energy as a function of the pressure for two electronic configurations for the K atom by using the exchange-only PBE functional

Table 8.5 Total and HOMO energies for the non-confined K atom. All quantities are in hartrees

	Clementi	Bunge	Thakkar
Total energy	−599.1645907	−599.1648610	−599.1648675
ε_{HOMO}	−0.147521	−0.147639	−0.147648

is zero is known as the critical radius because if we accept that the energy of the highest occupied molecular orbital (HOMO) represents an approximation to the ionization potential (*IP*) [27] then the critical radius indicates the confinement radius where we do not need energy to remove one electron. In fact, if we use the

Table 8.6 $-\varepsilon_{HOMO}$ obtained for several values of confinement radius (R_c) by using the Hartree-Fock (HF) method and two exchange-only functionals, PBE and OPTX

R_c	HF	PBE	OPTX
4.6	0.147073	0.268220	0.274415
4.8	0.100938	0.218258	0.224705
5.0	0.063049	0.176922	0.183573
5.5	−0.005785	0.100808	0.107827
6.0	−0.050224	0.050553	0.057822
6.5	−0.079793	0.016227	0.023690
7.0	−0.099932	−0.007858	−0.002224

exact exchange-correlation potential then $IP = -\varepsilon_{HOMO}$ [28]. Naturally, for hard walls the electron does not escape by the presence of the boundaries and therefore the *IP* concept is different for confined atoms than for free atoms, where the *IP* is evaluated as the energy difference between neutral and charged atoms. Díaz-García and Cruz have mentioned this problem and they treat the helium atom as an example [29]. However, when Ludeña applied the Hartree-Fock (HF) method on confined many-electron atoms he used the $-\varepsilon_{HOMO}$ to estimate the critical radius [30]. Unfortunately, the basis set functions used by Ludeña were not optimized for each confined radius, which is an important ingredient when the HF method is used on confined atoms. Recently we have published a methodology to obtain efficiently HF results for confined atoms [31]. This methodology has been applied on the K atom, in Table 8.5 we are presenting the basis set functions effect on the total and HOMO energies. For this case we have used three basis set functions based on Slater type orbitals and designed for non-confined atoms [32–34].

Evidently the basis set functions designed by Thakkar [34] gives the lowest energy. With this basis set the prediction to the *IP* by the HOMO is of 4.02 eV versus 4.34 eV, which corresponds to the experimental information [35].

By using as starting point the Thakkar basis set functions, in Table 8.6 we are reporting, for some values of R_c, the HOMO energy. Of course, we have optimized for each R_c the exponents of the basis set in accord with a previous HF study made by Garza and Vargas [36]. In the same table we are also reporting the HOMO energy obtained with two exchange-only functionals, PBE [23, 24] and OPTX [37].

From this table we appreciate large differences between the results obtained with PBE and OPTX with regard to those obtained with the HF method. It is well known that the wrong asymptotic behavior exhibited by several exchange-correlation functionals is the responsible of the mentioned differences [38–40]. For that reason the HOMO energy obtained by many exchange-correlation functionals do not give good estimations of *IP*. From these results it is evident that PBE and OPTX predict a critical radius larger than that radius predicted by the HF method. Even with these large differences between HF and PBE or OPTX we have found a linear correlation, $\varepsilon_{HOMO}^{HF} = m\varepsilon_{HOMO}^{x-only} - b$, between the corresponding HOMOs. For PBE we found

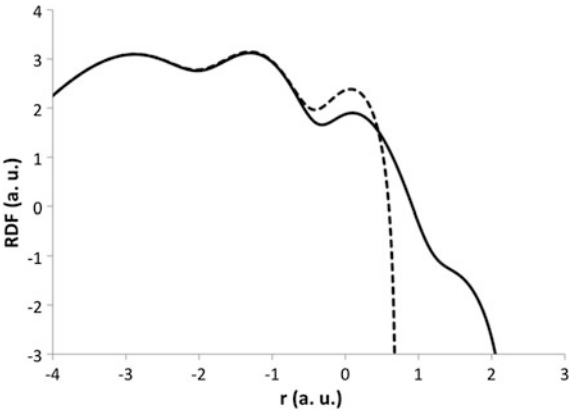

Fig. 8.6 Radial distribution function (RDF) for the K atom for R_c = 2.0 a.u. (*dotted line*) and R_c = 10.0 a.u. (*solid line*). Both axes are in logarithmic scale and in atomic units

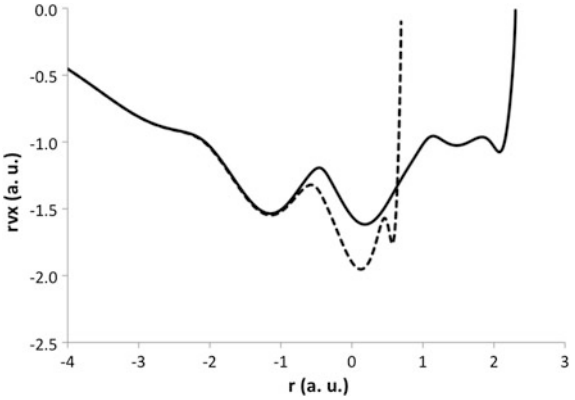

Fig. 7 Exchange-only PBE potential, times r, obtained for Rc = 2.0 a.u. (*dotted line*) and Rc = 10.0 a.u. (*solid line*), for K atom. r is in logarithmic scale

m = 0.8959, b = 0.0946 with a correlation coefficient of 0.9998. For OPTX m = 0.8971, b = 0.1007 and a correlation coefficient of 0.9997. Even with this linear relationship between ε_{HOMO}^{HF} and ε_{HOMO}^{KS} it is evident that the argument of the wrong asymptotic behavior as responsible of this difference is not enough since the confinement radii tested in this example do not belong to the asymptotic region. Thus, there is a contribution, in the non-asymptotic region, on the exchange potential that contributes to the behavior of the orbital energies, in particular the HOMO energy.

In this section we have discussed approximations to the *IP* for confined atoms. However, by its nature the electron propagator is the best technique to estimate this quantity, [41–43] in particular for confined atoms. Thus, it is necessary an implementation of this technique on the HF codes reported for confined atoms.

8.4.3 The Response of the Shell Structure to the Confinement

The impact of the confinement on orbital energies is also mapped on the electron density and local properties. For example, the radial distribution function (RDF $(r) = 4\pi\, r^2\rho(r)$) for the K atom, for two confinement radii, is presented in Fig. 8.6. Clearly this atom presents different number of shells depending on the applied confinement. A discussion about the RDF for confined atoms, within the KS context, is presented in Ref. [44].

Evidently, the RDF is not the only local quantity that is affected by the confinement imposed by the rigid walls. For example, the exchange-correlation functional depends explicitly on the electron density and consequently this quantity also must exhibit changes when the atom is confined, as it is shown in Fig. 8.7, where the exchange-only PBE potential ($r\, v_x$) for the K atom is contrasted between two confinement radii.

From Fig. 8.7 we can conclude that the shell structure in an atom can be studied by using several tools, in our case we use the radial distribution function and the exchange-only potential. Clearly, for large confinement radii the last shell for K atom is better appreciated when the exchange-only potential is used. Evidently, there are other quantities that are used to analyze the shell structure that must be implemented in confined atoms codes to obtain insight about the electron-electron interaction in these systems [45].

8.4.4 Correlation Energy from DFT in Confined Atoms

There are few works where the correlation energy is estimated for confined atoms. In particular, the helium atom is the system that has been studied in detail with many techniques [46–52]. For this system, it is found that the correlation energy is almost constant for any confinement radius, with a value around of −0.042 hartrees; there are no reports about this topic with DFT. In Table 8.7 we present the total energy obtained by several exchange-correlation functionals and by a Hylleraas wave functions expansion (HWF) for the confined helium atom [47]. For this case, PBEPBE represents to the PBE functional for the exchange and for the correlation contributions. PBELYP uses the PBE for the exchange energy and LYP [53] for the correlation contribution. BLYP uses the Becke88 [54] functional for the exchange and LYP for the correlation. It is important to remark that these functionals were designed for non-confined atoms. Thus, it is interesting to see the behavior exhibited by these exchange-correlation functionals for confined atoms. From this table we conclude that the BLYP exchange-correlation functional shows an impressive performance since it gives total energies closer to the HWF results.

In order to see the contribution of each part of the exchange-correlation functionals, in Table 8.8 we are reporting the exchange energy obtained by three functionals and they are contrasted with the HF results reported in Ref. [36].

Table 8.7 Total energy for the helium atom for several confinement radii

R_c	HWF	PBEPBE	PBELYP	BLYP
2.0	−2.60403	−2.57286	−2.55830	−2.59126
3.0	−2.87246	−2.85451	−2.85177	−2.86828
3.5	−2.89354	−2.87835	−2.87736	−2.89144
4.0	−2.90042	−2.88668	−2.88642	−2.89950
4.5	−2.90264	−2.88959	−2.88963	−2.90231
5.0	−2.90337	−2.89060	−2.89076	−2.90330
6.0	−2.90368	−2.89107	−2.89128	−2.90376
7.0	−2.90370	−2.89112	−2.89134	−2.90382

All quantities are in hartrees

Table 8.8 Exchange energy, in hartrees, for helium atom estimated by several methods

R_c	HF	PBEPBE	PBELYP	BLYP
2.0	−1.24412	−1.19019	−1.17462	−1.23251
2.5	−1.12763	−1.08124	−1.06577	−1.12663
3.0	−1.07118	−1.02756	−1.01217	−1.07647
3.5		−1.00135	−0.98597	−1.05321
4.0	−1.03342	−0.98881	−0.97341	−1.04273
4.5		−0.98297	−0.96754	−1.03817
5.0	−1.02682	−0.98032	−0.96489	−1.03624
6.0	−1.02589	−0.97867	−0.96324	−1.03514
7.0		−0.97838	−0.96295	−1.03496

From this table we appreciate two important results. (1) The PBE exchange functional underestimate always the exchange energy for any confinement radius. (2) The Becke88 exchange functional does not show a regular behavior because for some confinement radii this functional underestimates the exchange energy and for others it overestimates. From this observation it is clear that if we want to modify these exchange-only functionals, it seems easier to do this work with the PBE proposal.

By the side of the correlation energy, in Table 8.9 we are reporting this quantity for several confinement radii. The first thing we note is the relevance of the exchange functional used when it is coupled with the correlation functional since the LYP functional predicts different values depending of the exchange functional coupled with it. In general we can say that the correlation functionals predicts correlation energy almost constant for moderate confinements, $R_c \geq 4$. However, when the confinement is increased these correlation functionals predict correlation energies with important differences with respect to the HWF results.

Table 8.9 Correlation energy, in hartrees, for helium atom estimated by three correlations functionals and a Hylleraas wave functions expansion

R_c	HWF	PBEPBE	PBELYP	BLYP
2.0	−0.0415	−0.0494	−0.0387	−0.0492
3.0	−0.0414	−0.0432	−0.0432	−0.0434
3.5	−0.0417	−0.0419	−0.0435	−0.0423
4.0	−0.0418	−0.0412	−0.0434	−0.0418
4.5	−0.0419	−0.0409	−0.0433	−0.0415
5.0	−0.0420	−0.0407	−0.0433	−0.0414
6.0	−0.0420	−0.0406	−0.0432	−0.0414
7.0	−0.0420	−0.0406	−0.0432	−0.0414

Without doubt, calculations with several exchange-correlation functionals are needed for extreme confinements and they must be contrasted with techniques based on the wave-function, such as many-body perturbation theory, configuration interaction, coupled cluster, quantum Monte Carlo [55] or Hylleraas wave functions expansion. Evidently, correlated methods based on the wave-function must be developed around of the confined many-electron atoms.

8.5 Perspectives

In this report we have discussed some results obtained by the density functional theory, for many-electron atoms confined by a sphere with infinity potential at its surface. Clearly, there are several issues that must be treated with more detail. For example, the prediction of ionization potentials for confined atoms must be performed by sophisticate techniques, such as the electron propagator or by exchange-correlation potentials corrected on the asymptotic behavior. The performance exhibited by several exchange-correlation functionals is an issue that must be carried out. Our position is that with the confined atoms model we can extract useful information in order to design new functionals or correct some of them. Evidently, this issue has impact on the exchange-correlation potential and consequently on orbital energies.

Acknowledgments This work has been supported by CONACYT, México, through the projects 154784, 155698 and 155070. The authors thank the facilities provided by the Laboratorio de Supercómputo y Visualización en Paralelo at the Universidad Autónoma Metropolitana-Iztapalapa.

References

1. Parr RG, Yang W (1989) Density-functional theory of atoms and molecules. Oxford University Press, New York
2. Engel E, Dreizler RM (2011) Density functional theory: an advanced course (theoretical and mathematical physics). Springer, Berlin
3. Martin RM (2004) Electronic structure: basic theory and practical methods. Cambridge University Press, Cambridge
4. Degroot SR, Tenseldam CA (1946) Physica 12:669
5. Jaskolski W (1996) Phys Rep—Rev Sect Phys Lett 271:1
6. Michels A, De Boer J, Bijl A (1937) Physica 4:14
7. Sommerfeld A, Welker H (1938) Annalen Der Physik 32:56
8. Hohenberg P, Kohn W (1964) Phys Rev 136:B864
9. Fermi E (1928) Zeitschrift Fur Physik 48:73
10. Thomas LH (1927) Proceedings of the Cambridge Philosophical Society 23:542
11. Kohn W, Sham LJ (1965) Phys Rev 140:1133
12. Slater JC, Krutter HM (1935) Phys Rev 47:559
13. Abrahams AM, Shapiro SL (1990) Phys Rev A 42:2530
14. Parr RG, Ghosh SK (1986) Proc Nat Acad Sci U S A 83:3577
15. Kato T (1957) Commun Pure Appl Math 10:151
16. Feynman RP, Metropolis N, Teller E (1949) Phys Rev 75:1561
17. Díaz-García C, Cruz SA (2008) Int J Quantum Chem 108:1572
18. Cruz SA (2009) Advances in quantum chemistry, vol 57. Elsevier Academic Press Inc, San Diego, p 255
19. Boeyens JCA (1994) J Chem Soc-Faraday Trans 90:3377
20. Sarkar U, Giri S, Chattaraj PK (2009) J Phys Chem A 113:10759
21. Garza J, Vargas R, Vela A (1998) Phys Rev E 58:3949
22. Ekstrom U, Visscher L, Bast R, Thorvaldsen AJ, Ruud K (2010) J Chem Theory Comput 1971:6
23. Perdew JP, Burke K, Ernzerhof M (1996) Phys Rev Lett 77:3865
24. Perdew JP, Burke K, Ernzerhof M (1997) Phys Rev Lett 78:1396
25. Sen KD, Garza J, Vargas R, Vela A (2014) Proc Indian Natn Sci Acad 70A, 675
26. Guerra D, Vargas R, Fuentealba P, Garza J (2009) Advances in quantum chemistry, vol 58. Elsevier Academic Press Inc, San Diego, p 1
27. Koopmans T (1934) Physica 1:104
28. Perdew JP, Parr RG, Levy M, Balduz JL (1982) Phys Rev Lett 49:1691
29. Díaz-García C, Cruz SA (2006) Phys Lett A 353:332
30. Ludeña EV (1978) J Chem Phys 69:1770
31. Garza J, Hernández-Pérez JM, Ramírez JZ, Vargas R (2012) J Phys B-At Mol Opt Phys 45:015002
32. Clementi E, Roetti C (1974) At Data Nucl Data Tables 14:301
33. Bunge CF, Barrientos JA, Bunge AV, Cogordan JA (1992) Phys Rev A 46:3691
34. Koga T, Tatewaki H, Thakkar AJ (1994) Theoretica Chimica Acta 88:273
35. Sansonetti JE, Martin WC (2005) J Phys Chem Ref Data 34:1559
36. Garza J, Vargas R (2009) Advances in quantum chemistry, vol 57. Elsevier Academic Press Inc, San Diego, p 241
37. Handy NC, Cohen AJ (2001) Mol Phys 99:403
38. Sen KD, Garza J, Vargas R, Vela A (2000) Chem Phys Lett 325:29
39. Garza J, Nichols JA, Dixon DA (2000) J Chem Phys 112:1150
40. Garza J, Vargas R, Nichols JA, Dixon DA (2001) J Chem Phys 114:639
41. Vonniessen W, Schirmer J, Cederbaum LS (1984) Comput Phys Rep 1:57
42. Ortiz JV (1999) Adv Quantum Chem 35:33

43. Linderberg J, Öhrn Y (2004) Propagators in quantum chemistry, 2nd edn. Wiley-Interscience, New Jersey
44. Garza J, Vargas R, Vela A, Sen KD (2000) J Mol Struc Theochem 501:183
45. Navarrete-López AM, Garza J, Vargas R (2008) J Chem Phys, 128:104110
46. Ludeña EV, Gregori M (1979) J Chem Phys 71:2235
47. Aquino N, Garza J, Flores-Riveros A, Rivas-Silva JF, Sen KD (2006) J Chem Phys 124:8
48. Flores-Riveros A, Rodríguez-Contreras A (2008) Phys Lett A 372:6175
49. Gimarc BM (1967) J Chem Phys 47:5110
50. Rivelino R, Vianna JDM (2001) J Phys B-At Mol Opt. Physics 34:L645
51. Wilson CL, Montgomery HE, Sen KD, Thompson DC (2010) Phys Lett A 374:4415
52. Le Sech C, Banerjee A (2011) J Phys B-At Mol Opt. Physics 44:9
53. Lee CT, Yang WT, Parr RG (1988) Phys Rev B 37:785
54. Becke AD (1988) Phys Rev A 38:3098
55. Sarsa A, Le Sech C (2011) J Chem Theory Comput 7:2786

Chapter 9
Study of Quantum Confinement of H_2^+ Ion and H_2 Molecule with Monte Carlo. Respective Role of the Electron and Nuclei Confinement

Antonio Sarsa and Claude Le Sech

9.1 Introduction

The properties of atoms and molecules undergo significant changes when they are spatially confined in either penetrable or impenetrable surfaces. Quantum confinement means confinement on a scale comparable to the atomic size, as opposed to ordinary confinement when the cavity is very much larger than the atom. The confinement of a particle in a potential is a well known problem of basic quantum mechanics. A direct application of this model in nuclear physics is the understanding of the alpha radioactivity assuming a square well potential when the particle is inside the nucleus, and a coulombic potential outside the nucleus. Consideration about confinement is also useful in a number of fields of physics: the effect of the pressure on the energy levels, the polarizability and the ionization threshold of atoms and molecules, artificial atoms like quantum dots, wires and quantum well and in several other areas like astrophysics. These problems have addressed a lot of attention and they become a field of active research due to the possibility to load nanocavities with molecules and to observe their modifications by efficient new techniques, see e.g. [15] and references therein. We refer also to the recent reviews [7, 8, 10, 16, 22] available for the interested reader.

The theory of chemical binding, see e.g. [28] is one of the first outstanding result of the quantum mechanics. In most of the theoretical approaches, describing molecular systems by quantum chemistry, the electron-pair of the covalent bond are

A. Sarsa (✉)
Departmento de Física, Campus de Rabanales Edif. C2,
Universidad de Córdoba, 14071 Córdoba, Spain
e-mail: fa1sarua@uco.es

C. Le Sech
CNRS, Institut des Sciences Moleculaires d'Orsay-ISMO (UMR 8214),
Université Paris Sud 11, 91405 Orsay Cedex, France
e-mail: Claude.lesech@u-psud.fr

K.D. Sen (ed.), *Electronic Structure of Quantum Confined Atoms and Molecules*,
DOI 10.1007/978-3-319-09982-8_9

allowed to span the whole space without any constraint. However it is well known that the probability density associated to the wave function is larger between the nuclei in the ground σ state. This raises a pending question: what will be the changes induced in the molecular bond by the modification of the probability density of the binding electrons? When the binding electrons are subjected to external electrostatic forces, for instance in a polar cavity, the available space where they can be located is different from the free state. This remark leads to the problem of quantum confinement of the particles constituting the molecule. When confined molecules are investigated in order to study the dynamical changes of trapped molecules in nanocavities, the simplest molecular systems like H_2^+ or H_2 are very suitable. They are convenient to study the effects of confinement on the bonding electron and to analyze the variation of the energy levels or internuclear distances [6, 19, 23, 26]. These systems are a model to study the changes of the molecular covalent bond properties when the electrons are confined by an external constraint.

The hard-wall confinement model is far to be only an academic problem. It is very useful to study atoms and molecules confined by a model of impenetrable wall. It might be considered also as the starting point of a more accurate description of a spatially limited system by a soft boundary surface instead of a hard one. For instance molecules like H_2 placed in the inner cavities of fullerene allow for differences in their physical and chemical properties. Considerations relative to a significant decrease of the barrier of fusion between the nuclei resulting from confinement have been reported [27] and this issue will be briefly illustrated in the last section.

Within the Born-Oppenheimer approximation the Schrödinger equation for H_2^+ is separable in elliptic coordinates. In reference [20] the exact values for the energy when the ion is confined inside hard prolate spheroidal boxes have been reported. Recent studies have completed the understanding of this molecular ion under spheroidal confinement using a simple accurate wave function for H_2^+, including the Dirichlet boundary conditions and soft confinement when the boundary surface is penetrable, in a variational approach [9]. The Rayleigh-Ritz variational method is one of the most popular method for calculating accurately the ground or excited state energy of an atomic or a molecular system and its extension to confined systems is useful to study confined systems.

In the present work a study of the confined H_2^+ ion and H_2 molecules, placed inside spherical hard boxes, is presented in the frame work of a variational approach beyond the Born-Oppenheimer approximation. Jacobi coordinates are used to describe the three and four-body system. An approximate wave function is constructed taking into account accurately the dynamics of the nuclei in the lowest rovibrational state and the interelectronic correlation in the case of the neutral molecule. In the frame work of this approach it becomes possible to study the respective role of the electronic or nuclei confinement on the internuclear distances and energy values. It will be shown that electronic confinement reduces the internuclear distances and increases the energy level of the molecules resulting in a metastable state compared to the free system i.e. when constrain is removed.

The paper is organized in the following manner. In Sect. 9.2 the derivation of the approximate functions the for H_2^+ molecular ion and the H_2 molecule, including the cut-off function, is presented and the computational methodology is discussed. In Sect. 9.3 we show the results obtained with the present choice of the wave function. First and in order to ascertain the accuracy of our ansatz we compare our variational results with the exact ones for those special cases where the later can be obtained. This is the case of a confined hydrogen atom and the H_2^+ ion with clamped nuclei inside spheroidal surfaces with different eccentricities. The second part of Sect. 9.3 reports the results for the confined H_2^+ molecular ion and H_2 molecule including nuclear dynamics. Finally a brief discussion is devoted to some consideration relative to enzymes and a possible role of electronic confinement in the their catalytic properties. A short discussion about a possible increase of nuclear cold fusion rate by quantum confinement of bounding electron in cavities is proposed at the end of this section. The conclusion of this work are presented in Sect. 9.4.

Atomic units are used throughout this work unless otherwise indicated.

9.2 Theory

9.2.1 H_2^+ *Molecular Ion Including Motion of Nuclei*

9.2.1.1 Schrödinger Equation

The Schrödinger equation for a confined H_2^+ like ion can be written using atomic units

$$\left(-\frac{\nabla^2_{\mathbf{r}_e}}{2m}-\frac{\nabla^2_{\vec{\mathbf{R}}_1}}{2M_1}-\frac{\nabla^2_{\vec{\mathbf{R}}_2}}{2M_2}+V\right)\Psi(\mathbf{r}_e,\mathbf{R}_1,\mathbf{R}_2)=E\,\Psi(\mathbf{r}_e,\mathbf{R}_1,\mathbf{R}_2) \tag{9.1}$$

where $\mathbf{r}_e$ is the position vector of the electron and $\mathbf{R}_1$ and $\mathbf{R}_2$ the position vectors of the two nuclei with masses M_1 and M_2 respectively, and m is the electron mass, $m = 1$, in atomic units. The potential, V, is given by

$$V=\frac{1}{R}-\frac{1}{r_A}-\frac{1}{r_B}+V_{ce}+V_{cN} \tag{9.2}$$

with

$$R=|\mathbf{R}_2-\mathbf{R}_1|,\quad r_A=|\mathbf{r}_e-\mathbf{R}_1|,\quad r_B=|\mathbf{r}_e-\mathbf{R}_2| \tag{9.3}$$

and the potentials V_{ce} and V_{cN} are infinitely high when the electron or one nucleus is at the respective defined boundary surfaces—spheroidal or spherical—and equal zero when particles are inside the volume limited by the confining surfaces.

This equation can be simplified by using Jacobi coordinates as follows. The origin is placed in the center of mass of the nuclei and we introduce, **r**, the position vector of the electron relative to this origin and, **R**, the relative vector of the two nuclei. By using these two coordinate we have

$$r_A = \sqrt{x^2 + y^2 + \left(z + \frac{R}{2}\right)^2}, \quad r_B = \sqrt{x^2 + y^2 + \left(z - \frac{R}{2}\right)^2} \tag{9.4}$$

and the Schrödinger equation for the intrinsic coordinates, once the center of mass motion has been removed, becomes

$$\left(-\frac{\nabla_{\mathbf{r}}^2}{2\varepsilon} - \frac{\nabla_{\mathbf{R}}^2}{2\mu} + V\right)\Psi(\mathbf{r}, \mathbf{R}) = E\,\Psi(\mathbf{r}, \mathbf{R}) \tag{9.5}$$

where ε and μ are reduced masses

$$\varepsilon = \frac{m(M_1 + M_2)}{m + M_1 + M_2}, \quad \mu = \frac{M_1 M_2}{M_1 + M_2} \tag{9.6}$$

For the H_2^+ molecular ion we use $M_1 = M_2 = 938.2720\ \mathrm{MeV/c^2}$ and $m = 0.5109989\ \mathrm{MeV/c^2}$ obtaining $\varepsilon = 0.9997278$ and $\mu = 918.0763$ in atomic units of mass.

9.2.1.2 Trial Function for the Free H_2^+ Molecular Ion

In this work, the following trial wave function, $\Psi_t(\mathbf{r}, \mathbf{R})$, is employed

$$\Psi_t(\mathbf{r}, \mathbf{R}) = F(\mathbf{R})\,\phi(r_A, r_B, R) \tag{9.7}$$

where $F(\mathbf{R})$ describes nuclear vibration and rotation and $\phi(r_\mathrm{A}, r_\mathrm{B}, R)$ the motion of the electron and nuclei.

The lowest rotational and vibrational level is considered here and the following form is assumed for $F(\mathbf{R})$

$$F(\mathbf{R}) = \frac{e^{-\delta(R - R_0)^2}}{R} \tag{9.8}$$

with δ and R_0 variational parameters.

For $\phi(r_\mathrm{A}, r_\mathrm{B}, R)$, the form proposed by Guillemin and Zener, GZ, [11] is employed

$$\phi(r_A, r_B, R) = e^{-Z(R)r_A} e^{-a r_B} + e^{-Z(R)r_B} e^{-a r_A} \tag{9.9}$$

This function is written by using prolate spheroidal coordinates (ξ, η, φ)

$$\xi = \frac{r_A + r_B}{R}, \quad \eta = \frac{r_A - r_B}{R} \tag{9.10}$$

and φ is the azimuthal angle. The domain of these variables is

$$1 \leq \xi \leq \infty, \quad 1 \leq \eta \leq 1, \quad 0 \leq \varphi \leq 2\pi. \tag{9.11}$$

In terms of these variables, the function, ϕ, (9.9) becomes

$$\phi(\xi, \eta, R) = \exp\left(-\frac{Z(R) + a}{2} R\xi\right) \cosh\left(\frac{Z(R) - a}{2} R\eta\right) \tag{9.12}$$

When the nuclei are fixed R is a parameter, as in the Born-Oppenheimer approximation and the coefficients $Z(R)$ and a are optimized variationally at each internuclear distance $R = R_0$. For instance, at the equilibrium distance $R_0 = R_e = 2.0$ au, the optimal values are $Z(R_e) + a = 1.36$ and $Z(R_e) - a = 0.92$, providing an energy $E_{GZ} = -0.60244$ au to be compared to the accurate Born-Oppenheimer value $E_{BO} = -0.60263$ au.

If the motion of the nuclei is considered, $Z(R)$ becomes a function of R. It is reasonable to assume that $Z(R)$ tends toward 1 when the nuclei are far apart each other. The following simple choice is made to take into account the variation of Z versus R

$$Z(R) = 1 + \frac{\gamma}{R} \tag{9.13}$$

with γ a variational parameter. With this choice, Eq. (9.12) reads

$$\phi(\xi, \eta, R) = \exp\left[-\left(\frac{\gamma}{2} + \frac{1 + a}{2} R\right)\xi\right] \cosh\left[\left(\frac{\gamma}{2} + \frac{1 - a}{2} R\right)\eta\right] \tag{9.14}$$

Defining the new parameters α and β

$$\begin{aligned} \alpha &= \frac{\gamma}{2} \\ \beta &= \frac{1 + a}{2} \end{aligned} \tag{9.15}$$

we have a two-parameter factor, ϕ, (9.9) describing the motion of the electron and the nuclei

$$\phi(\eta, \xi, R) = \exp[-(\alpha + \beta R)\xi] \ \cosh\{[\alpha + (1 - \beta)R)]\eta)\} \tag{9.16}$$

Thus, final form of the trial wave function employed here to describe the free molecular ion H_2^+ including the nuclear motion is

$$\Psi_t(\mathbf{r}, R) = \exp[-(\alpha + \beta R)\xi] \cosh\{[\alpha + (1 - \beta)R)]\eta)\} \frac{e^{-\delta(R-R_0)^2}}{R} \tag{9.17}$$

The parameters α, β, δ and R_0 are to be fixed variationally. It is worth mentioning here that a more general trial wave functions such as

$$\Psi'_t(\mathbf{r}, R) = \exp[-(\alpha + \beta R)\xi] \cosh[(\alpha' + \beta' R)\eta] \frac{e^{-\delta(R-R_0)^2}}{R} \tag{9.18}$$

containing six variational parameters could be considered. However this option will not be studied here. As we shall see, the four parameters wave function of this work provides an accurate description of the confined molecular H_2^+.

9.2.1.3 Trial Function for the Confined H_2^+ Molecular Ion

For a confined quantum system with hard surfaces, the wave function vanishes at the surface. In order to fulfill this condition, a cut-off factor is included in the variational wave function.

$$\Psi_{tc}(X) = \Psi_t(X)\, \omega(X) \tag{9.19}$$

where X represents the coordinates of the system and $\omega(X)$ the cut-off factor. For the H_2^+ molecular ion, the following form of the cut-off factor is considered here

$$\omega(\mathbf{r}, \mathbf{R}) = w_{r_{ce}}(r)\, W_{r_{cN}}(R) \tag{9.20}$$

where the first term is a cut-off factor for the electron and the second for the nuclei. The functional form here employed is

$$w_{r_{ce}}(r) = \left(1 - \frac{r}{r_{ce}}\right) \ \exp\left(\frac{r}{r_{ce}}\right) \tag{9.21}$$

$$W_{r_{cN}}(R) = \left(1 - \frac{R}{R_{cN}}\right) \ \exp\left(\frac{R}{R_{cN}}\right) \tag{9.22}$$

with $r = |\mathbf{r}|$ and r_{ce} and R_{cN} are the radius of the limiting hard surfaces confining the electron and the nuclei respectively. This type of cut-off functions was proposed in Ref. [17] and this choice was found to provide accurate results in previous

studies of confined atoms [18, 25]. By using $r_{ce} \neq R_{cN}$ one can study separately the effect of the electron and nuclear confinement.

Finally the approximated wave function for a spherically confined H_2^+ molecular ion in its ground state, including nuclear motion is

$$\Psi_{tc}(\mathbf{r}, R) = \exp[-(\alpha + \beta R)\,\xi]\cosh\{[\alpha + (1-\beta)R)]\eta)\}\,\frac{e^{-\delta(R-R_0)^2}}{R} \times \left(1 - \frac{r}{r_{ce}}\right)\left(1 - \frac{R}{R_{cN}}\right)\exp\left(\frac{r}{r_{ce}} + \frac{R}{R_{cN}}\right) \tag{9.23}$$

9.2.2 H_2 Molecule Ion Including Motion of Nuclei

9.2.2.1 Schrödinger Equation

The kinetic energy operator, T, for a molecular-like four body problem in atomic units is

$$T = -\frac{\nabla_{\mathbf{s}_1}^2}{2m} - \frac{\nabla_{\mathbf{s}_2}^2}{2m} - \frac{\nabla_{\mathbf{R}_1}^2}{2M_1} - \frac{\nabla_{\mathbf{R}_2}^2}{2M_2} \tag{9.24}$$

where M_i and $\mathbf{R}_i$ are the masses and position vectors of the nuclei and m the electron mass ($m = 1$ in atomic units) and s_i the position vectors of the electrons.

The following Jacobi coordinates are used here

$$\begin{aligned} \mathbf{R}_c &= \alpha_1\mathbf{R}_1 + \alpha_2\mathbf{R}_2 + \beta\mathrm{s}_1 + \beta\mathrm{s}_2 \\ \mathbf{R} &= \mathbf{R}_1 - \mathbf{R}_2 \\ \mathbf{r}_1 &= -f_1\mathbf{R}_1 - f_2\mathbf{R}_2 + \mathbf{s}_1 \\ \mathbf{r}_2 &= -f_1\mathbf{R}_1 - f_2\mathbf{R}_2 + \mathbf{s}_2 \end{aligned} \tag{9.25}$$

with

$$\begin{aligned} \alpha_i &= \frac{M_i}{M_1 + M_2 + 2m}, \quad i = 1, 2 \\ \beta &= \frac{m}{M_1 + M_2 + 2m} \\ f_i &= \frac{M_i}{M_1 + M_2}, \quad i = 1, 2 \end{aligned} \tag{9.26}$$

After change of coordinates we obtain the following form of the kinetic energy operator

$$T = -\frac{1}{2M}\nabla^2_{\mathbf{R}_c} - \frac{1}{2\mu}\nabla^2_{\mathbf{R}} - \frac{1}{2\varepsilon}\nabla^2_{\mathbf{r}_1} - \frac{1}{2\varepsilon}\nabla^2_{\mathbf{r}_2} - \frac{1}{M_1+M_2}\nabla_{\mathbf{r}_1}\cdot\nabla_{\mathbf{r}_2} \tag{9.27}$$

where each one of the Laplacian operators are with respect to the coordinates given in Eq. (9.25), M is the total mass of the system and μ and ε are the reduced masses given in Eq. (9.6).

For the H_2 molecule, we have $M_1 = M_2$ and

$$m \ll M_n$$

so that contribution of the mass polarization term in Eq. (9.27), $(-1/(M_1+M_2)\nabla_{\mathbf{r}_1}\cdot\nabla_{\mathbf{r}_2})$, to the ground state energy is very small and it can be considered as a perturbation. The same mass values as for the H_2^+ molecular ion are employed here, see Sect. 9.2.1.1.

The potential energy operator written in terms of the relative coordinates employed in this work becomes

$$V = \frac{1}{R} - \frac{1}{r_{1\mathrm{A}}} - \frac{1}{r_{1\mathrm{B}}} - \frac{1}{r_{2\mathrm{A}}} - \frac{1}{r_{2\mathrm{B}}} + \frac{1}{r_{12}} + V_{\mathrm{conf}} \tag{9.28}$$

with

$$R = |\mathbf{R}|, r_{i\mathrm{A}} = |\mathbf{r}_i - \mathbf{R}_1|, r_{i\mathrm{B}} = |\mathbf{r}_i - \mathbf{R}_2|, \quad i = 1,2,\ r_{12} = |\mathbf{r}_1 - \mathbf{r}_2| \tag{9.29}$$

and V_{conf} stands for the confinement potential giving the Dirichlet condition at the boundary limits.

The center of mass can be removed when using this coordinate system and the following intrinsic Schrödinger equation is obtained

$$\left(-\frac{1}{2\mu}\nabla^2_R - \frac{1}{2\varepsilon}\nabla^2_{\mathbf{r}_1} - \frac{1}{2\varepsilon}\nabla^2_{\mathbf{r}_2} + V\right)\Psi(\mathbf{r}_1,\mathbf{r}_2,\mathbf{R}) = E\,\Psi(\mathbf{r}_1,\mathbf{r}_2,\mathbf{R}) \tag{9.30}$$

9.2.2.2 Trial Function for the Free H_2 Molecule

The trial wave function Ψ_t employed here to describe the ground state of a H_2 molecule in a non- adiabatic scheme is a generalization to a two electron molecule of the trial function employed for the H_2^+ molecular ion of Sect. 9.2.1.2 and it includes electronic correlations

$$\Psi_t(\mathbf{r}_1,\mathbf{r}_2,\mathbf{R}) = F(\mathbf{R})\,\Phi(\mathbf{r}_1,\mathbf{r}_2,R)J(r_{12}) \tag{9.31}$$

The factor $F(\mathbf{R})$ describes the nuclear vibration and rotation. The lowest rotational and vibrational level will be considered here. Two different geometries will

be considered, spherical and cylindric symmetry with the molecule lying along the internuclear axis Z. For spherical symmetry, $F(\mathbf{R})$, will be parameterized as in Eq. (9.8). For cylindric symmetry the following functional form is used

$$F(Z) = \exp[-\delta(Z - Z_0)^2] \tag{9.32}$$

where Z is the internuclear distance and δ and Z_0 are variational parameters. This form corresponds to the ground state of a one dimension harmonic oscillator.

The factor Φ in Eq. (9.31) describes the motion of the nuclei and the two electrons and it is written as follows

$$\Phi(\mathbf{r}_1, \mathbf{r}_2, R) = \phi(\eta_1, \xi_1, R)\phi(\eta_2, \xi_2, R) \tag{9.33}$$

where the function $\phi(\eta_i, \xi_i, R)$ describes the three-body wave function for the nuclei and the electron i and is taken as the two parameter function given in Eq. (9.16) with confocal elliptic coordinates for each electron

$$\begin{aligned} \xi_i &= \frac{r_{iA} + r_{iB}}{R}, \quad 1 \le \xi_i \le \infty \\ \eta_i &= \frac{r_{iA} - r_{iB}}{R}, \quad -1 \le \eta_i \le 1 \end{aligned} \tag{9.34}$$

and $r_{i\mathrm{A}}$ and $r_{i\mathrm{B}}$ are the distances of electron i to the nuclei A and B respectively as given in Eq. (9.29).

Finally, the factor $J(r_{12})$ in the wave function of Eq. (9.31) is a Jastrow term describing the interelectronic correlation. The following form is employed here

$$J(r_{12}) = \exp\left(\frac{br_{12}}{1 + cr_{12}}\right) \tag{9.35}$$

with b and c variational parameters.

9.2.2.3 Trial Function for the Confined H_2 Molecule

For a confined H_2 molecule, the same approximation as in the case of the H_2^+ molecular ion is employed to consider confinement, see Eq. (9.19). Two different confinement geometries are considered. First, boundary hard spherical surfaces centered mid point to the nuclei. The cut-off ω taken to fulfill the Dirichlet conditions is [17, 18, 25]

$$\omega(r_1, r_2, R) = \left(1 - \frac{r_1}{r_{ce}}\right)\left(1 - \frac{r_2}{r_{ce}}\right)\left(1 - \frac{R}{R_{cN}}\right)\exp\left(\frac{r_1}{r_{ce}} + \frac{r_2}{r_{ce}} + \frac{R}{R_{cN}}\right) \tag{9.36}$$

This is a generalization to a two electron case of the cut-off factor employed for the H_2^+ molecular ion, Sect. 9.2.1.3.

Cylindrical boundary conditions will be also considered in this study. The confining surface is a non penetrable cylinder of radius ρ_{ce}. The cylinder axis is the molecular axis. The cut-off factor employed for this case is

$$\omega(\rho_1, \rho_2) = \left(1 - \frac{\rho_1}{\rho_{ce}}\right)\left(1 - \frac{\rho_2}{\rho_{ce}}\right) \exp\left(\frac{\rho_1}{\rho_{ce}} + \frac{\rho_2}{\rho_{ce}}\right) \tag{9.37}$$

with

$$\rho_i = \sqrt{x_i^2 + y_i^2}, \quad i = 1, 2$$

where only electronic confinement is considered.

In Eqs. (9.8), (9.33) and (9.35) for spherical confinement or (9.37) for cylindric confinement, the parameters α, β, b, c, δ, R_0 or Z_0 are fixed variationally.

9.2.3 Dirichlet Boundary Conditions and Variational Monte Carlo Approach

The expectation value of the Hamiltonian of the H_2^+ molecular ion and the H_2 molecule with the wave trial functions described in Sects. 9.2.1 and 9.2.2 respectively will be carried out by using the Variational Monte Carlo (VMC) method. The Variational Monte Carlo method is based on the variational approach with expectation values calculated by using random walks, see e.g. [12] for a complete description of the technique.

For a free molecule, the integration volume is the full configuration space of the system and the trial wave function vanishes at the infinity. In our case, we have a molecule inside a hard wall so that the wave function vanishes at the boundary of the surface, $\partial\tau$. We have included this boundary condition in our ansatz by means of a cut-off factor $\omega(X)$, see Eq. (9.19). Analytical transformation of the multi dimension integral leads to a convenient form of the functional for the VMC [25]. As we shall see below, with this manipulation minor changes are requested in order to include the constraint in an VMC code working for an unbound system.

The expectation value of the Hamiltonian for a confined system enclosed by impenetrable surfaces with the trial wave function of Eq. (9.19), can be written as follows

$$\langle \Psi_{tc}|H|\Psi_{tc}\rangle = \int_{\tau(\partial\tau)} \Big\{ -\frac{1}{2}[\omega^2(X)\Psi_t(X)\nabla^2\Psi_t(X) + \omega(X)\Psi_t^2(X)\nabla^2\omega(X) + 2\omega(X)\Psi_t(X)\nabla\omega(X)\cdot\nabla\Psi_t(X)] + V(X)\,\omega^2(X)\Psi_t^2(X)\Big\} dX \tag{9.38}$$

where $\tau(\partial\tau)$ represents the volume enclosed by the surface $\partial\tau$ and ∇ is the Gradient respect the coordinates of all the particles.

The term with the Gradients can be simplified by using

$$\int_{\tau(\partial\tau)} [\omega(X)\nabla\omega(X)] \cdot [\Psi_t(X)\nabla\Psi_t(X)]dX = \frac{1}{4}\int_{\tau(\partial\tau)} \nabla\omega^2(X) \cdot \nabla\Psi_t^2(X)dX$$

and applying a Green transformation

$$\int_{\tau(\partial\tau)} \nabla\omega^2(X) \cdot \nabla\Psi_t^2(X)dX = \int_{\partial\tau} \Psi_t^2(X)\nabla\omega^2(X) \cdot dS - \int_{\tau(\partial\tau)} \Psi_t^2(X)\nabla^2\omega^2(X)dX$$

In this equation the surface term vanishes because of the Dirichlet condition and the volume term can be rewritten as follows

$$\int_{\tau(\partial\tau)} \Psi_t^2(X)\nabla^2\omega^2(X)dX = 2\int_{\tau(\partial\tau)} \Psi_t^2(X)\omega(X)\nabla^2\omega(X)dX + 2\int_{\tau(\partial\tau)} \Psi_t^2(X)[\nabla\omega(X)]^2dX$$

the first integral cancels out when substituted in the expectation value of the Hamiltonian, Eq. (9.38), and the following result is obtained

$$\langle\Psi_{tc}|H|\Psi_{tc}\rangle = \int_{\tau(\partial\tau)} |\Psi_t(X)|^2\left\{\omega^2(X)E_L^t(X) + \frac{1}{2}[\nabla\omega(X)]^2\right\}dX \tag{9.39}$$

$$= \int_{\tau(\partial\tau)} |\Psi_{tc}(X)|^2\left\{E_L^t(X) + \frac{1}{2}[\nabla\ln\omega(X)]^2\right\}dX \tag{9.40}$$

where

$$E_L^t(X) \equiv \frac{H\Psi_t(X)}{\Psi_t(X)}$$

is the local energy for the unconfined molecule.

Equation (9.40) is specially suited for a VMC calculation [12]. By using the Metropolis algorithm configurations sampled from $\Psi_{tc}(X)$ can be generated and the integral in (9.40) is evaluated starting from the term in braces calculated for each one of the configurations. Equation (9.39) can also be employed by using configurations distributed according to the wave function corresponding to the free molecule and using weights to account for the cut-off factor and the normalization.

This leads to an, in general, less efficient calculation. It is worth to remark here that by using either expression, one can calculate bound systems by performing minor changes in a working VMC code for the corresponding free system. Finally it is worth to remark here that this formalism is general and can be used for any confined atom or molecule with a trial function written as in Eq. (9.19).

9.2.4 Dirichlet Boundary Conditions and Diffusion Monte Carlo Approach

To improve the energies of the confined molecular systems here studied, a Quantum Monte Carlo calculation is carried out. More specifically, we shall use in this work the Diffusion Monte Carlo (DMC) method. We recall briefly here the main ideas underlying the DMC approach. Further details relative to this powerful approach to solve the Schrödinger by simulating the Green's function of the system in question by statistical methods can be found in e.g. Ref. [12]. The variationally optimized wave functions shown in Sects. 9.2.1.3 and 9.2.2.3 will be employed as guiding functions, see below.

Consider the following general Hamiltonian

$$H = D\nabla^2 + V$$

where V is the potential operator, ∇^2 is the Laplacian with respect to all of the coordinates of the N particle system and $D = \hbar^2/(2m)$. For simplicity in what follows all the particles' masses, m, are identical. Generalization for different particle mass is straightforward. DMC method starts from the time dependent Schrödinger equation in imaginary time, that becomes classical diffusion equation.

$$\frac{\partial\psi(X,\tau)}{\partial\tau} = D\nabla^2\psi(X,\tau) + [E_t - V(X)]\psi(X,\tau) \tag{9.41}$$

where E_t is a constant and τ the imaginary time

$$\tau = it$$

In the limit $\tau \to \infty$, the asymptotically stationary behavior is obtained and the partial derivative with respect to imaginary time vanishes. In that limit, Eq. (9.41) becomes the time-independent Schrödinger equation.

Let us note that the factor, $E_t - V(X)$, will present large fluctuations along the configuration space of the system. In order to develop an efficient Monte Carlo algorithm to solve Eq. 9.41 in the asymptotic regime, it is necessary to use a noise reduction technique called importance sampling. Importance sampling starts from a guiding function, $\Psi(X)$, used to bias the sampling. This guiding function is an

approximation to the exact ground state wave function. Then the following distribution function is defined

$$f(X,\tau) = \phi(X,\tau)\Psi(X) \tag{9.42}$$

If we multiply Eq. (9.41) by $\Psi(X)$ and rewrite this equation in terms of $f(X,\tau)$ we obtain

$$\frac{\partial f(X,\tau)}{\partial \tau} = D\nabla^2 f(X,\tau) - D\nabla\cdot[f(X,\tau)\mathbf{F}(X)] + [E_t - E_L(X)]f(X,\tau) \tag{9.43}$$

where

$$F(X) \equiv 2\frac{\nabla\Psi(X)}{\Psi(X)}, \quad E_L(X) \equiv \frac{H\Psi(X)}{\Psi(X)} \tag{9.44}$$

In Eq. (9.43), the term $\mathbf{F}(X)$ represents a drift in the Monte Carlo that bias the simulation towards those regions of the configuration space where the probability, given by the guiding function is larger. In the form given by Eq. (9.43), the term giving rise to fluctuations is the local energy, $E_L(X)$. The local energy is a constant if the exact wave function is employed as guiding function. Therefore it is convenient to use an accurate wave function as guiding function in order to reduce the statistical noise of the simulation. However, very involved parameterizations, which generally are time consuming, will slow down the calculation due to the fact that the Gradient and the Laplacian of the guiding function must be calculated for all of the configurations at every step of the Monte Carlo simulation. Hence, compact and concise and still accurate wave functions are ideal as guiding functions.

In order to solve Eq. (9.43) by using Monte Carlo methods, this equation is written in integral form

$$f(X,\tau) = \int dX'\tilde{G}(X,X';\tau)f(X,0) \tag{9.45}$$

where $\tilde{G}$ is the importance sampling imaginary-time Green's function or propagator. This function is not exactly know in general. However, for small values of the imaginary time, approximations to the imaginary-time Green's function can be employed as the following one

$$\tilde{G}(X,X';\delta\tau) = \tilde{G}_D(X,X';\delta\tau)\tilde{G}_B(X,X';\delta\tau) + \Theta[(\delta\tau)^2] \tag{9.46}$$

where

$$\tilde{G}_B(X,X',\delta\tau) = e^{-(1/2[E_L(X)+E_L(X')]-E_t)\delta\tau} \tag{9.47}$$

$$\tilde{G}_D(X, X'; \delta\tau) = \frac{1}{(2\pi\sigma^2)^{3N/2}} e^{-(X-X'-\sigma^2\mathbf{F}(X'))/(2\sigma^2)} \tag{9.48}$$

where

$$\sigma^2 \equiv 2D\delta\tau$$

and N is the number of particles.

The Diffusion Monte Carlo algorithm is based in the integral form of the Schrödinger equation in imaginary time, Eq. (9.45) with the approximate form of the propagator given in Eqs. (9.46) and (9.48).

The DMC algorithm is as follows. A small value of the time step, $\delta\tau$, is fixed. An initial set of configurations, drawn for example from the guiding function is generated. Starting from each one of the configurations a new one is proposed based on the anisotropic diffusion part of the propagator, $\tilde{G}_{\mathrm{D}}$. This configuration is replicated m times according to the branching part of the propagator, $\tilde{G}_{\mathrm{B}}$. A complete and detailed description of this and other algorithms tailored to simulate the propagation given by Eq. (9.45), can be found in [12]. The propagation is iterated many times until the asymptotic regime of large imaginary time steps is reached. Then the exact ground state energy, within the statistical error, is obtained by calculating the average value of the local energy, $E_L(X)$, Eq. (9.44) in the asymptotic set of configurations. Several simulations for different time step values, $\delta\tau$, are carried out in order to extrapolate the results to $\delta\tau = 0$ removing the finite time step error of the propagator (9.46)

Fermion systems present some additional problems due to the antisymmetry of the wave function. This is not the case of the molecules here considered because they present spatially symmetric states. Finally, let us note that more elaborate approximations for the short time Green's function have been proposed and employed in the literature, see e.g. [24, 29].

9.3 Results and Discussion

This section presents the results obtained for the confined H_2^+ and H_2 molecular systems. As a first step we study the accuracy of the variational ansatz, including a check for the choice of the cut-off factor. In order to do that, calculations are made for different systems and the results are compared with the data available in the literature.

For this purpose, the energy values of the hydrogen atom located at one of the foci confined by a hard spheroidal surface have been calculated. Exact values are known for this problem, allowing for a check of the approximate wave function of this work. Secondly the energy values of the molecular ion H_2^+ under spheroidal constraint, in the frame work of fixed nuclei, will be calculated and compared to the exact values also available for this system.

Table 9.1 Energy and optimal parameters for the confined hydrogen atom with the wave function of this work, Eq. (9.49) as compared with the exact and another approximate calculation

ξ_c	E_{exact} [a]	E [b]	$E_{thiswork}$	Z_{eff}	b
10	−0.4999	−0.4997	−0.4998	1	0
4.1098	−0.475	−0.4713	−0.4730	0.95	0
3.3931	−0.425	−0.4217	−0.4239	0.97	0
3.0697	−0.375	−0.3721	−0.3740	1	0
2.5918	−0.225	−0.2225	−0.2234	1.04	0.09
2.4142	−0.125	−0.1223	−0.1207	1.05	0.13

[a] Ref. [20], [b] Ref. [9]

9.3.1 *Confined Hydrogen Atom Located at One of the Foci Confined by a Hard Spheroidal Surface*

The calculation for hydrogen atom confined by a hard spheroidal surface can be seen as a check of the cut-off function chosen here. The hydrogen atom is located on the axis **oz** at one of the focus i.e. A, with charge $Z_A = 1$, separated from the other focus, B, by a distance R. The charge at the focus B is taken $Z_B = 0$ in order to study a confined hydrogen atom. The spheroidal impenetrable surface is defined by the value of ξ_c = constant. The trial wave function including the cut-off is

$$\Psi(\mathbf{r}) = \begin{cases} \exp(-Z_{\text{eff}}\, r_A)(1+bz)\left(1-\frac{\xi-1}{\xi_c-1}\right)\exp\left(\frac{\xi-1}{\xi_c-1}\right) & \text{if} \quad \xi \le \xi_c \\ 0 & \text{if} \quad \xi > \xi_c \end{cases} \tag{9.49}$$

In this function Z_{eff} and b are variational parameters. The factor $(1+bz)$ is needed to describe the polarizability of the atom along the **oz** axis when relatively large eccentricities $1/\xi_c$ values are considered.

In Table 9.1 we report the variationally optimized values for the energy of the confined hydrogen atom. The comparison with the exact results and those of reference [9] shows a good agreement and validate the choice of the present wave function in this case.

9.3.2 *Clamped Nuclei H_2^+ Molecular Ion Confined by a Spheroidal Surface*

The H_2^+ molecular ion is standing along the **oz** axis and the nuclei are located at the centers A and B with charges $Z_A = 1$ and $Z_B = 1$. The foci A and B are separated by a fixed distance $R = R_0 = 2$ au. The spheroidal hard surface is defined

Table 9.2 Energy and optimal parameters obtained from the wave function of Eq. (9.50) with fixed internuclear distance as compared with the exact and another approximate calculation

ξ_c	E_{exact} [a]	E [b]	E_{thiswork}	Z_t	a
5.6924	−0.6025	−0.6022	−0.6022	1.3	0.92
2.9162	−0.525		−0.5237	1.27	0.88
2.4196	−0.375		−0.3746	1.38	0.81
2.2237	−0.25	−0.2499	−0.25	1.49	0.75
1.9934	0	0.0001	0.85×10^{-5}	1.68	0.57
1.6150	1.0	1.025	1.0072	2.44	0.0

[a] Ref. [20], [b] Ref. [9]

by the value of ξ_c = constant. Thus the trial wave function here proposed for this case is

$$\Psi(\mathbf{r}, R_0) = \begin{cases} \exp(-Z_t\,\xi)\cosh(a\eta)\left(1-\frac{\xi-1}{\xi_c-1}\right)\exp\left(\frac{\xi-1}{\xi_c-1}\right) & \text{if} \quad \xi \le \xi_c \\ 0 & \text{if} \quad \xi > \xi_c \end{cases} \tag{9.50}$$

The exact energy for this problem has been reported in reference [20] for different values of ξ_c. A comparison with these values and other approximate values will provide a check of the accuracy of the function proposed here for this ion.

The parameters Z_t and a are variationally optimized. In Table 9.2 we report the results here obtained as compared to those calculated in reference [9] and to the exact values, [20].

The agreement is found to be good even for relatively large values of the eccentricity, $1/\xi_c$. This make us confident on the reliability of the variational anzatz here employed to describe the $1s\sigma_g$ ground state of the confined H_2^+ ion when nuclei are fixed.

9.3.3 *Confined Three-Body* H_2^+ *Molecular Ion by a Spherical Surface*

When the vibration and the rotation of the H_2^+ ion are considered the symmetry of the lowest energy state, $v = 0$, and $K = 0$, is spherical with respect to the origin located mid of the nuclei. For this problem, with spherical symmetry, it is necessary to make the choice of spherically symmetric boundary hard surfaces. The boundary hard surfaces considered now are two spheres with center at the mid of the nuclei. The cut-off radii are, respectively, r_{ce} and R_{cN}. The present approach allows to make different choices like $r_{ce} = R_{cN}$ or $r_c \neq R_{cN}$ in order to study the respective role of the electron or nuclei confinement.

Table 9.3 Energy and optimal parameter for different confinement

$r_{ce} = R_{cN}$	α	β	δ	R_0	E_{VMC}	E_{DMC}	$\langle R \rangle$
∞	0.14	0.61	5.27	2.07	−0.596690(6)	−0.59714(3)	2.05580(5)
20	0.14	0.60	6.20	2.05	−0.596543(6)	−0.59713(3)	2.03789(5)
5.0	0.07	0.58	6.80	2.05	−0.594984(9)	−0.59637(4)	2.02685(5)
4.0	0.11	0.55	7.60	2.00	−0.58835(1)	−0.59062(2)	1.97514(5)
3.5	0.10	0.54	6.50	1.95	−0.57679(1)	−0.57905(8)	1.91265(6)
3.0	0.05	0.53	5.20	1.90	−0.54615(2)	−0.5496(3)	1.83127(6)
2.5	0.08	0.53	3.40	1.80	−0.47034(2)	−0.4772(2)	1.64659(5)
2.0	0.12	0.55	2.50	1.70	−0.27894(2)	−0.2916(1)	1.38087(4)

The accurate energy for the unconfined molecular ion [14] is −0.597 139 063 1 au. In parentheses we show the statistical error in the last figure

Table 9.4 Energy and optimal parameter for different confinement

r_{ce}	R_{cN}	α	β	δ	R_0	E_{VMC}	E_{DMC}	$\langle R \rangle$
2.0	20	0.11	0.55	6.60	1.35	−0.28714(1)	−0.29173(8)	1.33915(2)
20	2.0	0.16	0.61	5.80	2.05	−0.582429(5)	−0.58308(1)	1.70460(1)

In parentheses we show the statistical error in the last figure

The parameters α, β, δ and R_0 are optimized variationally. The optimum values and the VMC and DMC energies, E_{VMC} and E_{DMC} respectively and the expectation value of the internuclear distance $\langle R \rangle$ are reported in Table 9.3 for different confinement radii.

The results for the unconfined ion are also reported. The variational energy in this case $E_{VMC} = -0.596\,690(6)$ au is in a very good agreement with the result that can be considered as exact $E = -0.597\,139\,06$ au of [14] while the DMC agrees with this energy within the numerical error. When confinement becomes stronger the energy is increased. It can be remarked that even for relatively large confinement radii, for example $r_{ce} = R_{cN} = 4$ au, the energy is significantly different from the ground state one, though the internuclear distance is almost unchanged.

In Table 9.4 we show results obtained when different confinement radii are used for the electron and the nuclei. Two different limiting situations are considered.

From these results it is clear that when the confinement of the electron is strong, $r_{ce} = 2$ au, whereas the confinement of the nuclei is large, $R_{cN} = 20$ au, the mean internuclear distance is much more decreased than in the opposite situation, $r_{ce} = 20$ au and $R_{cN} = 2$ au. This finding illustrates the fact that in the former case the larger screening of the nuclei, induced by the strongly confined electronic charge, reduces the internuclear distance more efficiently that in the reverse situation. In reference [27] it has been suggested that this property might be useful to decrease the fusion barrier of protons. It is worthy also to remark that the raise in energy, $E = -0.29173(8)$ au, is much more important when electron is confined

Table 9.5 Different expectation values and the quantum pressure as a function of the confinement

r_{ce}	R_{cN}	$\langle r \rangle$	$\langle r_{\mathrm{eN}} \rangle$	$\langle \theta \rangle$	P (atm)
20.0	20.0	1.42755(9)	1.6893(1)	89.992(6)	
5.0	5.0	1.39745(7)	1.6621(1)	90.005(7)	2.2×10^3
4.0	4.0	1.33424(7)	1.5922(1)	89.995(7)	2.2×10^4
3.5	3.5	1.28052(6)	1.5337(1)	90.000(7)	7.3×10^4
3.0	3.0	1.21271(5)	1.45892(8)	90.000(6)	2.0×10^5
2.5	2.5	1.06899(5)	1.29649(7)	90.001(6)	1.0×10^6
2.0	2.0	0.88670(4)	1.08293(6)	90.001(6)	3.8×10^6
2.0	20.0	0.88380(4)	1.06984(6)	90.002(6)	
20.0	2.0	1.29936(9)	1.5091(1)	90.003(7)	

In parentheses we show the statistical error in the last figure

than when nuclei are confined $E = -0.58308(1)$ au. Under electronic constraint the energy of the molecular ion can be raised above the dissociation limit of the free system and the expectation value of the internuclear distance $\langle R \rangle$ is smaller in the confined system than in the unconfined one. The electronic constraint results in a sort of metastable bound state - high energy metastable state by confinement - compared to the free system. Some possible consequences of such mechanism is illustrated below along with a possible role in the catalytic mechanism of enzymes.

In Table 9.5 we show different radial expectation values $\langle r \rangle$, electron to origin distance, and $\langle r_{\mathrm{eN}} \rangle$, electron nucleus distance, along with the mean value of $\langle \theta \rangle$ the angle between the radius of the electron $\mathbf{r}_e$ and the internuclear axis **oz**.

The expectation values, $\langle r \rangle$, and $\langle r_{eN} \rangle$ decrease when the confinement is increased. This is further illustrated in Fig. 9.1, where we plot the energy and the radial expectation values $\langle R \rangle$, $\langle r_{\mathrm{eN}} \rangle$ and $\langle r \rangle$ as a function of the confinement for the case of $r_{ce} = R_{cN}$. For both kind of confinement, electron or nuclei, the $\langle r \rangle$ values are smaller than that those corresponding to the free system. It is interesting to note that the confinement due to the nuclei, $R_{cN} = 2.0$ au, $r_{ce} = 20.0$ au gives $\langle r \rangle = 1.299$ au, a value almost equal to $\langle r \rangle = 1.280$ au when the electron confinement is set to $r_{ce} = 3.5$ au. The mean value of the angle $\langle \theta \rangle$ remains always close to $\pi/2$. This means that, on the average, the electron stays in the mid plane between the nuclei perpendicular to the axis **oz** for all values of the confinement radii.

The mean quantum pressure, P, exerted on the spherical box of radius $r_{ce} = R_{cN}$ is calculated starting from

$$\begin{aligned} P &= -\frac{dE}{dV} \\ &= -\left[\frac{1}{4\pi r^2}\frac{dE}{dr}\right]_{r=r_{ce}} \end{aligned} \tag{9.51}$$

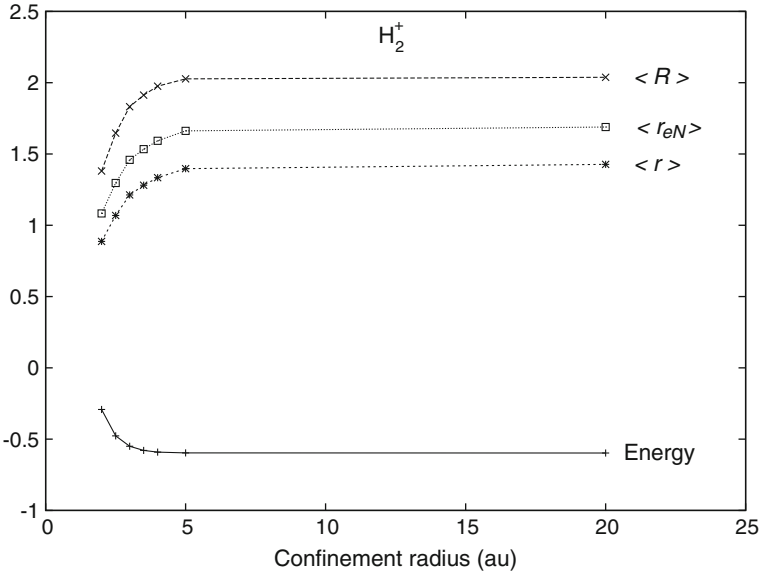

Fig. 9.1 Energy and the expectation value of the internuclear distance $\langle R \rangle$, mean electron-nuclei distance $\langle r_{eN} \rangle$, and the distance of the electron to the center of mass of the two nuclei, $\langle r \rangle$ for different values of the confinement radius for the H_2^+ molecular ion. The lines are for guiding the eye and the error is smaller than the size of the symbols

The numerical results for the pressure, in atmosphere (1 au (pressure) = 2.913 06 $\times 10^8$ atm) are reported in Table 9.5 as a function of the constrain radius. As expected the pressure augments very rapidly when the confinement is stronger.

In practice the boundary conditions limiting the space available to electrons can be realized, for example, by cages like those existing in fullerene, as proposed by different authors, see for example reference [27].

9.3.4 Confined Four-Body H_2 Molecule by a Spherical Surface

Following a similar approach made to study the H_2^+ ion, the VMC method is used first to make the variational optimization of the parameters α, β, δ, b, c and R_0 or Z_0 in the wave function of H_2^+. The optimized wave function is next employed as a guiding function in the DMC approach. For the ground state this method provides the exact non-relativistic energy up to the numerical precision, because the nodal surface is exactly defined through the Dirichlet conditions. A check of the accuracy can be made easily considering the calculated dissociation energy D_0 for the ground state of

Table 9.6 Variational Monte Carlo, E_{VMC} and Diffusion Monte Carlo E_{DMC} ground state energies for the spherically confined H_2^+ molecule for different confinement radii

$r_{ce} = R_{cN}$	E_{VMC}	E_{DMC}	α	β	b	c	δ	R_0
∞	−1.15304(3)	−1.16403(5)	0.11	0.60	0.72	0.45	8.8	1.46
20	−1.15286(3)	−1.16400(4)	0.11	0.60	0.72	0.45	8.8	1.46
5.0	−1.14572(3)	−1.16025(9)	0.10	0.55	0.60	0.40	9.2	1.45
4.5	−1.13945(3)	−1.15465(9)	0.10	0.56	0.57	0.33	9.9	1.43
4.0	−1.12522(3)	−1.14193(9)	0.10	0.56	0.62	0.35	11.0	1.40
3.5	−1.09516(3)	−1.11216(9)	0.10	0.56	0.57	0.33	11.5	1.35
3.0	−1.02532(4)	−1.04381(8)	0.10	0.57	0.70	0.36	15.0	1.26
2.5	−0.8709(4)	−0.88488(8)	0.10	0.56	0.56	0.34	16.5	1.13
2.0	−0.47909(4)	−0.49408(8)	0.10	0.59	0.60	0.41	19.5	1.02

The optimum parameters in the VMC calculation α, β, b, c, δ and R_0 are also shown. In parentheses we show the statistical error in the last figure

free H_2^+ molecule. In the present work we have obtained $D_0 = 36{,}120 \pm 11\ \mathrm{cm}^{-1}$ to be compared to the experimental value $D_0 = 36118\ \mathrm{cm}^{-1}$ [2]

In Table 9.6 we provide the Variational Monte Carlo (E_{VMC}) and Diffusion Monte Carlo (E_{DMC}) energy values and the expectation values of radial distances between nuclei and electrons and the variational parameters employed for different confinements radii with $r_{ce} = R_{cN}$. It is of interest to notice that the energy is increasing with the strength of the confinement. Even for a relatively soft confinement the change in energy is significant as already noticed in Ref. [4]. For instance at $r_{ce} = R_{cN} = 4$ au the calculated energy is $E = -1.1412$ au to be compared to the ground state energy $E_{GS} = -1.1641$ au.

It is worth to remark here that the expectation value of the mass polarization term, Eq. (9.27) is of the order of $10^{-5} - 10^{-4}$ au.

In Table 9.7 some expectation values of interest for the different confinement considered are reported. $\langle R \rangle$ is the expectation value of the internuclear distance; $\langle r_{eN} \rangle$ is the mean electron-nucleus distance; $\langle r \rangle$ is the expectation value of the electron-nuclear center of mass distance; $\langle r_{ee} \rangle$ is the average value of the interelectronic distance; $\langle \theta_{ee} \rangle$ is the expectation value of the angle subtended by the position vector of the electrons and $\langle \theta(r, R) \rangle$ is the expectation value of the angle subtended by each electron with the molecular axis (internuclear vector). The interparticle distances decrease with the confinement. For instance the mean internuclear distance is $\langle R \rangle = 1.03$ au when $r_{ce} = R_{cN} = 2$ au to be compared to $\langle R \rangle = 1.453$ au for the free molecule. The electronic confinement of the bonding electrons is able to shorten significantly the internuclear distances. This result was already noticed by Segal et al. [27] in relation with the cold fusion problem. The values of the angles $\langle \theta(r, R) \rangle$ remain in all cases close to $\pi/2$ illustrating that the bonding electrons stay on the average in the mid-plane perpendicular to the nuclei axis.

Table 9.7 Different expectation values

$r_{ce} = R_{cN}$	$\langle R \rangle$	$\langle r_a \rangle$	$\langle r \rangle$	$\langle r_{ee} \rangle$	$\langle \theta_{ee} \rangle$	$\langle \theta(r,R) \rangle$
∞	1.45304(2)	1.55848(5)	1.40469(7)	2.1470(1)	98.094(4)	90.000(4)
20	1.45267(2)	1.55403(5)	1.39993(7)	2.1393(1)	98.089(4)	89.997(4)
5	1.38090(2)	1.48033(5)	1.33585(6)	2.0445(1)	98.765(4)	90.002(4)
4.5	1.41983(2)	1.48637(5)	1.33557(6)	2.0338(1)	98.321(4)	90.005(4)
4	1.38921(2)	1.44020(5)	1.29167(5)	1.9680(1)	98.614(4)	90.002(4)
3.5	1.33746(2)	1.36707(5)	1.22215(5)	1.8538(1)	98.217(4)	89.998(4)
3	1.24811(1)	1.27225(4)	1.13696(4)	1.73378(8)	99.239(4)	89.999(4)
2.5	1.11746(1)	1.13663(4)	1.01510(4)	1.52644(7)	97.577(4)	90.001(4)
2	1.00311(1)	0.97833(3)	0.86400(3)	1.28947(5)	96.918(4)	90.002(4)

In parentheses we show the statistical error in the last figure

In Table 9.8 we show the energy values for cylindric confinement calculated by using the VMC and DMC approaches. It is important to recall here that only the electrons are confined in this case. Nuclei are not confined, see Eq. (9.37). However cylindrical hard boundary surfaces constraint induces a significant raise in energy, even for relatively soft confinement condition, as already noted in the case of the spherical confinement. The results show the raise in the energy and the decrease of the mean internuclear distance even when the Dirichlet boundary conditions are not a closed surface and concern only the electrons. However the cylindrical constraint needs a stronger confinement, $\rho_{ce} < r_{ce}$, in order to reach the same energy increment as that of the spherical confinement.

In Fig. 9.2 we plot the DMC energy values for different radii of constraint for both the H_2^+ molecular ion and the H_2 molecule. In the upper curves of Fig. 9.2 we compare the results for the energy obtained by using the Born-Oppenheimer approximation, BO curve, as a function of the internuclear distance R for a free H_2^+ molecular ion and the confined non adiabatic energies of this work versus $\langle R \rangle$. The same is shown in the lower curves of Fig. 9.2 for the H_2 molecule, including both spherical and cylindrical symmetry. In both cases, steep raise in energy is obtained.

The constraint gives rise to a *metastable state* with higher energy than the free molecule. It is of interest to analyze the fate of the metastable state when the constraint is removed. For instance, let us consider the metastable state represented by the point M in the Fig. 9.2, and assume a sudden relaxation of the constraint. The symmetry of the metastable state (g) is identical as the free state. This precludes an electronic radiative dipolar transition. The final state will be a vibrationally excited state of the $^1\Sigma$ ground state of the molecular bond represented by the broken line in Fig. 9.2, assuming that the removal of the constraint is ideally sudden.

The question of how such metastable state can be obtained in practice with the help of a suitable confinement is of importance. To achieve a significant decrease in the bond length following the electronic confinement it is necessary that the forces are set on the bonding electrons during a sufficient long time in order that the nuclei,

Table 9.8 Results for cylindric confinement. In parentheses we show the statistical error in the last figure

ρ_{ce}	α	β	b	c	δ	Z_0	E_{VMC}	E_{DMC}	$\langle Z \rangle$	$\langle r_{ee} \rangle$
20	0.106	0.60	0.48	0.30	9.0	1.49	−1.15304(4)	−1.1640(1)	1.48180(2)	2.1423(1)
5.0	0.088	0.60	0.52	0.28	9.5	1.46	−1.15100(4)	−1.1626(3)	1.45094(2)	2.1083(1)
4.0	0.082	0.60	0.58	0.30	10.0	1.42	−1.14140(4)	−1.1552(4)	1.41131(2)	2.0608(1)
3.0	0.085	0.60	0.58	0.32	11.5	1.36	−1.09329(4)	−1.1094(3)	1.35254(2)	1.9065(1)
2.5	0.085	0.59	0.58	0.32	11.5	1.30	−1.01248(4)	−1.0270(1)	1.29378(2)	1.8162(2)
2.0	0.115	0.58	0.45	0.35	11.5	1.20	−0.79687(4)	−0.8125(5)	1.19702(2)	1.5777(1)

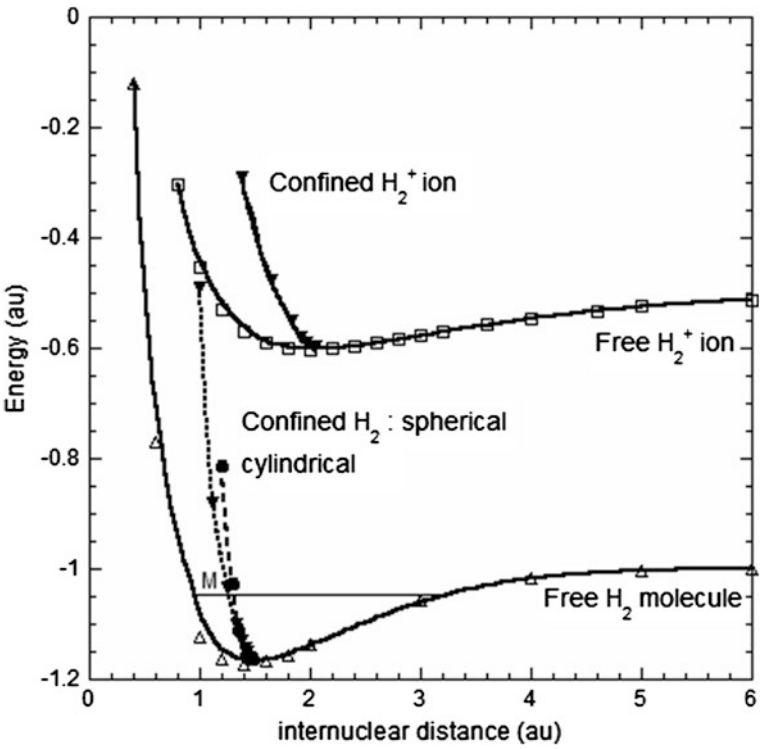

Fig. 9.2 Illustration of the energy changes induced by confinement. Upper curves: H_2^+ ion, open squares BO results; filled triangles confinement by spherical hard surfaces of different radii. Lower curves: H_2 molecule, open triangles BO approximation; filled triangles spherical confinement; filled circles cylindrical confinement

which are heavy particles, have enough time to move. Such long constraint in time cannot be obtained in a strongly polar solvent, for example, because the forces due to the electrostatic environment are not coherently reoriented during a sufficiently long time due to the thermal dispersion in continuum solvent models. Confinement is probably not a relevant mechanism of the chemical reactions in water solutions.

9.3.5 Consideration of Confinement in Active Site of Enzymes

Polar cavities, with a stable preorganized electrostatic environment, look suitable to induce the right confinement on the substrate molecules. One of the common features in the catalysis by enzymatic transformations is the confinement of the substrate in the enzyme pocket. Compression of the *nuclei* of the substrate inside

the cavity is often invoked to contribute to the catalytic power of the enzymes by lowering the distance between reactive termini thus facilitating nuclear tunneling across the activation barrier [3, 21]. Different works concerned with the problem of catalytic transfer of hydrogen atom in red-ox reactions argue that the distance between donor and acceptor is decreased by compression [13].

The analysis made above shows that compression/decompression of the bonding electrons is a mechanism able to produce a vibrationally excited state of the chemical bond. The net result will be similar to an increase of the temperature of the substrate making easier an atomic rearrangement to give the products. Such a compression/relaxation cycle by electrostatic forces of the bonding electrons might occur in the polarized active site of the enzyme, when the enzyme-substrate complex is formed, and driven by the molecular dynamics of the enzyme that governs the shape and volume of the active cavity.

Such mechanism can explain qualitatively the primary and secondary kinetic isotope effect (KIE) observed in some catalyzed reactions made by the enzymes. Let us consider the reaction of a transfer of an hydrogen atom and the substitution by a deuterium atom (primary KIE) in the reactant. As the deuterium is twice heavier than the proton it moves slower than the proton when the same pulse of force is applied on the bonding electrons. As a direct consequence the metastable state reached by the D isotope during the compression/relaxation cycle, which is assumed to be identical for both atoms, will result in a metastable state with lower energy. Relaxation of the constraint induces a transition to the ground state with a smaller vibrational quantum number v than for the H case. This analysis predicts that the reaction rate should be larger for the H atom transfer from a C–H bond compared to C-D case.

A secondary KIE corresponding to an isotope substitution in the enzyme, even at a large distance from the active site, will affect the molecular dynamic of the enzyme cavity. The final outcome is a reduced catalytic activity of the enzyme due to a lower efficiency of the compression/relaxation cycle process.

In summary we suggest that the induction of the vibrational excitation via electronic confinement/relaxation in the particular molecular bond concerned by the chemical reaction of the substrate, is a basic molecular mechanism that increases the reaction rate. We propose that this mechanism plays a role in the catalytic power of the enzymes.

9.3.6 Decreasing the Coulomb Barrier for the Fusion of Protons by Electronic Confinement

The fusion of two protons in a molecular ion H_2^+ under normal condition of pressure and temperature—cold fusion—is a highly unprobable event. Under these conditions the fusion rate has been estimated [5] to be 10^{-74} s^{-1}. The muon catalyzed fusion, as demonstrated by Alvarez [1], is based on the decreasing of the

internuclear distance when the electron is replaced by a muon in the molecular ion. The present results on the compressed H_2^+ ion indicate that the electronic confinement can induce a significant lowering of the internuclear distance. A rough estimation of the enhancing of tunneling through the Coulomb repulsive barrier is presented following [27].

The rate of the fusion reaction w is related to the following probability

$$w \sim |\Psi(R_N)|^2 \tag{9.52}$$

where R_N is the distance between the protons when the strong nuclear forces are present i.e. $R_N = 10^{-7}$ nm. In order to reach such small distances the protons must tunnel through the repulsive Coulomb potential from the classical turning point R_t given by $E = V(R_t)$. In the frame work of the JWKB semi-classical approximation the nuclear probability can be estimated by the integral

$$|\Psi(R_N)|^2 \sim \exp\left\{ 2 \int_{R_t}^{R_N} \sqrt{\frac{2\mu}{\hbar^2}(V(R) - E)} dR \right\} \tag{9.53}$$

The fusion rate for the ground state $E = E_0$ can be estimated as

$$w \sim \frac{2\mu E_0}{4\pi^2 \hbar^2 A_\mu} \exp\left[1 - \pi \sqrt{2 \frac{R_t}{A_\mu}} \right] \quad \text{where } A_\mu = \frac{\hbar^2}{\mu e^2} \tag{9.54}$$

with μ the reduced mass.

The lowering of R_t by a factor c $\leq$ 1 gives a turning point $R_t' = cR_t$. The approximated tunneling rate w' is given, in a more quantitative way, by [5]

$$\frac{w'}{w} = \exp\left[\pi \sqrt{\frac{2R_t}{A_\mu}} (1 - \sqrt{c}) \right] \tag{9.55}$$

Taking for example for the value of the classical turning point in the ground state $R_t = 0.1$ nm and $A_\mu = 2.9 \times 10^{-5}$ nm, a decrease of about 40 % in R_t is obtained i. e. c = 0.6. The corresponding enhancement in the tunneling factor is $w'/w \sim 10^{25}$. Results from Table 9.5 show that such enhancement is reached for a confinement of about $r_{ce} = 2.0$ au, corresponding to a pressure of 3.8×10^6 atm. The gain is not sufficient to sustain cold fusion. However, it is of interest to keep in mind that the confinement of the electron decreases significantly the fusion barrier. An additional transitory increase of pressure by a shock wave, for example, might induce more events of fusion and could be of significant interest for cold fusion purpose and its applications to obtain energy.

9.4 Conclusions

Most of the studies presently available concerning the constrained H_2^+ molecular ion and the H_2 molecule are performed under the hypothesis of clamped nuclei. The boundary surfaces, where Dirichlet conditions are fulfilled, are usually spheroidal surfaces. Exact values have been calculated for the latter situation and should be considered to be a check of any other approach.

In the present work we have developed approximate wave functions to describe the H_2^+ ion and H_2 molecule in their ground rovibrational state using the Jacobi coordinates. A different cut-off radius is fixed for the electron or the nuclei allowing for a quantitative analysis of the respective role of the electron or nuclei confinement. Using the Variational and Diffusion Monte Carlo approaches the energy and several expectation values including the quantum pressure have been obtained for different radii of the constrain. It is found that the electron confinement is much more efficient to decrease the mean internuclear distance as compared to the nuclei confinement. As a consequence the raise in energy of the ion is more important when electron confinement is considered.

Confinement by hard surfaces, not necessarily closed surfaces, of the bonding electrons augments the energy and decreases the interparticle distances. Due to the confinement a metastable state with higher energy is obtained. This raises the interesting question of the fate of such metastable state when the constraint is removed. We have discussed the formation of a vibrationally excited state induced induced when a confinement/deconfinement cycle is considered. As a consequence a sudden release of the constraint will result in an excited vibrational state of the chemical bond in the free system. Such mechanism might play a significant role if molecules are located in a cavity, like the active pocket of an enzyme, assuming that a fluctuation of the surrounding charges induces the right pulse of constraint.

Acknowledgment AS thanks partial support for this work to the Spanish Dirección General de Investigación Cientfica y Técnica (DGICYT) and FEDER under contract FIS2012-39617-C02-02 and by the Junta de Andalucía.

References

1. Alvarez LW, Bradner H, Crawford FS, Crawford JA, Falk-Vairant P, Good ML, Gow JD, Rosenfeld AH, Solmitz F, Stevenson ML, Ticho HK, Tripp RD (1957) Phys Rev 105:1127
2. Balakrishnan A, Smith V, Stoicheff BP (1992) Phys Rev Lett 68:2149
3. Basner J, Schwartz S (2005) J Am Chem Soc 127:13822
4. Bielinska-Waz D, Diercksen GHF, Klobukowski M (2001) Chem Phys Lett 349(3–4):215
5. Bracci L, Fiorentini G, Mezzorani G (1990) J Phys G: Nucl Part Phys 16(1):83
6. Colín-Rodríguez R, Cruz SA (2010) J Phys B-At Mol Opt Phys 43:235102
7. Connerade JP, Kengkan P (2003) Idea-Finding Symposium. EP Systema, Debrecen, Frankfurt, Germany, pp 35–46

8. Cruz S (2009) Adv Quantum Chem 57:255–284 (ed. by J. Sabin, E. Brändas (Elsevier, San Diego, CA)
9. Cruz SA, Colín-Rodríguez R (2009) Int J Quantum Chem 109:3041
10. Dolmatov V, Baltenkov A, Connerade JP, Manson S (2004) Radiat Phys Chem 70:417
11. Guillemin V Jr, Zener C (1929) Proc Natl Acad Sci USA 15:314
12. Hammond BL, Lester WA Jr, Reynolds PJ (1994) Monte Carlo methods in ab initio quantum chemistry. World Scientific, Singapore
13. Hay S, Scrutton N (2012) Nat Chem 4:161
14. Hilico L, Billy N, Grémaud B, Delande D (2000) Eur Phys J D12:449
15. Horsewill AJ, Panesar KS, Rols S, Johnson MR, Murata Y, Komatsu K, Mamone S, Danquigny A, Cuda F, Maltsev S, Grossel MC, Carravetta M, Levitt MH (2009) Phys Rev Lett 102:013001
16. Jaskolski W (1996) Phys Rep 271:1
17. Laughlin C, Chu SI (2009) J Phys A: Math Theor 42:265004
18. Le Sech C, Banerjee A (2011) J Phys B-At Mol Opt Phys 44:105003
19. LeSar R, Herschbach DR (1981) J Phys Chem 85:2798
20. Ley-Koo E, Cruz SA (1981) J Chem Phys 74:4603
21. Masgrau L, Roujeinikova A, Johannissen L, Hothi P, Basran J, Ranaghan K, Mulholland A, Sutcliffe MJ, Scrutton N, Leys D (2006) Science 312:237
22. Sabin J, Brändas E, Cruz S (eds) (2009) Theory of confined quantum systems, vol 57 and 58. Academic Press, New York
23. Sarsa A, Alcaraz-Pelegrina JM, Le Sech C, Cruz SA (2013) J Phys Chem B 117:7270
24. Sarsa A, Boronat J, Casulleras J (2002) J Chem Phys 116:5956
25. Sarsa A, Le Sech C (2011) J Chem Theory Comput 7:2786
26. Sarsa A, Le Sech C (2012) J Phys B-At Mol Opt Phys 45:205101
27. Segal D, Seideman T, Kurizki G, Shapiro M (2006) Chem Phys Lett 420:241
28. Slater JC (1960) Quantum theory of molecules and solids, vol I. McGraw-Hill, New York
29. Umrigar CJ, Nightingale MP, Runge KJ (1993) J. Chem Phys 99:2865